THE LONG-TERM BEHAVIOUR OF BUTT FUSION WELDS IN POLYETHYLENE PIPELINE SYSTEMS

A thesis submitted for the degree of Doctor of Philosophy

by

Ravindra Parmar

Department of Materials Technology, Brunel University

April 1986

CONTENTS

ACKNOWLEDGEMENTS

I wish to thank the Polymer Engineering Directorate of the SERC, the Water Research Centre (Engineering) and the Associated Octel Company Ltd., for finanical support. I have appreciated the help given to me during my experimental work by all the technicians in the Department of Materials Technology and in particular like to thank Mr W Price for the maintenance of heaters and manufacture of various fixtures in the pipe testing laboratory.

Many of the ideas presented in the thesis have been discussed with my supervisors Dr J Bowman and Professor M Bevis and I would like to express my thanks to them for spending some of their time with me. I am particularly grateful to them for their advice and encouragement.

Many thanks are due to my father - Narsibhai, mother - Gangaben and my sister, Paroo for their moral support and constant encouragement they have given in completing the manuscript. Last but not least special thanks to my wife, Neeta for being patient with me and also for her accurate typing of the manuscript.

SUMMARY

The objective of the study was to examine factors that influence the strength of butt welds and gain an understanding of the process of failure. The study was divided into several sectors. The first and primary part of the programme was to determine the extent to which the pipe system's long-term strength under both internal fluctuating and constant pressure is reduced by the presence of axially misaligned butt welds. The second objective was to examine fracture initiation sites and crack propagation paths of the failed aligned and misaligned butt welded samples in relation to the melt flow zone and the weld bead in order to establish the cause of failure. Finally the project considered the influence of selected welding parameters on the fatigue performance of aligned butt fusion welds and an investigation into the influence of elevated temperature (79°C) testing technique on the basic material's properties.

Fatigue and stress-rupture lifetimes were found to decrease significantly with increasing axial misalignment at the butt fusion weld in 63, 90 and 125mm MDPE pipe systems at 79°C in a water environment. In the butt fusion weld having axial misalignment of 20 per cent of the wall thickness and above, the reduction in the fatigue and stress-rupture lifetime was greater than 50 per cent compared to the aligned weld. It was not clear whether there is a pipe size effect or not; there was no marked change in the fatigue performance of misaligned butt welds for the three pipe diameters examined. However, the fatigue performance of the aligned butt welds in 90 and 125mm was noticeably better compared to 63mm pipe systems. The stress rupture performance of misaligned butt welds in 90 and 125mm MDPE pipes was more than halved compared to those in 63mm pipe systems.

Both the fatigue and stress rupture performance of misaligned butt welds could be explained in terms of amplified axial stress

and in general, the Ory expression for evaluating the increase in axial stress due to misalignment appears to be valid.

The temperature dependence of the fatigue performance of aligned and misaligned butt fusion welds in 63 and 90mm MDPE pipe systems suggests that if continuous internal fluctuating pressure under the conditions examined is maintained, then the butt fusion welds with axial misalignment of below 10 per cent of the wall thickness may well meet the design lifetime of 50 years at the service termperature. Under stress-rupture conditions, all the misaligned butt welds considered in the three pipe diameters surpassed the minimum specified requirement of 170 hours at 79°C. The fatigue was the most aggresive condition of the two for minor misalignment.

Examination of the circumferential butt weld failures revealed that the crack invariably initiated from the notch located at the inner weld bead and no preferred crack propagation path was taken in relation to the melt flow zone. It was proved that the notch was responsible for the observed circumferential failure of aligned butt welds in 63mm MDPE pipes by testing these butt fusion welds where the internal weld bead was machined off. The failure site for the internal weld bead machined off sample was in the pipe remote from the weld inferring that the material in the melt flow zone does not constitute any weakness.

The effect of elevated temperature (79°C) testing in 63mm HDPE pipe was found to increase the density (and crystallinity) signifying a slow annealing process in the material. However, the changes in these parameters were not of sufficient scale to strongly influence the performance. The main effect of elevated temperature testing in water environment appears to be the extraction of stabiliser from the base polymer as was indicated by the rapid decrease in oxidation induction time with the ageing times.

LIST OF TABLES

LIST OF FIGURES

Fig. 2.10 Geometrical defects at the butt weld (a) due to displacement of the wall and (b) due to shrinkages (After Ref 125)

Fig. 2.11 Effect of testing variables on specimen temperature. (a) effect of ambient temperature on nylon 6 (After Ref. 160), (b) effect of frequency on LDPE (After Ref. 162) and (c) effect on applied stress amplitude on nylon 6.10: curve 1, 260 kg/cm^2; curvé 2, 280 kg/cm^2; curve 3, 340 kg/cm^2. (After Ref. 158)

Fig. 2.12 Stress amplitude, σ_a, versus logarithm cycles-to-failure, N_f for a potyacetal copolymer +, 0.167; ∇ ,0.5; □ , 1.67; 0, 5.0; Δ, 10.Hz (note difference between thermal and mechanical fatigue failure mechanism and their different dependencies upon frequency). (After Ref. 166)

Fig. 2.13 Fatigue crack propagation behaviour in amorphous and crystalline polymers. The fatigue crack growth rate, da/dN, is plotted against K_I (= K_{Imax} - K_{Imin}) (After Ref. 151)

Fig. 2.14 Influence of loading frequency on (a) number of cycles to failure and (b) the time at maximum stress for various small diameter MDPE/HDPE pipes. (After Ref. 109)

Fig. 2.15 Model of discontinuous crack propagation mechanism. (After Ref. 186)

Fig. 2.16 Mechanism of fatigue crack propagation in semi-crystalline thermoplastic (HDPE) (After Ref. 192)

Fig. 2.17 Mechanism, of fatigue crack propagation in an amrophous polymer (uPVC) (After Ref. 181)

Fig. 3.1 Sample location site for the density, DSC, DTA and IR analysis of the untested and tested butt welded specimen at 79°C.

Fig. 3.2(a) Perkin-Elmer Differential scanning calorimeter system.
(b) Instrument circuit daigram for Differential Thermal Appratus
(c) Plots of (i) sample temperature and (ii) programmed temperature against furnace temperature.
(d) Plot of difference in temperature for the same curve.

Fig. 4.12(a) Logarithm amplified axial stress versus logarithm time to failure for 63mm SDR11 Rigidex 002-50 MDPE pipe systems.
ML = Pipe manufacture's line (After Ref.3).

Fig. 4.12(b) Logarithm amplified axial stress versus logarithm time to failure for 90mm SDR11 Rigidex 002-50 MDPE pipe systems.
ML = Pipe manufacture's line (After Ref.3).

Fig. 4.12(c) Logarithm amplified axial stress versus logarithm time to failure for 125mm SDR11 Rigidex 002-50 MDPE pipe systems.
ML = Pipe manufacture's line (After Ref.3).

Fig. 4.13 Definition of $t_{fatigue}$.

Fig. 4.14 Comparison of fatigue and stress-rupture data in terms of t, t_f and t_{SR} for 63mm SDR11 Rigidex 002-60 HDPE pipe systems.

Fig. 4.15 Comparison of fatigue and stress-rupture data in terms of t, t_f and t_{SR} for SDR11 Rigidex 002-60 HDPE pipe systems in (a) 63, (b) 90 and (c) 125mm pipe systems.

Fig. 4.16 Comparison of observed t_f and predicted t_f for (a) 63, (b) 90 and (c) 125mm SDR11 Rigidex 002-50 pipe systems.

Fig. 5.1 Low magnification optical photomicrograph of the etched surface of (a) nominally aligned and (b) nominally 44% misaligned butt weld in 63mm SDR11 Rigidex 002-50 MDPE pipe.

Fig. 5.2 Schematic of three different types of crack propagation path by which aligned and misaligned butt welds failed in the circumferential plane;
(a) Type I, (b) Type II and (c) Type III.

Fig. 5.3 Low magnification optical photomicrographs of the etched surface of (a) nominally aligned and (b) nominally 9% and (c) 18% misaligned butt weld failures in 63mm SDR11 Rigidex 002-60 HDPE pipes.

Fig. 5.4 Low magnification optical photomicrographs of the etched surface of (a) nominally aligned and (b) nominally 9%, (c) 18% and (d) 44% misaligned butt weld failures in 63mm SDR11 Rigidex 002-50 MDPE pipes.

Fig. 5.5 Low magnification optical photomicrographs of the etched surface of (a) nominally aligned and (b) nominally 9%, (c) 18% and (d) 44%misaligned butt weld failures in 90mm SDR11 Rigidex 002-50 MDPE pipes.

Fig. 5.6 Low magnification optical photomicrographs of the etched surface of (a) nominally 18% and (b) 44% misaligned butt weld failure in 63mm SDR11 and, (c) 18% misaligned butt weld failures in 90mm SDR11 Rigidex 002-50 MDPE pipes under stress rupture condition.

Fig. 5.7 Low magnification optical photomicrograph of the etched surface of a nominally aligned butt weld failure in 63mm SDR11 DuPont Blue Aldyl 322A.

Fig. 5.8 Photomicrograph showing the pipe failure remote from the internal weld removed region.

Fig. 5.9 Scanning Electron micrographs of the inner weld bead region showing the notches present in nominally aligned and nominally 44% misaligned butt welds in (a) 63, (b) 90 and (c) 125 mm SDR11 Rigidex 002-50 MDPE pipe.

Fig. 5.10 Low magnification photomicrographs of the fracture surfaces of aligned butt weld failures in (a) 63 and (b) 90 mm pipe systems.

Fig. 5.11 Low magnification photomicrographs of misaligned butt weld fracture surfaces of (a) 9% and (b) 44% tested at ΔP=9.5 bar; (c) 9% and (d) 44% tested at ΔP=6.5 bar in 63mm SDR11 MDPE pipe systems.

Fig. 5.12 Low magnification photomicrographs of misaligned butt weld fracture surfaces of (a) 9% and (b) 44% tested at ΔP=9.5 bar; (c) 9% and (d) 44% tested at ΔP=6.5 bar in 125mm SDR11 MDPE pipe systems.

Fig. 5.13 Low magnification photomicrographs of misaligned butt weld fracture surfaces of (a) nominally aligned and (b) 44% misaligned butt weld in 63mm SDR11 MDPE pipe systems tested under stress-rupture conditions.

Fig. 5.14 Low magnification photomicrographs of misaligned butt weld fracture surfaces of (a) nominally 9% and (b) 44% misaligned butt welds in 125mm SDR11 MDPE pipe systems tested under stress-rupture conditions.

Fig. 5.15 Low magnification optical photomicrographs of axial cracks in the aligned butt welds in (a) and (b) 63; (c) and (d) 90mm SDR11 MDPE pipe.

Fig. 5.16 Fracture surfaces of axial butt weld failures in (a) and (b) 63; (c) and (d) in 90mm SDR11 MDPE pipe.

Fig. 5.17 Fracture surfaces of pipe failures (a) and (b) in 63mm and (c) and (d) in 90mm SDR11 pipes tested at ΔP=9.5 bar.

Fig. 5.18 Fracture surfaces of pipe failures (a) and (b) in 63mm and (c) and (d) in 90mm SDR11 pipes tested under stress-rupture conditions at 9.5 bar.

Fig. 5.19 SEM micrographs of fracture surface of 9% misaligned butt weld tested at ΔP=9.5 bar; (a) low magnification and high magnification region of (b) initiation site, (c) intermediate distance and (d) on approach to the final stages of rupture.

Fig. 5.20 SEM micrographs of fracture surface of 44% misaligned butt weld tested at ΔP=9.5 bar; (a) low magnification and high magnification region of (b) initiation site, (c) intermediate distance and (d) on approach to the final stages of rupture.

Fig. 5.21 SEM micrographs of fracture surface of 9% misaligned butt weld tested at ΔP=6.5 bar; (a) low magnification and high magnification region of (b) initiation site, (c) intermediate distance and (d) on approach to the final stages of rupture.

Fig. 5.22 SEM micrographs of fracture surface of aligned butt weld tested under constant pressure of 9.5 bar; (a) low magnification and high magnification region of (b) initiation site and (c) on approach to the final stages of rupture.

Fig. 5.23 SEM micrographs of fracture surface of 44% misaligned butt weld tested under constant pressure of 9.5 bar; (a) low magnification and high magnification region of (b) initiation site.

Fig. 5.24 SEM micrographs of fracture surface of axial butt weld failure; (a) and (b) low and high magnification micrographs respectively of initiation site, (c) and (d) low and high magnification micrographs respectively of MFZ at mid-wall and (e) and (f) low and high magnification micrographs respectively of the final stages to rupture.

Fig. 5.25 SEM micrographs of fracture surface of pipe failure tested at ΔP=9.5 bar; (a) low magnification and high magnification region of (b) initiation site and (c) intermediate distance from the bore to mid-wall.

Fig. 5.26 SEM micrographs of fracture surface of pipe failure tested at a constant pressure of9.5 bar.

Fig. 5.27 SEM micrographs showing initiating particles in (a) and (b) 63mm; (c) and (d) 90mm pipe failures.

Fig. 5.28 Creep rupture cracks in pressure butt welds with heated tool; (a) cracks on the welding surface, (b) crack starting from notch and (c) crack in the base material.

Fig. 6.1 DSC thermograms of surface specimen taken from the butt weld (MFZ) and 15-20mm away from it of the control butt welded MDPE pipe samples aged for 000, 200 and 8000 hours.

Fig. 6.2 DSC thermograms of surface specimen taken from the butt weld (MFZ) and 15-20mm away from it of the pressure tested butt welds in MDPE pipe sample for 200 and 8000 hours.

Fig. 6.3 Decrease in Oxidation Induction Time of both the control and pressure tested samples taken from butt welds in MDPE pipe with the ageing/pressure testing time.

Fig. 6.4 Infrared spectrum obtained for the bore skin of MFZ taken (a) from the untested butt welded MDPE pipe sample and (b) from pressure tested butt welded MDPE pipe sample to greater than 8000 hours.

NOMENCLATURE

A, B, C, D, E, n	Constants
A_p	Area of a perfect annulus
A_m	Area of misaligned annulus
a	Thermal diffusivity, Crack length
c_p	Specific heat
D	Diffusion coefficient
d	Internal diameter, Outside diameter, Weld bead depth
da/dN, da/dt	Crack growth rate
E	Energy dissipation rate
E(t)	Time dependent elastic modulus
E_m', H	Apparent energy
e	Axial displacement at the weld
F_m	Longitudinal force
f	Welding factor, Frequency
ΔH_f	Enthalpy of fusion
$\Delta H_f^{\ominus}$	Enthalpy of fusion for a 100% crystalline linear polyethylene
h	Planck's constant
I	Permeation constant
J"	Loss compliance
K_c	Fracture toughness
ΔK	Stress-intensity range
ΔK_{th}	Threshold value of ΔK
k	Boltzmann's constant
L_o	Thickness of melted zone
M_m	Fractional misalignment
Mn	Number average molecular weight
Mw	Weight average molecular weight

N_f	Number of cycles to failure
n_m	Average apparent viscosity
P	Applied internal pressure
P_f	Welding pressure
P_1	Inside pressure
P_2	Outside pressure
ΔP	Pressure range
R	Gas constant
R_c	Plastic zone size
r_i	Inside radius
r_o	Outside radius
S	Solubility constant
T	Absolute temperature
T_{f1}	Flow temperature (melt temperature)
T_h	Surface temperature of the heater plate
T_U	Ambient temperature
ΔT	Temperature rise per unit time
t	Wall thickness, Time to fracture/failure
t_c	Cyclic time
t_d	Time to drop to the minimum pressure
t_E	Total heating time
$t_f, T_{fatigue}$	pseudo stress-rupture or cyclic stress-rupture lifetime
t_{max}	Time under maximum stress
t_r	Time to reach the maximum pressure
V', β	Apparent volume
V_{m2}	Average flow speed
v_{f1}	Flow speed
w	Weld bead width

Y	Geometric factor
γ	Angle of inclination at the weld
$\delta c/\delta x$	Concentration gradient
ϵ	Strain rate
ρ	Specimen density
ρ_c	Density of the crystalline phase
ρ_a	Density of the amorphous phase
σ	Butt weld strength, peak stress
σ_D	Strength dependent on Diffusion process
σ_R	Strength dependent on Relaxation process
σ_{fl}	Strength dependent on Flow speed
σ_H	Hoop stress
σ_A	Axial stress
σ_r	Radial stress
$[\sigma_H]_r$	Hoop stress at radius, r
$[\sigma_A]_r$	Axial stress at radius, r
$[\sigma_r]_r$	Radial stress at radius, r
$\Delta\sigma$	Stress range, Chosen/Applied nominal stress range
$\Delta\sigma_h$	Hoop stress range
$\Delta\sigma_a$	Axial stress range
σ_a	Increase in axial stress due to axial misalignment Applied stress amplitude
σ_h	Increase in hoop stress due to axial misalignment
σ_a'	Increase in axial stress due to angular misalignment
σ_h'	Increase in hoop stress due to angular misalignment
σ_Y	Stress at the plastic zone
σ_{cs}	Craze stress
σ_Y'	Plane-strain yield stress
τ	Characteristic relaxation time of the activated process

τ_{SR}	Stress-rupture lifetime
χ_c	Crystallinity

ABBREVIATION

ASTM	American Society for Testing and Materials
ABS	Acrylonitrile-butadiene-styrene copolymer
BS	British Standard
DSC	Differential Scanning Calorimetry
DTA	Differential Thermal Analysis
GPC	Gel Permeation Chramatography
HAZ	Heat affected zone
HDPE	High Density Polyethylene
HRT	Heat removal time
HSPVC	High Strength Polyvinyl Chloride
HST	Heat soak time
IR	Infrared
ISO	International Standard Organisation
LDPE	Low Density Polyethylene
MDPE	Medium Density Polyethylene
MFI	Melt flow index
MFZ	Melt flow zone
NDT	Non-Destructive Testing
OIT	Oxidation induction time
PMMA	Polymethyl methacrylate
PS	Polystyrene
PVC	Polyvinyl chloride
uPVC	unplasticised polyvinyl chloride
SEM	Scanning Electron Microscope
WAA	Water Authority Association
WP	Welding Pressure

CHAPTER 1 - INTRODUCTION

High density polyethylene, HDPE, pressure pipe systems have been available since the mid 1950's and over the last decade the usage has increased dramatically. In Europe, between 1973 and 1984 the consumption (1,2) of medium density polyethylene, MDPE and HDPE for pipe applications rose from about 30,000 to 132,000 tonnes, an increase of 340 per cent. Both MDPE and HDPE pipe systems find application in the gas, water and chemical process industries. The main advantages which these pipe systems offer include; the economical benefits of installation, easier handling, flexiblity, outstanding chemical resistance and availablity of good jointing methods.

In all the three industrial applications an important engineering aspect of the pipe is its long-term behaviour under constant internal pressure. The relationship between the hoop stress and lifetime is one of the essential pieces of information required by the designer. In water and gas service distribution, the pipe system is usually designed for the minimum lifetime of 50 years at 20°C, the design stresses for which are primarily selected on the basis of the results of long-term hydrostatic tests. The grades of material installed today differ from those used in the early systems; therefore there is a need to evaluate the long-term performance of new grades.

Typical stress/creep-rupture curves for MDPE pipes (3) are shown in figure 1.0. Such curves are generated by determining time to failure of pipes at different levels of constant pipe hoop stress and at a range of temperatures in order to accelerate failure and predict their long-term performance. In the case of MDPE, when a plot of logarithm hoop stress against logarithm time to failure is made, two distinctive regions are apparent with an intermediate "knee" area in between. At high stresses and short times the failure occurs by a local, large scale

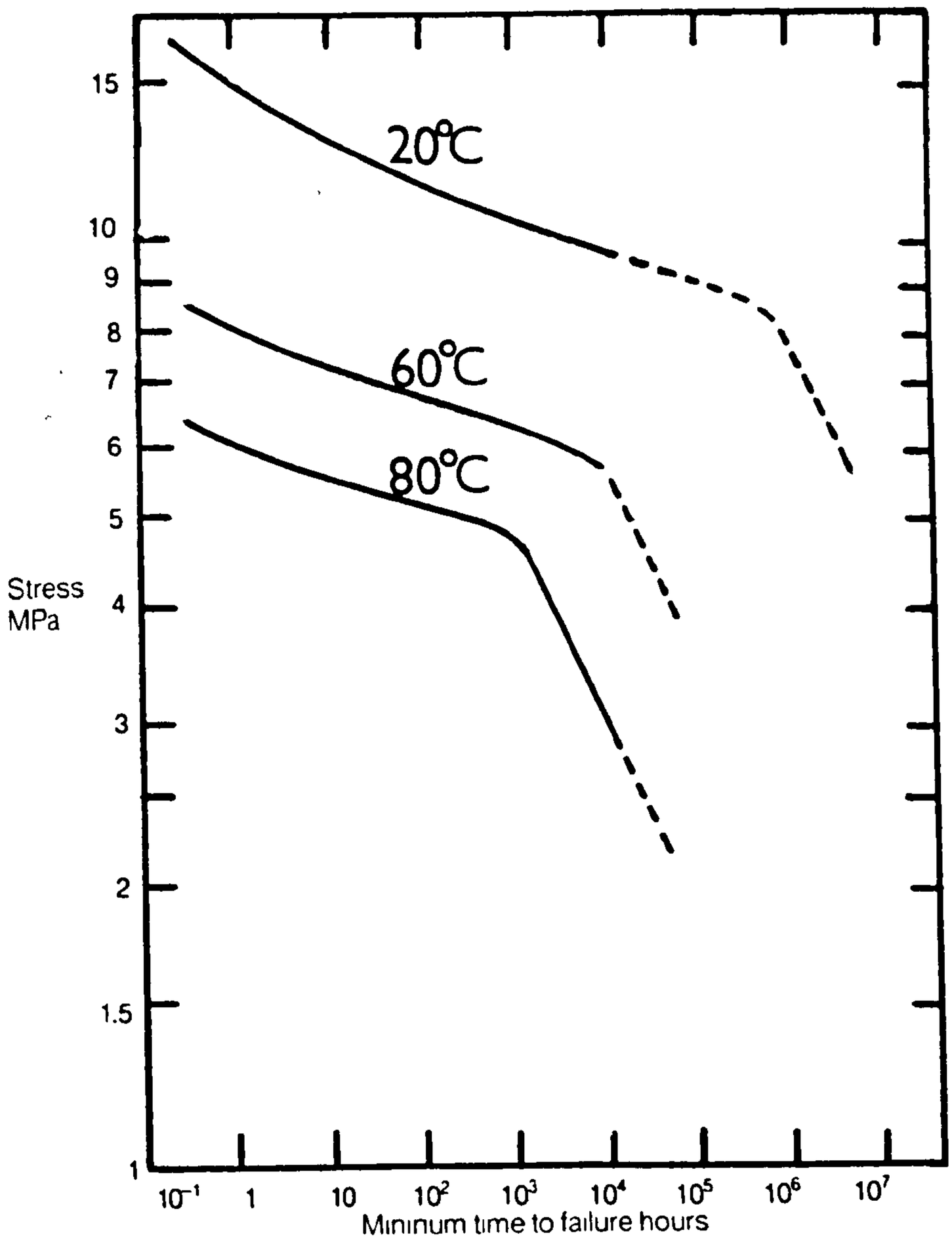

Fig. 1.0 Pipe stress-rupture performance of Rigidex PC 002-50 MDPE (After Ref. 3)

deformation which is clearly visible; this failure mode is referred to as ductile failure. However at lower stresses and longer times the failure occurs by a slit mechanism in which no visible large scale deformation is apparent; this mode of failure is referred to as brittle. In the knee region both the ductile and brittle modes of failure are observed.

There are various methods (4-9) for predicting the lifetime of MDPE/HDPE pipe based on emprical relationships between the hoop stress and time to failure which have been applied successfully over the past 20 years. The commmon feature of these methods is that the predicted design stress for 50 years lifetime is based on an extrapolation of the experimental data. For example in the North American Method described in ASTM D2837 (5), the design stress is evaluated from an extrapolation of the linear region representing the ductile mode of failure whereas the European Graphical Method (4) evaluates the design stress on the extrapolation through the point at which the knee occurs. A safety factor of 1.3 or 2 is normally incorporated in the design stress as a good practice. Typically some of the grades of MDPE/HDPE pipe are characterised by a design stress of $5MNm^{-2}$. Recently, the fracture mechanics concept has been utlised in predicting the lifetime of MDPE/HDPE pipe (24-26) and statistical approaches to predicting the lifetime of pipes have also been examined (32-33). However none of these methods have been applied for the prediction of joints and fittings as extensively as the prediction of pipe failure.

The integrity of pressure pipeline systems depends not only on the extruded pipe but also on the components in the system, namely joints (butt fusion welds, socket fusion and electrofusion in the case of MDPE/HDPE pipe systems) and fittings (90° bend, 90° equal tees, etc). The difference in stress-rupture performance of the extruded pipe and the components in the pipe system are recognised and accepted by the plastic pipe industry and major users of these systems. Demanding users of MDPE/HDPE pipe systems take account of these

differences in stress-rupture lifetime by mainly increasing the safety factor when indentifying the operating conditions. Clearly then, there is a need to assess the long-term performance of joints in order to determine the design stress which is not under or grossly over-estimated unneccessarly. In the case of butt fusion welds, various studies into the stress-rupture performance of properly made butt fusion welds (49,56,83,84,87,88) and butt fusion welds made under limited (72,73) and a wide range (61) of welding conditions have found the strength of a butt fusion weld can equal or exceed the minimum specified stress-rupture time for unwelded pipe.

In the field, deviation from the optimum welding conditions may occur due to prevailing weather conditions and in addition there is also a potential danger of butt fusion welds having misalignment, that is, creating a step at the weld which can result from any one or combination of; pipe wall thickness and outside diameter being at extremes of tolerance range, ovality, damaged pipe ends and carelessness. Geometrical defects such as the misalignment of the butt welds have been acknowledged (38,47-51,88,106) and its consequence on down rating the performance has been recognised. However, no systematic studies into this important problem, which may well result in field failures, has been undertaken. This is one of the main aspects of the project - the evaluation of misaligned butt fusion welds in the new grade of MDPE.

In a water distribution system, the water pressure will normally be varying. Such variation will occur as a result of consumption as well as through the manipulation of pumps and valves (104,105). Pressure surges caused by the latter effect can lead to fatigue of the material. Therefore it would be pertinent to test pipe systems under fluctuating pressure rather than constant pressure. A good number of research programmes have been devoted to the study of the fatigue behaviour of uPVC pipe grade material (97-99), uPVC pipe (100-103) and fittings (93-96) but the same is not true of MDPE/HDPE pipe systems. Of

those limited fatigue studies carried out on MDPE/HDPE pipe system (107-109), butt welds (107-109), and fittings (107-109) have been identified as a source of weakness.

Objectives

The prediction of the service performance of thermoplastics pipeline systems is required in order to install systems with confidence. To assess performance by room temperature short term testing will not provide the necessary information for such prediction. However, the method of elevated temperature testing, which involves pressure testing of pipes at a range of temperatures (80,60 and 40°C) and extrapolating the data to service conditions offers a means of assessing the long-term performance of pipe systems. This method has been used successfully over the last twenty years and has assisted in developing the better grades of MDPE/HDPE pipes. Pressure testing of pipes at 80°C provides guidelines to the relative long-term lifetime of the different grades of polyethylenes. The work presented in the thesis forms a part of the major on-going programme at Brunel University aimed at evaluating the long-term performance of MDPE/HDPE pipe systems, which includes identifying the performance of fittings, joints, materials and processing variables under flucatuating and constant internal pressure at 80°C in a water environment. The primary objective of the current project is to provide basic design information relating to the strength of butt fusion welds that will enable confident use of these MDPE pipe systems.

The butt fusion weld is one of the typical jointing techniques used with MDPE/HDPE pipes and the only technique available for jointing large diameter pipes. One of the problems associated with the use of the butt fusion welding techniques is that it may introduce misalignment in the joint which would result in premature failure in service. To what extent the systems performance is reduced by the presence of axially misaligned butt welds is of concern. To elucidate this problem the

relationship between the axial misalignment of the butt weld and lifetime is examined with thoroughness under fatigue and stress-rupture conditions at 80°C in a water environment for three different diameters of MDPE pipes in order to provide guidelines for specification. The stress levels chosen for the study are those inducing brittle mode of failure.

The cause of butt weld failure in the circumferential plane is not clear; it has been reported due to poor welding conditions (61,73), thermal degradation (52-54) and due to the notch at the weld bead (49,56). Therefore the second objective of the project was to examine fracture initiation sites and crack propagation paths of the failed aligned and misaligned butt welded samples in relation to the melt flow zone and weld bead in order to establish the cause of failure and also to carry out a fractography study.

Finally the project considers the influence of selected welding parameters on the fatigue performance of aligned butt welds and an investigation into the influence of elevated temperature testing techinque on the basic materials properties and its fatigue performance.

CHAPTER 2 - LITERATURE REVIEW

2.1.0 Materials

Types of Polyethylene There are three types of polyethylene available depending on the density and the method of production. Type one is the low density polyethylene, LDPE (910-925 kgm^{-3}) produced by the high pressure process, Type 2 is the medium density polyethylene, MDPE (926-940 kgm^{-3}) and Type 3 is the high density polyethylene, HDPE (941-965 kgm^{-3}). MDPE and HDPE are produced by the low pressure process utlising either metal oxide catalysts (the Philips process) or the aluminium alkyl or similar material (the Ziegler process) (110). With respect to pipe application, LDPE is normally used for low pressure pipe system and is not of concern here. MDPE and HDPE are usually used for the higher pressure pipe systems (up to 12 bar gauge) and are of importance with regards to the current project.

For any material in general there is triangular inter-ralationship between structure, processing and properties as shown below:

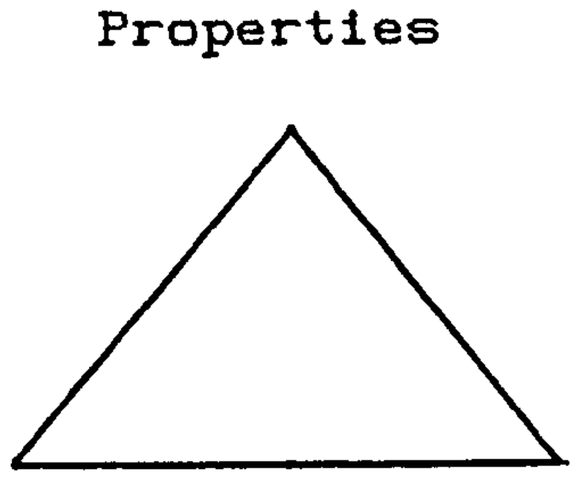

Polyethylene is no exception to this rule. In the following section a brief review of how the molecular structure, micro-structure and processing influences the properties in general, but in particular the effect on mechanical properties is considered.

2.1.1 Structure of Polyethylene

(i) Molecular structure Polyethylene is essentially a long chain aliphatic hydrocarbon of the type:

$$-CH_2-CH_2-CH_2-CH_2-$$

In general the difference in properties of various types of polyethylene arises in the main due to the following (110)

(a) variation in the degree of short chain and long chain branching in the polymer.

(b) variation in the average molecular weight.

(c) variation in the molecular weight distribution.

(ii) Chain Branching The presence of branching interferes with the ease of crystallisation; thus, the long chain branching produced in polymers made by the high pressure processes have the lowest density (since close packing due to crystallisation is reduced) whereas the polymer produced from Phillips or Ziegler process have a controlled amount of short chain branching (the molecules are able to pack relatively closely) and therefore higher density. In the Phillips process (110), comonomers such as propylene and but-1-ene are used to produce a controlled degree of short chain branching and some retardation in the growth of large crystal structure. Polyethylene produced in this way has better creep, environmental stress cracking and thermal cracking resistance than the corresponding homopolymer. Degree of crystallinty and the density of a particular grade of polyethylene have an important bearing on the properties of the polymer as discussed in section 3.1.2.

(iii) Molecular Weight and Molecular Weight Distribution The molecular weight of a polymer has a very important bearing on its mechanical behaviour, morphology, kinetics of crystallisation and thermodynamic properties (111). The molecular weight distribution is just as important as molecular weight since the distribution of chain lengths will also effect the polymer morphology, processing and properties.

There are various measures of average molecular weight; two of the most commonly used to characterise polyethylene and other polymers are the number average molecular weight, Mn and the weight average molecular weight, Mw. They are defined as:

$$Mn = \frac{\Sigma NiMi}{\Sigma Ni} \qquad (2.1)$$

and

$$Mw = \frac{\Sigma NiMi^2}{\Sigma NiMi} \qquad (2.2)$$

where Ni is number of molecules of species i of molecular mass Mi.

The general effect of molecular weight on some of the mechanical properties and thermal properties of polyethylene is clearly shown in the table 2.1 (110). Molecular weight differnces affect properties that involve large deformation such as ultimate tensile strength, elongation at break, melt viscosity and low temperature brittle point (110). Resistance to environmental stress cracking increases with increasing molecular weight. Brown and Ward (112) have found brittle fracture stress of linear polyethylene increases with increasing molecular weight and relate the improvement due to increases in the tie moelecule concentration; that is the higher the molecular weight the greater the number of points of attraction and entanglement between molecules. Muller and Gaube (113) and Gebler (114) have shown that an increase in molecular weight improves the stress-rupture performance of pipe as seen by the shift in the knee to the right in the plot of logarithm hoop stress against logarithm time to failure (see figure 2.2(a)).

Table 2.1 The general effect of molecular weight and density on some mechanical and thermal properties of polyethylene.

Property	*Test*	*Density ≃ 0·92 g/cm³ (high pressure polymers)*					*Density ≃ 0·94 g/cm³ high pressure polymers*	*Density ≃ 0·95 g/cm³ Ziegler-type polymers*			*Density ≃ 0·96 g/cm³ Phillips-type polymer*	*Density ≃ 0·98 g/cm³ poly-methylene*
Melt flow index	BS2782	0·3	2	7	20	70	0·7	0·02	0·2	2·0	1·5	—
Tensile strength (lb in⁻²)	BS903	2,200	1,800	1,500	1,300	—	3,000	3,200†	3,350†	3,350†	~4,000	~5,000
(MN/m²)		15·3	12·5	10·2	8·9	—	20·7	22·0	23·0	23·0	~27·5	~34·5
Elongation at break (%)	BS903	620	600	500	300	150	—	>800	380	20	500	~500
Izod impact strength (ft lb)	BS2782	~10	~10	~10	~10	~10	—	3·2	2·0	1·5	5·0	—
(J)		~13·5	~13·5	~13·5	~13·5	~13·5	—	4·3	2·7	2·0	6·8	—
Vicat softening point (°C)	BS2782	98	90	85	81	77	116	124	122	121	—	—
Softening temperature (°C)	BS1493	—	—	—	—	—	—	110	110	106	122	—
Crystalline melting point (°C)	—	~108	~108	~108	~108	~108	125	~130	~130	~130	~133	136
Number average molecular weight	—	48,000	32,000	28,000	24,000	20,000	—	—	—	—	—	—
CH_3 groups per 1,000 C atoms	—	20	23	28	31	33	—	5–7	5–7	5–7	<1·5	unbranched

† Yield strength

De Charentenary et al (192) examined the fatigue crack propagation, FCP behaviour of several HDPEs whose Mw varied in the range 45,000-200,000 and found FCP to be retarded for higher Mw grade of HDPE.

Polyethylenes also vary in their molecular weight distribution. The ratio of weight average molecular weight to number average molecular weight (Mw/Mn) provides a useful parameter to describe the dispersivity of molecular weight. It is generally considered, that with other structural factors constant a decrease in Mw/Mn tends to an increase in impact strength, tensile strength, toughness, softening point and resistance to environment stress cracking. There is also a pronounced influence on melt flow properties, the narrower distribution materials being less sensitive to shear rate but more liable to sharkskin effect (110).

(iv) Microstructure: Spherulities It has been well establised that the single crystal of polyethylene, large enough to be resolved in the light microscope can be grown in 0.01% xylene solution, crystallised at 70-80°C. Such a single crystal consists of thin plates or lamellae but crystallisation from the melt does not normally yield individual crystals on this scale. Under these less favourable growth conditions the region of crystallographic regularity form radially symmetric polycrystalline arrays called spherulites which show a characteristic Maltese cross pattern in cross-polarised light (111,126). They form by nucleation at different points in the sample and grow as spherical entities. The growth of the spherulites stops when impingement of adjacent spherulites occurs. Spherulites vary in size from less than one micrometer to a millimeter in diameter depending on nucleation rate and crystallisation temperature. In commercial grades of polyethylene various additives are present and the rate of cooling is rapid, and these two factors lead to a high rate of nucleation and there may not be characteristic

spherulitic structure but some other fine morphological features.

Spherulites consists of numerous crystals radiating from a central nucleus. The typical extinction patterns seen in polarised light are due to the orientation of the crystals, within the spherulites (126). Analysis of the Maltese cross pattern has indicated that the molecules are normally aligned tangentially in spherulites. It has been shown that the b crystal axis is radial in polyethylene spherulites and the a and c crystallographic direction are tangential.

Degree of Crystallinity Melt-crystallised polyethylene can never be completely crystalline. This is because there are an enormous number of chain entanglements in the melt and it is impossible for the amount of organisation requried to form a 100% crystalline polymer to take place during crystallisation. The degree of crystallinity, χ_c is of great technological and practical importance and it is related to the specimen density, ρ and the density of the crystalline ρ_c and amorphous, ρ_a components by the following relationship (126) :

$$\chi_c = \frac{\rho_c(\rho - \rho_a)}{\rho\ (\rho_c - \rho_a)} \qquad (2.3)$$

ρ is determined using density gradient column,
ρ_c is calculated from the knowledge of the crystal structure,
ρ_a is measured directly if the polymer is obtained by rapid cooling or extrapolating technique.

The degree of crystallinity in a given grade of polyethylene has a profound effect upon its mechanical behaviour. Figure 2.1 (data of Wong reported by Young (126)) shows how the Young's modulus of a linear polyethylene increases as the crystallinity is increased through the use of different heat treatments. Brown and Ward (112) noted that the fracture stress of linear polyethylene increased with increasing cooling rate, whilst Muller and Gaube (91) have shown that stress-rupture graph of

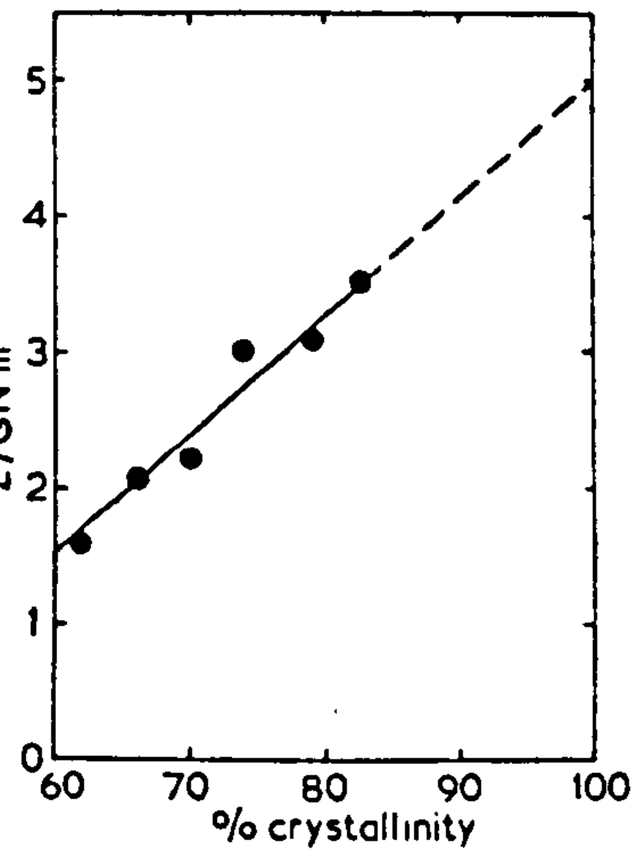

Fig. 2.1 Dependence of the modulus of polyethylene upon crystallinity (After Ref. 126)

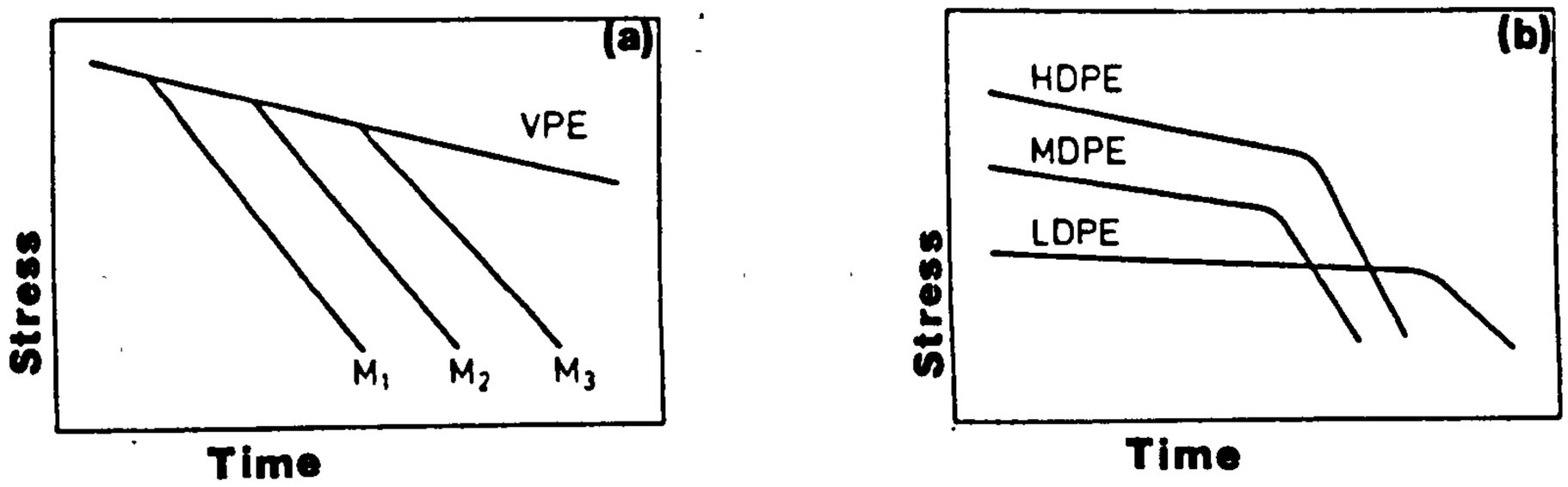

Fig. 2.2 Dependence of the stress-rupture performance of polyethylene pipe
(a) with varying average molecular weight ($M_1 < M_2 < M_3$) and
(b) with varying density (LDPE, MDPE, and HDPE) (After Ref. 91)

polyethylene shifts upwards with increasing density or differing degree of crystallinity (figure 2.2(b)) that is the stress-rupture performance improves with increasing density; LDPE>MDPE>HDPE. Crystallinity changes due to ageing of HDPE pipes at room temperature (133) and due to testing of pipes at elevated temperature has also been determined (13,135).

2.1.2 Effect of Processing on Polyethylene Pipes

(i) General Pipes are manufactured by an extrusion process. In principle the extrusion process consists of metering polymer, usually in the granular form, into a heated barrel in which a screw is rotating. The rotation of the screw causes the granules to move up the barrel where they are forced under pressure through the breaker plate and into an annular die. The resulting extruded pipe is calibrated by means of water cooled sizing die or vacuum sizing (115). To monitor and control the dimensions of the finished product various ultrasonic devices are used (116).

The nature of pipe extrusion is such that it can introduce a range of defects such as gas bubbles, foreign particles and spiderlines which reduces the stress-rupture performance of pipe depending on the size of the defect. Extrusion, combined with the cooling phase, also introduces changes in structure and residual stress through the pipe wall due to differential cooling rate (117) and as a result can affect the mechanical properties. In addition the extrusion process tends to orient molecular chains in a non-random fashion (118) thus imparting a degree of anisotropy.

(ii) Density Density profiles through the pipe wall thickness have been determined (114,117) and it is observed that the external surface has a lower density compared to the bore region. This is because the external surface has cooled rapidly and hence is expected to have relatively greater amorphous content compared to the bore region. For example Gebler (114)

found that with 190mm HDPE pipe the external surface layer had a density of 952kgm^{-3} whereas the bore layer had a density of 959 kgm^{-3}.

(iii) Residual Stress Residual stresses resulting from the temperature gradient which exists while the extrudate pipe solidifies have been measured (119-123). As mentioned above, the outer wall of the pipe solidifies first, on the inside the material is still in a molten state. As cooling progresses, the material on the inside of the pipe attempts to contract, but is prevented from doing so by the material in the outer wall that has already solidified. The result is that compressive stresses build up in the outer wall due to constrained elongation (123).

The outside machining layer removal method using bending measurement appears to be the common method for measuring residual stresses in the pipes. Typical values for 63mm MDPE pipe in the hoop direction are -3MNm^{-2} on outside and 1.5MNm^{-2} on the inside (119,122). However, the profile of residual stress through the pipe wall will depend on the thermal history, pipe diameter and wall thickness. Reinke and Potente (125) have reported compressive residual stresses on the outside and at the mid-wall in 110mm (6.3mm thick) HDPE pipe of magnitude 12Nmm^{-2} and 0.25Nmm^{-2} respectively, while a tensile residual stress of magnitude 5Nmm^{-2} exists near the bore (see figure 2.3). Excessive residual stresses in the pipe due to poor processing superimposed by external stress during transport or handling of pipes can lead to surface cracks and making pipes unusable. The changes in the residual stresses due to the testing of pipes at elevated temperature (80°C) has also been measured (135) where it was noted that residual stresses relaxed. More recently Bhatnagar and Broutman (193) investigated the effect of annealing on residual stresses in polyethylene pipes, and showed that annealing time and temperature altered the residual stress distribution in pipes and these stresses can be completely removed by annealing at temperature between 100°C and 120°C for a time of approximately one hour.

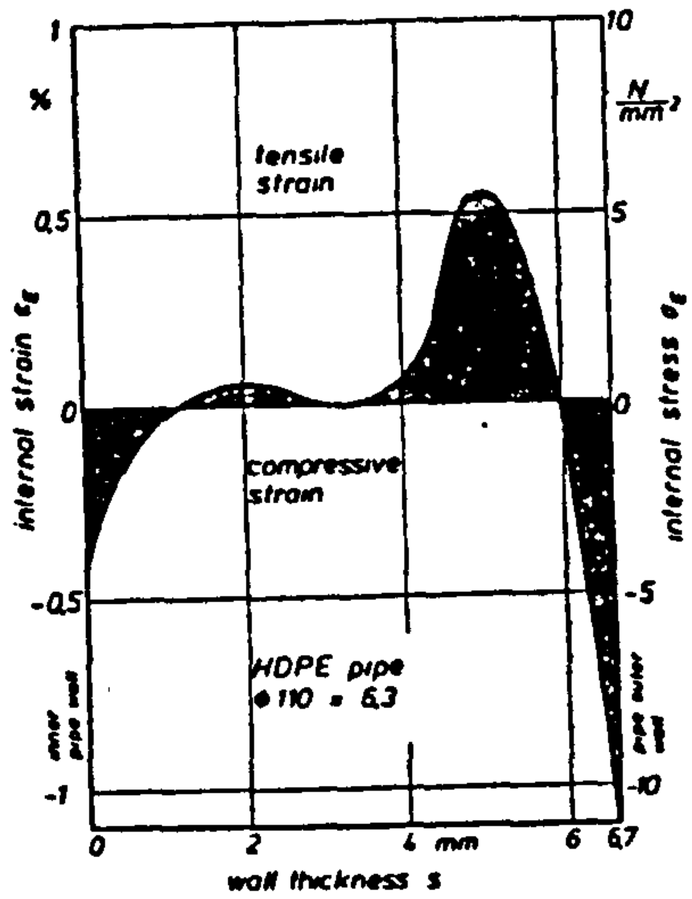

Fig. 2.3 Axial stress/strain distribution as a function of wall thickness (After Ref. 125)

(iv) Thermal Oxidation Although Marshall et al (122) found no correlation between a range of processing conditions and stress-rupture lifetime of 63mm MDPE and HDPE pipes, it is possible that for the larger outside diameter pipes (>180mm) this may not be the case. Since the rate of extrusion is slow for larger outside diameter pipes there is a greater probability of thermal oxidation of the material at the inner wall surface of pipe due to prolonged exposure to an oxygen contaning atmosphere at high temperature. Muller and Gaube (113) state that it has been proved that processing under unfavourable conditions can lead to considerable oxidation damage on the internal surface of an HDPE pipe which results in a shorter effective lifespan. This is true even in the case where the damage layer on the inside of the pipe is only very thin (100 micrometers). Gedde et al (127-130) report the thickness of the oxidised layer in larger outside diameter HDPE pipes (200-1000mm) to be typically about 0.1-0.2 mm and they go onto mention that the strength of an oxidised pipe is in most cases significantly lower than the strength of a non-oxidised pipe.

2.1.3 Mechanical and Other Properties of Polyethylene

Both the short term and the long term mechanical properties of polyethylene are very dependent on the molecular weight and degree of branching of the polymer as was indicated in section 2.1.1. As with other polymers the short-term properties are also dependent on the rate of testing, the temperature of test, the method of specimen preparation, the size and shape of the specimen and the conditioning of samples before testing. Table 2.1 (after Brydson(110)) clearly shows the general effect of molecular weight and density on some of the short term mechanical and thermal properties of polyethylene, but it should be remembered that under different test conditions different results may be obtained. In general, increasing the density or testing rate or decreasing temperature causes an increase in modulus and less ductile behaviour.

MDPE and HDPE pressure pipe system find application in the water and gas distribution and in the chemical industrial, because of the following properties it possesses:-

- economics of installed cost
- light weight (easy to transport)
- does not crack or shatter on impact
- high elongation at 0°C
- low friction losses
- outstanding resistance to chemical and soil
- does not impart toxic ingredients to water and most foodstuff
- maximum operating temperature 40-60°C
- jointing method available (insert fitting, heat fusion and variety of mechanical joints)

The specific properties of the main grade of MDPE used in this project are given in table 3.2 as supplied by the raw material manufacture.

2.1.4 Additives

Although polyethylene can be, and indeed often is used without additives a number may be blended into the polymer for various reasons (110). The additives normally present in the polyethylene pipe material are considered here.

(i) Stabilsers In general, stabilsers are used to reduce the adverse effects due to heat, sunlight and ozone. Antioxidants such as 4 aminophenol N-sterate, 4,4'-thiodi-(6-terbutyl-m-cresol) and 1,1,3-tri-(5-terbutyl-4-hydroxy-2-methylphenyl)butane (see BS3284) of the order of 0.3% by mass are added to provide protection against degradation during processing. Ideally, the antioxidant used should not show any tendency to bloom, bleed and discolour.

(ii) Carbon Black The weathering properties of polyethylene are improved by the incorparation of carbon blacks. Maximum

protection is observed using blacks with average particle size 0.010-0.025μm and a content of 2.5 ± 0.5% by mass.

(iii) Colouring Material Pipe material in the U.K. are colour coded, for the pressure pipe application using the following code: Yellow for Gas, Blue for potable water, Black for sewers/chemical. The principal requirements of pigments used are that these should have a high covering power-cost ratio and that it should withstand processing and service conditions. Special care is taken in the selection of pigments to ensure that pigment does not catalyse oxidation as inorganic pigments based on cobalt, cadium and manganese are known to produce this effect (110).

2.2.0 Butt Fusion Welds in MDPE/HDPE Pipes

Introduction A brief mention of the technique used in general for joining pipes is mentioned first in order to place butt fusion welding into its proper perspective. Next, the butt welding procedure is scrutinised; this is followed by a review of the theroetical nature of the fusion process which is largely the work of Potente. The studies into the microstructure of butt fusion welds are reviewed and more imortantly determination of weld quality / strength is examined extensively. The cause of misaligned butt welds is explained and its consequences on the long-term strength considered. Finally the nature in which butt welds fail is also considered.

2.2.1 Jointing Of Plastics Pipes

In general, there are four principal methods of jointing plastics pipes to one another and to fittings:

(i) heat fusion technique (used principally for polyethylene and polypropylene),

(ii) solvent cement jointing (used for uPVC),

(iii) elastomeric seal (used for uPVC) and

(iv) mechanical (can be used in any plastic pipes).

The selection of jointing method is dependent upon many factors, such as:-

- materials to be joined
- cost
- jointing time
- jointing performance
- jointing condition
- jointing equipment
- appearance of joint

For polyethylene pipeline systems the most common technique used for jointing is heat fusion. Qualitative description of the heat fusion method are available in a number of books (35-38) and standards (39,40). The basic principle of the heat fusion technique is to form sufficient melt to flow and intermix across the joint so as to produce a joint comparable in strength with that of the parent components. Within the heat fusion technique there are mainly two types of jointing method; socket fusion and butt fusion. A third technique of jointing polyethylene pipe, which is gaining acceptence is electrofusion welding, used for pipes outside diameters up to 180mm.

Socket Fusion This method is used to extend straight pipelines or introduce special purpose fittings (e.g. bends, tees) for pipes outside diameters up to 125mm. In principle a hot shaped tool is used to heat the inside bore of the fitting and outside surface of the pipe. The heating tool is then removed and the pipe introduced into the fitting and held in position until the joint has cooled.

The long term performance of the socket fusion joint is usually inferior to that of the butt fusion joint and failure normally initiates from the notch at the internal fusion bead which constitutes a stress concentration and leads to stress cracking under bending and pressure load.

2.2.2 Butt Fusion Welding

The butt fusion welding procedure is the most popular technique and the only technique of jointing large outside diameter (>180mm) polyethylene pipe as the welds usually have a similar strength to the original pipe and its performance is better than socket fusion.

In butt fusion welding the pipes are aligned and secured in a robust machine and after the pipe ends have been faced parallel to one another the welding procedure is as follows:

(i) A polytetrafluroethylene coated heater plate which is thermostatically maintained at a given temperature, T_H (usually 205±5°C for MDPE), is inserted between the pipe ends which are then brought up against the plate for a certain time, t_H. An initial welding pressure, P_H is used to melt any asperties so that subsequently heating occurs equally around the faces. This is called the Heating Up period, t_H.

(ii) The pressure is then reduced to zero to prevent melt from being extruded out between the plate and the unmelted part of the pipe. The pipe ends are left touching the heater plate for a certain time. This is called the Heat Soak Time, t_{HS}.

(iii) After a sufficient amount of melt has been formed, the pipes are withdrawn from the plate which is then quickly removed. The period between the withdrawal and the butting of the pipe is called the Removal Time, t_r.

(iv) The pipes are then butted, t_f and held under pressure, P_f for a certain time, t_c until the weld has cooled.

The complete list of variables which are needed to describe butt welding comprehensively are; T_H, t_H, P_H, t_{HS}, t_r, P_f, t_f, and t_c. The procedure is shown schematically in figure 2.4.

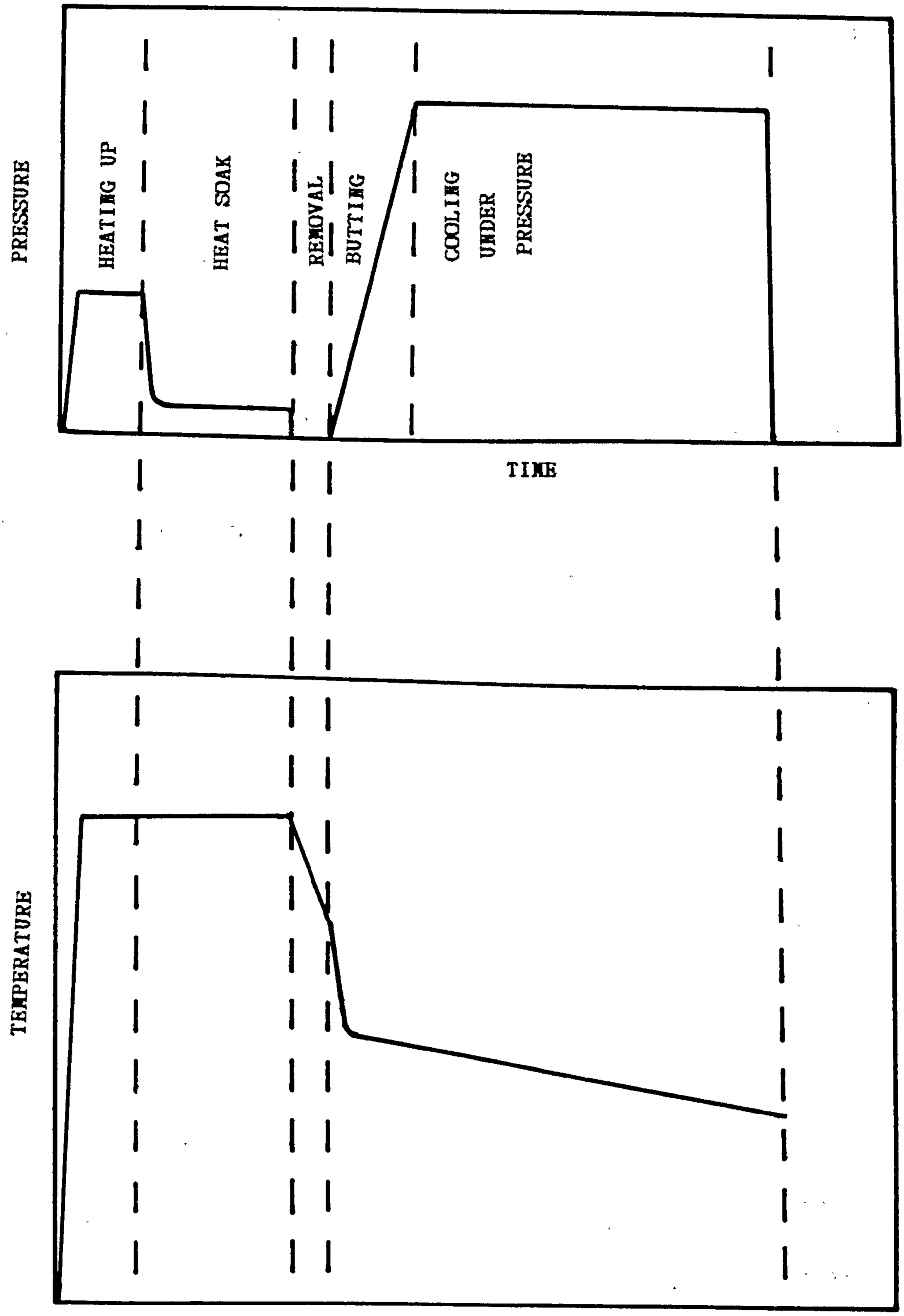

Fig. 2.4 Schematic pressure and temperature profile as a function of time during the butt fusion welding process.

The most critical aspects of the method are the melt temperature and sufficient melt formation (41-46,61,62) which depends primarily on heater plate temperature and heat soak time respectively, welding pressure (41-47,61,62) to a certain extent, degreasing of the pipe ends and the alignment of pipe (47-51). Weakness in the butt fusion weld may arise due to any one or any combination of following:-

(i) Incomplete adhesion giving rise to cold fusion may arise because of insufficent heating or welding temperature being too low (due to chilling) or heating time being too short or insufficient pressure (41-47,61,62).

(ii) Thermal degradation may result because of excessive heating or too high a heater plate temperature (52-54).

(iii) Void formation may result due to entrapment of air or evolved degradation product or due to contraction on cooling (52-54).

(iv) Narrow or thin welds due to too high a welding pressure (41-46,61,62).

(v) Geometrical defects due to misalingnment / mis-match of the pipe wall, that is a misaligned butt weld (47-51).

2.2.3 Theory of Butt Fusion Welding

Potente (63) after considering the theoretical mechanism of the diffusion theory (64) and viscoelastic contact theory (65-70) to explain the adhesion of polymer, mathematically describes the welding process in terms of flow speed of the melt. Assuming that the butt weld strength, σ depends on three parameters; diffusion (σ_D), relaxation process (σ_R), and a flow speed (σ_{fl}) that is:

$$\sigma = \sigma_D + \sigma_R + \sigma_{fl} \qquad (2.4)$$

then, further making the assumption that flow speed has the dominant effect on the butt weld strength, so as a first approximation

$$\sigma \simeq \sigma_{f1} \simeq v_{f1} \qquad (2.5)$$

the weld strength now is solely dependent on the flow speed, i.e. one only needs to optimise the flow speed, v_{f1} in order to obtain high weld strength since all the welding parameters are contained in the flow speed.

By considering the welding process to involve two distinct time phases, the Heating phase and Joining phase, the flow speed was derived. It was shown that the Heating phase can be represented by:

$$\frac{T_{f1} - T_a}{T_h - T_a} = \text{erfc}\ \frac{L_o}{2\sqrt{at_E}} \qquad (2.6)$$

where T_a = ambient temperature

T_h = surface temperature of the heater plate

T_{f1} = flow temperature (melt temperature)

L_o = thickness of melted zone

t_E = total heating time

a = thermal diffusivity

Then let $$A = \frac{T_{f1} - T_a}{T_h - T_a} \qquad (2.7)$$

and let $$B = \frac{L_o}{2\sqrt{at_E}} \qquad (2.8)$$

$$\therefore \quad L_o = 2B\sqrt{at_E}$$

For the joining process considering the speed field (70) as shown in figure 2.5(b), the average speed to be a fuction of heat history i.e. melted zone and welding pressure P_f

$$V_{m2} = \frac{8\ P_f L_o^2}{\pi\ n_m t} \qquad (2.9)$$

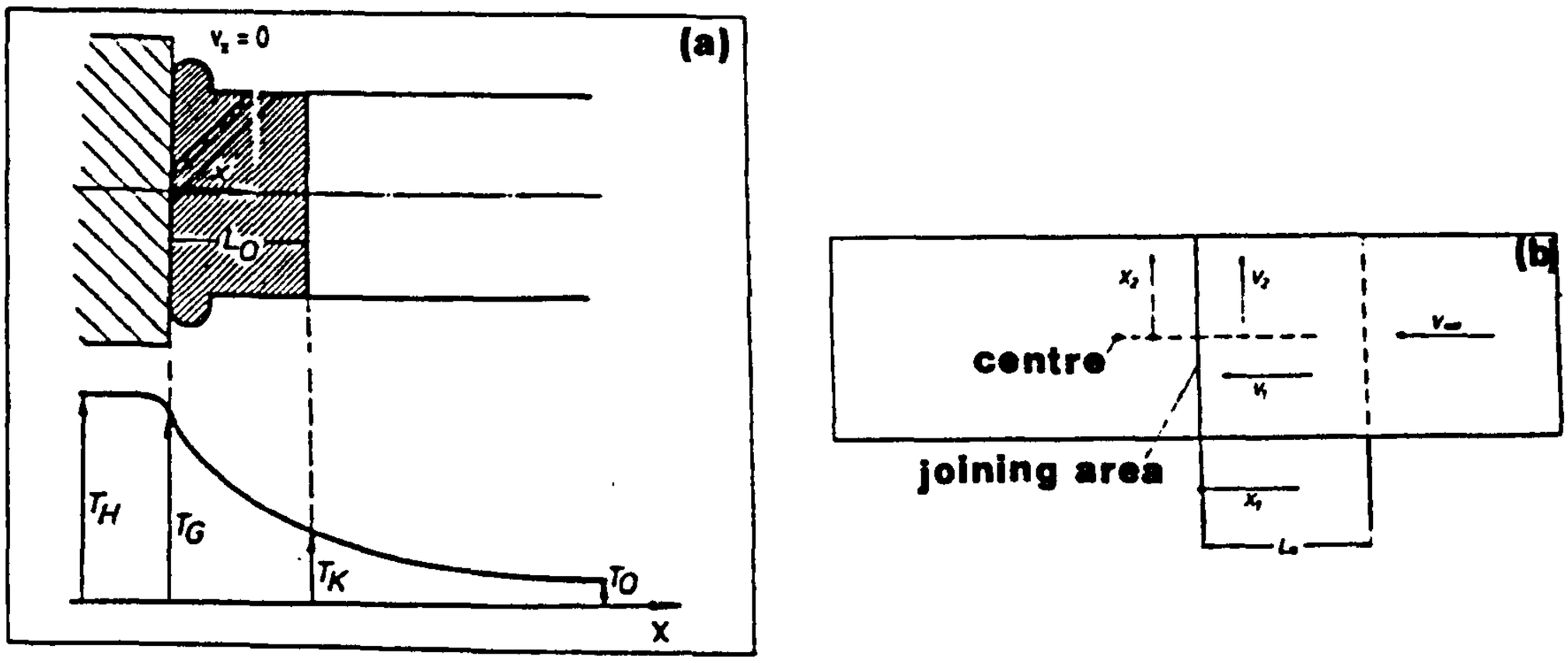

Fig. 2.5(a) Melt layer thickness Lo after the heating process.
(b) Sketch showing principle of speed areas. (After Ref 63)

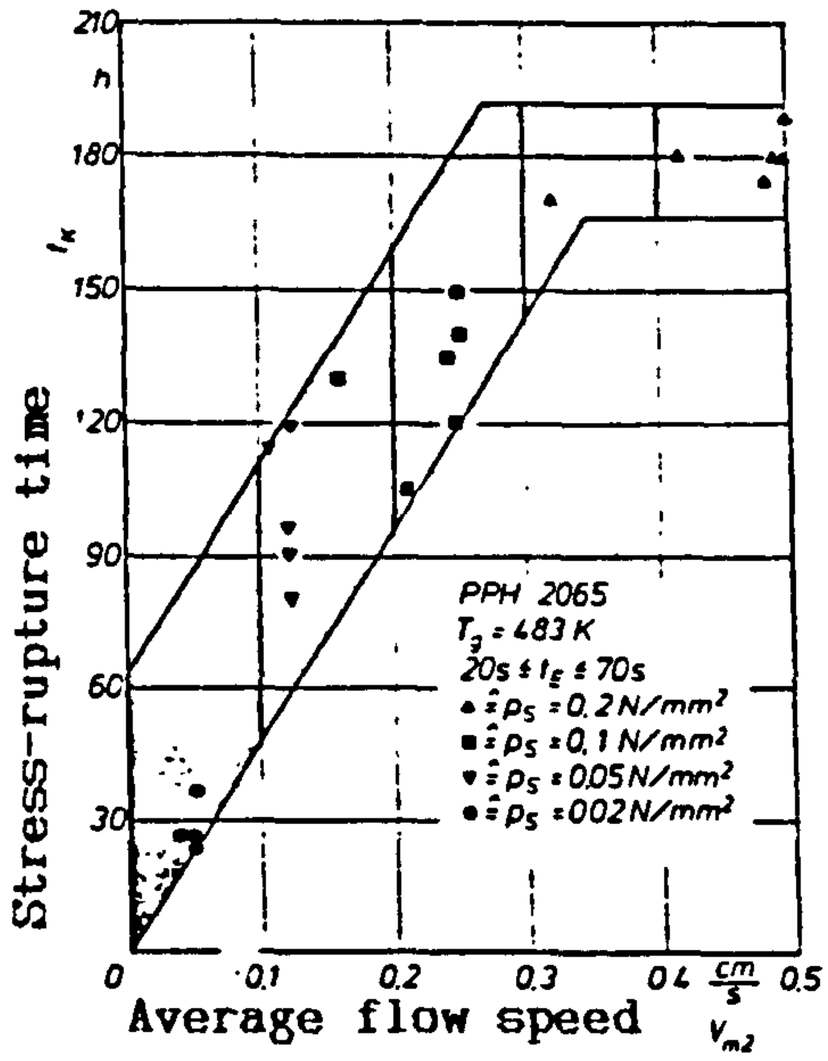

Fig. 2.6 Stress-rupture performance dependence on flow speed for polypropylene at different welding conditions. (After Ref. 63)

where V_{m2} as defined in figure 2.5(b)

n_m = apparent viscosity averaged over the cross-section

t = wall thickness

on subsituting for L_o the flow speed is

$$V_{m2} = \frac{32\ a\ B^2 P_r t_E}{\pi\ n_m\ t} \qquad (2.10)$$

Note that in the equation 2.10 all the welding parameters are combined.

To prove the equation 2.5 is valid a plot of stress rupture lifetime against the average flow speed for polypropylene butt welds was made as shown in figure 2.6 and a linear dependence was found as predicted by the equation. Potente goes onto state that a minimum flow speed can be defined which when exceeded, does no longer improve the weld strength, i.e. the optimum of the weld strength lies above this flow speed. It is also expected at the limiting flow speed, failure will no longer occur in the weld but begins in the basic material or emanates from especially stress concentration, the shearing zone between the melt and solid material or the notch between the bead and the basic material.

Brinken (71), like Potente reviews the diffusion theory (64) and viscoelastic contanct theory (65-70) and in addition considers two other theories; adhesion theory (76) and flow process theory (63). Assuming the validity of all these theories, Brinken established a set of criteria for the compatibility of various polyethylene types. Brinken declares that for the butt fusion technique it is necessary that the MFI of pipes to be jointed do not differ too much from each other and in theory material with greater difference in MFI value could be jointed by using different heating up times.

Whilst Malguarnera and Earles (45) seem to favour the diffusion theory, they believe the strength of the joint is directly due

to diffusion of molecular segments from one pipe end to the other. This in turn is strongly effected by the temperature and time of the joining operation. Regions of insufficient fusion, "cold joint" are a consequence of insufficient temperature and time during joining or too much pressure which consequently leaves only cool material to form the weld.

2.2.4 Microstructure of Butt Fusion Welds

The microstructure study of butt fusion welds has been carried out by a number of research investigators (41-47,57-60). Menges and Zohren (59) using the transmitted light and reflected light microscopy techniques characterised the microstructural features and identified five zones in a polyethylene butt weld. Bukin (57) also carried out optical examinations of sections from the weld in 32mm pipe in transmitted and reflected light and in addition investigated the fine structure by taking carbon replicas from the fractured surface of the specimen cooled in liquid nitrogen. Unlike any of the research workers who studied microstructure of butt welds in MDPE/HDPE pipe, Bukin (57) reports small spherulitic structural formation in the welding plane. The microstructures of the different zones in welds was found to differ greatly; it also differed from the microstructures of the surface away from the weld. The width of the welded zone was stated to be ≃100 μm and in the heat affected zone, HAZ (1.5-2mm from the weld) a quite well defined spherulitic structure was observed and it was suggested that heterogenity in structure near the weld may affect the strength of the welded joint.

Barber and Atkinson (41,42) and DeCourcy and Atkinson (43,44) observed the microstructural features in the microtomed section of polyethylene butt welds using the combined techniques of transmission optical microscopy and chromic acid etching of butt welded section and also examined the etched surface in SEM. The microstructures were explained on the basis of temperature

gradients measured in the region of the welds and the flow of molten material during welding. The etched surface of the butt weld exhibited five different zones, a similar observation to Menges and Zohren (59). These five zones were identified because of the differential attack by the chromic acid within the small fused region. The differential attack was explained by Barber and Atkinson (41-42) in terms of amorphous or low molecular weight fraction being attacked first leaving the crystalline material behind or because of a crystalline structure which is suspectible to chromic acid. They suggested that there are columnar crystals in zone 3 and long-term weakness may result because of the columnar structure separating at their boundaries. However, the later work of DeCourcy and Atkinson (43,44) suggests that zone 3 represents an area of molecular orientation in the welds and it is this fact which determines the extent of the etching in chromic acid rather then any differences in crystal structure. The latest view according to DeCourcy and Atkinson (44) is that a butt fusion weld with its inevitable molecular orientation would be more susceptible to cracking due to external loading or environment effects than the rest of the pipe.

Barton (60,61) and Cherry (61) applied the same techniques as Barber and Atkinson to study morphological features of butt welds in HDPE pipe. They also considered alternative etching methods and found etching in toluene vapour for 15 seconds to support the observation made under the chromic acid etch. In their opinion the degree of attack by the etchant depends on the angle the flow lines make with the boundary. The degree of flow or deformation of the melt was detected in the microtomed section of the weld taken between crossed polarisers. Barton and Cherry (61) believe that the contrast between the weld and the HAZ is due to the differences in orientation of the material. However neither Atkinson et al (41-44) nor Barton and Cherry (60,61) carried out an X-ray examination of the melt flow zone to confirm that there is preferred crystalline orientation in the MFZ (that is in the fused area).

In order to demonstrate the effects of welding conditions upon the melt flow zone, Bucknall et al (46) undertook an elegant experiment involving butt welding of compression moulded specimens fabricated from alternate sheets of black and white pigmented polypropylene. They discovered that at a low displacement, the amount of flow was small, trapped air remained in the weld and the weld bead was small. At the highest displacements the maximum flow had occurred and the weld bead was large.

This section of the literature review is concluded by recording that the microstructural studies have been carried out with the view that microstructure may have an effect on the strength of the joint. In these studies, microstructure was characterisied with varied success. However in none of the studies was microstructure correlated to long-term strength.

2.2.5 Butt Fusion Weld Quality and Testing

(i) Non-Destructive Testing (NDT) Determining whether a particular heat-fused joint is of satisfactory quality is a difficult problem. Non-Destructive and Destructive Testing Techniques are reviewed in this section.

(a) Visual Inspection A visual inspection of the external bead can indicate joint quality but is no guarantee (35-38,41,45,47). The bead should be completely uniform around the circumference and equal amounts formed from each pipe end. Unevenness is usually caused by poor joint preparation. This technique is limited to detecting those welds which show surface defects such as insufficent melting as evidenced by too small a melt bead, discoloured material due to overheating or surface cracks and flaws due to contamination or mechanical damage. Evaluation by this means is highly dependent on the experience and training of the inspector (35-38) and it is possible to produce welds which look perfectly satisfactory but which fracture easily in a brittle fashion (35-38,41,45,47).

(b) Radiographic and Ultrasonic Examination Two of the most important non-destructive testing methods for polyethylene butt fusion welds are radiation and ultrasonic testing which have been used with varying degrees of success (38,45,47,74).

X-ray Examination In view of the poor absorption properties of plastics, soft x-rays are employed for radiation testing. The excitation voltage varies between 30kV and 80kV depending on the thickness. Field evaluation of the fusion joint are conducted using a double wall, single image technique (47) with the x-ray set working at a maximum of 50kV. Although x-ray photographs may reveal defects such as inclusions of foreign material, voids, cracks and thereby indicating that the weld is unsatisfactory, the reverse is not always true, that is the absence of defects is no guarantee that a satisfactory weld has been made.

Ultrasonic Examination Ultrasonic examination of polyethylene butt welds is done using calibrated equipment. Transducers having a frequency of 2.5MHz and the element dimension of 7mm x 7mm are used (77). For wall thickness up to 15mm, the head of transducer is inclined at angle of 70° and for thickness greater than 15mm at angle of 65°. The principle of ultrasonic examination is based on the propagation of a high frequency sound wave through the wall thickness and measuring the intensity of the reflected wave, any defects in the wall thickness will cause the speed of the propagating and reflective wave to be altered, resulting in a deviation from normal signal. The resolving power of this method allows localisation of faults at depth of from 15 to 60mm with 1 to 3mm lateral range. The sensitivity of the test method also depends on the situation of the fault in relation to the propagation direction of sound waves. This technique is limited to detecting flaws such as cracks and voids rather than "cold" weld regions (75).

Other NDTs which have been used included spark testing technique (38) and Holographic Interferometry (78). The later technique

also enables one to measure residual stresses and strains and slight surface shifts due to loading. However, none of the NDT or visual inspection methods for polyethylene can ensure total integrity.

(ii) Destructive Testing In order to determine the optimum welding condition, to obtain information on the operatives and/or suitablity of the jointing method and for routine quality control, a test method is required which gives good differentiation and can be carried out quickly. Destructive testing is the suitable means of obtaining such information. Two types of destructive testing method are available namely the short term testing and long term testing.

(a) Short Term Testing: Tensile Test The tensile test is one of the popular tests applied to the routine evaluation of the material/weld. The sample preparation is straight forward to carry out, the test is inexpensive and results generation is not a time consuming process. In the case of a butt welded pipe, longitudinal samples are taken from the welded region such that the weld lies in the middle of the test specimen. The usual procedure is to carry out a tensile test with the weld bead left on and also with the weld bead removed. A welding factor, f, defined by equation (2.11) is then reported (41).

$$f = \frac{\text{yield strength of welded material}}{\text{yield strength of basic material}} \qquad (2.11)$$

Atkinson and coworkers (41-44) and Malguarnera and Earles (45) seem to favour the tensile test method to evaluate the optimum welding conditions. The results, reported in terms of welding factors, f showed little change in f with the welding condition ranges examined. For example the highest variation in welding factor was found to vary between .89-.95 for the welding temperature variation of 150 to 250°C; for the other grades of

polyethylene tested f was noted to be between .98-1.0 or .95-.98 when the welding temperature was varied in the similar range. Malguarnera and Earles (45) working with Drisco 6500 pipe have reported the result in terms of yield stress. A significant reduction in the yield stress of the butt welded specimen was apparent at the very low welding temperature (204°C) and at very high welding temperature (370°C) for the low heating time (5 seconds), low heating pressure (5 psi, 3.5MNm^{-2}) and low fusion pressure (20 psi, 14MNm^{-2}).

Most of the research investigators (47,49,50,56,72,73,83) do not prefer to use tensile tests for assessing optimum welding conditions of butt welds because the results obtained using this test method vary only slightly as examplified by Atkinson et al (41-44) and Malguarnera and Earles (45) work. It overestimates the weld strength (f of .95-1.0), and it only detects a very bad weld (butt welds made under poor/extreme conditions). In addition, it is well known that the mechanical properties of thermoplastic materials are time dependent; bearing in mind that pipe systems are usually designed for 50 years, the tensile test provides, at best, only a limited guide to the long-term behaviour. Furthermore, the failure obtained under a tensile test is not similar to service failures.

Finally, although Potente and Tappe (62) disapprove of the tensile test, they favour two modified short term testing procedures proposed by Herfort (79), Hessel and John (80) and Menges and co-workers (195,190). Herfort (79) proposal involves the low temperature bending test and Menges and co-workers (195,196) proposal involves the short-term tensile test to be carried with a hole notch at the butt weld and use the breaking strain rather than yield stress for the evaluation.

(b) Long-Term Testing For plastic pipes the resistance to internal water pressure is normally used as a quality control test and to predict long-term properties. Lack of time and testing capacity requires that accelerated tests (stress-rupture

test at elevated temperature) are used, the results being subsequently extrapolated to the desired requirements - an expected admissible hoop stress after fifty years under static load is the basic design criterion used in the UK (197,198). However, before examining the review on Long-Term Testing it is appropriate at this juncture to consider and introduce the stresses in pipes under internal pressure.

Stresses in Pipes Under Internal Pressure

Pipes as Thin-Walled Cylinders If a pipe is allowed to expand and extend freely and is subjected to an internal pressure, three mutually perpendicular stresses will be produced as shown in figure 2.7. Such stresses are generally termed hoop or circumferential, axial or longitudinal and radial stresses (199,200).

Hearn (199) considers that a criterion for the assumption that a pipe is a thin-walled circular cylinder is if the ratio of the wall thickness to the inside diameter of the pipe is less than 1/20. If such is the case it is possible to assume that the hoop and axial stresses remain constant through the wall thickness and that the radial stress is small enough to be neglected. (In practice its value increases from zero on the outside surface to equal the internal pressure at the inside surface of the pipe). In this approach the effects of any end fittings are considered so far removed as to be negligible.

For the above conditions the hoop stress generated in a thin-walled pipe is given by

$$\sigma_H = \frac{Pd}{2t} \qquad (2.12)$$

where σ_H is the hoop stress

d is the internal diameter

t is the wall-thickness

P is the applied internal pressure

The longitudinal or axial stress in a pipe wall produced under similar conditions is given by

$$\sigma_A = \frac{Pd}{4t} \qquad (2.13)$$

where σ_A is the axial stress. For axial stresses to apply the pipe system must have closed ends and the system be axially unconstrained. Once again the ends are considered as having no reinforcing effect on the pipe.

From these equations it is evident that

$$\sigma_H = 2\ \sigma_A \qquad (2.14)$$

Another relation for the effect of internal pressure on a thin-walled pipe is known as Barlow's formula. It is considered to be a reasonable description of circumferential stresses in pipes of most thickness ratio and is expressed as

$$\sigma_H = \frac{Pd}{2t} \qquad (2.15)$$

where σ_H, P, and t are defined as before and d is the outside diameter of the pipe.

The Nadai formula is a further variation on the hoop stress/pipe dimensions relationship and is given by

$$\sigma_H = \frac{P\ (d - t)}{2t} \qquad (2.16)$$

where all symbols have meanings prevously defined. This is the relationship which has been applied in the first instance, to all the experimental data reported in later chapters. The approach concurs with the method of obtaining hoop or comparative stresses in thermoplastics pipes used by most manufacture: and other workers in the field of internal pressure testing.

Pipes as Thick-Walled Cylinders The theoretical treatment of stresses in thin-walled cylinders under internal pressure with free ends assumes that:-

(a) The hoop stress is constant across the cylinder wall
(b) There exists no pressure gradient across the cylinder wall.

Neither assumption is valid for thick-walled pipes or cylinders and in reality the hoop stress will vary in all SDR 11 pipes (SDR - Standard Dimension Ratio is defined as the ratio of the pipe outside diameter, d to wall thickness, t). The hoop stress on the inside surface of the pipe can be greater by about 25% than the hoop stress experienced on the external surface. The expression describing this variation is developed from the Lame equation and is given by

$$[\sigma_H]_r = P\left[\frac{r_i^2}{r_o^2 - r_i^2}\right]\left[1 + \frac{r_o^2}{r^2}\right] \qquad (2.17)$$

where $[\sigma_H]_r$ is the hoop stress at radius r and r_i and r_o are the inside and outside radii of the pipe respectively.

An equation such as that above will enable the true hoop stress at any point within a pipe wall to be identified. Expressions describing the variation in axial stress, σ_A radial stress, σ_r is given by (199).

$$[\sigma_A]_r = \frac{P_1 r_i^2 - P_2 r_o^2}{r_o^2 - r_i^2} \qquad (2.18)$$

where P_1 is the inside pressure and P_2 the external pressure.

$$[\sigma_r]_r = P\left[\frac{r_i^2}{r_o^2 - r_i^2}\right]\left[\frac{r^2 - r_o^2}{r^2}\right] \qquad (2.19)$$

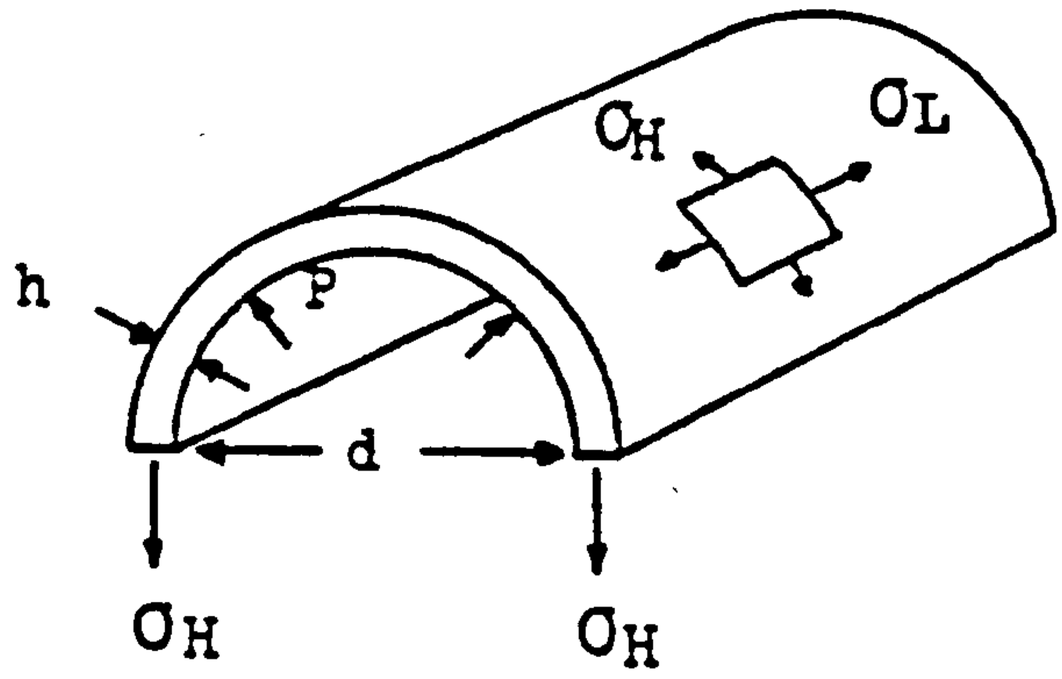

$$\sigma_H = \frac{Pd}{2h}$$

Fig. 2.7 Half of a thin cylinder subjected to internal pressure showing the hoop and longitudinal/axial stresses acting on any element in the cylinder surface. (After Ref. 199)

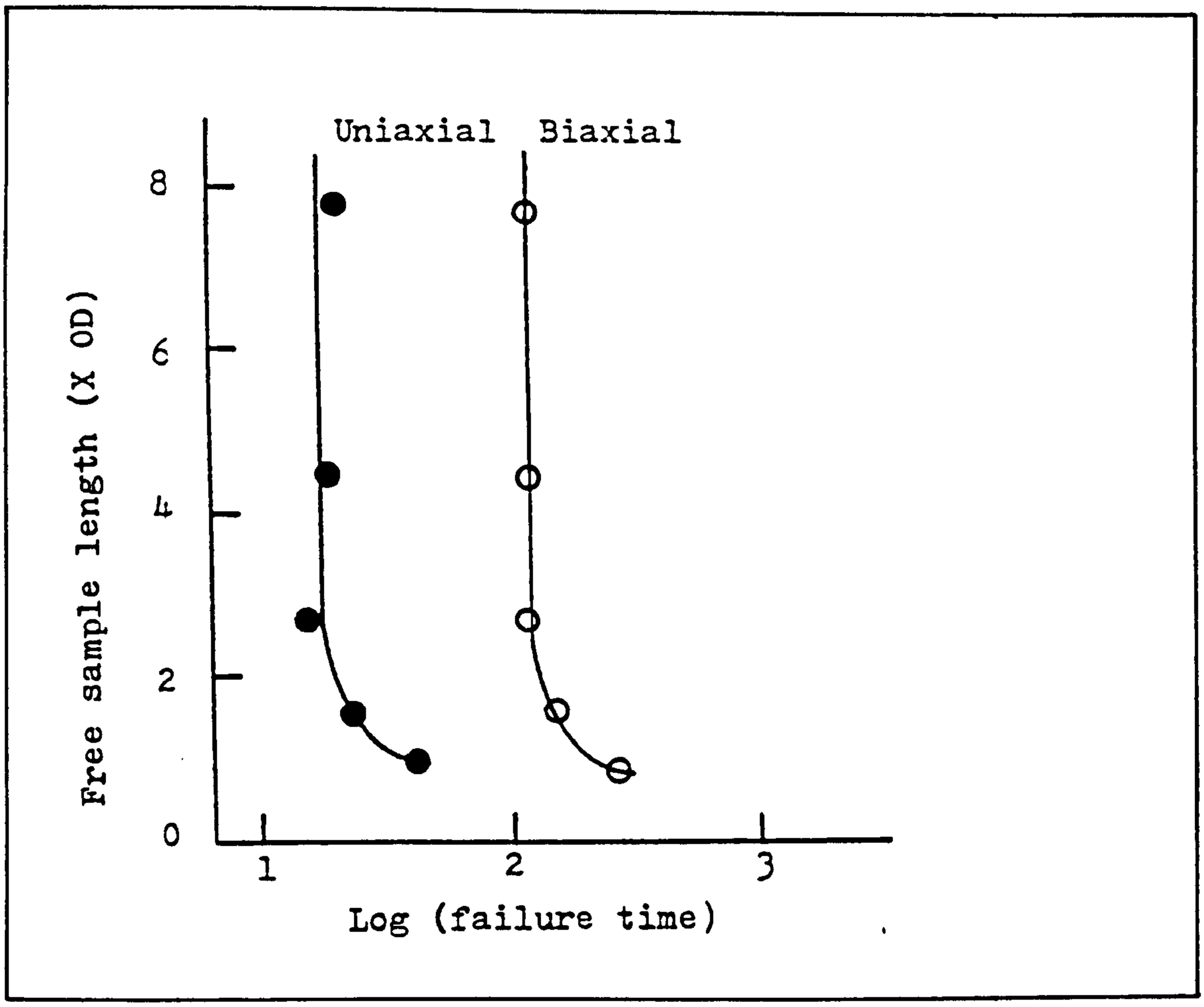

Fig. 2.8 Dependence of failure time on free sample length of uPVC pipe expressed in outside diameter units (xOD) for uniaxially and biaxially stressed pipes. Temperature 20°C; Hoop Stress 39.3 MPa, Pipe OD 110mm and wall thickness 3.3mm. (After Ref.197).

Long-Term Testing Two different types of test methods are utilised to determine the long-term properties of pipe systems; the tensile creep rupture (43,73) and the internal pressurisation of the pipe systems (49,50,56,61,72,73,83). These tests require a large initial investement in the equipment, they occupy large ammounts of space, require maintenance and results generation is rather a wearisome process compared to short-term tensile tests. However, the information obtained from the long-term testing is invaluable and of paramount importance. Both the tests are carried out at a series of elevated temperatures (typically for HDPE, at 40,60 and 80°C) and the results extrapolated to the desired requirement. The internal pressure testing of pipe systems is conducted according to relevant standards; ASTM 1598, BS 3284, BS 4728, British Gas Corporation Standard PS/PL2 and Water Authority Association Specification 4-32-(02-04).

Test parameter consistency is required for the test results to be of use, particularly temperature, pressure and specimen dimensions (197). Figure 2.8 shows the effect of the free length on a thermoplastic pipe can have on the failure times at 20°C. The diagram also indicates the variation induced by unconstrained and constrained ends (197) which can result in biaxial or uniaxial stress systems in a pressurised pipe altering the slopes and position of stress rupture curves, possibly a reflection of a craze criterion such as proposed by Sternstein and Ongchin (201) for the failure of thermoplastics under this type of stress.

Diedrich and Gaube (49) and Diedrich and Kemp (50) have shown that if tensile creep rupture of the sample taken across the welded sample is carried at 20,50 and 80°C in water, then the long-term welding factors of between .9 and 1.0 are obtained and lifetimes are ten times that of the butt welded pipe tested under constant internal pressure (stress-rupture test) which is subjected to biaxial stress ie pipe tested with no end constraint. In this respect, it is interesting to note that

Barton and Cherry (61) investigating internal pressure strength of the butt welded pipe with end constraint and without end constraint found that the pipe tested without end constraint failed earlier compared to the sample tested with end constraint. They opted for the test inducing a biaxial stress condition because failure occurred at the weld under this more aggressive test mode.

There have been a limited number of studies (82,106) where the internal pressure has been made to fluctuate (fatigue) rather than remain constant. The fatigue testing of butt welded pipe samples is resorted to because of increasing demands made on MDPE/HDPE pipe systems and increasing improvement in the performance of pipe means the stress-rupture testing takes longer to generate the results.

Finally Atkinson and DeCourcy (44) have criticised stress-rupture testing of pipe at elevated temperature on the following counts:-

(1) Predicting long-term behaviour using an elevated temperature of 80°C is dangerous because Schonefeld and Wintergerst (135) have shown that the density, internal stress and bursting strength of polyethylene pipe are all altered by being subjected to a temperature of 80°C for prolonged periods.

(2) Stress-rupture tests are lengthy and expensive and it is not usually practical to carry out sufficient tests to determine optimum welding conditions.

(3) Most stress-rupture tests are obtained with the pipe in contact with water and this may accelerate failure.

However, the above criticism can be equally argued on the following counts:-

(1) Predicting long-term behaviour by use of accelerated

testing at elevated temperatures, although not ideal, is not invalidated as long as effects due to elevated temperature testing can be identified and accounted for in the proposed failure mode (82).

(2) The expense put into the long-term testing is justified because the test condition has the advantage of simulating the service condition as the failure mode obtained under test are identical to failures which occur in service. This type of testing has been successfully used for the past 25 years to predict the service temperature performance and improve the grades of MDPE/HDPE material.

(3) Stress-rupture tests have been carried out in water and air (131), and the lifetime was not found to differ significantly.

2.2.6 Misaligned Butt Weld

Axial misalignment of the butt weld or the mis-match of the weld at the butt weld can be caused by any one or combination of following; pipe outside diameter and wall thickness lying at the extreme opposites of tolerance range, ovality, damaged pipe ends, out of aligned welding machine, carelessness, joining coiled pipes and there is also the case of jointing of pipes with different wall thickness classes. It is interesting to note that the tolerence limit for wall thickness increases with outside diameter as stated in the ISO specification (see reference 3). Thus with increasing outside diameter pipe there is a greater potential for misalignment of the butt weld. For example the outside diameter tolerance range for nominal 250mm pipe is 250.0 to 252.3 and wall thickness tolerances for SDR11 are 22.7 to 25.2, that is potentialy a misalignment of magnitude over 20% of nominal wall thickness can occur.

On the one hand the ISO tolerances for pipe dimensions are generous such that potentially axial misalignment of over 20% of

nominal wall thickness can occur in practice while on the other hand the values quoted in the literature for maximum misalignment of the butt weld varies from 5 per cent (38) to 10 per cent (47), which in practice would be unachievable if ISO specification (see reference 3) is followed. In this connection it is also interesting to note that a field survey was carried out by the author to assess the magnitude of axial misalignment occurring in practice. Figure 4.0 shows the results of the survey. For 82 per cent of the butt fusion welds examined (from 6 different sites where 90/125mm MDPE pipe was laid), the maximum axial misalignment was under 5 per cent of the nominal pipe wall thickness. However, 6 per cent of the butt fusion welds had a significant axial misalignment in the range 15-20 per cent of the nominal pipe wall thickness. The limited survey therefore indicated that gross misalignment of the butt weld can occur in the field.

Various research workers have commented on the problem of misaligned butt welds and its consequence on the reduction in the lifetime of butt welds has been recognised (38, 47-51,88,106). Sucherck (51) shows some typical geometry defects which can be introduced in the butt weld due to variations in the dimension of pipes and problem with the welding process itself - see figure 2.9. Greig (47), Albrecht (48), Diedrich et al (49,50) and Vancrombrugge (88) point out that butt welds in which the welding surfaces are not flush but staggered so that there are sharp transitions, then a displacement of the lines of forces give considerably reduced rupture times. Greig (47) believes that a step of over 10% of the pipe wall thickness is unacceptable and a step wall substantially weakens the weld joint not only through the reduction in the area fused but due to the introduction of sharp notches in the region of the bead produced during fusion.

Albrecht (48), is the only research investigator to the authors knowledge who has carried out stress-rupture tests on the pipe systems containing a wall thickness step at the butt weld

resulting from different wall thickness pipe; in this study by Albrecht the pipe axis were parallel and aligned. The test results showed that the presence of a step on the inside wall of pipe prevents the test specimen from reaching the minimum failure time of 170 hours at 80°C. However, Albrecht (48) does not report what was the magnitude of the misalignment and examination of the relationship between misalignment and lifetime was not carried out in any detail.

Reinke and Potente (125) quote Ory's work in which the increase in axial stress, σ_a and hoop stress, σ_h due to axial misalignment defined in figure 2.10(a) and due to shrinkage at the weld (due to relaxation of residual stresses) defined in figure 2.10(b) can be accounted for by the following sets of equations:-

$$\sigma_a = P\left(\frac{d - t}{4t}\right)\left(1 + \frac{3e}{t}\right) \qquad (2.20)$$

$$\sigma_h = P\left(\frac{d - t}{2t}\right)\left(1 + \frac{0.2789e}{t}\right) \qquad (2.21)$$

$$\sigma_a' = P\left(\frac{d - t}{4t}\right)\left(1 \pm 1.14\gamma\sqrt{\frac{d - 1}{t}}\right) \qquad (2.22)$$

$$\sigma_h' = P\left(\frac{d - t}{2t}\right)\left(1 \pm 0.658\gamma\sqrt{\frac{d - 1}{t}}\right) \qquad (2.23)$$

where P = applied internal pressure
d = outside diameter
t = wall thickness
e = axial displacement at the weld-see figure 2.10(a)
γ = angle of inclination at the weld-see figure 2.10(b)
σ_a' = increase in axial stress due to angular misalignment
σ_h' = increase in hoop stress due to angular misalignment

Note that in equations 2.20 to 2.23 when there are no defects, that is when e = 0 and γ = 0 the equations reverts to identifying the axial and hoop stress in plain pipe. Reinke and

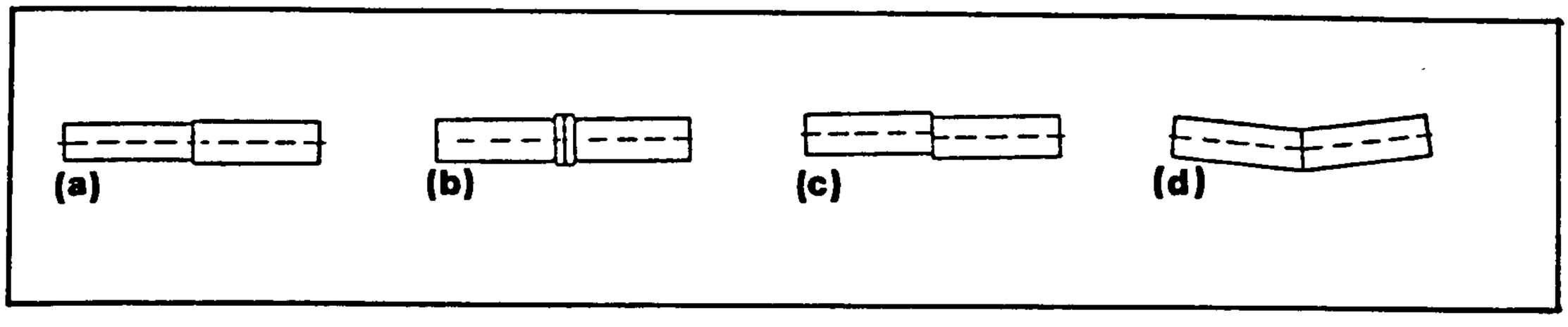

Fig. 2.9 Geometrical defects in plastic pipes butt welded ; (a) unequal diameter, (b) grooving, (c) displacement and (d) sharpe bend. (After Ref. 51)

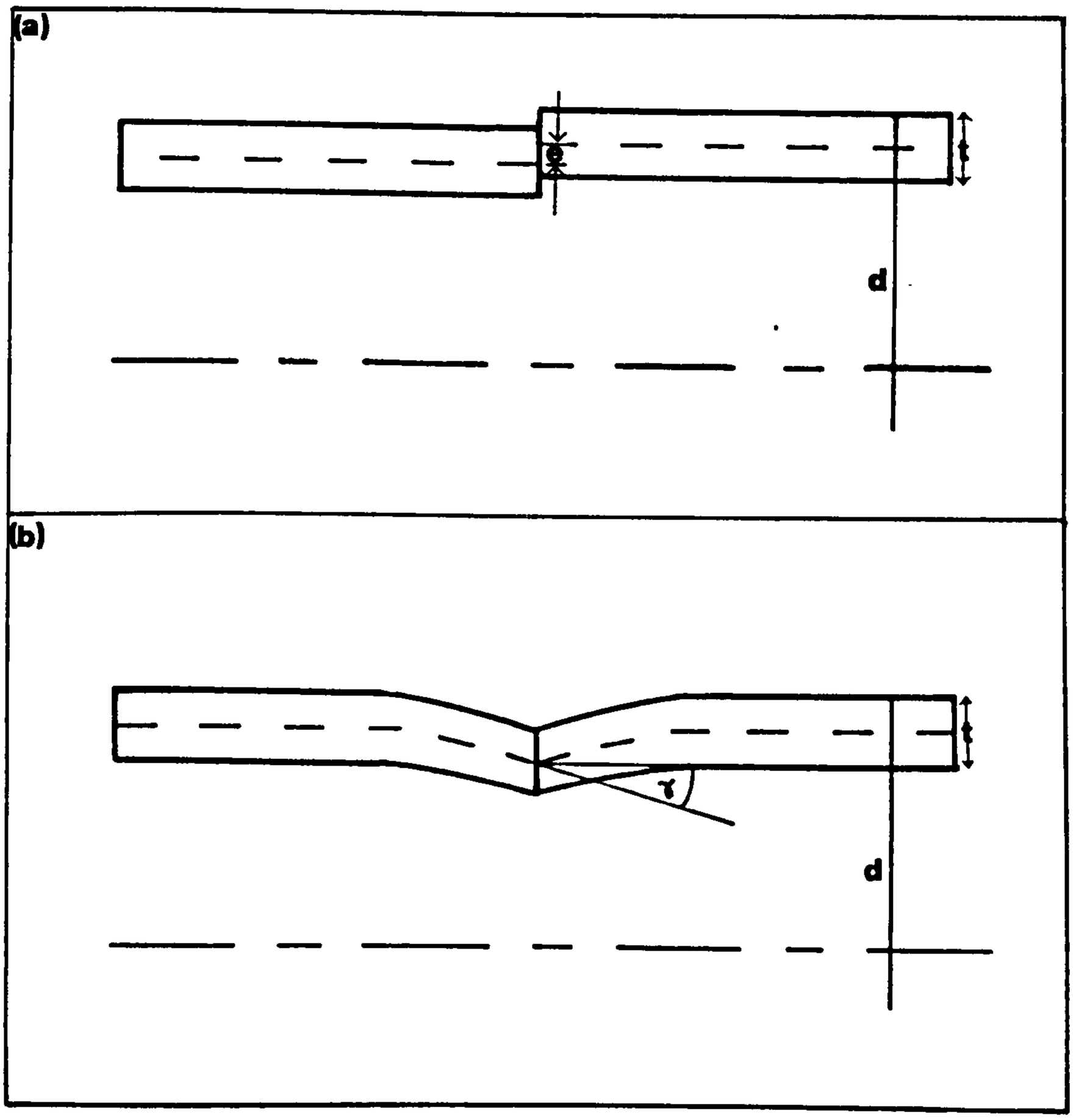

Fig. 2.10 Geometrical defects at the butt weld
(a) due to displacement of the wall and
(b) due to shrinkages (After Ref 125)

Potente (125) comment that as a rule, it is the axial stress which is responsible for the breaking of the weld seam.

It is clear from the literature review that the problem of misaligned butt welds has been recognised by the various research workers. However, no one has carried out any systematic study into the problem and the information on how misaligned butt welds influence the service lifetime of the pipe systems is scarce.

2.2.7 Butt Weld Failure

The failure of pipe (49,72,73,83,84,88,95) and axial (72,82,106) and circumferential (49,56,61,82) brittle cracking in butt welds has been reported when butt welded samples of HDPE pipe were tested under stress-rupture and fatigue conditions. Diedrich and Gaube (49), Wolters and Venema (73), Menges and Roberg (95) and Uancrombrugge (88) found that when butt fusion welds were tested under stress-rupture conditions, most of the samples did not fail at the weld but in the pipe itself. However, Diedrich and Gaube (49) did observe two other types of failure at the butt fusion weld;

(i) circumferential failure as a result of insufficient melt penetration and

(ii) circumferential failure due to a notch effect at the weld bead.

Wolters and Venema (73) tested butt fusion welds produced under a broad range of welding conditions using internal pressure tests. In these tests only pipe failures were observed, no failure occurred in the weld region. In the opinion of Wolter and Venema (73) only very bad welds would lead to premature failure in the weld zone during stress-rupture tests.

John (72), recently carried out stress-rupture tests on butt

welds in 90mm SDR11 HDPE pipe made at a low environment temperature and observed that all the samples had an axial crack in the pipe or in the butt weld and no circumferential failures were observed. In contrast to John (72), Kashkovskay and Kaigorodov (56) found only the circumferential failure due to the notch at the inner weld bead in more than 700 butt welds and socket fusion joints in five different grades of HDPE pipe of outside diameter of 100mm and 150mm under stress-rupture testing conditions. Potente et al (124) believe that in the case of faultless joints the notch between the weld bead and the pipe constitute the weakest point, whilst the other case where welding conditions have deviated, the abrupt transition from residual compression to residual tensile stress during the progress of cooling contributes towards the width of scatter of the weld seam quality value. Potente et al (124) determined axial residual stresses for a range of welding conditions and concluded that with the internal pressure test, bending stresses can occur; and the residual stresses can weaken the weld, hence they should be avoided

Zaitsev et al (52-54), have suggested that the circumferential failure of butt fusion welds is caused by the welding conditions not being observed, deviations from the optimum joint designs, the presence of internal-stresses, changes in the structure of welds, thermal degradation and bubbles of air or pores in the central zone of the weld and also near the weld bead.

In fatigue loading of butt welds in HDPE pipe, Cowley and Wylde (106) observed only the axial failure at the butt weld while Barker (82) found both axial and circumferential failure of butt welds in HDPE pipe.

2.3.0 Fatigue Behaviour Of Thermoplastics

2.3.1 Introduction

Fatigue or dynamic fatigue failure is the phenomenon of fracture of a material or structure under repeated or oscillating loading. The importance of fatigue is that under fluctuating loads materials will fail at stress levels much lower than they withstand under static loading.

The list of experimental variables which needs to be considered when designing fatigue tests is shown in the table 2.2. The objective of fatigue testing is to determine the relationship between the applied stress amplitude (or mean stress or maximum stress) and number of cycles to failure as a function of an experimental variable e.g. frequency, wave form, grade of material, a notch, an environment, etc. The results are presented in the classical fatigue curves referred to as 'S-N' or Wohler curves, a plot of logarithm stress amplitudes, S against logarithm number of cycles to failure, N. Such curves provide basic design information on the performance of the material under the experimental conditions but do not provide much information concerning the mechanism of the fatigue failure processes. They do not establish whether crack initiation or propagation is the dominant phase in the fatigue life. Therefore, to gain an insight into both the kinetics and the mechanisms of fatigue crack growth, fracture mechanics principles have, over the last decade or so, been applied. In these crack propagation studies, the objective is to ascertain the factors that control crack growth rate, da/dN which is usually examined using the stress-intensity range ΔK, (stress-intensity factor describes the stress field ahead of the crack).

There is a fairly extensive literature concerning the fatigue properties of polymeric materials; there are several excellent reviews (142-147) and the subject has been covered by the

Table 2.2 List of experimental variables which need to be considered when designing fatigue test.

1. A periodically varying stress system having a characteristic stress amplitude, σ_a [$\sigma_a = \frac{1}{2}(\sigma_{max} - \sigma_{min})$].

2. A corresponding fluctuating strain amplitude ϵ_a.

3. A mean stress level, σ_m [$\sigma_m = \frac{1}{2}(\sigma_{max} + \sigma_{min})$].

4. A mean strain, ϵ_m.

5. A stress ratio, $\sigma_{min}/\sigma_{max}$.

6. A strain ratio, $\epsilon_{min}/\epsilon_{max}$.

7. A frequency, ν_d.

8. A characteristic wave-form (sinusoidal, square, etc.).

9. The amount and internal temperature of the specimen which in general will not be the same.

10. Environmental effects and

11. The specimen geometry.

polymer fracture monograph (48-152) and comprehensively in the book by Hertzberg and Manson (151). Therefore a brief review of the two fundamental mechanism of fatigue failure in thermoplastic materials namely thermal and mechanical fatigue is considered; failure resulting from cyclic creep (due to application of positive square wave form) is also considered. These three sections mainly concern the sample in the conventional form of sheet or a rod in the unnotched and notched form and the fatigue test conducted by controlling stress amplitude, although deflection or strain controlled testing have been reported. The overview of the fatigue behaviour of thermoplastics is followed by a more specific review on the fatigue behaviour of HDPE pipe systems in which the sample is in the form of a pipe subjected to internal fluctuating pressure and important factors influencing its lifetime are considered. Then, the prediction of the fatigue lifetime is examined and finally the study on the fractography and fatigue mechanism is reviewed.

2.3.2 Thermal Fatigue Failure

The major cause of thermal failure is generally believed to be due to a combination of accumulated hysteresis energy generated during each loading cycle and a low thermal conductivity causing significant temperature rise in the polymer such that the sample melts, thereby preventing it from carrying any loads. The energy dissipation rate, E according to Ferry (153) may be described by

$$E = \pi f J''(f,J)\sigma^2 \qquad (2.24)$$

and the temperature rise per unit time, ΔT is given by

$$\Delta T = \frac{\pi f J''(f,J)\sigma^2}{\rho c_p} \qquad (2.25)$$

where f is the frequency, J'' is the loss compliance, σ is the peak stress, ρ the density, and c_p the specific heat.

The temperature rise in bulk polymers undergoing cyclic deformation has been measured for several polymers (149). Figure 2.11 shows the increases in specimen temperature T with number of deformation cycles N (T-N curves) for nylon 6 (160), nylon 6,10 (158), and LDPE (162). The three sets of curves show that increasing ambient temperature, cyclic frequency or maximum stress level all promote parallel changes in the T-N curves. Different polymers exhibit vastly different susceptibilities to thermal fatigue failures. For example, Sauer and Richardson (164) have noted for polystyrene, which has a very low internal friction, it is possible to run a fatigue test about 30Hz and at maximum stresses of about 15 MPa with the accompanying temperature rise being less than 2K (165). However, under the same conditions polyethylene samples would rapidly melt and PMMA, which has a viscoelastic damping maximum near room temperature, would fail by thermal rupture unless the applied stresses were maintained at a low level. The significant effect that frequency has upon the form of the applied stress amplitude, σ_a versus number of cycles to failure, N_f when a thermal fatigue mechanism is operating may be clearly seen from figure 2.12. This data also demonstrates that the thermal and mechanical fatigue mechanism may be thought of as competing failure mechanisms and Crawford and Benham (166) described the transition from one mechanism to the other in terms of a critical value of applied stress amplitude. The critical value for the transition in mechanism is dependent upon mean stress, frequency, wave-form and specimen surface area - to volume ratio, apart from obviously also being dependent upon the material.

In conclusion then, it is clear from the above that the thermal fatigue failure may be suppressed by several factors such as (151); limiting the applied stress amplitude, decreasing test frequency, allowing for perodic rest periods, or cooling the test sample, and by increasing the samples surface area to volume ratio.

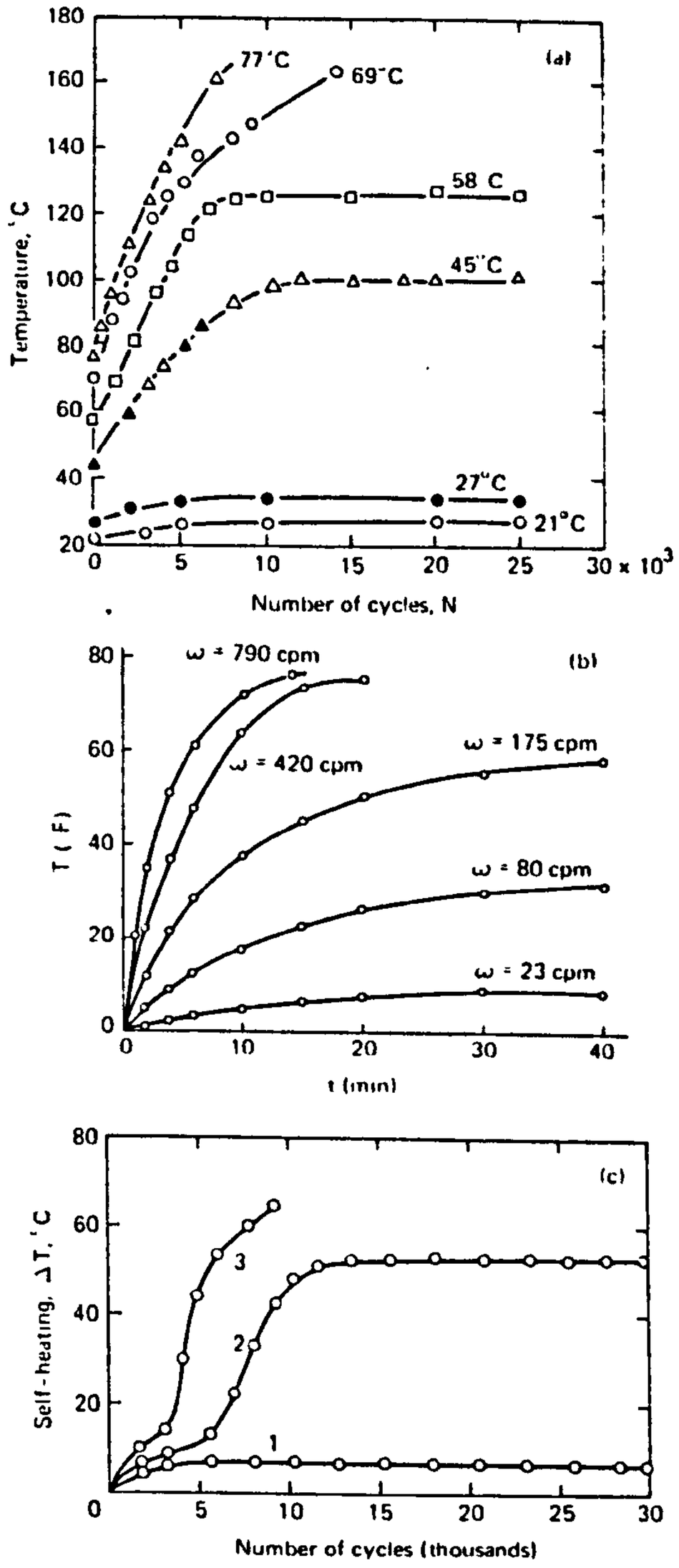

Fig. 2.11 Effect of testing variables on specimen temperature. (a) effect of ambient temperature on nylon 6 (After Ref. 160), (b) effect of frequency on LDPE (After Ref. 162) and (c) effect on applied stress amplitude on nylon 6.10: curve 1, 260 kg/cm²; curve 2, 280 kg/cm²; curve 3, 340 kg/cm². (After Ref. 158)

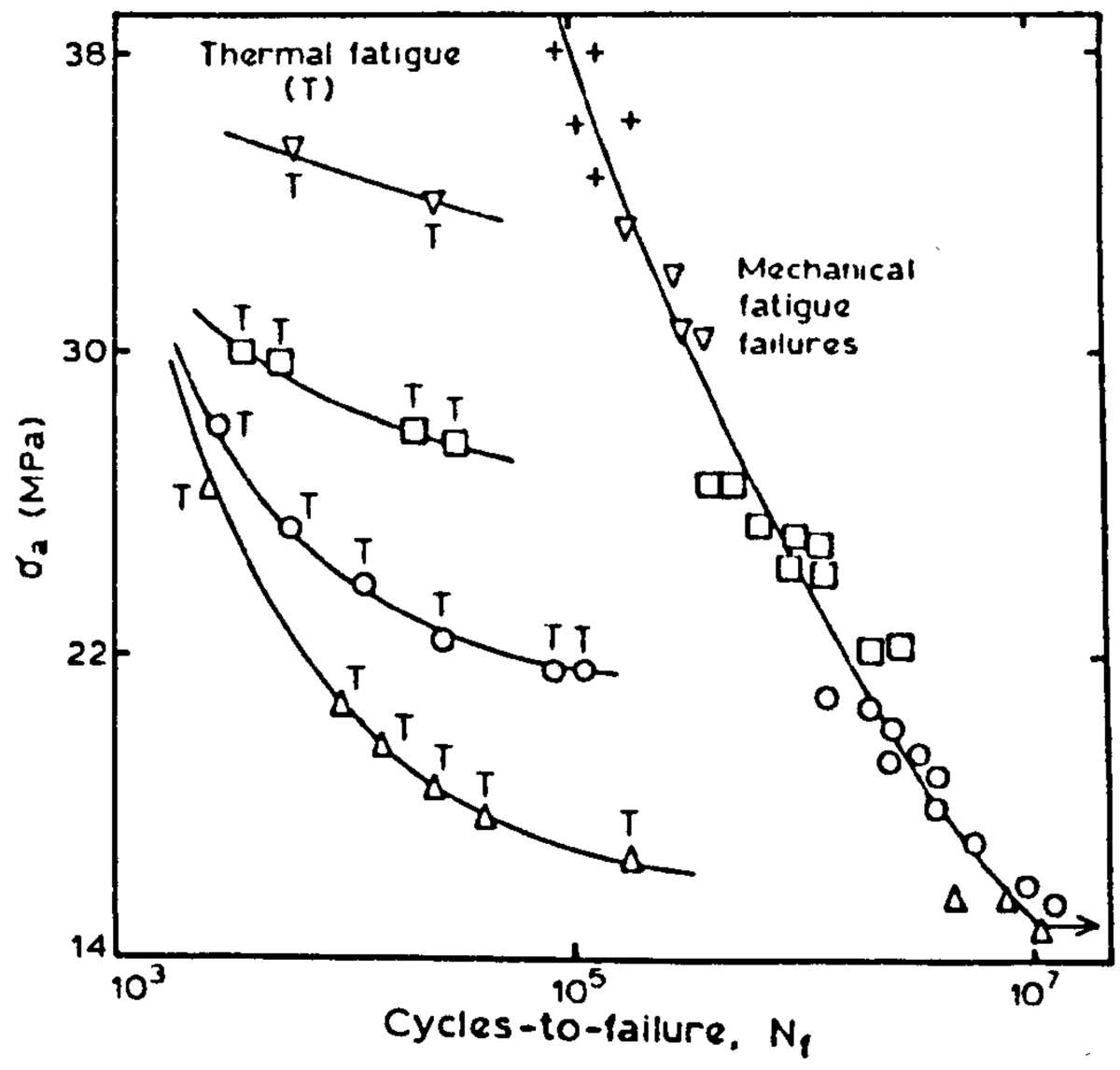

Fig. 2.12 Stress amplitude, σ_a, versus logarithm cycles-to-failure, N_f for a potyacetal copolymer +, 0.167; ∇ ,0.5; □ , 1.67; O, 5.0; Δ, 10.Hz (note difference between thermal and mechanical fatigue failure mechanism and their different dependencies upon frequency). (After Ref. 166)

2.3.3 Mechanical Fatigue Failure

The other main mechanism of failure is mechanical fatigue which involves the initiation of a crack and its subsequent propagation due to the alternating stress. Most of the interest has been focussed upon the growth of a crack which has macroscopic dimensions since it is this phase of the mechanical fatigue failure mechanism which often controls the fatigue life. However, before considering crack propagation studies, a limited review of what is known of the crack initiation processes is examined.

(i) Initiation of Fatigue Cracks Both crack initiation and crack propagation can occupy substantial portions of the total fatigue life for polymeric materials (148-152). The possibility thereby exists to greatly increase the fatigue life by reducing the frequency of crack initiation. However, little attention has been paid to the initiation process itself.

It appears as though the nucleation events in polymeric solids bear some relation to those observed in metals. For instance, nucleation at grain boundries is sometimes observed in metals (143). Andrews and Walker (167) have observed the analogous process of fatigue crack initiation at spherulite boundaries in LDPE. In a large number of cases, fatigue fracture of metals initiates at persistent slip bands ie in regions where extensive and highly localised plastic flow has taken place. Again, there is evidence as shown by Rabinowitz et al (168,169) that fatigue fracture in many polymers initiates at craze sites, an analogous case for crack initiation at a zone of high and very localised plastic deformation.

Finally there is evidence that internal or surface flaws can act as nucleation sites. Crawford and Benham (163) report that submillimeter internal flaws formed during moulding of an acetal copolymer act as sites for crack nucleation. Rabinowitz et al (168) observe such defects can act as nucleation sites in

polystyrene. Feltners (180) however, finds no such effect of internal flaws in PMMA, but rather, indicates that cracks initiate due to stress and temperature instability at the base of shallow surface cracks.

(ii) Fatigue Crack Propagation FCP The most popular approach to describe the fatigue crack growth rate (da/dN) as a function of applied stress amplitude, crack length and material properties has been to employ Paris's equation (171,172):

$$\frac{da}{dN} = A_f \Delta K_I^m \qquad (2.26)$$

where A_f and m are constants but their values depend upon the material, and the test variables of temperature, frequency, stress ratio and environment. ΔK_I is the stress-intensity factor range ($\Delta K_I = K_I \max - K_I \min$), the general formula which describes the stress field ahead of the crack is:

$$\Delta K = Y \Delta \sigma (\pi a)^{1/2} \qquad (2.27)$$

where $\Delta\sigma$ is the chosen/applied nominal stress range, Y is the geometric factor - allowing for shape, size and orientation of the crack and size of component, while a is the length of the crack. The main assumption being made in equations (2.26) and (2.27) is that linear elastic fracture mechanics is obeyed. That is, the size of plastic zone ahead of the crack is negligible compared to crack length and specimen dimensions and the polymer is in the linear elastic region (152).

Experimentally the crack length, a, in a notch bar is monitored against the number of cycles, N to give a plot of crack length against number of cycles. These data are replotted as crack growth rate, da/dN against the stress intensity range, ΔK. The crack propagation studies are carried out at a lower range of frequencies, usually below 5Hz for polymers.

Fatigue crack growth rate data in the form, of da/dN against ΔK on a log-log plot have been cited for a range of amorphous and semicrystalline thermoplastics. Figure 2.13 shows such a linear plot for several of these polymers (151). Generally semicrystalline polymers tend to show superior resistance to FCP in comparison with the amorphous polymers, ie lower FCP rates at a given value of ΔK, or higher values of ΔK to drive the crack at the same velocity. The superior FCP behaviour exhibited by polycarbonate and Nylon 6,6 was related to the availability of significant energy dissipation mechanisms that are linked to main chain segmental motion (173). For the case of Nylon 6,6 superior FCP behaviour also may be due to crystalline regions acting in a manner that would retard crack advance, for example by deformation and disruption of the crystallites (84). Hertzberg amd Manson (151) speculate whether polystyrene and polymethylmethacrylate, the worst materials shown in figure 2.13, possess this dubious distinction as a result of their low fracture energy and/or tendency to craze.

In some instances the relationship between da/dN and ΔK may be sigmoidal in shape due to A_r and m not being truly constant. Crack growth rates are then found to decrease to very low values as ΔK_I approaches to some limiting threshold value, ΔK_{Ith}, and to increase to very high values as $K_{I}max$ approaches the typical K_{Ic} values for crack growth under short-term monotonic loading conditions.

To describe FCP response over a wide range of loading conditions and to reflect viscoelastic effects implicit in changes in frequency, waveform and temperature, a general FCP law can be written as

$$\frac{da}{dN} = D\ f(\Delta K, K_c, \Delta K_{th}, m) \qquad (2.28)$$

where K_c, ΔK_{th}, D and m are the fracture toughness, threshold value of ΔK, and material parameters, respectively and $da/dN \rightarrow 0$ and ∞ at K_{th} and K_c respectively (175). Hertzberg and Manson

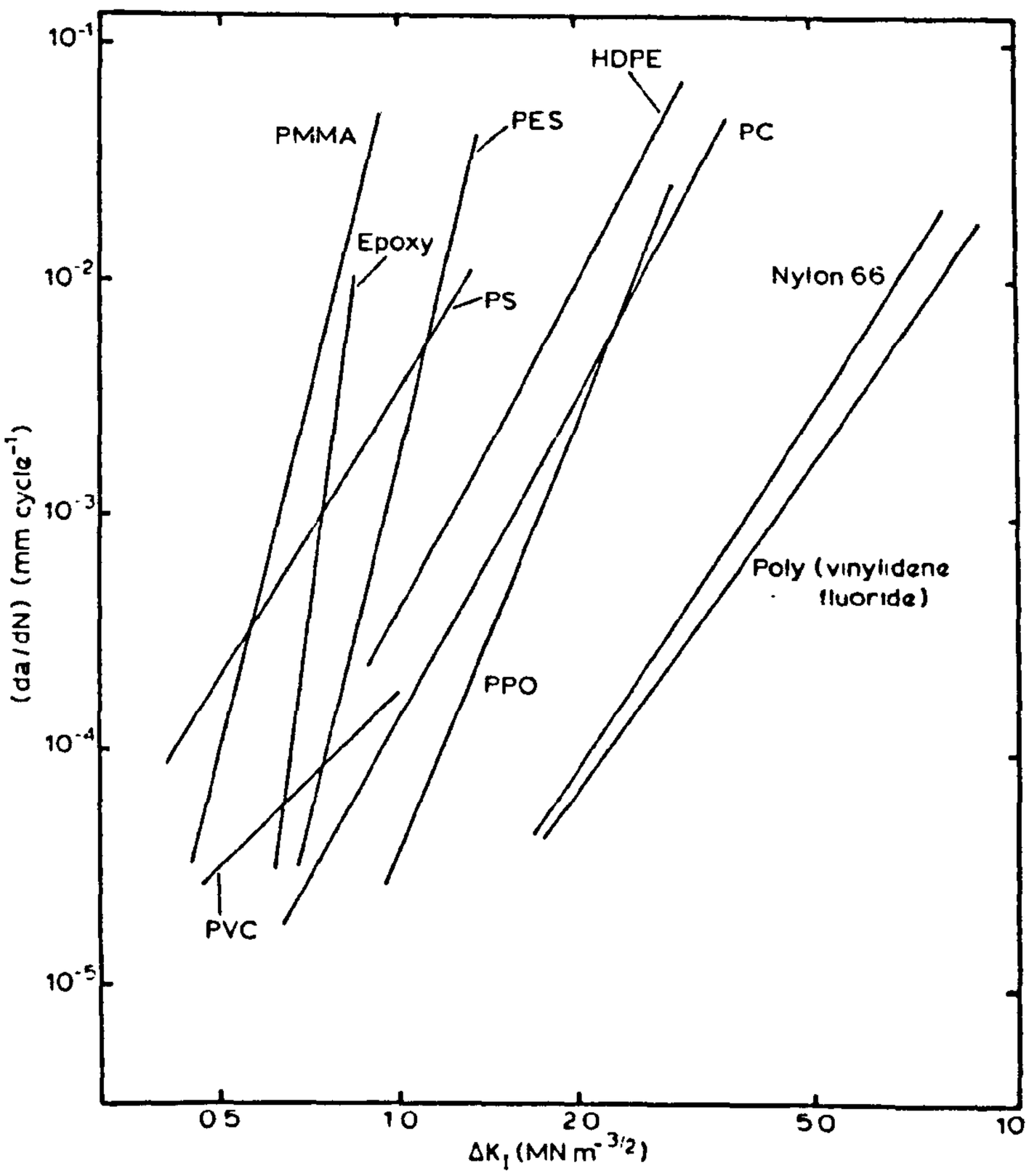

Fig. 2.13 Fatigue crack propagation behaviour in amorphous and crystalline polymers. The fatigue crack growth rate, da/dN, is plotted against ΔK_I (= K_{Imax} - K_{Imin}) (After Ref. 151)

(175) have recently proposed a model to describe the FCP between ΔK_{th} and K_c which combines both the molecular (rate process theory) and continuum elements. The essential feature of the model is to express da/dN as $f(\Delta K)/\tau$ where τ is a characteristic relaxation time of the activated process in the plastic zone (disentanglement, bond rupture, etc). In the simplistic case, τ (a function of the appplied stress function σ (t)) depends on the material, but not ΔK and may be expressed as

$$\tau = \tau_o \exp [(E_a' - V'\sigma_{y,m})/RT] \qquad (2.29)$$

where $\sigma_{y,m} = \sigma_y [(1 + R)/2]$; R is the gas constant, σ_y is the stress at the plastic zone boundary, and E_a' and V' the apparent energy and volume of activation, respectively. According to Hertzberg and Manson (175) the model has been used successfully to describe the effects of several tests and material variables. However, the application of the approach to much wider fatigue studies awaits good information.

2.3.4 Cyclic Creep

A basic hypothesis of the fracture mechanics approach outlined in the previous section is that the fracture process depends upon the magnitude of the stress range and not specifically on the time of its application. Cyclic or interrupted creep studies reveal, however, that fatigue behaviour depends at least in part on the loading - unloading process itself and time under load in the fatigue loading profile. This is seen in two types of measurement, one involving the total time to rupture and the other involving the creep rate. In either case the specimen is subjected to square wave loading, the lower limit of which may be either zero or tension or compressional. The duration of the stress pulses is such that experiments are generally sufficiently long (seconds to hours) that viscous heating effect could be realised only near the tip of the moving crack.

Schultz (149) discusses the results on the total time to failure τ_f which have been reported for PMMA, LDPE, PVC, ABS, plasticised epoxy and PS by various research workers, and comments that in all cases except LDPE the time to failure is decreased, relative to the static creep value, by the loading - unloading process. Natov and Glushov's result on LDPE (154) and on PVC (155) are of special interest, because these are the only investigations in which the time under load and the time at zero load are varied independently of each other. For PVC, the lifetime τ_f at constant zero load time decreases as the length of time under load decreases from 20 minutes to 1 minute. On the other hand, τ_f increases with decreasing load time from 120 minutes to 20 minuties for LDPE. The effect of increasing the time at zero stress in the case of LDPE is to increase τ_f above the static lifetime and for PVC is at first to reduce τ_f, but at longer zero stress times an increase towards the static lifetime is observed. No mechanistic interpretation has as yet been placed on these results. They broadly show, however, that the process of loading and unloading produces itself marked effects on the failure life of materials. Harris and Ward (156) too have shown that for some polymers the life is cycle, not time - dependent, in agreement with the thesis that the process of loading and unloading is intrinsically important.

2.3.5 Fatigue Behaviour Of MDPE/HDPE Pipe System

In contrast to PVC (93-104), the study on the fatigue behaviour of MDPE/HDPE (94,105-109) pipeline system has been some what limited. Each of the studies on MDPE/HDPE is reviewed and the uPVC study is omitted since it does not concern the current project.However some mention on uPVC will be made in order to illustrate some specific points. In the review presented here, the fatigue loading is considered to arise from fluctuation in the pressure of the fluid within the pipe, at a very low frequency (<1Hz) and at test temperatures ranging from 20 to 80°C.

Lortsch (94) carried out pulsation testing under high maximum pressures at 20°C on black pigmented LDPE and HDPE pipes of diameter 32mm and 2.9mm wall thickness (SDR11). Ductile failures were observed and from the results Lortsch (94) deducted that pulsation increases the strength of the pipe (in the ductile region) and related this increase to the higher rate of loading, ie the higher the rate of loading the greater the stress at upper yield. Lortsch also concluded that pressure waves do not damage the HDPE as long as the mean stress does not exceed the stress at pressure. According to Lortsch then the fatigue does not reduce pipe lifetime where lifetime is defined by the time to pipe failure under maximum load.

Fedosoff and Szpak (105) tested 160mm outside diameter HDPE pipe at 23°C to two different fatigue loading patterns; pressurising the pipe to a level causing a hoop stress of 12.8MPa for 15 minutes followed by an instantaneous drop to give a hoop stress of 4.9MPa, this sequence was repeated every 12 hours, giving frequency of 2.5×10^{-5}Hz, and a waterhammer loading every 12.5 second. Waterhammer sequence was as follows; fast closing valve opens, pump starts and flow reaches equilibrium, fast closing valve cocks itself ready to fall, fast closing valve starts and pump stops. For both the cases no fatigue weakness was identified up to 968 cycles (11,610hours) in the first case and up to 41,500 cycles (144 testing hours) in the second case.

Cowely and Wylde (106) investigated systematically the behaviour of butt fusion welded HDPE (density 955kg/m^3, MFI 0.3g/10min 2.16kg at 190°C) pipe and fittings subjected to fatigue loading Using HDPE pipe of 160mm diameter and 9.1mm wall thickness (SDR18) subjected to dynamic square wave fatigue at a fixed frequency of four cycles per minute (.066Hz) and a pressure of 6.3kgfcm^{-2}, tested at 50 and 70°C the pipe system lifetime was significantly reduced in comparison to the creep life of the pipe, and failure was shown to be due in part to the incorporation of injection-moulded fittings. They observed that crack initiation occurred at weld defects, that is all the

failures at pipe to pipe butt fusion welds were found to occur at weld defects caused by pipe wall misalignment and weld mismatch during welding. They also observed that some of the failures remote from welds were associated with pipe defects, such as bubbles trapped during extrusion of the pipe, and pointed out that the size of the defect may be important in controlling the times to failure. Cowely and Wylde (106) had also carried out tests in water, methanol and in a weak sodium chloride solution; no obvious relationship was apparent between time to failure and environment.

Barker, Bowman and Bevis (107-109) report data on the fatigue response of three different small diameter (60/63mm) SDR11 MDPE/HDPE pipe systems which included pipe to pipe butt fusion welds, 90° equal tees and 90° bends. These were tested at 79.5°C using maximum stress values which lay in the brittle region of the stress-rupture curve and the loading profile was trapezoidel. The influence of loading frequencies in the range .014 to .143Hz was also investigated for various small diameter MDPE/HDPE pipes. The frequency was varied by varing the time at maximum stress while maintaining a fixed time off load. Barker et al support the observation of Cowley and Wylde (106) that pipe network lifetime can depend on the integrity of the injection moulded fittings or welds between fittings and pipe, as opposed to the strength of the extruded pipe. Since Barker et al used a trapezoidal wave form, it enabled the fatigue performace, defined by

$$\tau_{fatigue} = N_f \times t_{max} \qquad (2.30)$$

where t_{max} = time under maximum stress

N_f = number of cycles to failure

to be compared to stress rupture time, τ_{SR} under equivalent stress and testing temperature. The data of Barker et al is presented in figure 2.14 (a) and (b). It is clear from the results that for two of the pipes (PE1 and PE3) the value of N_f

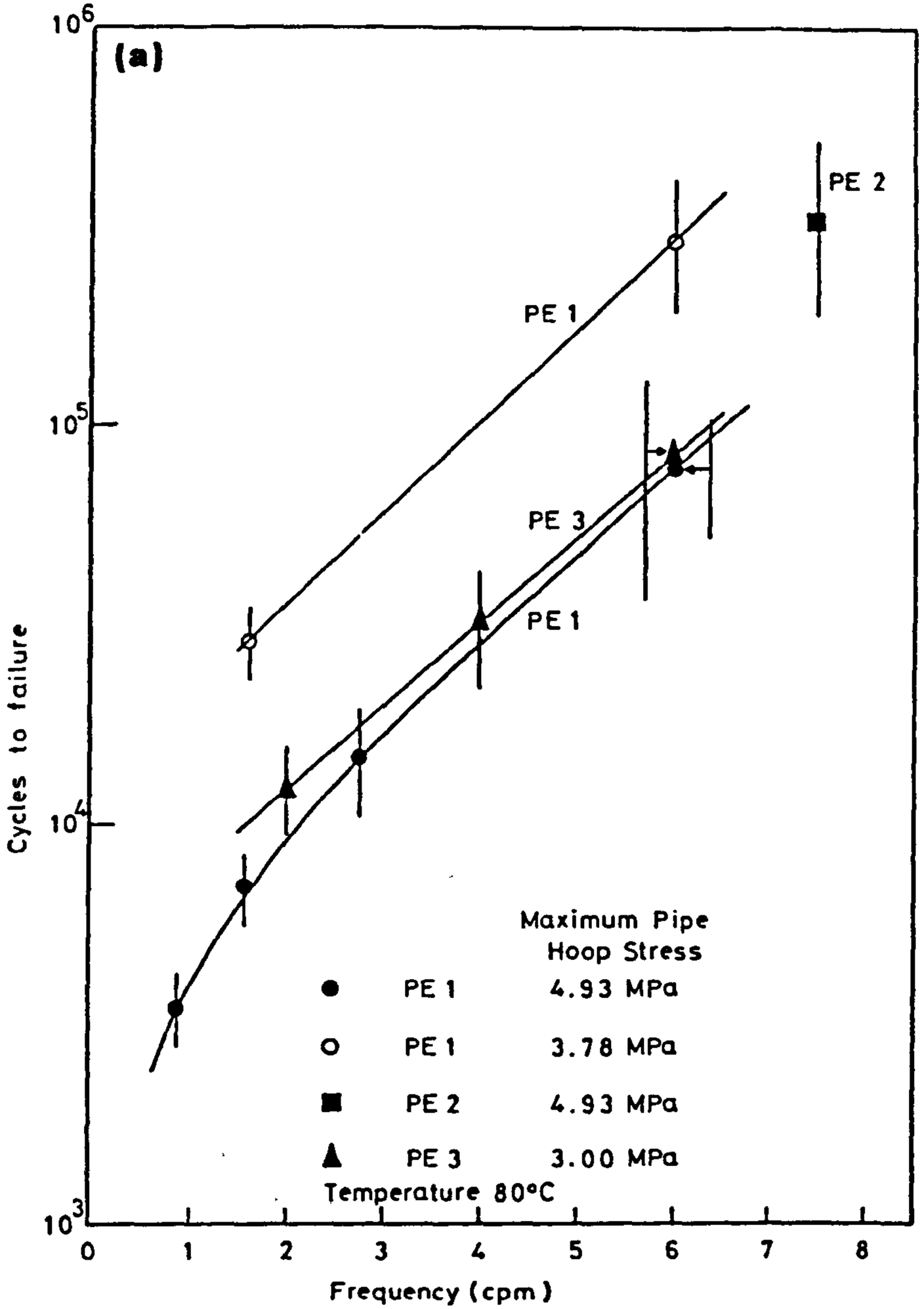

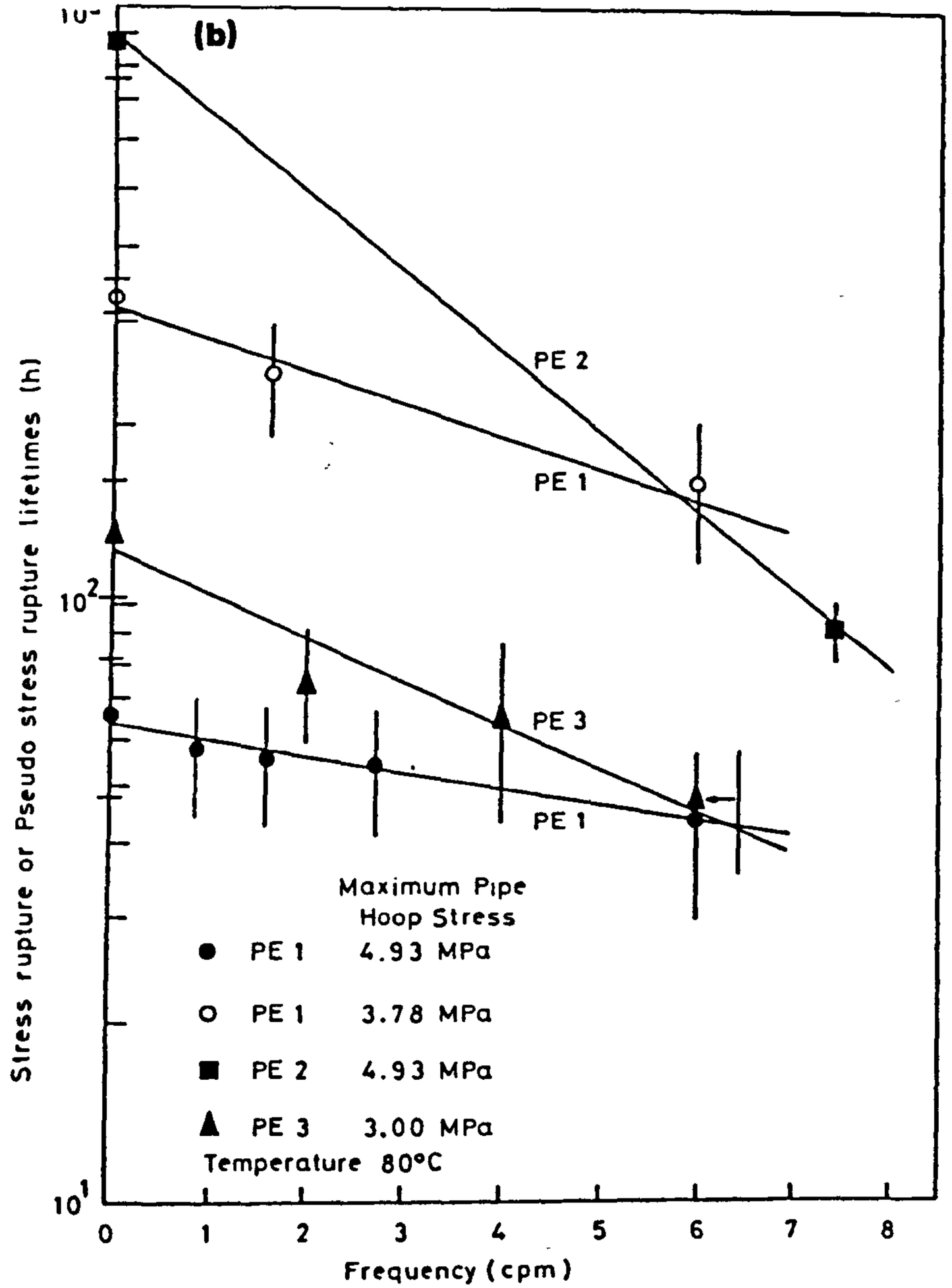

Fig. 2.14 Influence of loading frequency on (a) number of cycles to failure and (b) the time at maximum stress for various small diameter MDPE/HDPE pipes. (After Ref. 109)

can be strongly frequency dependent over the limited frequency range of the fatigue loading studied. From their results it appears that in the brittle region of the stress rupture curve the failure under fatigue is due to the accumulated creep/stress rupture damage. However, for one of the pipes there was evidence of a real fatigue weakness, since the ratio to $\tau_{fatigue}/\tau_{SR}$ was of the order of 0.1 and $\tau_{fatigue}$ lay to the left of the material manufacture's stress rupture curve. Tests on other long stress-rupture lifetime MDPE/HDPE pipes using a single frequency and hoop stress range, revealed a similar reduced performance under fatigue when compared to constant stress loading ($\tau_{fatigue}<0.048\tau_{SR}$).

2.3.6 Effect Of Fatigue Testing Variables

In general, the fatigue properties of thermoplastic materials, in particular fatigue crack propagation, FCP, can be affected by a variety of parameters such as frequency, test temperature, environment, molecular properties and morphology, and sample size. Effects of these variables are fully discussed by Hertzberg and Manson (151). There is therefore no intention to reproduce their survey. However, it is proposed to discuss the possible effect of a relevant selection of such parameters on MDPE/HDPE pipe system lifetime; the effect of test frequency, wave form and pipe size will be considered.

(i) Test Frequency The importance of test frequency has to certain extent, been discussed in section 2.3.2 and 2.3.3 on the mode of failure. For polyethylene, thermal fatigue failure is observed at a frequency of 30Hz (165); to obtain mechanical fatigue failure the frequency normally used is less than 15Hz depending on the applied stress. The review which follows discusses the effect of test frequency on mechanical fatigue failure, since it is this mode which is of concern.

As a general rule for semi-crystalline thermoplastics the lower the frequency (<1Hz) of the applied load, the fewer the number

of cycles to failure, and the greater the period of test (which equals the number of cycles multiplied by the cycle time) (97,99,157,159). Mckenna and Penn (159) report an immediate contradiction to this general rule. For conditions of zero tension, sinusoidal fatigue testing, they found that the the lifetime (time of test), of polyethylene increases with increasing test frequency. For polymethymethacrylate, PMMA, increasing frequency caused the fatigue lifetime to decrease. Thus PMMA obeys the "general rule" as suggested by Stapel (99) but PE does not. Natov and Glushkov (154,155) investigating the effect of loading time at constant cyclic recovery using a square wave form on the lives of PVC and LDPE have also made similar observation to Mckenna and Penn (159). Natov and Glushkov (154,155) found that for PVC the total testing time increased with decreasing frequency in accordance with the general rule but the opposite effect was observed for LDPE, the total testing time decreased with decreasing frequency.

De Charentenary et al (192) investigated the influence of frequency in the range .1 to .15Hz on the fatigue crack propagation,FCP of the conventional fatigue sample of HDPE. At a given stress intensity factor range, the decrease in frequency from 15 to .1Hz was found to increase the crack growth rate by two decades. They report a fatigue sensitivity factor, FSF of 5 for HDPE, the highest ever reported. FSF is defined as the multiple by which FCP rate chages per decade change in test frequency, after Hertzberg and Manson (151). De Charentenay et al (192) state that high sensitivity to frequency is consistent with the hypothesis of Hertzberg (151) concerning the fit between molecular jump frequency and the test frequency. The observation of a damaged zone in the front of the crack tip showed that this zone was larger for the low frequency. Thus microvoiding appeared to be enchanced at a low frequency.

There have been a limited number of studies on fatigue properties of MDPE/HDPE pipe system (94,109) and in general only

at one frequency, so that comparison cannot be drawn to identify any frequency induced effect on lifetimes. However, Barker et al (108,109) experimenting on the 60/63mm outside diameter MDPE pipe samples using a trapozidal wave form have carried out tests at a range of frequencies from .86 to 8.6 cycles per minute (.014- .143Hz) and at test temperature of 79.5°C and found the number of cycles to failure increases with increasing frequency, obeying the "general rule". There would appear to be some process at work in PE which is not yet obvious, but may be something to do with the waveform of the applied load.

For pipes of uPVC, Stapel (99) discusses the effect of a range of fatigue frequencies from 0.1 to 23 cycles per minute, cpm. Stapel reports that Hucks (96) found no significant differences in the performances of the pipes fatigued in the stated frequency range. However, Dukes (103), for uPVC pipe, reports the cycles to failure increasing with increases in operating frequency (from 10 to 100 cpm) at 15MNm^{-2} while at higher stresses frequency changes seem to have little effect in real terms. By comparison, an increase of about 15 times was reported by Gotham and Hitch (97) on conventional fatigue samples of well processed uPVC over the same frequency range at 35MNm^{-2}.

Jacobi subjected injection moulded uPVC tee fittings to two frequencies at several pressures in a range up to about.606±.202MPa and at a temperature of 20°C. He found increased frequency (80cpm) reduced the lifetime of the tee significantly, compared with a lower frequency of 2cpm. Jacobi considered such failures to be related to the effect of processing and went on to say that the results from his work prove the unsuitability of short term tests and recommended that pipe fittings which are subjected to periodically changing stresses should be tested with alternating internal pressure in order to obtain information regarding the lifetime.

(ii) <u>Wave Form</u> Stapel (99) refers to work by Oberbach and Heese (176) which suggests that square wave loading profiles

lead to failure sooner than either sinusoidal or sawtooth types of waveforms. It appears that such differences occur more markedly at high stresses, whereas at lower stresses no significant differences are apparent.

The reason for this appears to be due to the effect of creep deformation which has a greater influence at elevated stresses; coupled with this is the reasonable assumption that since a rectilinear waveform imposes a maximum stress for longer compared with a sinusoidal or sawtooth, the amount of creep damage per cycle would be greater.

Hertzberg and Manson (151) discuss the effect of loading profile on fatigue crack propagation and propose theories which conflict to some extent with those suggested by Oberbach and Heese (176).A change in strain rate is brought about by altering the waveform from rectilinear to sinusoidal or triangular and this will affect the material's stiffness as well as its yield strength, particularly with non-linear viscoelastic polymers such as HDPE. The higher the strain rate, the stiffer the material and the higher its yield stress.

To summarise Hertzberg and Manson's (151) opinion, the effect of loading profile on fatigue behaviour has been examined on a number of polymers where, for example, a square waveform has provided a strongly beneficial effect (for vinyl urethane), no effect (for polycarbonate) and a deleterious effect (for polymethylmethacrylate). Since polymers such as PE, uPVC and others differ with respect to their viscoelastic response, the different strain rates provided by the three types of a waveform mentioned above will have different effects on each material. There is apparently no hard and fast rule to enable a prediction of behaviour to be made.

However, because the various loading profiles result in different load-time integrated areas and different loading rates, the effects due to creep deformation and load appliction,

as described by Oberbach and Heese, have to be isolated. Hertzberg and Manson (151) show for a number of thermoplastics (excluding PE) that for the same loading rate, crack growth rates were consistently higher in association with the square wave which possesses twice the load-time integrated area, compared with the negative sawtooth waveform. In accordance with Hertzberg and Manson's suggesstion, Dukes (103) observed that the cycles to failure of both HSPVC and extruded uPVC pipe were marginally increased by changing the form of loading from square to sinusoidal with a near zero minimum load. There was also some evidence that the endurance limit is higher for both types of pipe under sinusoidal conditions and not under square waveform but comments that more work is required on both materials at long testing times.

For any work specifically related to PE plastic pipes, it is necessary to refer to Lortsch (94), who found that a sinusoidally varying internal pressure on HDPE pipe increases the time to failure if compared with a static load.

From the preceeding discussion it becomes clear that both loading rate and load-time integrated area must be considered for the fatigue response in PE pipe systems. This will supply only part of the solution, however, since stress levels and frequency will also produce significant effects for reasons described previously. Fatigue response in PE is thus apparently a result of a complex interaction of a number of variables, which have not been clearly defined in the literature to date.

(iii) Pipe Size A limited number of studies on the influence of pipe diameter and wall thickness on fatigue performance of uPVC have been reported (177-179). The findings of these studies are summarised below:-

(a) Large diameter pipes do not, of necessity, exhibit lower fracture strength under fatigue at the same maximum hoop stress (177).

(b) Pipes of larger wall thickness exhibit lower fatigue strength and allow the process of fatigue crack propagation to progress more easily (177).

(c) Small diameter pipes last longer than larger diameter when subjected to the same maximum hoop stress, all other parameters being equal (179).

(d) Tests on pipes with different SDR's indicate that the thin walled pipes sustain fatigue loadings better than thick walled pipes, for the same maximum hoop stress (178).

The conclusions drawn in (a) by Moore et al (177) and in (c) by Kirstein (179), although not exactly contradicting, certainly do not reinforce each other's findings. In other words, by increasing the pipe diameter and maintaining the same wall thickness, but subjecting all pipes to the same hoop stress, the lifetime under fatigue may or may not be reduced.

2.3.7 Prediction Of Fatigue Lifetimes

Lifetime predictions of a plastic component subjected to certain fluctuating loads have been successfully undertaken by using the concepts of cumulative damage and cycle dependent failure which can be described in terms of fracture mechanics.

The cumulative damage concept of fatigue failure assumes damage accumulates only during the time when the part is subjected to stress, failure occurring when the accumulated damage reaches a critical value (159). For simple loading profiles, such as a rectilinear waveform, the cumulative damage model is able to predict the number of cycles to failure, N_f using an expression similar to that of Stapel (99).

$$N_f = \frac{[I_{SR}]}{[t_{max}]_{T,\sigma}} \qquad (2.31)$$

where τ_{SR} is the stress rupture lifetime and t_{max} is the section of the time cycle under the set maximum load, both at the same stresses and temperature. In theory equation 2.31 is frequency independent and no restriction is placed on the length of the period t_{max} spent at maximum stress during each cycle. There is also no allowance made for recovery of damage, so that it must be assumed that the recovery or the time off load is negligible.

In cycle dependent fatigue failure the repeated application of stress, rather than the time for which the stress is applied, induces damage and causes a crack to propagate. It implies that a component will fail after a given number of fatigue cycles and the total lifetime to failure decreases proportionately with increasing test frequency. Mckenna and Penn (159) have shown that PE subjected to sinusoidal fatigue loading does not fail in a cycle dependent manner, nor can the previously described cumulative damage concept describe the material's frequency dependence.

It was discussed in section 2.3.3 under fatigue crack propagation, FCP; the actual rate of crack propagation in terms of the number of loading cycles, N is normally expressed in a form attributed to Paris (171,172) as given by (2.27) which is reproduced here

$$\frac{da}{dN} = A_f \Delta K_I^m \qquad (2.26)$$

and

$$\Delta K = K_{max} - K_{min} = Y(\Delta\sigma)(\pi a)^{1/2} \qquad (2.27)$$

where all the terms are as previously defined in section 2.3.3. In this mode of fatigue failure, for plastics, the frequency of loading can have a considerable influence on both "constant" A_f and m.

Equations (2.26) and (2.27) can be integrated with respect to N between the limits of initial crack length a_o and the final

crack length, which for pipes is taken to the wall thickness, t (25,26). Thus we have:

$$N_f = \frac{2}{m-2}\left[a_o^{(1-m/2)} - t^{(1-m/2)}\right]\left(\frac{Y(\Delta\sigma)\sqrt{\pi}}{A_f}\right)^{-m} \qquad (2.32)$$

This equation (2.32) assumes that the geometrical correction factor, Y remains constant between a_o and t. If, however, Y depends strongly upon crack length then the equation for N_f must be evaluated numerically.

When $t>>a_o$, its contribution to the expression for N_f is very small and the equation can be simplified to

$$N_f = \frac{\text{constant}}{\Delta\sigma^m} \qquad (2.33)$$

which can prove useful for determining stress level effects on the fatigue crack propagation lives of samples with identical geometries and flaws (19,20).

2.3.8 Fractography and Micromechanism

(i) General The literature on the features of fatigue fracture surfaces and the proposed micromechanisms for the failure resulting from mechanical fatigue is reviewed. In general two different sets of fatigue marking may be found on the fracture surface of the same polymer, each band corresponding to either one (striation formation) or as many (discontinuous crack growth band) as 1000 load cycles.

(ii) Striation Formation At relatively high ΔK_I values and low frequencies most polymers with the exception of PVC, experience incremental crack extension where the striation marking produced on the fracture correspond to successive positions of the advancing crack front as a result of individual load excursion (151). For polymethylmethacrylate, polysulfone, polystyrene and

polycarbonate, excellent one-to-one agreement between striation width and macroscopic growth rate has been observed (151). This implies that in the ΔK regime where striations are found, they represent the only fatigue crack advance micromechanism and account for the entire crack increment during a given loading cycle. By way of confirmation, no other fracture mechanism is seen in these materials in the ΔK regime where striations are found.

The surface of each striation contains a fine linear structure oriented normal to the striation line itself which may be reflecting material tearing during its formation. Overall, there appears to be no change in morphology from one side of the striation to the other. The morphology and mechanism of fatigue striation formation have been considered by several investigators (180-183) McEvily et al (181) and Feltner (180) described striation formation in PMMA, PC and Polyethylene (PE) in terms of the crack-tip blunting model proposed by Laird and Smith (184), wherein the crack-tip is considered to blunt and resharpen during loading and unloading portions of the stress cycle, respectively. The development of a bundle of crazes rather than a single craze has been suggested to be a possible crack tip blunting mechanism (185).

(iii) Discontinuous Crack Growth Bands The other sets of parallel fatigue markings have been found at low ΔK levels and at high test frequencies in PC, PS, PMMA, and at all stress levels in PVC and PE (149,151). These bands are too large to be caused by the incremental extension of the crack during one loading cycle. Instead, they correspond to discontinuous crack advance following several hundred loading cycles during which the crack tip remains stationary. The fatigue fracture sequence that produces these markings together with the model of discontinuous crack propagation mechanism is shown in figure 2.15. The damaged zone ahead of the crack is a single craze, or a few crazes at most, develops continuously, although it is characterised by a decreasing rate with increasing length. When

the craze reaches a critical length, the crack advances abruptly across the entire craze and then arrests. With further cycling, a new craze is developed and the process is repeated. Several authors (185-190) have used the Dugdale plastic-zone model to describe the craze length ahead of the fatigue crack tip. Skibo et al (186) have determined the craze length, R_c by measuring the band spacing and deduced the craze surface stress, σ_{cm} using equation:

$$R_c \simeq \frac{K_{Ic}^2}{8\pi\sigma_{cm}^2} \qquad (2.34)$$

and taking $K_{Ic}=K_{Imax}$. For a range of polymers there was a reasonable correlation between the computed value of σ_{cm} and the measured plane strain yield stress, as may be seen from the table below.

Values of the craze surface σ_{cm}, deducted from the Dugdale model and plane-strain yield stress, σ_y' (186)

Polymer	σ_{cm}(MPa)	σ_y' (MPa)
Polystyrene	38	38
Polyvinylchloride	51	47-65
Polysulphone	79	67-80
Polycarbonate	81	61-82

(iv) Fractography and Fatigue Failure Mechanisms in Polyethylene

This section is specifically devoted to fractography and fatigue mechanisms in polyethylene. Papers published by the following are dicussed; White and Teh (191) on LDPE and HDPE,
De Charentenary et al (192) for results specifically related to FCP in HDPE, Cowley and Wylde's (106) observations with the fracture morphology and mechanism of fatigue failure in HDPE pipe systems and Barker et al (109) characterisation of initiation site in fatigue and stress-rupture.

White and Teh (191) using a specially constructed fatigue rig at a frequency of 0.24Hz (15cpm) tested HDPE (Mn ≈ 10^5, Mw ≈ 10^4, density 960Kgm^{-3}) compression moulded parallel sided dumb-bells where the internal stresses had been removed. They indicated that stress whitening was found to occur at the crack tip prior to crack growth. The surface showed a fibrous type of failure where the fibrillation was more extensive and developed to a degree greater than in the other polymers examined in their investigation. Microfibrils were observed with lengths of the order of nanometers and were found to be comparable to the well developed microfibrils produced by "cold drawing" of HDPE at elevated temperature. The fractured fibril remnants were generally less than 3μm in length.

During large cyclic crack advance it is often the case that fatigue striations are formed particularly under conditions of high tensile strain and during the final stages of fracture; slow crack growth in HDPE is usually related to rough fibrous regions on the fracture surface. The striations, it is proposed, normally form at the rate of one per cycle, however microstriations are also shown to be present. They are not thought to be caused by a mechanism of crack arrest, rather the microstriations were consistent with their identification as lamellae, either exposed ends or fractured sections which lie parallel to the crack front. Hertzberg and Manson (151), however, consider that the 0.5μm wide bands found on fracture surfaces in their own studies may represent a cluster of several lamellae or different sections through such crystalline units.

The lines referred to by White and Teh (191) which lie in the direction of crack propagation are determined, it is thought, by interspherulitic paths at slightly different levels. Similarly the generally undulating appearance of the fracture surface when tracing paths in a radial direction from the nucleating spherulite can also be related to the boundaries between the spherulites, though plastic deformation can mask such evidence.

De Charentenary et al (192) carried out their fractographic and mechanistic analysis on HDPE's of various molecular weights and crystallinities. The specimens were notched prior to the 20°C testing, σ_{max} was maintained throughout the test and no compressive stresses were applied to the samples; frequency was varied in the range .1 to 15Hz. It was found that the lower molecular weight samples of Mw = 45,000, 70,000 and 72,000 showed extensive microductility arising from micronecking and cracking of damaged regions (voids) in a continuous propagating mechanism, ie no striations. The discontinous propagating mechanism in the cracking of a high molecular weight sample (Mw=200,000) was shown by the presence of several crack arrest lines. In the area preceeding the crack arrest lines microstriations were observed. They suggest that microscopic growth calculated on the basis of one striation space for one cycle is much larger than macroscopic observation and it is proposed that a step-wise mechanism, with the formation of a crack in the process zone behind the crack tip gives a reasonable explanation of the fracture surface as shown in figure 2.16.

This is somewhat different to the mechanisms proposed by McEvily et al (181) for LDPE, who describe a crack tip blunting model for fatigue striation formation. Figure 2.17 shows that during the stress-off period of the fatigue cycle, elastic contraction of the plastic zone ahead of the crack tip imposes a residual compressive stress on the tip. This resharpens the cracks, reduces the material ductility ahead of the crack front and produces a fracture surface of alternating troughs and flat regions, where the two surface are mirror images.

Cowley and Wylde (106) carried out a fatigue study of HDPE pipe systems at elevated temperatures (43-70°C) and at a constant frequency of 4cpm with square waveform. They separate their study of fatigue fracture surface into discussions relating to crack intiation and crack propagation. They indicate that environmental and/or microstructural effects do not have the

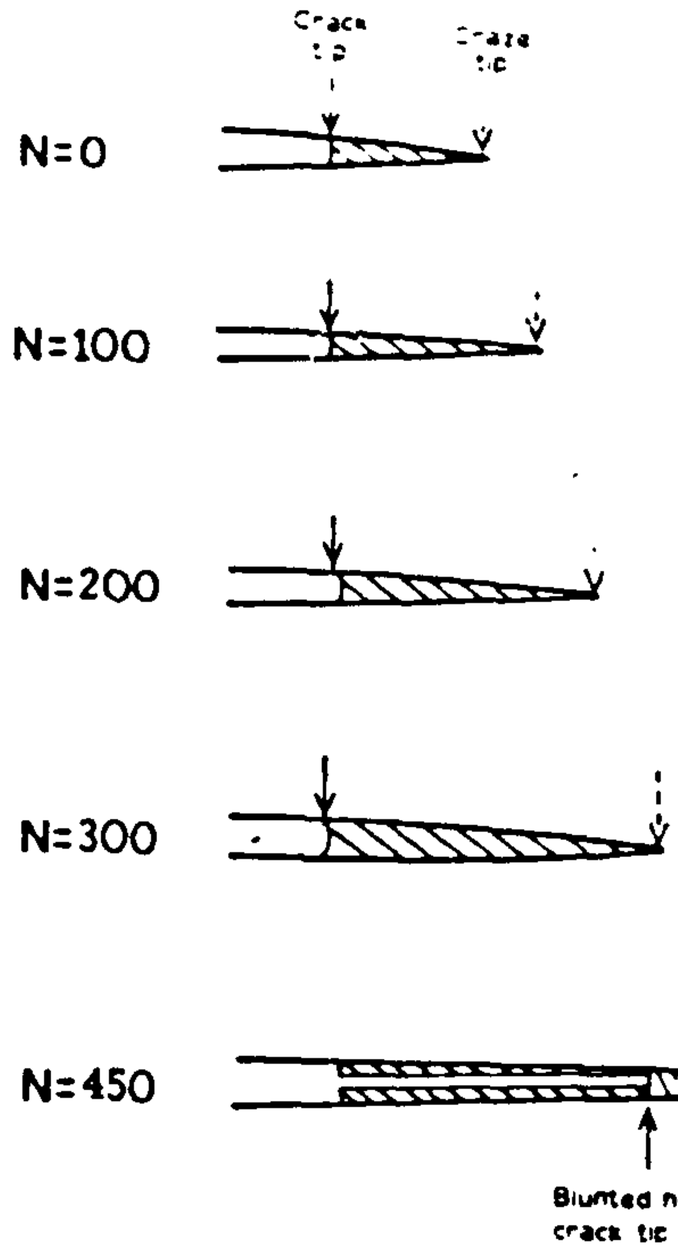

Fig. 2.15 Model of discontinuous crack propagation mechanism. (After Ref. 186)

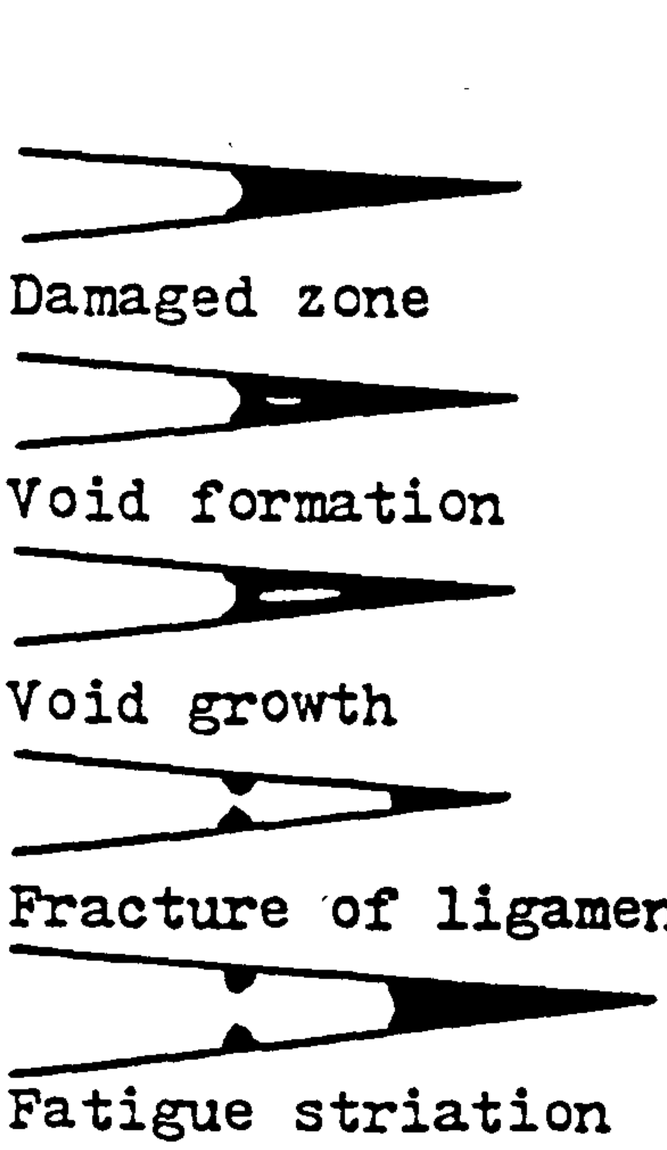

Fig. 2.16 Mechanism of fatigue crack propagation in semi-crystalline thermoplastic (HDPE). (After Ref. 192)

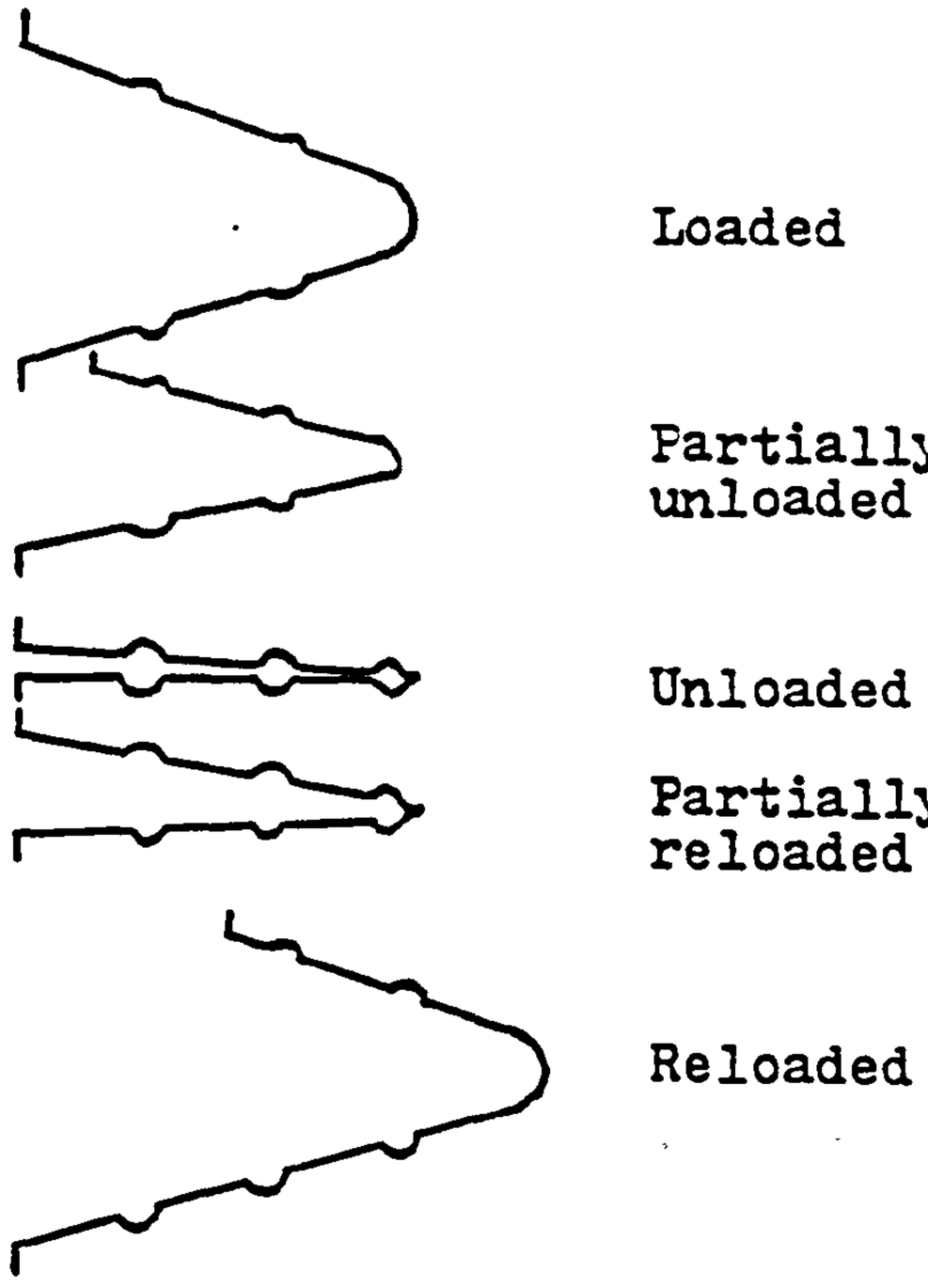

Fig. 2.17 Mechanism of fatigue crack propagation in an amorphous polymer (uPVC). (After Ref. 181)

most significant effect on the initiation of cracks. They observed failures at pipe/pipe welds, made at the recommended welding temperatures, in a water and methanol environment and suggest that the factors causing failure must operate in the absence of environment. They go on to say that failures in pipes were also observed well away from the heat affected zones near butt-welds, where there has been signifcant microstructural change, but which is not considered as a prerequisite for crack initiation. In general it appeared that failures occurred from either voids within pipe walls or at pipe/pipe welds where defects caused by wall misalignment and weld mismatch could be seen.

In a second series of tests in pipe/fittings welds, failures initiated at weld bead discontinuities produced by the effect of internal weld lines in injection moulded fittings. The weld defects act as stress raisers and during cyclic loading cracks are initiated at such points. The application of scanning electron microscopy confirmed that whatever the mode of crack initiation, the crack growth took the same form in these pipe systems. All surfaces revealed a banded structure which were concentric and allowed the nucleation site to be located. The general structure of the failure surface consisted of light areas with a high degree of fibrillation.

The mechanism used by Cowley and Wylde to explain these fracture surfaces is similar to that proposed by McEvily et al (181). A reduction of ductility ahead of the crack tip during the crack-arrest of the stress-off part of the cycle is assumed and when the stress is applied again the crack propagates through the now less ductile zone and then into the more ductile normal material producing dark and light bands. Evidence for this effect is also drawn from the fact that the two fracture surfaces for each failure are indeed mirror images of each other.

Barker et al (109) investigated fatigue and stress-rupture response of three different grades of PE in the form of

one large (160mm) and three small diameter pipe systems (60/63mm labelled as PE1, PE2 and PE3) at a temperature of (79±.5°C). Fracture surface studies were carried out using reflected light microscopy to examine the macrofeatures and scanning electron microscopy to examine the microfeatures. The latter technique was mainly used to characterise the shape and size of fracture initiating particle and to determine their elemental composition using the EDX facility available on SEM. For two of the pipe grade polyethylenes (PE1 and PE3) in small diameter pipe systems, no beach markings were visible. However, for PE2 beach markings (discontinuous crack growth band) were revealed; it is interesting to note that these were also observed for the pipe failure obtained under stress-rupture condition.

In PE1 pipes, Barker et al (109) found that over 95% of failures initiated from particles of whose size was predominantly below 700μm. Elemental analysis of the particles showed 52% initiated from particles where no elements could be detected, 16% from calcium rich and the remainder from iron or titanium based particles. In the large diameter pipe (160mm) fracture initiated mainly from macro-voids in the pipe wall.

2.4.0 Stress Rupture Behaviour Of MDPE/HDPE Pipe

2.4.1 Stress Rupture Data and Failure Modes

The behaviour of polyethylene pipe subjected to a static internal pressure (creep loading) is characterised by a family of stress rupture curves. There is general agreement in Europe that the stress rupture curves for both MDPE and HDPE pipe have the general form shown in figure 1.1, where for each curve there are two distinct regions separated by a "knee". Above the knee the material deforms in a gross ductile manner with significant local straining of the material prior to failure, whereas below the knee a brittle crack propagates through the pipe wall with little or no evidence of ductility, and strains of usually less than 3% (84,150). At longer times and lower stresses, the mode

of failure of HDPE and MDPE pipe is by the propagation of a brittle crack through the wall of the pipe. Experience has shown that such cracks nucleate on the inside wall of a pipe and propagate through to the outside (84). In general this effect would be expected considering hoop stresses are greatest on the inside wall of a pipe. It may be necessary, however, to modify this reasoning if the pipe materials are not completely free of inhomogeneities (which inevitably they are not). Cracks may then initiate at positions lying away from the inside surface where local stresses may be greater due to the presence of inclusions or voids or other nucleation sites. When pipes do fail by the propagation of a brittle crack, the fracture lies parallel with the pipe extrusion direction forming in response to the largest stress in the hoop or circumferential direction (106).

The processing effects and the geometry of pipes make it necessary to determine the stress rupture behaviour on the pipe itself. It is not really valid to rely entirely upon uniaxial tensile creep tests.

2.4.2 Prediction Of Stress Rupture Lifetimes

In the main, two different approaches to calculate the lifetimes of plastics pipes subject to static loads or stress have been proposed, one based upon the application of fracture mechanics (25,26) to slow stable growth, the other from the theory of activated rate processes developed by Eyring et al (10) and applied to thermoplastics pipes by Barton and Cherry (12,13), Bragaw (14,15), Palermo (16), Geffroy and DeBlice (17) and Szpak and Rice (18). The fracture mechanics approach will be dealt with first.

Gray, Mallinson and Price (26) applied fracture mechanics to the case of slow stable crack growth in HDPE material and found that the rate of crack growth da/dt could be given by

$$\frac{da}{dt} = BK_c^b \qquad (2.35)$$

where B and b are material constants and K_c is the stress intensification at the tip of the growing crack, and is given by

$$K_c = Y\sigma\sqrt{\pi a} \qquad (2.36)$$

where Y is a geometrical correction factor

a is the crack length

σ is the applied stress

It was assumed that the PE pipes failed from the inside surface by the propagation of a brittle crack of initial defect size a_o. The crack was also considered to propagate from the defect immediately upon application of a load. With the factors Y, σ and temperature remaining constant (25,26) K_c can be substituted in the crack growth rate expression and integrating between the limits of a_o and t (the pipe wall thickness), the lifetime, τ_{SR} of the pipe under static internal pressure can be expressed as

$$\tau_{SR} = \frac{2}{b-2}\left[a_o^{(1-b/2)} - t^{(1-b/2)}\right]\frac{(Y\sigma\sqrt{\pi})^{-b}}{B} \qquad (2.37)$$

If the size of the defect changes such that Y varies significantly then the change in Y should be allowed for during integration.

If $t >> a_o$ and b is greater than 2, the above equation simplifies to

$$\tau_{SR} = \left[\frac{2(Y\sigma\sqrt{\pi})^{-b}}{(b-2)\ B}\right]a_o^{(1-b/2)} \qquad (2.38)$$

where the terms in square brackets are constant for testing at both a given fixed temperature and pipe hoop stress. Assuming that equation (2.36) is obeyed by the material, the lifetime of the pipe is then dependent upon the initial defect size. It also

implies that the initial crack growth dominates the lifetime since smaller cracks grow more slowly than larger ones.

As an example, for an unnotched HDPE pipe material (006-60), Price et al (25,26) demonstrated that lifetimes could be predicted using the above approach if defect sizes between 10 and 100μm were assumed. This material obeyed the crack growth rate law.

The same method was applied to another pipe material Rigidex MDPE 002-40 which is much tougher than conventional HDPE, but since it failed to obey equation (2.35), that is the crack propagation rate was not a straightforward function of stress intensity at the crack tip, then the equation used for predicting lifetimes became invalid.

It should be stressed that the model of creep crack propagation in HDPE pipes under constant internal pressure proposed by Price et al (25,26) does not allow any period spent initiating cracks. The theory assumes that for a particular value of the critical stress intensity factor there is a corresponding crack speed. However, Bragaw (27) has reported on work with MDPE pipe system and shown there is a significant incubation time for a crack to start growing in a slow, stable manner. He therefore casts doubt on the validity of the use of fracture mechanics concepts to determine the failure performance of such ductile materials. Price and Gray (25) answer this by insisting that although no incubation process has been included in their treatment, such an approach does describe the lower bound case of immediate stable crack growth. Also their experimental results agree with predicted values for HDPE pipes, which can be considered as having an insignificant period of crack initiation, that is, the cracks or defects are probably present prior to testing.

Activated rate processes have been used (12) to describe the rate at which activated complexes pass over an energy barrier and assuming a local critical failure strain the time to fracture under loading can be described by

$$t = \frac{Nh}{kT} \exp\left[\frac{H - B\sigma/2}{kT}\right] \qquad (2.39)$$

which leads to

$$\sigma = \frac{2kT}{\beta}\left[\ln N - \frac{\ln kT}{h} + \frac{H}{kT}\right] - \frac{2kT}{\beta} \ln t \qquad (2.40)$$

where N is a constant

σ is the applied stress

H and β are the activation energy and activation volume of the process leading to either ductile or brittle failure.

h and k are Planck's and Boltzmann's constants respectively

T is the absolute temperature.

Equaton (2.40) implies a linear stress - logarithm time to failure relationship with a slope of $2kT/\beta$ or in other terms the equation can be written as:

$$\sigma = A_1 - B_1 T \ln t \qquad (2.41)$$

sometimes referred to as the "Russian" method for the prediction of stress rupture performance.

Barton and Cherry (12,13) obtained stress rupture data for Hostalen GM5010 pipes and plotted the results in this linear stress - logarithm lifetime fashion. Reasonable curves at testing temperatures of 40, 60 and 80°C were constructed from the data using the activated rate process theory. However, evidence (12,13) suggests that for HDPE the activation volume β is not constant and will increase with temperature. Kubat et al (202) produced results indicating that β also varies with

stress. These effects are contradictory to the proposals by Barton and Cherry (12,13) since in order that they were able to produce curves to fit the pipe data more closely, a temperature dependent activation volume was required. In fact for GM 5010 HDPE pipes the value of β more than doubled as the test temperature increased from 20°C to 80°C.

In spite of these difficulties Barton and Cherry (13) formulated a general equation describing the brittle rupture time at any temperature for HDPE GM 5010 pipes, which is based on a knowledge of the temperature variation of the activation volume and other terms in the rate process equation, and is expressed as

$$\sigma = 7.10\times10^{16}T^{-4.30}(1.12\times10^{4}T^{-1} - 13.5 - \ln t) \qquad (2.42)$$

which at 20°C becomes

$$\sigma = 201 - 175 \ln t \qquad (2.43)$$

2.4.3 Fractography and Failure Mechanisms

In non-orieted thermoplastics such as HDPE and MDPE the failure mechanism under static loads is dominated by the development of creep cracks (180). The failure mechanism can be divided into three growth periods:-

(i) Homogeneous deformation which induces a crack to form
(ii) A period of slow stable crack growth
(iii) A period of unstable crack growth

Generally, this formation and growth of creep cracks can be examined from the resultant fracture surfaces which can exhibit a number of features. Although not always the case, cracks are often observed to initiate at defects within the material. A stable crack growth follows which is considered to be thermally activated (150). The supposed constant conditions

during this period cause a circular or elliptical smooth fracture surface to form which can extend across the thickness of the material, depending upon the applied stress. Higher magnifications reveal that for HDPE a cellular, locally highly drawn surface has formed in the mirror zone. Gaube (184) and their co-workers have found, with natural PE pipes, that the period taken to initiate a crack could account for 90% of the lifetime of the pipe.

From the fractographic analysis of surfaces of MDPE pipes, slowly spreading cracks and ring like traces of the crack front can be seen under low power light microscopy (203). Here a creep crack surface distinctly shows elliptical rings, the centre of which lies at the nucleation site. The crack had apparently propagated slowly, the surface being uniformly covered with drawn fibrils. High local ductile drawing occurs at or ahead of the crack tip, which Bragaw (203) suggests results from a craze preceeding the crack.

It is also indicated that the fatigue cracks in HDPE pipes reported by Cowley and Wylde (106) are due to creep type failure which is evident from the surface being covered with drawn fibrils, upon which, however, are superposed gross rings of a very different nature from sustained load markings. Bragaw (203) suggests that these rings are caused by a discontinuous crack growth.

Hannon (204) reports on the mechanism of crack growth in a variety of HDPE samples under constant stress in a water environment. His findings are that the fracture surface of an HDPE copolymer produced in a water environment at 60°C shows a macroscopically brittle mode of failure, the crack being preceeded by a void nucleation and growth process with considerable ductile deformation between the voids which results in the formation of fibrils.

To summarise, the brittle fracture of HDPE in a water environment at elevated temperature (≃60°C), under plane strain conditions, at stresses well below the yield stress, proceeds by a mechanism of hole nucleation, hole growth and finally followed by the plastic deformation (yielding) of the molecules surrouding the voids.

CHAPTER 3 - EXPERIMENTAL

3.0.0 Materials

Fatigue tests were undertaken on three different commercial grades of polyethylene supplied by two manufacturers. The list of the commercial grades of polyethylene pipes, together with pipe sizes and total pipe lengths used in the test programme is given in table 3.1.

Preliminary investigations into the feasibility of the project on the fatigue strength of misaligned butt welds were carried out using black HDPE pipe of standard dimension ratio (SDR) 11 and nominal outside diameter of 63mm. The black pipe was manufactured using BP Chemicals Limited Rigidex 002-60 grade of HDPE resin. The total pipe length of Rigidex 002-60 used in the study was 40 meters. Note that this grade of material was withdrawn by BP Chemicals Limited in mid 1983 and is no longer available. The majority of the work described in this thesis was executed on blue pipe of SDR 11 in three different nominal outside diameters of 63, 90 and 125mm. The blue pipe, as employed in the water distribution, was manufactured by Stewarts and Lloyds using BP Chemicals Limited Rigidex 002-50 grade of MDPE resin. The total length of each of the pipe sizes used for the fatigue testing programme was as follows: 116 meters of 63mm, 84 meters of 90mm and 32 meters of 125mm. The total length of pipe used in the stress-rupture testing was 28 meters of 63mm and 13 meters each of 90mm and 125mm.

A limited fatigue study was performed on the DuPont Blue Aldyl 322 grade of MDPE of SDR 11 and outside diameter of 63mm. The total pipe length of this grade of pipe used in the study was 12 meters.

Table 3.2 gives the relevant physical properties of the main materials (Rigidex 002-50) as published in manufacture's

Table 3.1 Polyethylene grades used in the testing programme.

Polyethylene Grade	Pipe Diameter, mm	Pipe Length Used, Meters
Rigidex 002-60 HDPE	63	40
Rigidex 002-50 MDPE	63	144
Rigidex 002-50 MDPE	90	97
Rigidex 002-50 MDPE	125	45
DuPont Aldyl 322 MDPE	63	12

Table 3.2 Typical properties of Rigidex PC 002-50 MDPE compound (after ref.3).

Property	Test Method	PC002-50	Unit
Density	BS3412(1976)AB_2B_3 ISO1872(Annex B)	950	kg/m^3
Melt Flow Index	BS3412(1976)-2.16kg load ISO1872-2.16kg load	0.2	g/10min
Tensile stress at yield	BS2782(1976)Method320A ISOR527:1966(Type2speedD)	19.0	MPa
Elongation at break	BS2782(1976)Method320A ISOR527:1966(Type2speedD)	750	%
Flexural modulus	BS2782:1976Method335A ISO178	700	MPa
Hardness	ISOR868(TypeD)	65	-
Vicat softening temperature	BS2782(1976)Method120A ISO306A50	116	°C
Brittleness temperature	ISO974	<-70	°C
Linear thermal expansion	Average value over temperature range20°Cto6°C	$1.5x10^{-4}$	W/m°C
Thermal stability	Oxidation induction temperature, ASTMD3350	260	°C
	Oxidation induction time Isothermal in O_2 at 200°C	>30	min

Table 3.3 Measured density and melt flow index of polyethylene grades. Manufacture's value are given in the bracket.

PE Grade	Rigidex 002-60	Rigidex 002-50			DuPont 322A
Pipe Diameter, mm	63	63	90	125	63
Density(mid-wall), kgm^{-3}	957.8 (960.0)	942.9 (950.0)	945.5 (950.0)	945.1 (950.0)	938.4 (940.0)
MFI, g/10min.(2.16kg load)	.182 (.200)	.203 (.200)	.208 (.200)	.197 (.200)	.576 (.600)

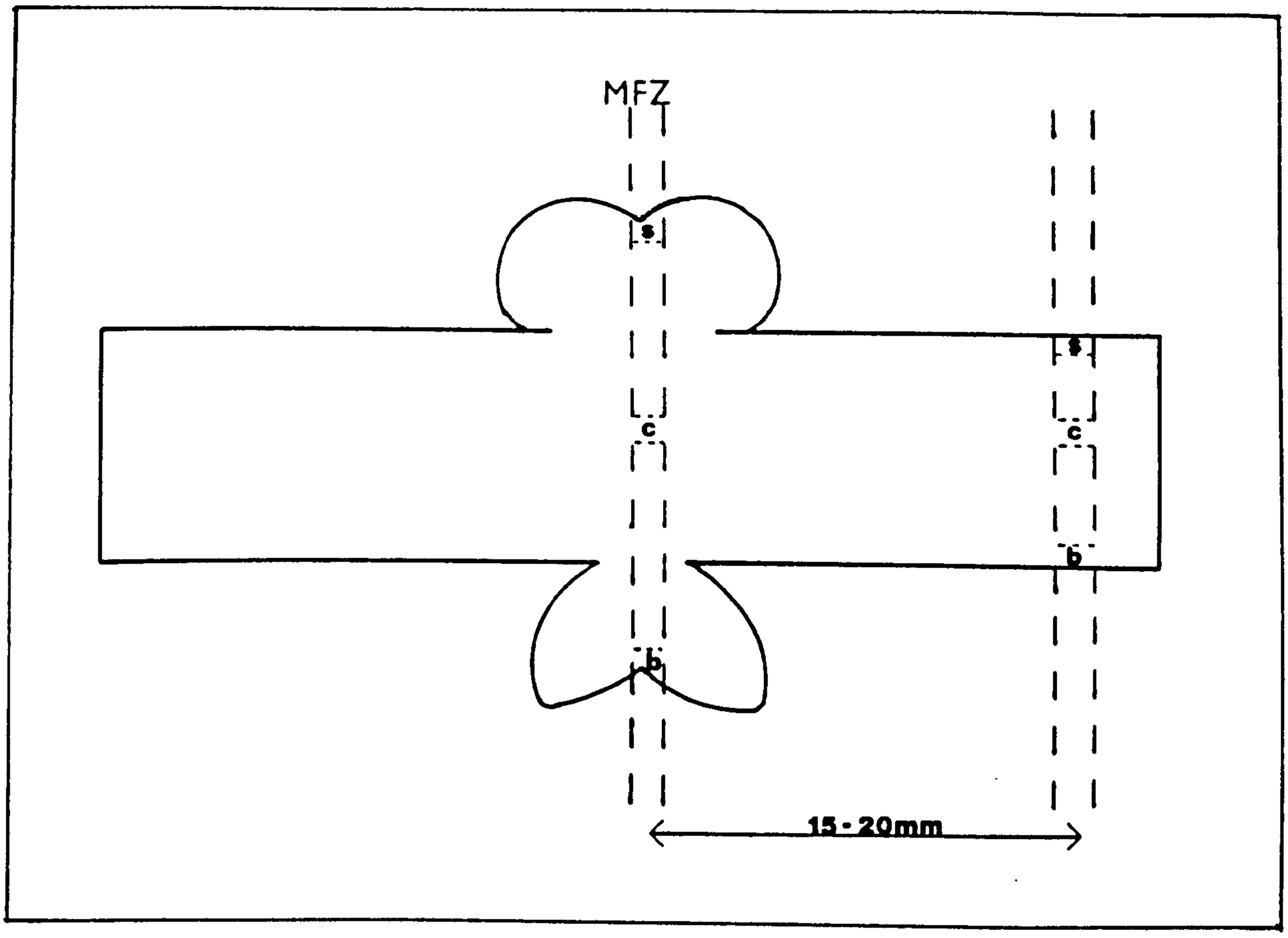

Fig. 3.1 Sample location site for the density, DSC, DTA and IR analysis of the untested and tested butt welded specimen at 79°C.

literature. All three resins were thermoplastic non-crosslinked MDPEs which are most easily characterised by a density and melt flow index (MFI). The density and MFI of these materials were determined and in all cases found to be within the manufacturers specification; the results are given in table 3.3.

3.1.0 Materials Characterisation

Materials characterisation techniques, in particular Density Gradient Column analysis, Differential Scanning Calorimetry, Differential Thermal Analysis and Gel Permeation Chromatography were applied to determine basic materials properties namely density, peak melting temperature and crystallinity, oxidation-induction time and number and weight average molecular weight respectively. Infrared Spectroscopy was also used to detect the presence of any carbonyl peak. All the above mentioned techniques were employed for a limited study into the physical and chemical ageing of the pipe material in order to identify the effect of elevated temperature testing (79°C) on the structure and hence the influence on the fatigue and stress-rupture performance of butt fusion welds in MDPE pipes at 79°C. Before considering the principle of measurement and application of each of the techniques, the sampling procedure adopted for the ageing study is given.

3.1.1 Sampling Procedure

Two series of tests were undertaken in the ageing study on butt fusion welds in 63mm SDR 11 Rigidex 002-50 MDPE pipes. In one case the samples for characterisation analysis were obtained from a butt fusion welded test specimen (see section 3.3.2, figure 3.10(a)) which had been subjected to either internal fluctuating or constant pressure for about 200, 1000, 2000 and 8000 hours of testing at 79°C in a water environment. In the other case the samples were obtained from a butt fusion welded specimen similar to that shown in figure 3.10(a) which was not subjected to any external stress and it is referred to as the

control or untested samples. In the control sample cases, the butt fusion welded specimen was filled with water and simply left in the water tank at 79°C for the ageing time of 200, 1000, 2000, and 8000 hours. The density, DSC, DTA, and IR of the tested and untested butt fusion welded specimens at 79°C for the various ageing times were measured on samples located at the surface, mid-wall and bore region of the butt weld and 15-20mm away from it as shown in figure 3.1. GPC measurements were carried out on samples located away from the butt weld.

3.1.2 Melt Flow Index

Principle and Instrumentation Melt flow index, MFI is the popular test employed to measure gravimetric flow rate of polymer melt extruded from a die of specific length and diameter under prescribed conditions of temperature and pressure. The apparatus consists of a simple piston-type capillary rheometer operating at low shear rates with accurate temperature control maintained thermostatically in order to obtain consistent and reproducible results. The weight extruded in 10 minutes under a standard load and temperature is defined as MFI.

Application Five to eight batches of random samples in the form of small rectangliods of dimensions in the range 2x2x2 to 3x3x3mm were cut from the through pipe thickness of each of the pipe sizes and pipe grades. MFI was determined in accordance with ASTM D1238 procedure (condition E) using a Davenport Melt Indexer Model 3/80 to verify the value quoted by the manufactures and assess the quality of the material.

3.1.3 Gel Permeation Chromatography

Principle and Instrumentation Gel permeation chromatography, GPC, is a rapid, efficient and reliable method of determining molar mass distribution compared to conventional fractionation techniques. The principle behind GPC is very simple. A polymer solution is injected into the column packed with porous gel

beads; as the dissolved polymer molecules flow past the porous beads, they can diffuse into the pore structure of the gel to an extent depending on their size and the pore-size distribution of the gel. Larger molecules can enter only a small fraction of the internal portion of the gel, or are completely excluded and so remain in the solvent going around the beads; smaller polymer molecules penetrate a large fraction of the interior of the gel, so their flow through the column is retarded. In this way, the larger the molecule the less time it spends inside the gel, and the sooner it flows through the column. The different molecular species are eluted from the column in the order of their size (molecular) as distinguished from their molecular weight, the larger emerging first and the molar mass distribution becomes spread out. Analysis of the solution leaving the column (measure of refractive index) therefore allows the complete distribution of molar mass to be determined. Full details of the GPC are discussed by Kirkland (132).

Application Since the Gel permeation chromatography was not available at Brunel University, the determination of the number and weight average molecular weight of the aged samples was carried out by the Rubber and Plastics Research Association, RAPRA, using a Waters Associates ALC/GPC - 501/502 equipment. At least two to three determinations were carried out on each of the untested and tested butt fusion welded pipe of various ageing/testing times.

Gel permeation chromatography was used under the following operating conditions:-

Column	- P.L. gel having pore size of $1x10^6$A, $1x10^4$A, 1x500A
Flow Rate	- 1.0 ml/minute
Solvent	- 1,2 dichlorobenzene stablised with 2,6di-tert-butyl-p-cresol
Temperature	- 140°C
Calibration	- Derived from polystyrene standards.

3.1.4 Density Gradient Column

Principle and Instrumentation Density gradient column technique is the most frequently employed and rapid means of determining the densities of plastics accurately. The basic principle of the technique depends upon the hydrostatic equilibrium between a solid specimen and a liquid of identical density. The apparatus consists of a column which contains a mixture of two liquids whose densities differ. The density of the liquid in the column varies in a linear scale from the top to bottom of the column. The entire tube is surrounded by a constant temperature water jacket which is kept at 23°C.

When a specimen is put into the column, it descends to a point where its density matches that of the solution. The column is calibrated using glass spheres of a known density which are noted in the column, the positon of the specimen is recorded and compared with the standard linear plot of density of floats against the float height.

Application The density of the samples obtained from the location site shown in figure 3.1 of the tested and untested butt fusion welded pipes aged for various times was determined. The samples had no surface roughness so as to prevent bubble formation. No less than three individual determinations were made for each of the sample locations.

The density gradient column was prepared in accordance with ASTM D1505 method B using an isopropanol-water density gradient column having density range of 928.8 to 959.2kgm^{-3} at 23°C.

3.1.5 Differential Scanning Calorimetry

Principle and Instrumentation Differential Scanning Calorimetry, DSC is one of the Thermal Analysis methods used to determine the energy change due to a phase transformation or transition in a polymer. DSC differs fundamentally from

Differential Thermal Analysis, DTA in that the sample and reference are both maintained at the temperature predetermined by the programme even during a thermal event. The amount of energy which has to be supplied to or withdrawn from the sample to maintain zero temperature differential between the sample and the reference is the experimental parameter usually displayed as the ordinate of thermal analysis curve.

The ordinate signal, the rate of energy evolution or absorption by the sample is proportional to specific heat of the sample since the specific heat at any temperature determines the amount of thermal energy necessary to change the sample temperature by a given amount. Any transition accompanied by a change in specific heat produces a discontinuity in the power signal and exothermic or endothermic changes give a peak whose area is proportional to the total enthalpy change. Figure 3.2(a) shows the experimental arrangement.

Critical discussion on DSC instruments and their limitation to measurement of crystallinity are presented by Mandalkern et al (136,137), Hay (138), Stil (139) and Ghijsels and Waals (140).

Application DSC analysis was conducted on a Perkin Elmer DSC-2 with thermal data station. A sample weight of approximately 5mg was used with the heating and cooling rate set at 10 K per minute. A sample size of five from each of the locations (see figure 3.1) was used and for each the peak melting temperature, the onset of melting and the heat of fusion were determined on the first heating run.

The percentage crystallinity was calculated from

$$\% \text{ crystallinity} = \frac{\Delta H_f}{\Delta H_f^o} \times 100 \qquad (3.1)$$

where ΔH_f was the enthalpy of fusion of the sample as obtained from DSC thermogram and ΔH_f^o was the enthalpy of fusion for a

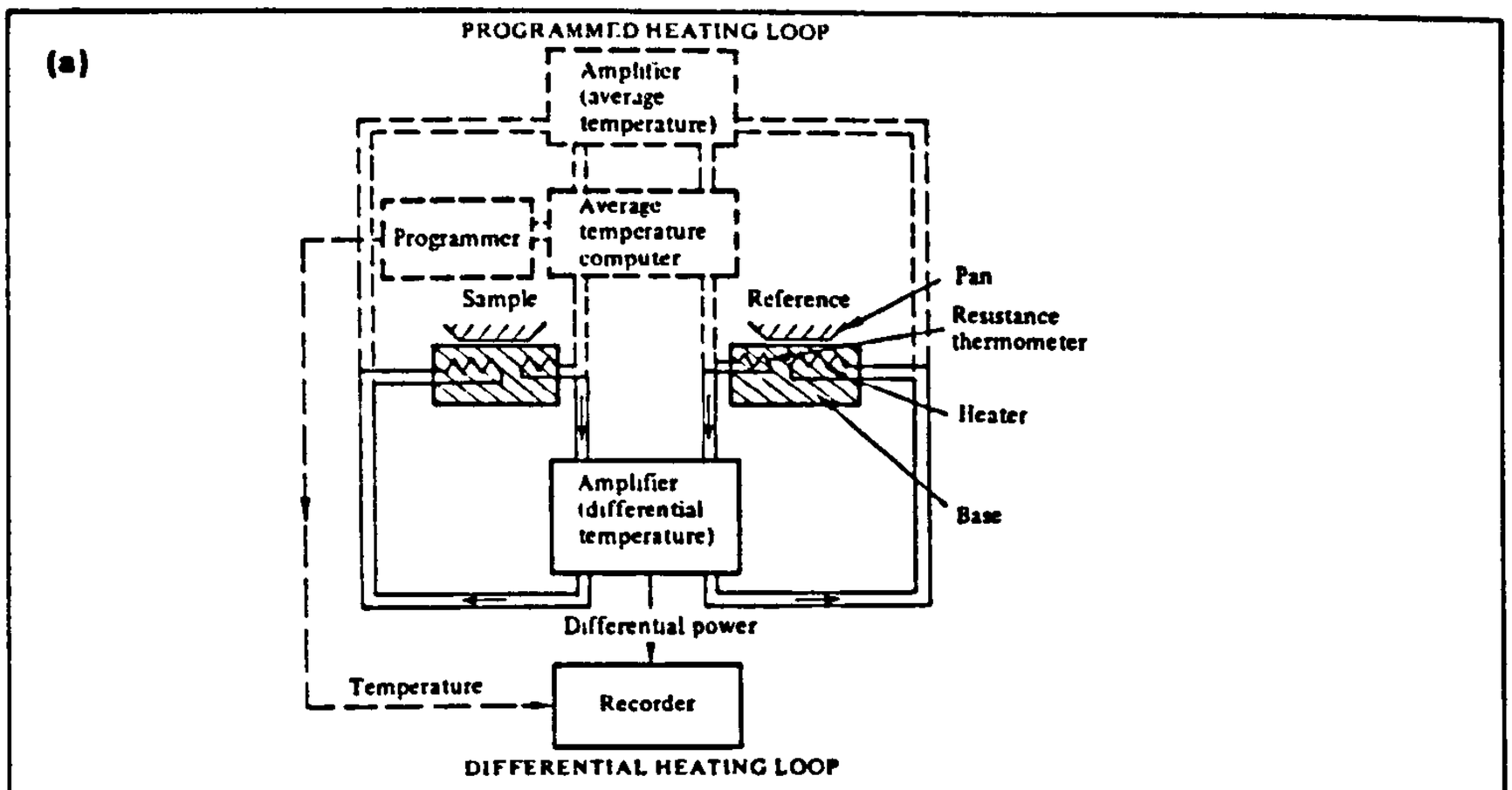

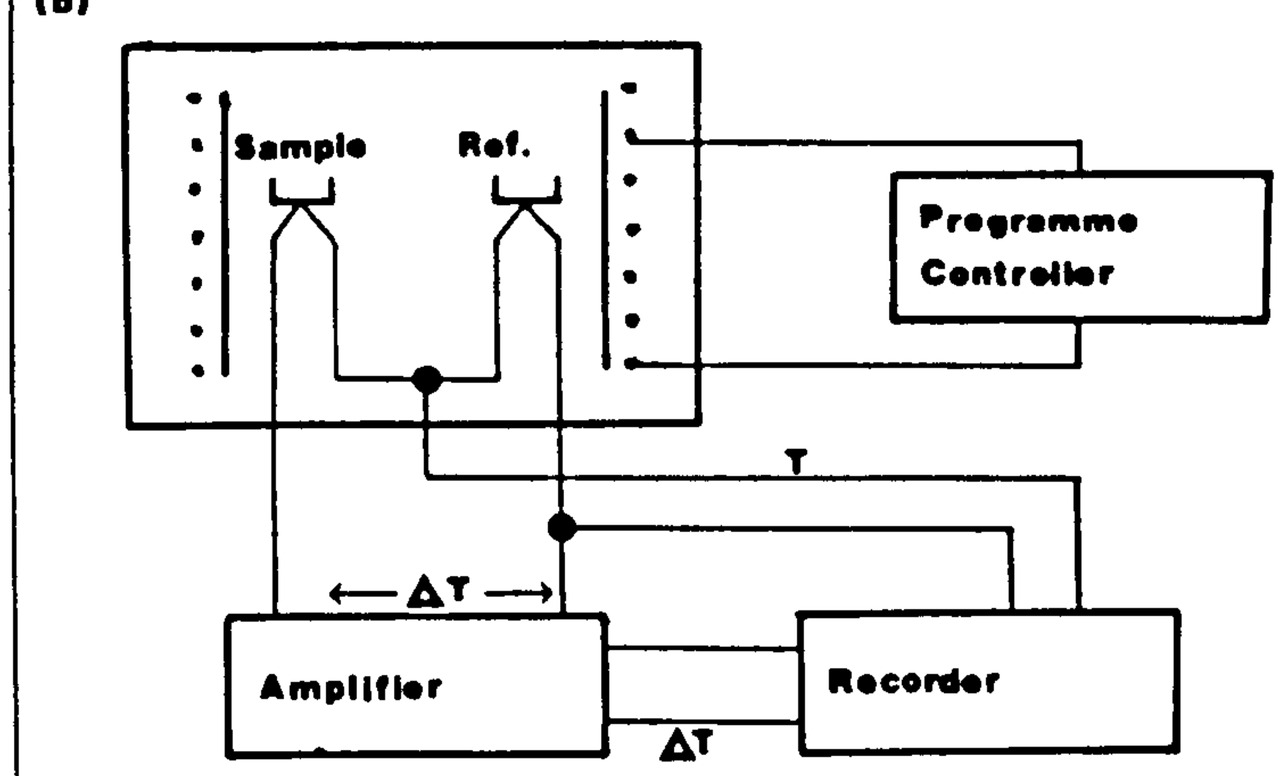

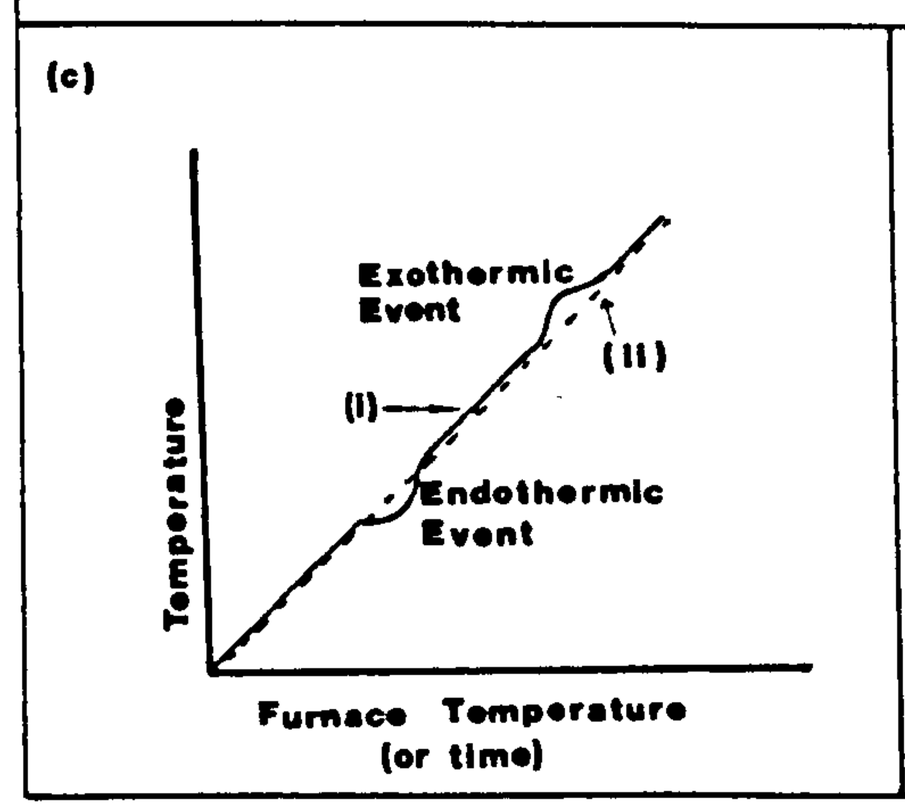

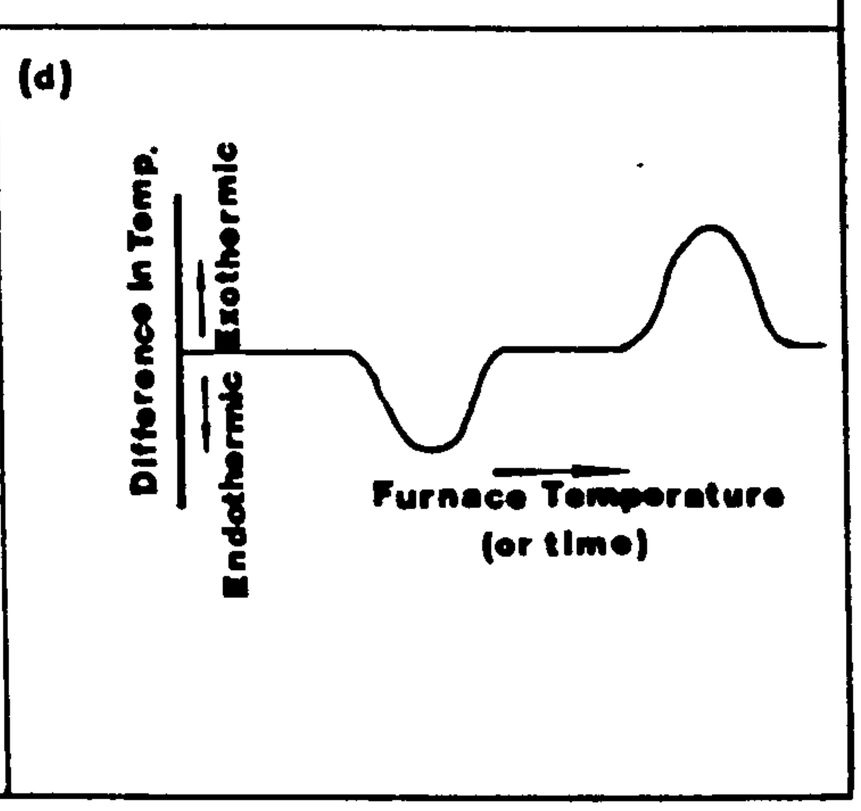

Fig. 3.2(a) Perkin-Elmer Differential scanning calorimeter system.
(b) Instrument circuit daigram for Differential Thermal Appratus
(c) Plots of (i) sample temperature and (ii) programmed temperature against furnace temperature.
(d) Plot of difference in temperature for the same curve.

100% crystalline linear PE. The value of $\Delta H_f^{\ominus}$ was taken as 293 kJ/kg^{-1} (127,137).

In all pipe materials examined pigment was present; the crystallinity values obtained are therefore underestimates as no attempt was made to determine the pigment content to provide for a more accurate crystallinity result. It was also assumed that the pigment dispersion was constant throughout the materials. The results must therefore be considered comparatively and are in no way absolute.

3.1.6 Differential Thermal Analysis

Principle and Instrumentation Differential Thermal Analysis, DTA, is used in the phase transformation and chemical reaction studies. The fundamental difference between DSC and DTA was as mentioned in the previous section. In DTA the sample and a reference material are separately heated in indentical environments. The reference material undergoes no thermal event in the temperature range under study, and therefore its temperature is the same as the programmed temperature throughout the heating, ie the temperature of the reference follows curve (ii) on figure 3.2(c). Hence, a plot of the difference between the sample and reference temperature against the furnace temperature is equivalent to the type of plot shown in figure 3.2(d). The instrument circuit diagram for DTA is shown in figure 3.2(b).

Application A parallel study to the one conducted for DSC measurement of the samples located at site as shown in figure 3.1 of tested and untested butt welds of various testing/ageing times was also carried out to determine the oxidation induction time, OIT which is an indicator of the thermal stability of the polymer. The thermal stability test of the pipe material was undertaken using DTA and followed closely to the test specified in the WAA specification 4-32-04.

Oxidation induction time determination was carried out at Stewarts and Lloyds on their purpose built DTA for the oxidative stability of a polymer. Thin samples of dimensions 3x2x1mm weighing 2-5mg were heated to 200°C in a nitrogen atmosphere to obtain the baseline. The atmosphere was then switched to pure oxygen supplied at a rate of 20ml per minute and the onset time of the main exotherm was measured by the base line extrapolation method. Three individual determinations were made on the samples taken from each of the locations as shown in figure 3.1.

It was assumed that the stabiliser was dispersed uniformly in the pipe material and the oxidation induction time results were considered to be comparative and are in no way absolute.

For any particular stabiliser, its effectiveness is dependent on its concentration in the polymer. However, the concentration of stabiliser in polymer decreases during long-term use. Because stability under which oxidation induction time is determined is a function of antioxidant, induction times can be used to estimate concentration of this component (34). Thermal analysis is regarded as an acceptable monitoring procedure for relative antioxidant content but is not itself an accelerated exposure test (208) and stability decreases caused by processing condition have been pinpointed by this procedure (209).

3.1.7 Infrared Spectroscopy

Principle and Instrumentation Infrared, IR, spectroscopy is used to investigate quantised molecular transition that absorb electromagnatic energy selectively from a broadband infrared source (194). Thus, it requires the spectral analysis of infrared energy transmitted through the sample. The spectral analysis is undertaken with a prism or grating monochrometer. The resulting signals are detected, amplified and recorded.

A molecule will absorb infrared radiation if it vibrates in such a way that its electric dipole moment changes during vibration. As a molecule vibrates, its charge distribution with respect to that origin may or may not change, depending upon the structure of the molecules. Thus not all vibrations of a particular molecular structure will necessarily absorb infrared radiation, but only those vibrations that cause the electric dipole moment to change.

Bascially, the infrared spectrum helps to reveal the structure of a compound by telling us what groups are present in - or absent from - the molecule. A particular group of atoms gives rise to characteristic absorption bands; that is to say, a particular group absorbs light of certain frequencies that are much the same from compound to compound. For example the hydroxyl, OH group of alcohols absorbs strongly at 3200 to 3600cm^{-1}; the carbonyl, C=O group in general around at 1700cm^{-1} the alkyl, CH_3 group at 1450 and 1375cm^{-1}. However, interpretation of an infrared spectrum is not a simple matter. Bands may be obscured by the overlapping of other bands.

Zaitsew et al (53,54) have used IR spectroscopy to examine the thermal degradation produced as a result of welding pipe face at 280°C for three minutes; the carbonyl peak, C=O in the IR spectrum was observed. Gedde et al (127-130) have identified C=O for the 0.1-0.2mm layer removed from the inner surface of thermally oxidised large outside diameter HDPE pipe.

<u>Application</u> Infrared spectroscopy was conducted on thin sections, (less than 4μm in thickness) microtomed from the butt weld in order to identify if any thermal oxidation was occurring at the butt weld of the untested butt welded samples and tested/aged butt welded samples.

A double beam, Perkin Elemer 577 Grating Infrared Spectrophotometer was employed for the analysis. A scan rate of 6 minute was used.

3.2.0 Butt Fusion Welding

3.2.1 Equipment

With the exception of DuPont's Blue Aldyl 322 pipe which needs to be welded on a Fusion Equipment BF2 Machine, all the other pipes (Rigidex 002-60 HDPE and Rigidex 002-50 MDPE) were butt welded on a Mark II butt welding machine manufactured by Haxey Engineering Limited see figure 3.3. The Haxey Butt Welding Machine uses compressed air for moving the shells/clamps, whereas Fusion Equipment BF2 machine uses hydraulics.

Pipes having outside diameters of 63, 90, 125 and 180mm could be butt welded on the Haxey Butt Welding Machine with the apt inserts or re-round clamps for the given outside diameter. It has four inserts; two of which are held in the one side of the machine which moves along the tie bars while the other two are fixed. A fluid operated ram system activates the moveable half of the pipe clamps, the direction of which can be chosen by a two-way selector switch. The rams are pressurised using a compressed air system to the inlet port. This enables component faces to be brought together or separated as required. The pressure gauge on the machine was calibrated by the use of an Instron load cell mounted horizontally in the welding machine, thus allowing an accurate determination of the forces on the pipe ends during welding; the calibration plot is given in figure 3.4.

The hot-plate provided with the Haxey Butt Welding machine was thermostatically controlled. It had a power rating of 1250 Watts and was covered on both faces with PTFE impregnated glass cloth which prevents the molten material adhering to the hot-plate and thus prevents damaging the plasticised surfaces. The temperature of the hot-plate was checked using a Digitron contact digital thermometer. Once the temperature had been set (205°C), it did not vary appreciably with time.

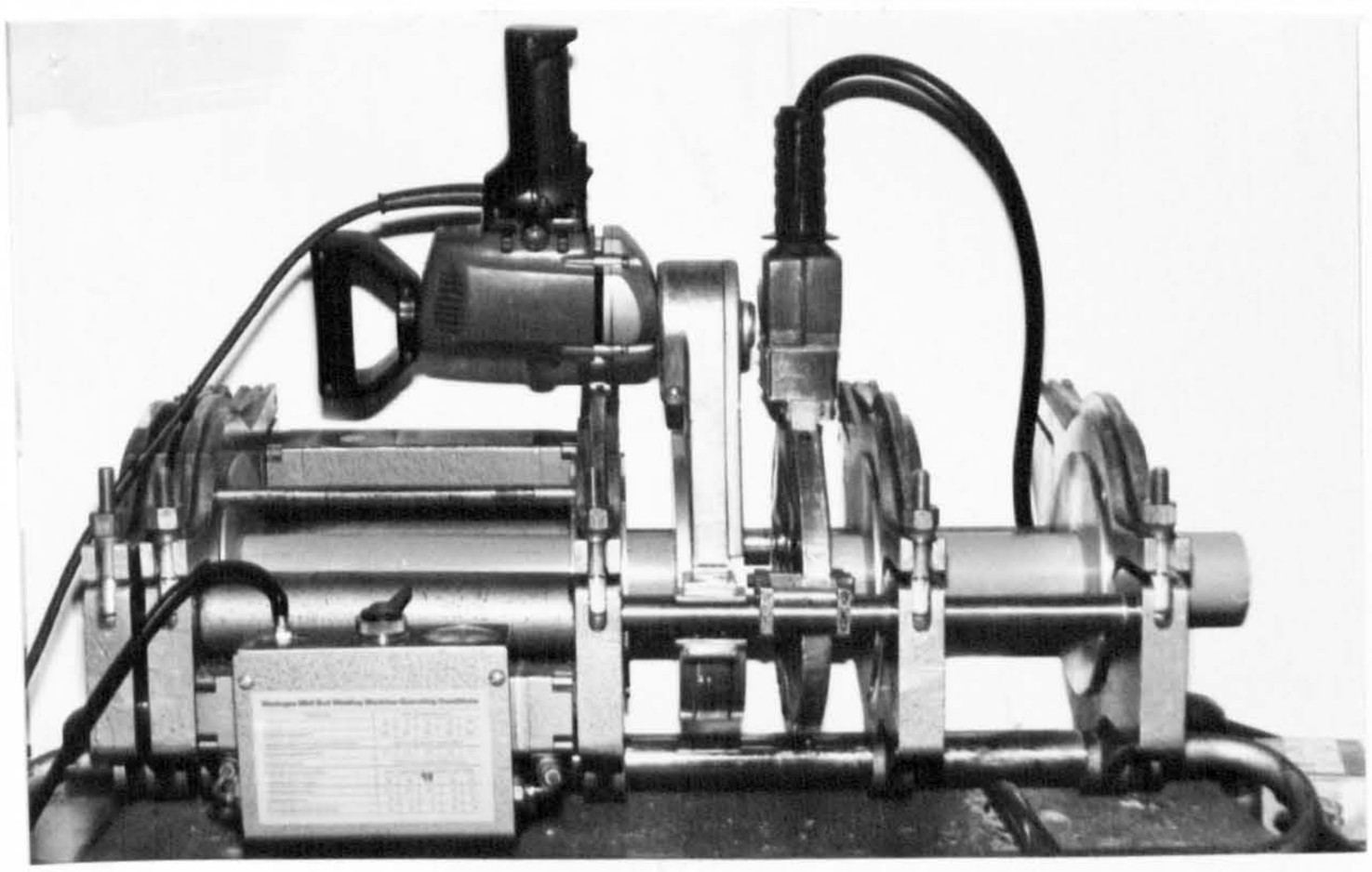

Fig. 3.3 Haxey Mk II Butt Welding Machine.

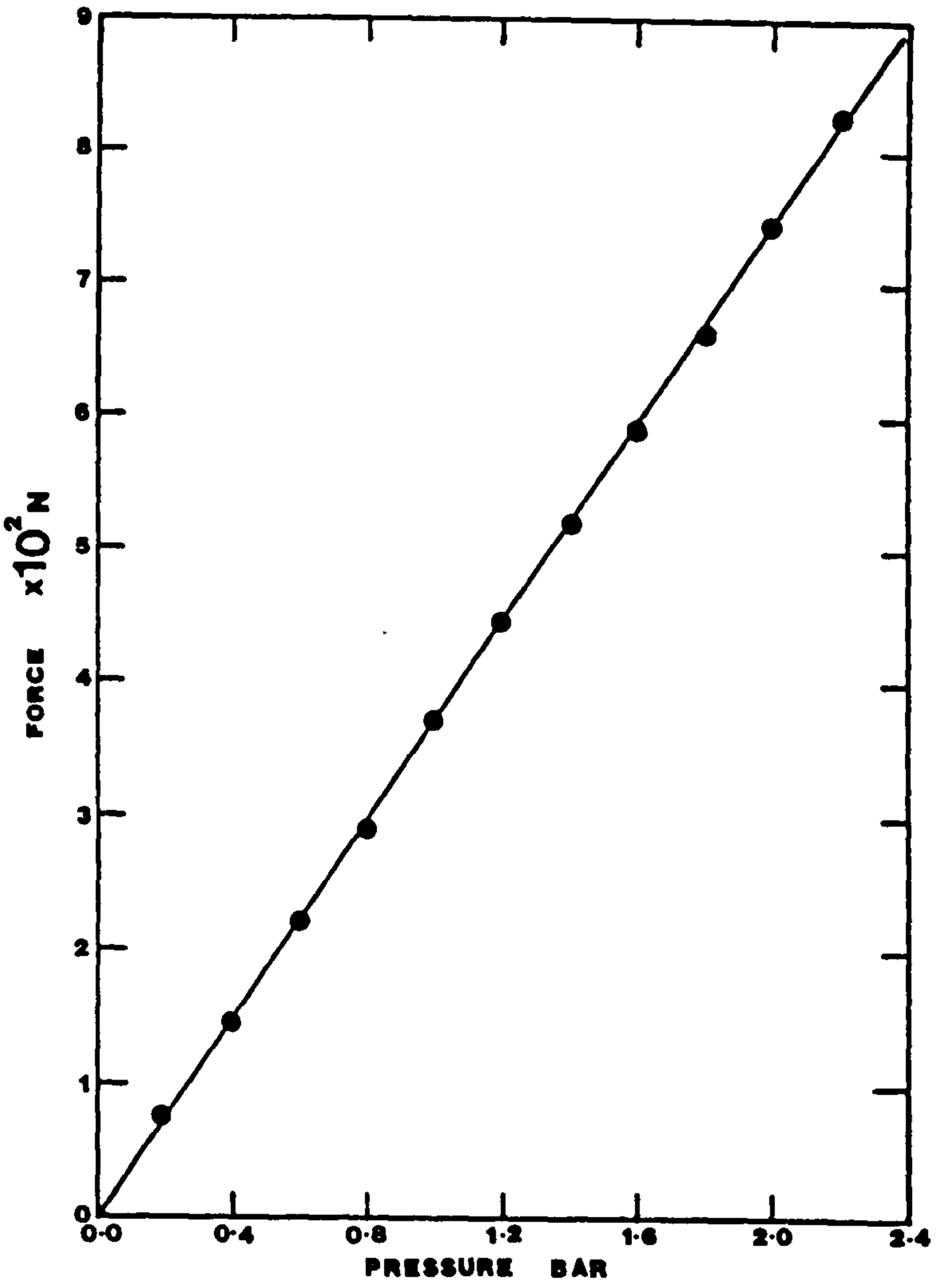

Fig. 3.4 Calibration of pressure gauge on Haxey MK II Butt Welding Machine.

Modification Of Inserts For Axially Misaligned Butt Weld Study

Special sets of inserts were manufactured for the Haxey Butt Welding Machine to produce "controlled" axial misalignment of the butt welds, the definition of nominal axial fractional misalignment is given in figure 3.5. Inserts employed to create misaligned butt welds had their centres off set axially as shown in figure 3.6. Table 3.4 gives the nominal axial offset value for inserts for the three pipe sizes, 63, 90 and 125mm. Inserts having their centres offset axially were manufactured to give nominal axial fractional misalignment of .09, .17, .34 and .44 of the nominal wall thickness for SDR11, 63, 90 and 125mm pipe systems.

3.2.2 Procedure

Butt fusion welded samples were produced in batches of 20-25 samples at a time for each of the axial misalignments under a constant welding condition for the fatigue and stress-rupture test programmes. The welding conditions adopted were those recommmeded by the manufactures of the Butt Fusion Welding Machines and pipe manufactures. All steps during the welding process and the specific conditions are tabulated for the Rigidex 002-60 HDPE and Rigidex 002-50 MDPE and three pipe sizes in table 3.5(a) and for DuPont Blue Aldyl 322 MDPE in table 3.5(b). Table 3.6 gives the range of welding conditions which were used for the limited investigation into the influences of welding conditions on fatigue performance of aligned butt welds.

In general butt fusion welding is a three step process; weld bead formation, heat soak and weld formation. The welding cycle is shown schematically in figure 2.4 in terms of pressure against time.

In all the cases the two pipes to be butt welded were obtained from one continuous pipe length and placed into the clamps with the permanent pipe markings aligned. This was carried out to minimise undue mismatch due to variation in outside diameter,

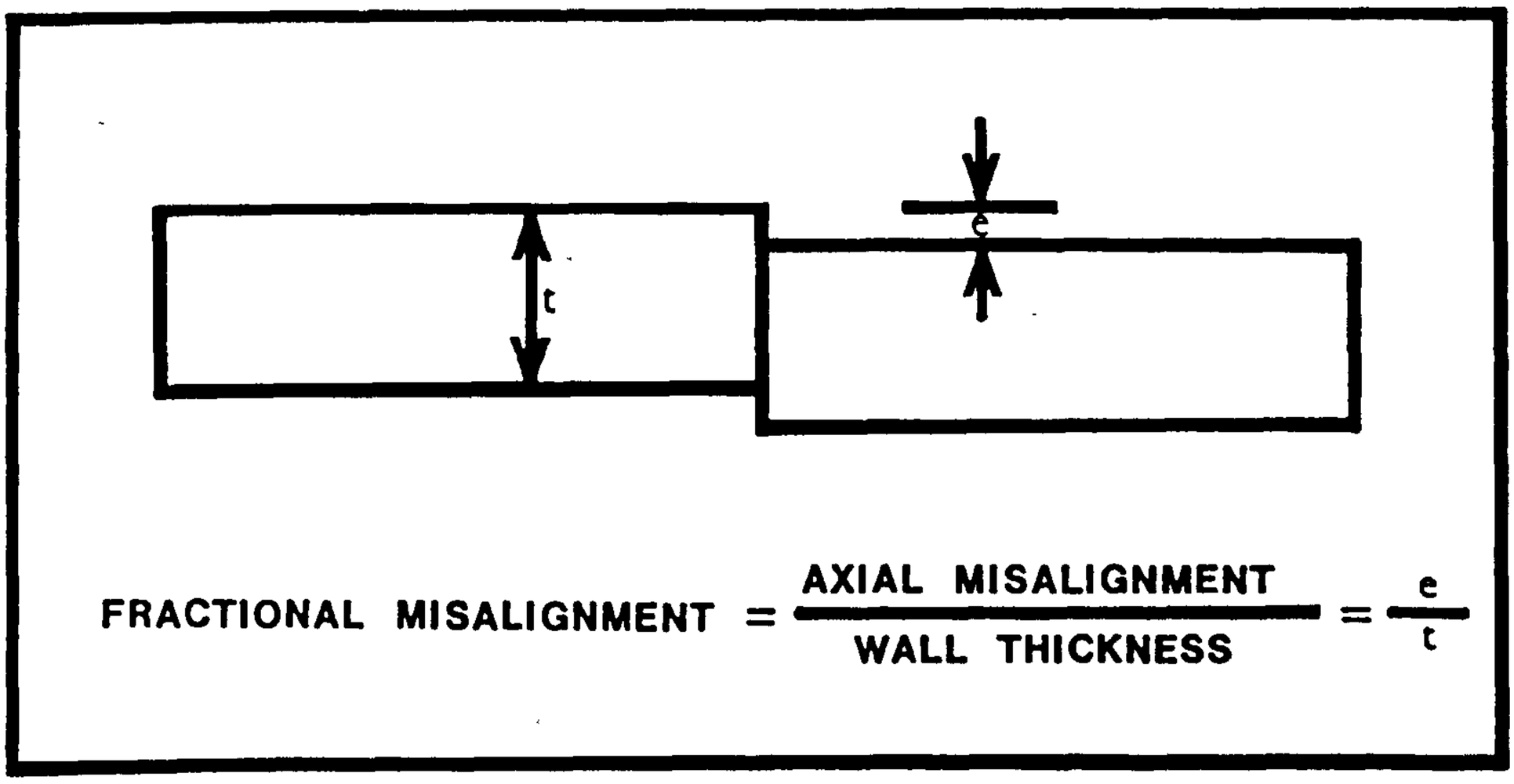

Fig. 3.5 Definition of fractional misalignment.

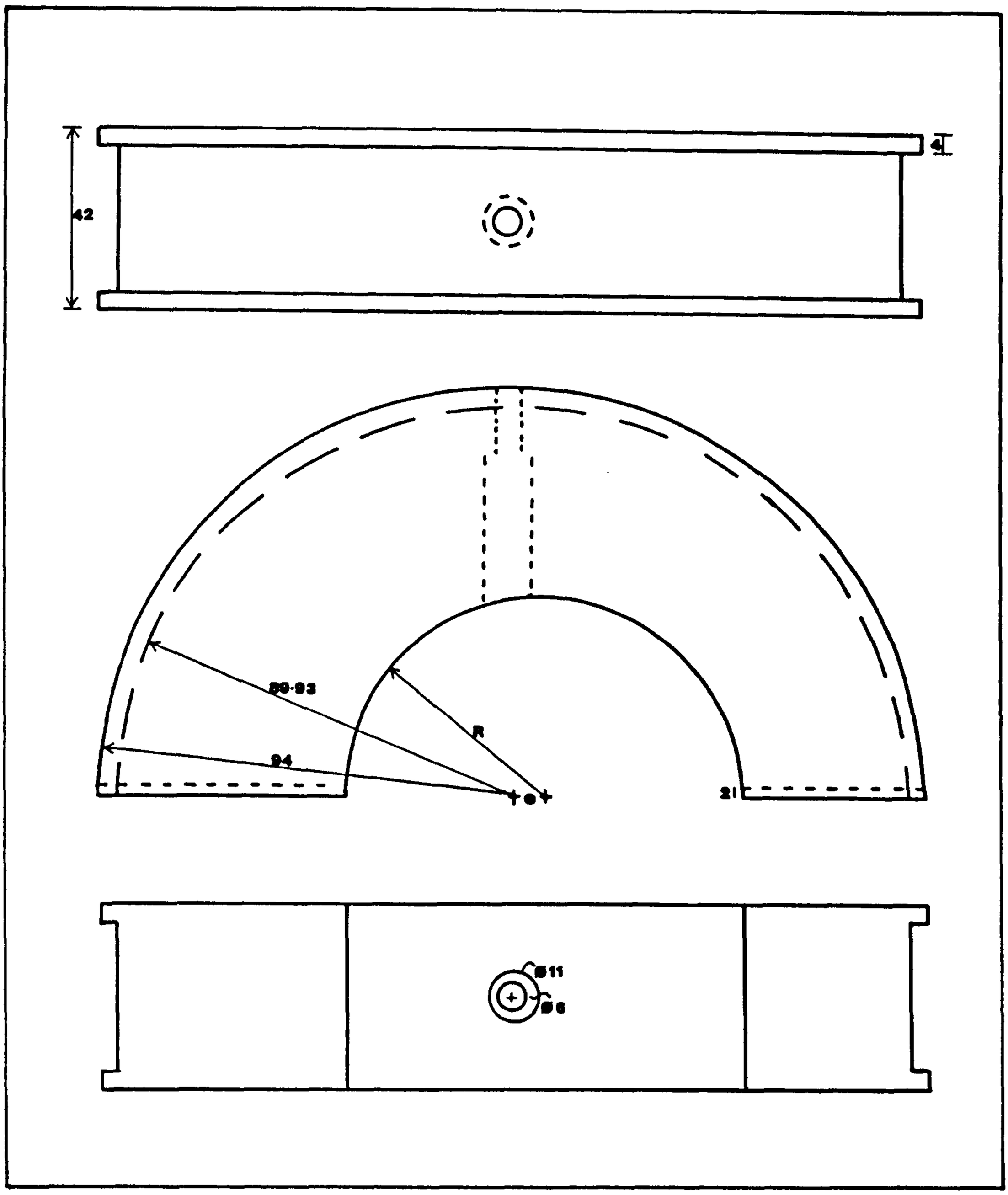

Fig. 3.6 Axial offset of the insert for Haxey MK II Butt Welding Machine. Diagram showing the top segment of the misaligned insert set.

Table 3.4 Axial Offset values of various inserts for the Haxey Butt Welding Machine.

Pipe Diameter, mm	Axial Offset of Inserts, mm			
	Nominal Fractional Misalignment			
	.09	.17	.35	.44
63	0.5	1.0	2.0	2.5
90	0.7	1.4	-	3.6
125	1.0	2.0	-	5.0

Table 3.5(a) The welding conditions used to butt weld Rigidex 002-60, HDPE and Rigidex 002-50, MDPE pipe on Haxey Butt Welding Machine. Pressures given in the table are those read from the pressure gauge on the machine.

Welding Parameter		Pipe Diameter, mm		
		63	90	125
Heater Plate Temperature,	°C	205±5	205±5	205±5
Initial Heating Pressure,	Bar	0.2 for 33 secs.	0.4 for 35 secs.	0.8 for 40 secs.
Heat Soak Time,	secs.	63±2	75±1	110±1
Heater Removal Time,	secs.	6±1	6±1	6±1
Welding Pressure,	Bar	0.4	0.8	1.6
Welding Time,	secs.	300	300	600

Table 3.5(b) The welding conditons for DuPont's Blue Aldyl 322A on the Fusion Equipment Limited BF2 machine.

Welding Parameter		
Heater Plate Temperature,	°C	205
Initial Heating Pressure,	Bar	20+Drag
Heat Soak Time,	secs.	15
Welding Pressure,	Bar	20+Drag
Welding Time,	secs.	180-300

Table 3.6 Independent effect of three welding variables which were examined.

Welding Parameter		
Heat Soak Time,	secs.	30, 180
Heat Removal Time		2xstandard, 3xstandard
Welding Pressure		0.5xstandard, 2xstandard

wall thickness and ovality. Despite the care taken to ensure to reduce unwanted misalignment some misalignment was present in nominally aligned butt welds and variations from the nominal value in "controlled" misaligned butt welds were found. Table 3.8 gives the variation in misalignment from nominal values as measured according to method described in next section.

3.2.3 Misalignment Measurement

The axial misalignment, of the butt weld was measured in order to determine the variation on the nominal "controlled value". The principle of how to determine the axial misalignment is schematically illustrated in figure 3.7 and figure 3.8 shows the apparatus used to determine the axial misalignment.

The measurement was carried out using an engineering surface plate, 'V' - blocks, cylindrical weights and a dial gauge having an accuracy of 0.01mm. The dial gauge was zeroed at a reference point and readings were taken 5mm from the weld bead on both sides of the butt weld, and at 10mm away from centre of the butt weld. The difference in the readings taken at 5mm from the weld bead was used to define the actual axial misalignment. Readings were also taken at a distance of 20mm from the centre of the butt weld and thereafter at an interval of 10mm up to 70mm on the both sides of the butt weld along a straight line. These readings were used to determine an extrapolated regression value. The latter method excludes the region next to the weld where shrinkage has occurred due to relaxation of residual stresses after the butt welding. Table 3.7 gives typical readings taken for a butt weld having a nominal axial misalignment of 1.0mm and the table also shows how the actual and regression misalignments were determined. Generally, no difference was found in the actual and regression misalignment values. However, it was the measured actual misalignment values of the failed butt welds which were used in analysis in later chapter.

Table 3.7 Typical measurement readings for the determination of axial misalignment. (Nominal axial misalignment = 1mm)

	Distance From The Butt Weld, mm							
	5	10	20	30	40	50	60	70
Reading taken on RHS of Butt Weld	-.2	-.11	+.01	+.01	.00	.00	.00	.00 (ref)
Reading taken on LHS of Butt Weld	+.78	+.89	+.88	+.78	+.66	+.53	+.44	+.35
Difference	1.07	1.00	.87	.77	.66	.53	.44	.35

Actual/measured misalignment = 1.07mm

Misalignment based on Regression Analysis of reading taken between 20 and 70mm away from butt weld = 1.08mm

Correlation Coefficient = .998

Table 3.8 The mean, standard deviation and the range of the measured axially misaligned butt weld for a given batch (20 samples) of nominal misaligned butt welds in 63mm pipe.

	Measured Axial Misalignment, mm		
Nominal Axial Misalignment, mm	Mean	Minimum	Maximum
0.0	0.09±.06	0.01	0.24
0.5	0.48±.11	0.33	0.68
1.0	0.89±.18	0.63	1.17
2.0	2.04±.13	1.82	2.31
2.5	2.42±.16	2.07	2.65

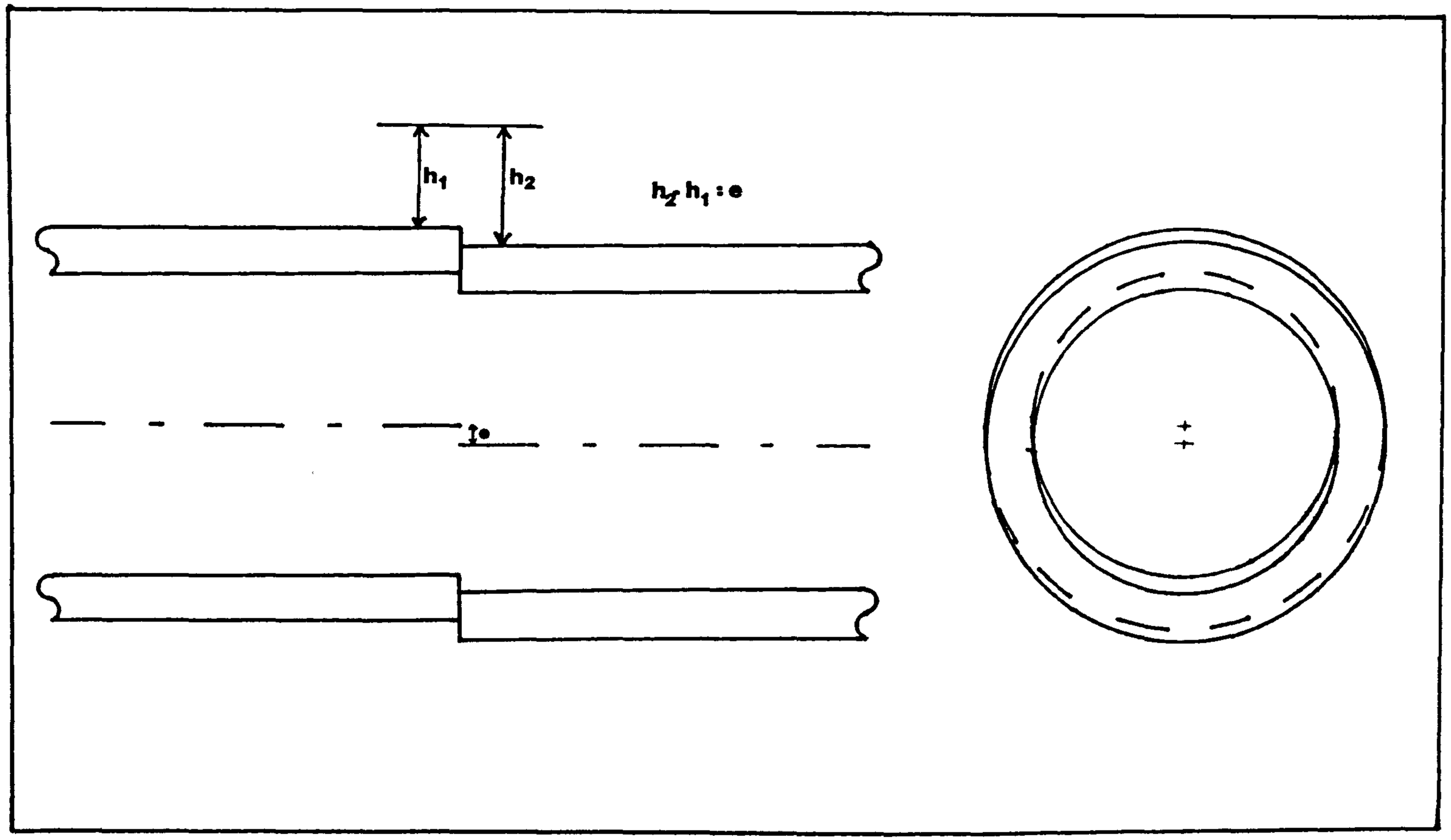

Fig. 3.7 Schematic representation of the main principle involved in determining the axial misalignment.

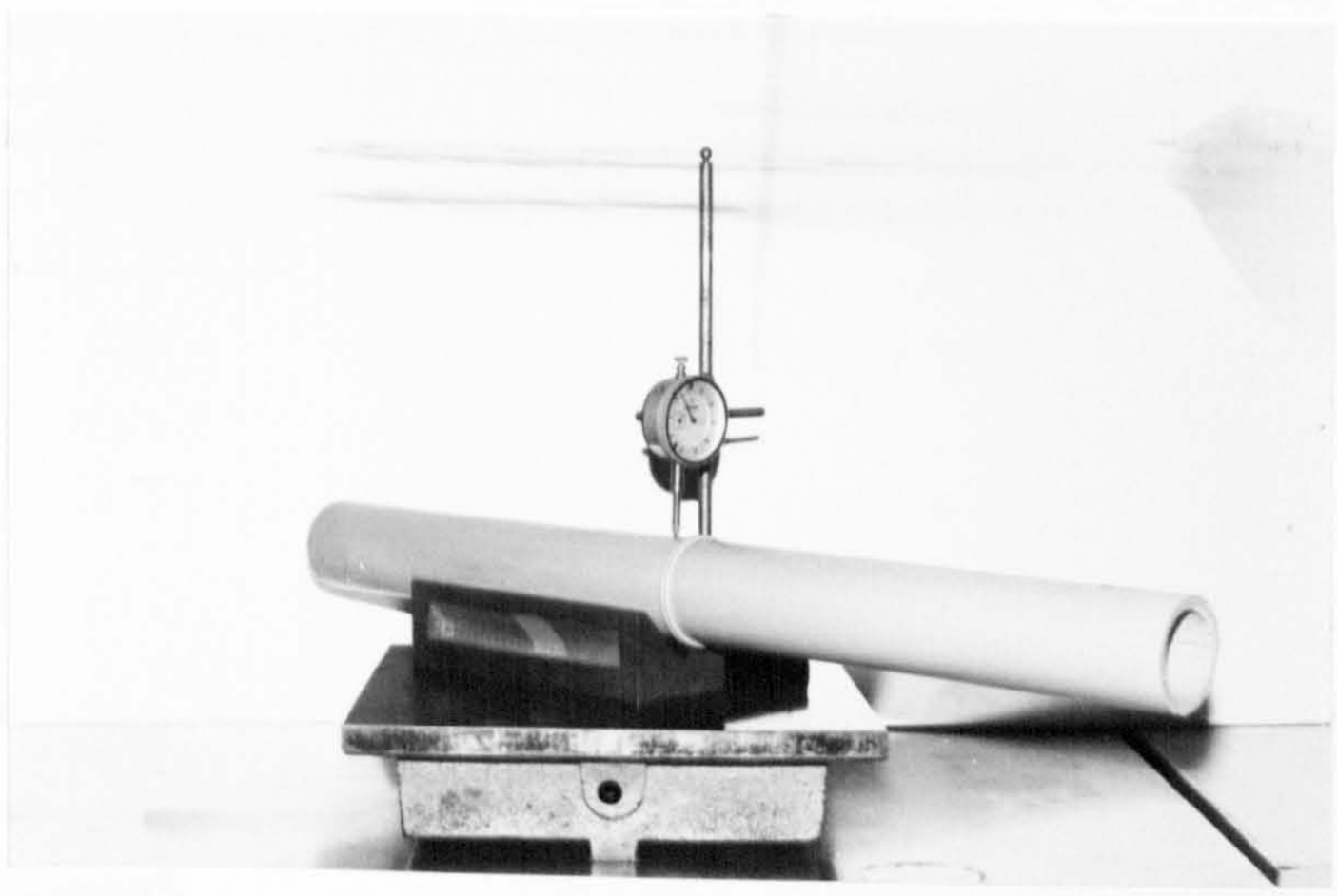

Fig.3.8 Apparatus used for the determination of axial misalignment.

3.3.0 Internal Pressure Testing

A laboratory was allocated and equiped for the purpose of internal pressure testing thermoplastics pipe systems with the following objectives in mind:-

(i) To test thermoplastics pipe systems with a range of outside diameters from 63mm up to 125mm.

(ii) To test as many pipe systems as possible at any time within the available space.

(iii) To test the pipe systems under a wide range of pressures and temperatures.

(iv) To enable a comparison of failure behaviour to be made for the pipe systems in two different modes of internal pressure testing, namely under constant pressure, that is stress rupture or creep or static fatigue testing, and under fluctuating pressure, that is fatigue or dynamic fatigue or intermittent creep testing.

These guidelines have led to to a flexible, reliable and comparatively inexpensive pressure testing facility.

3.3.1 Equipment

Descriptions of the equipment used for internal pressure testing of the thermoplastics pipe systems is given below.

(i) Testing Tank Four glass reinforced polyester tanks supplied by various manufactures were available for use. All the tanks were side insulated by 102mm thick polystyrene foam held by 6mm thick plywood. The tank bases were supported and also insulated by 13mm thick Tico-asphalate and the floor of the pipe room had rubberised anti-vibration pads on the concrete base.

Two small tanks had internal dimensions of 1.83x0.91x0.91 meters and two large tanks had internal dimensions of 1.83x0.91x1.22 meters. The maximum number of pipe samples which could be placed in the tank for each of pipe size of 63, 90 and 125mm was 150, 135 and 60 respectively. This was true for both the small and large tanks except that large tank could accommodate longer sample length (1.2m) compared to small tank (0.9m). The tanks were used continuously and contained ordinary tap water at a maximum temperature of 80°C.

One small tank was allocated for the fatigue tests at 79°C. All the 63mm pipes were tested first followed by 90mm and finally by 125mm. The total number of fatigue test samples on test in the small tank varied depending on the pipe size and availability of fatigue stations, but the maximum was 40.

Another small tank was allocated for fatigue testing at 69°C and at 59°C. This lower temperature work was carried out at a much later date in the test programme due to lack of availability of fatigue test stations. The total number of samples on test at 69°C was 8 for 63mm and 6 for 90mm pipe system.

One large tank was allocated for the stress-rupture testing at 79°C of pipe sizes 63, 90, and 125mm. The total number of samples which initially had to be maintained was 52. However this number was diminishing with time as samples failed.

Note then the total number of test samples (fatigue and stress-rupture) which had to be maintained in the pipe testing laboratory was about 100.

(ii) Heaters A total of eight heaters were available for heating the water. Six heaters were from Cornair Churchill and two of UTAC heaters. Three heaters were normally required on each of the fatigue and stress-rupture testing tanks for maintaining 79°C water bath. One heater was used for

maintaining the 69°C water bath and one spare heater was always available for emergency purposes.

Water in the tank was circulated by the pumping action of the heaters and the temperature of the water was monitored continuously using a digital thermometer. Checks on the thermal layering effect were made and it was found that the there was little variation (±0.2°C) in temperature of the water with the location or depth. Temperature control on the heaters kept the set temperature to within ± 0.5°C. Temperature variation of ± 1°C is allowed by BS 4728 and ± 2°C by ASTM D1598.

Regular maintenance work on the heaters was of paramount important as scale accumulated either in the pump or the heater element with time such that pumping action and/or control of water temperature became inefficient.

(The tap water in the Uxbridge area where all pressure tests were carried out was fairly hard, containing significant amounts of lime (calcium carbonate) which tended to coat the exposed surface of the pipe systems mainfesting itself as a fine whitesh film. A similar effect was observed on the fracture surface.)

(iii) Compressor Compressed air to the laboratory was supplied using a Atlas Copco Compressor. Figure 3.9 shows schematically the layout of the main supply line for compressed air and the seven branch/take off points available in the pipe testing laboratory. The main supply line was maintained at maximum gauge pressure of 14 bar (200psi) which decayed to minimum gauge pressure of 10.5 bar (150psi). This minimum gauge pressure in supply line corresponded to the lower limit to activate the compressor automatically. The compressor switched itself off when pressure had climbed up to maximum of 14 bar.

The time at which the maximum gauge pressure in the supply decayed to minimum gauge pressure depended on the demand of compressed air (on the number of outlets in use) and therefore

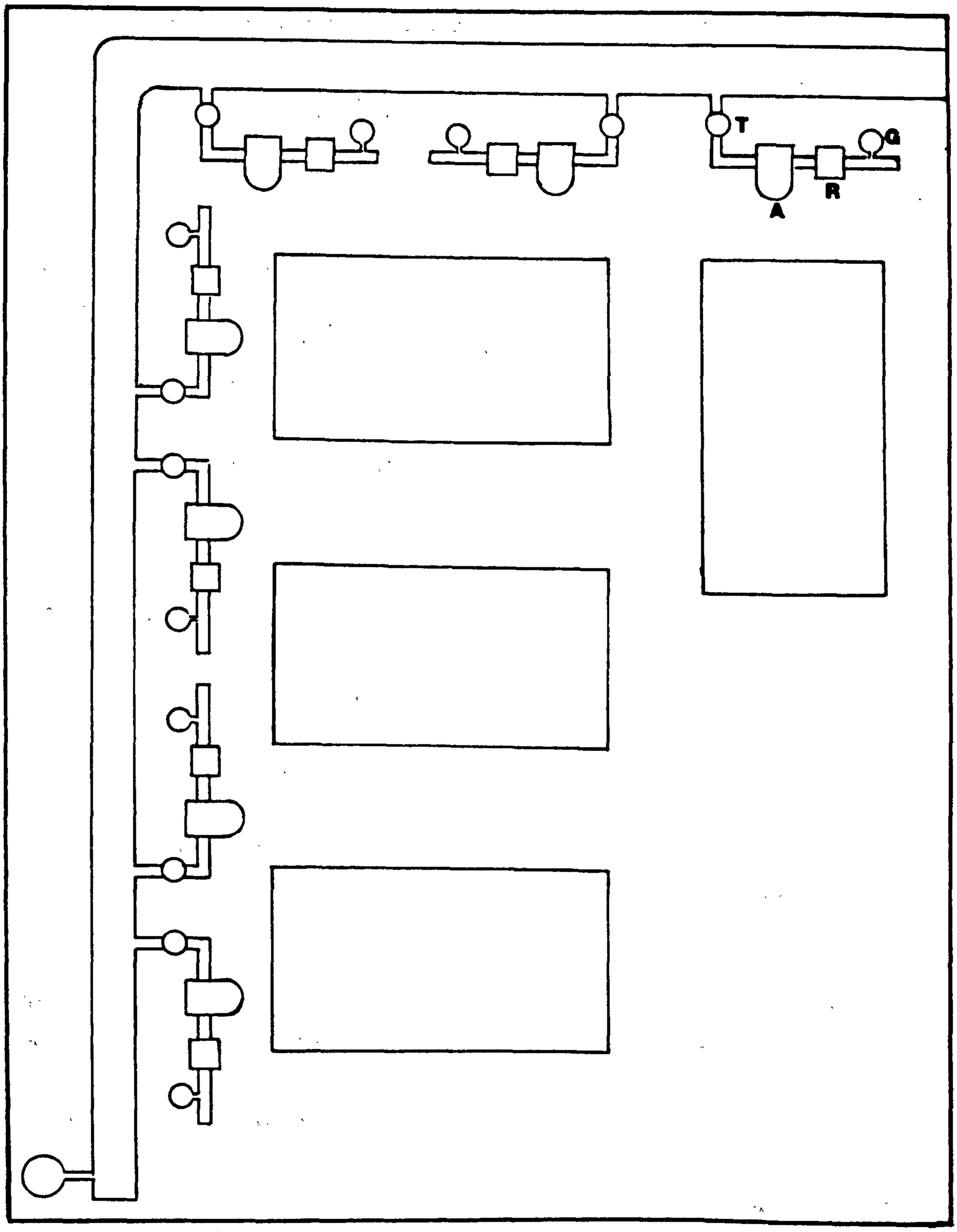

Fig 3.9 Lay-out of the main compressed air supply line and take off branche and also the testing tanks in the pipe testing laboratory.

G - Pressure Gauge, R - Air Regulator, A - Air Filter, T - Tap

the number of fatigue samples on test. Since all these were in use the decay time was 20 minutes; consequently the compressor was switching on three times per hour.

The decay of pressure in the main supply line resulted in apressure drop of 0.2bars for the test samples subjected to a maximum pressure of 9.5 bars. The pressure would thus drop to 9.3 bar, this pressure would climb back to 9.5 as soon as the supply pressure reached 12 bar. No pressure drop was experienced by the test sample subjected to pressure of less than 9.0 bar. (Pressure variation of ±2% is allowed by BS 4728 and only ±1% by ASTM D1598-76.)

3.3.2 Test Samples

The test specimens had one central butt weld which was 3 to 5 outside diameters away from the end caps depending on the pipe size and in no case was the butt weld less than 250mm away from the end cap. The dimensions of the test samples conform to WAA specification 4-32-04 and well within the BS 4728 and ASTM D1598. Figure 3.10(a) shows schematically a typical test specimen.

Of the various types of end closures available for the pipe system, the plastic (PE) end caps were preferred because the number of test sample to be tested at any one time was large (≈100) and the range of pipe sizes examined was wide. PE end caps were welded onto the pipe ends using a socket fusion tool. The only disadvantage of using PE end caps was that at times they failed earlier than the test weld thus interrupting the test and also creating unnecessary extra work in removing the failed end cap and replacing it with the new one. Figure 3.10(b) shows a detailed view of a top end cap which involved boring a 15.8mm (⅝") hole through the end cap and tightening a 15.8(⅝") bulk head fittings before welding on the top end cap.

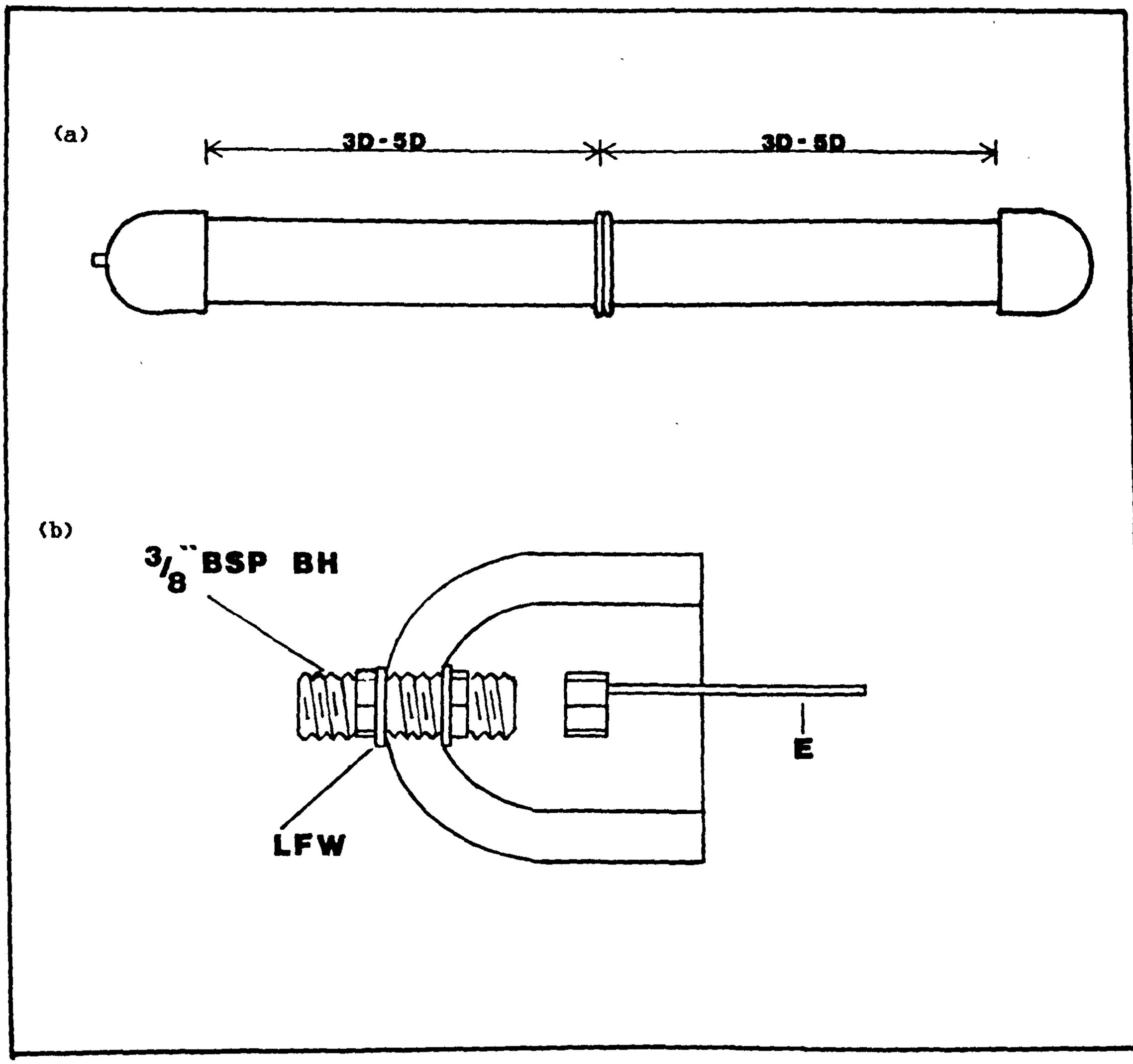

Fig. 3.10(a) Test specimen. (b) Detail - view of Top end Cap.
BH = Bulk Head Fitting LFW=Lucas Fluid Washer E=Electrode

The outside diameter and the wall thickness of each of the samples was measured at six different places in accordance with ASTM D2122. The local wall thickness near the failure site was also measured. The average minimum wall thickness (ie average of minimum wall thickness and the local wall thickness near the failure site) and average outside diameter of the pipe was used for calculating the hoop and axial stresses in the pipe.

The test samples were conditioned for 24 hours at the test temperature before commencing the fatigue or stress-rupture test. A sample size of four was used for each test pressure range except for the maximum test pressure range (9.5 bar) where a sample size of eight was used. The total number of butt welded samples tested in the programme are summarised below:

	Number of Butt Welded Samples					
	Fatigue Testing			Stress-Rupture Testing		
Material	Pipe Outside Diameter mm			Pipe Outside Diameter mm		
	63	90	125	63	90	125
Rigidex 002-60	34	-	-	24	-	-
Rigides 002-50	130	85	22	31	20	20
Blue Aldyl 322	12	-	-	-	-	-

Total number of samples tested = 378

3.3.3 Fatigue Testing

The arrangement employed for fatigue testing the pipe systems is shown in figure 3.11(a). Compressed air top loaded the water filled systems to provide the desired internal pressure which was made to cycle between zero gauge pressure and set maximum in the following manner. Compressed air from the regulator was supplied to a five-way solenoid valve. The five-way solenoid valve, controlled by an electronic timer, enabled compressed air

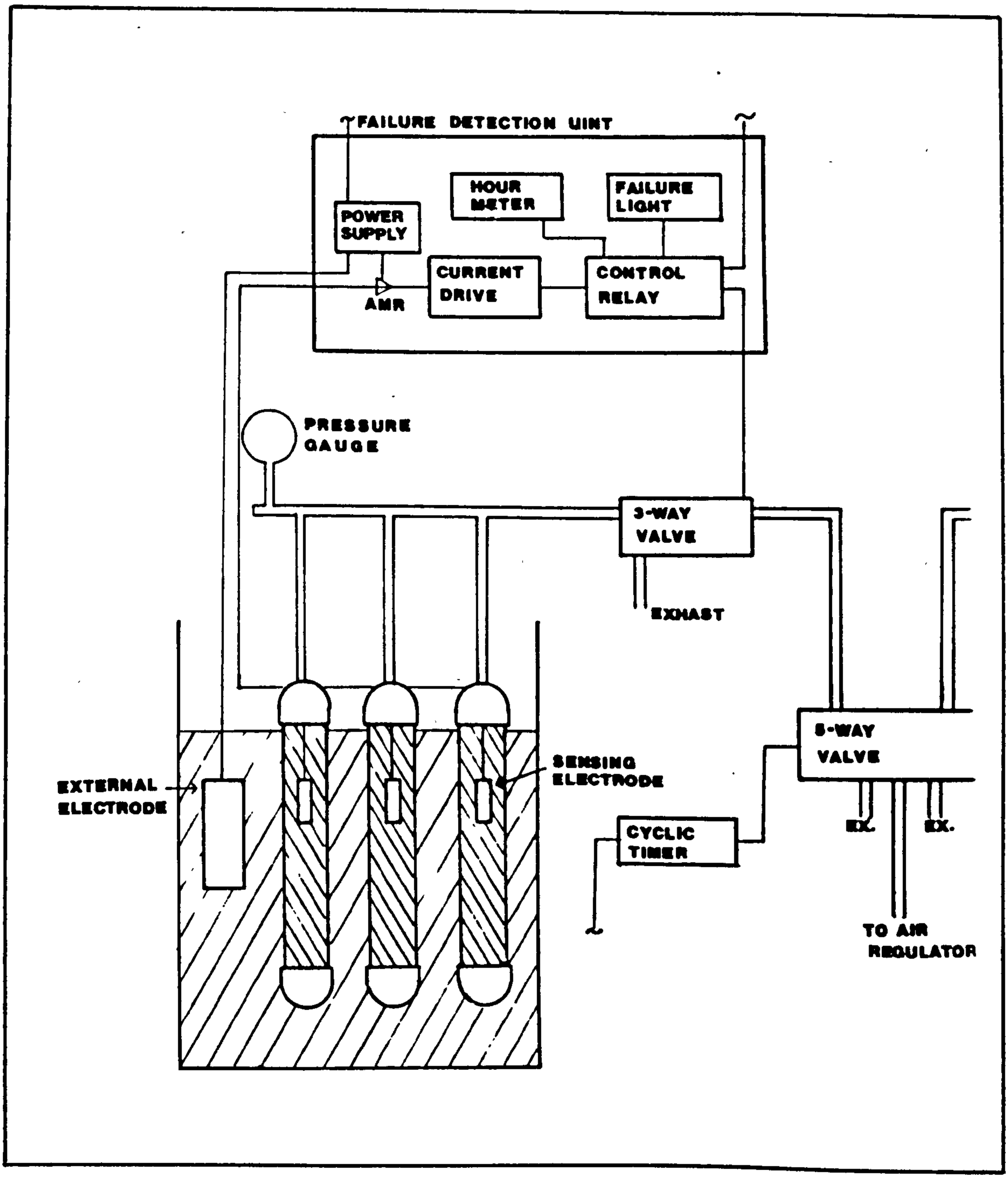

Fig. 3.11(a) Experimential arrangement for internal fatigue testing of pipes.

to fluctuate between the two outlet ports from which compressed air was directed to the system to internally pressurise and depressurise the water filled pipe samples at a set frequency. Compressed air was delivered to the samples via a normally open three way solenoid valve positioned between the five way valve and the samples under test. When a failure was detected by the failure detection system, the three way solenoid valve was actuated such that it would exhaust (depressurise) the sample and cut-off the supply from the five way-valve. At the same time it also stopped the timer on the failure detection unit. The details of how the failure detection units work are given in section 3.3.5.

The maximum number of samples which could be fatigue tested on one five-way solenoid valve depended on the rate of pressurisation which itself was a function of the pipe size and frequency. The maximum number of samples on test on a five-way solenoid valve was eight for 63mm pipe systems, six for 90mm pipe systems and four for 125mm pipe systems.

Variables:

(i) Pressure Range For all the internal pressure fatigue tests, the internal pressure was cycled between zero gauge pressure and the set maximum pressure giving a stress ratio $R(\sigma_{min}/\sigma_{max})$ of zero. Three different pressure ranges were applied in the test programme: 6.5, 8.0 and 9.5 bar and these correspond to nominal hoop stress ranges of 3.29, 4.05, and 4.81MNm^{-2} for SDR11 pipe system. These stress ranges were selected to induce the brittle mode of failure.

(ii) Frequency Test frequency was kept constant throughout the fatigue testing programme at .083Hz (5 cpm). This frequency was close to the decay frequency experiencd by water distribution system due to pressure surges.

(iii) Pressure/Time Testing Profile - Wave Form Internal test pressures were monitored by means of glycerine filled pressure gauges placed in the pressurising line and the pressure profile constructed from the measured time to reach the maximum pressure, t_r and time to drop to the minimum pressure, t_d.

The values of t_r and t_d were determined using a stopwatch accurate to .1 second; this was made possible because of the very low frequency employed in the test (5 cpm). Table 3.9(a) lists such average values together with variations in these values caused by the loss of water in the test samples which decreased the rate of pressurisation, whilst table 3.9(b) gives the rate of pressurisation and depressurisation based on t_r and t_d values. In general, a trapezoidal type of wave form was applied. However, the wave from was not identical for each of the pipe sizes as apparent from t_r and t_d values in table 3.9(a). Figure 3.12 shows schematically a series of pressure profiles as constructed form the knowledge of t_r, t_d and applied frequency for different pressure ranges and different pipe sizes.

Note the loss of water in the samples was via water vapour during each depressurising part of the cycle and this effect was prominent for the test pressure range of 9.5 bar. The loss of water consequently decreased the rate of pressurisation. To minimise this effect and to maintain the rate of pressurisation more or less constant over its entire test specimen life, all the fatigue tests had to be interrupted in order to top-up the samples with water every 24 hours. This problem was inherent due to the nature of fatigue test method employed.

(iv) Test Temperature The majority of the fatigue tests were carried out at 79±1°C. However, a limited test were conducted at 69±1°C and 59±1°C.

Table 3.9(a) Measured time to reach the maximum pressure, t_r and time taken to fall to minimum pressure, t_d in seconds at three different pressure ranges at 79°C and frequency of 5 cpm.

	Pressure Range, bar					
	6.5		8.0		9.5	
Pipe Outside Diameter, mm	t_r	t_d	t_r	t_d	t_r	t_d
63	0.7±.1	2.0±.2	1.0±.2	2.1±.3	1.6±.4	2.2±.5
90	1.1±.1	2.3±.2	1.4±.3	2.6±.4	1.9±.7	3.1±1
125	1.4±.3	2.5±.4	-	-	2.5±.7	3.2±.9

Table 3.9(b) Rate of pressurisation, R_p and depressurisation, R_d at three different pressure ranges at 79°C and frequecy of 5 cpm derived from t_r and t_d values.

	Pressurisation Rate, bars/sec. (corresponding Hoop stress rate $MNm^{-2}s^{-1}$)					
	Pressure Range, bar					
	6.5		8.0		9.5	
Pipe Outside Diameter, mm	t_r	t_d	t_r	t_d	t_r	t_d
63	9.30 (4.65)	3.25 (1.65)	8.00 (4.00)	3.80 (1.90)	5.95 (2.95)	4.30 (2.15)
90	5.91 (2.95)	2.83 (1.41)	5.70 (2.85)	3.10 (1.55)	5.00 (2.50)	3.07 (1.53)
125	4.64 (2.32)	2.60 (1.30)	- -	- -	3.80 (1.90)	2.97 (1.48)

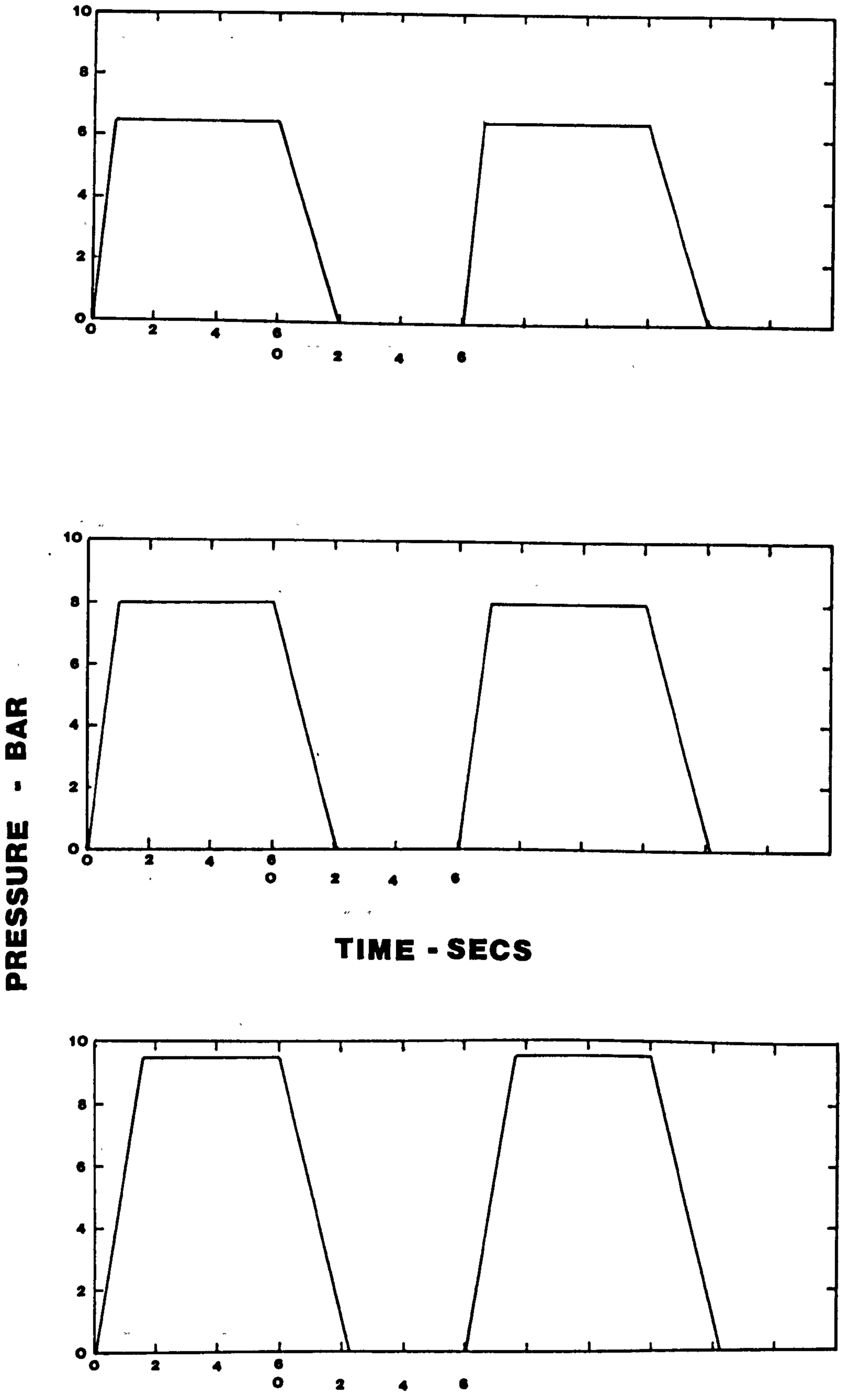

Fig. 3.12(a) Schematic pressure profile based on measured time to reach the maximum pressure and time to reach the minimum pressure for 63mm pipe systems.

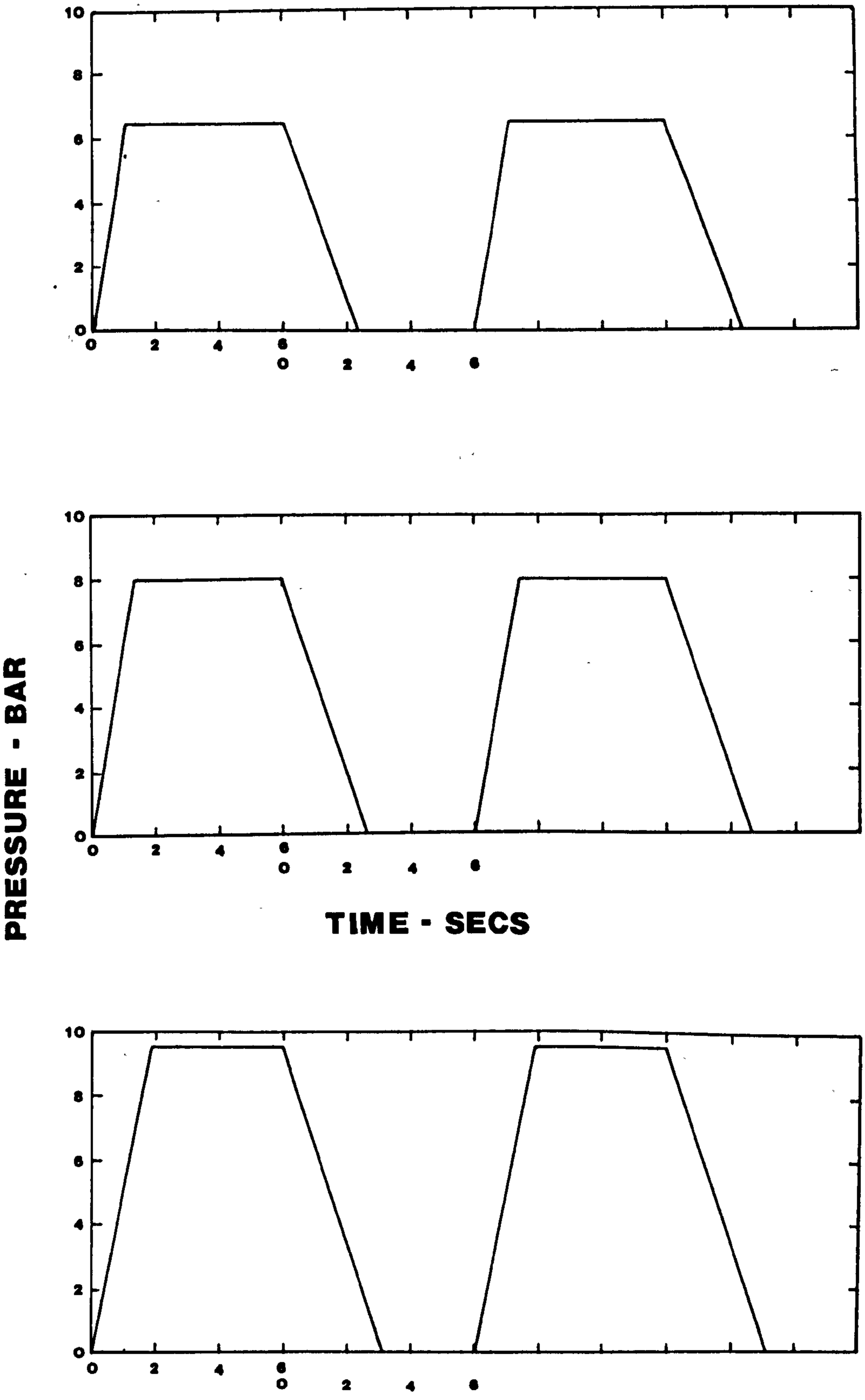

Fig. 3.12(b) Schematic pressure profile based on measured time to reach the maximum pressure and time to reach the minimum pressure for 90mm pipe systems.

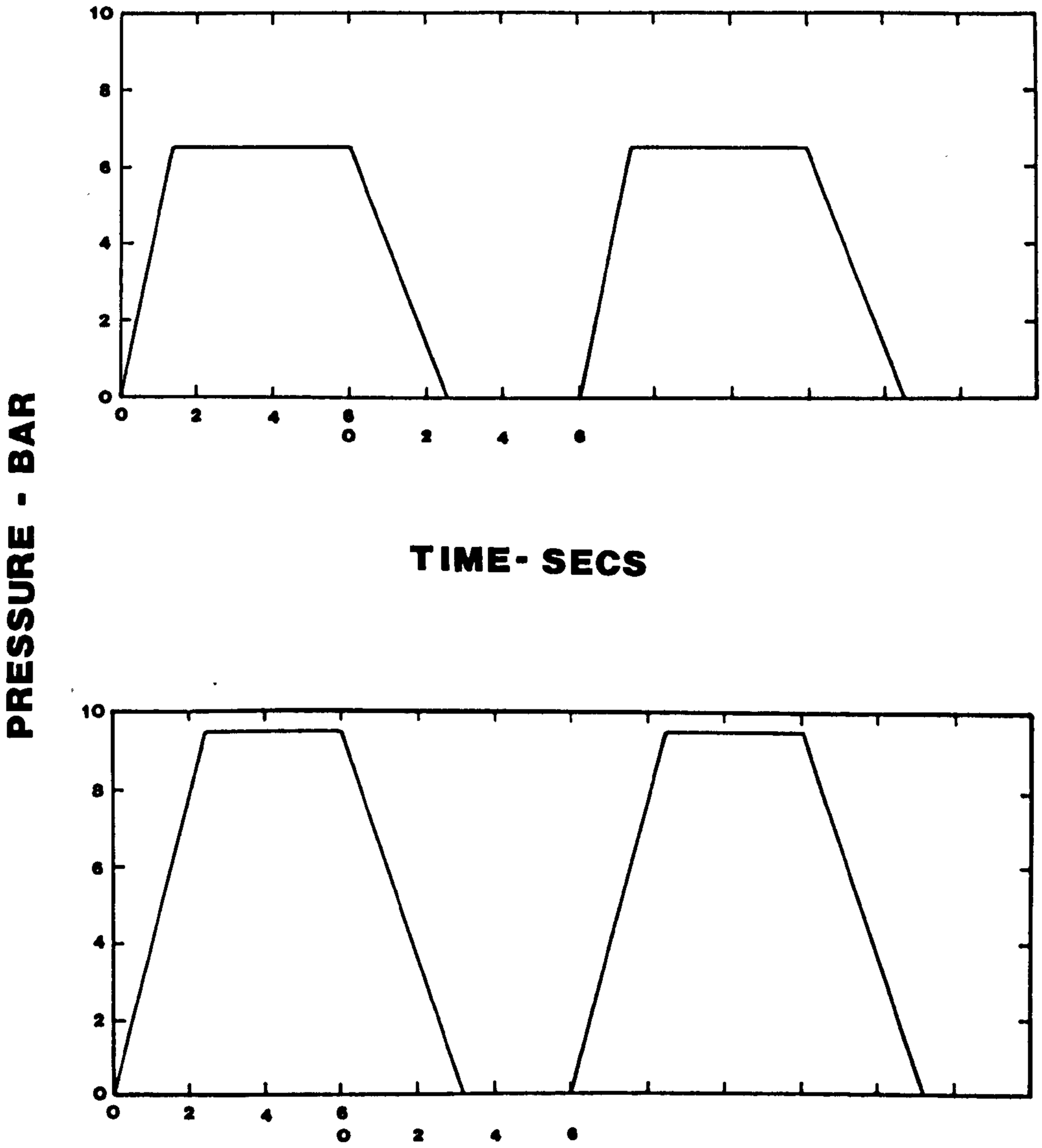

Fig. 3.12(c) Schematic pressure profile based on measured time to reach the maximum pressure and time to reach the minimum pressure for 125mm pipe systems.

3.3.4 Stress Rupture Testing

The arrangement utlilised for stress-ruture testing of the sample is shown in figure 3.11(b). It is much simpler than the fatigue testing and easy to maintain since the pressure is constant with time; thus there is no need for a five-way solenoid valve or the timer.

Stress-rupture tests were carried out in accordance with ASTM D1598 by pressurising water filled systems with either compressed air or nitrogen. A normally open three-way solenoid valve was placed between the pressurising mechanism and the pipe systems which were immersed in the test tank filled with tap water at the desired temperature. The three-way solenoid valve was activated when a failure was detected; on activation it would depressurise the sample and cut-off the supply of compressed air from the regulator thus isolating the system. At the same time it would stop the timer on the Failure Detection Unit.

Test Pressure and Test Temperature All the stress-rupture tests were conducted at one gauge pressure of 9.5 bar corresponding to a nominal hoop stress of 4.81MNm^{-2} for SDR11 pipe systems and in a water bath at 79±1°C.

3.3.5 Failure Detection System

A schematic representation of the failure detection device is shown both in figure 3.11(a) and (b). The principle of operation relies on the fact that a pipe test specimen is filled with an electrically conductive fluid, which in this instance was tap water, with the pipe system itself being immersed in a bath of similar fluid. Electrodes were inserted internally and externally to the pipe system. The external electrode was connected to a positive bias voltage derived from the amplifier power supply, thus sustaining a potential between both electrodes.

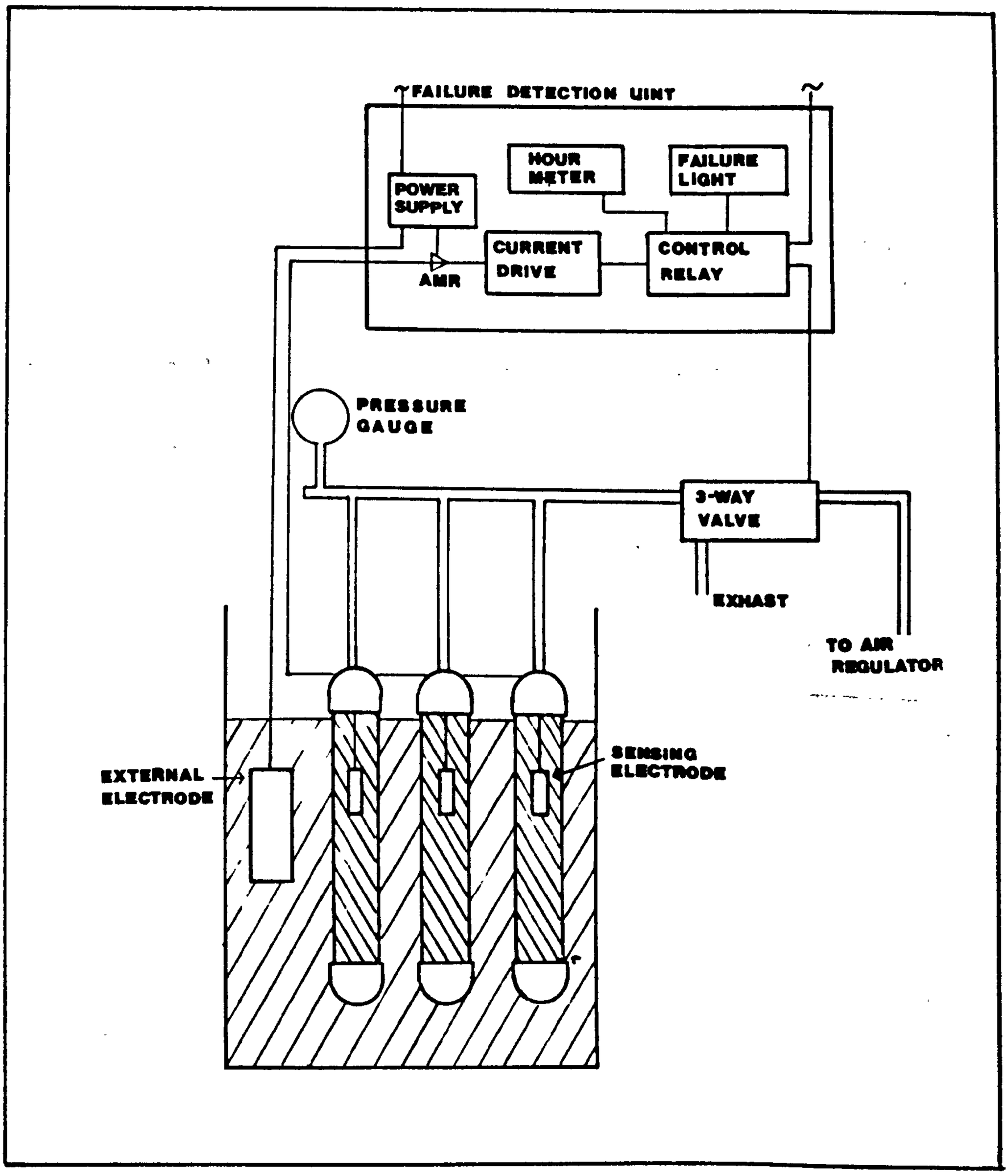

Fig. 3.11(b) Experimential arrangement for stress-rupture testing of pipes.

When a crack propagates through the complete wall of the pipe system an electric current (of the order of microamps) can flow between the internal and external electrodes. This signal current turns on the amplifier which is biased off with a small negative voltage. (The sensitivity of the device can be altered by changing the negative bias voltage.) When the output from the amplifier becomes positive, the current driver is turned on which then operates a relay. This relay was fitted with a sufficient number of contacts to operate whichever control or indicating devices were required for the pressure testing. The relay when activated because of failure, stopped a timer, isolated the failed system from the compressed air and vented any excess pressure remaining. Visually, failure was indicated by a red warning light on the appropriate control module.

3.4.0 Failure Analysis

All the butt welds and pipe failures were isolated. In the case of butt weld failures which had failed in the circumferential plane two types of examination were carried out; crack propagation path studies and fracture surface examination.

(i) Crack Propagation Path Study Extensive examinations of the crack propagation path of circumferential butt weld failures were conducted using a combined technique of etching and microscopy.

Etching A series of etchants were tried in order to delineate the melt flow zone within butt fusion welds. The organic solvents used were found to swell the polymer and concentrated sulphuric acid and nitric acid had little effect on the surface of MDPE. The most successful etchant was the saturated chromic acid, a technique used by Barber et al (41).

Longitudinal sections were cut from the failed butt welded pipes and were polished on the hand grinder, starting on the coarse grade of 220 mesh size and moving in turn onto the finer grade

of 320, 400 and 600 mesh size. The samples were subsequently polished on the 6μm wheel for 20-40 minutes followed by 3μm wheel for 5 minutes. The samples were cleaned ultrasonically in a solvent before moving onto finer polishing grades.

Fresh staturated chromic acid was prepared for the etching in the following manner; 10g of sodium dichromate ($Na_2Cr_2O_7.2H_2O$) was dissolved in 5ml of water in a 250ml beaker, 100ml concentrated sulfuric acid (H_2SO_4) was then added slowly with constant stirring.

Samples were etched in the chromic acid at 75°C for 8 to 12 hours. After etching samples were washed in hydrogen peroxide solution followed by distilled water.

The etched surfaces were examined with a light microscope using reflective light. The crack propagation path was studied using a Wild Heerbrugg Microscope under low angle illumination employing Intralux fibre optics light source. The etched surfaces were sputter coated using a gold palladium electrode before examination with a reflective light microscope. Coating was found to enhance the contrast and it enabled the melt flow zone to be seen more clearly.

(ii) Fracture Surface Features The macro-features of fracture surfaces were examined with the aid of Wild Heerbrugg Microscope under low angle illumination employing Intralux fibre optics light source. The micro-features of fracture surfaces were examined by a scanning electron microscope (SEM) on a Cambridge Instrument Stereoscan S250 with accelerating voltage for the beam set at 10KV. The fracture surface for SEM examination were coated using gold palladium electrode on an Edwards Sputter Coating unit so as to make the surface conductive and prevent excess static charge build up. The facility of elemental analysis on the SEM was utilised to determine the composition of any initiating particle in the pipe failure.

CHAPTER 4 - FATIGUE AND STRESS-RUPTURE PERFORMANCES OF BUTT FUSION WELDS AT ELEVATED TEMPERATURES

4.0 Results: Introduction

The results recorded here cover a broad study into the long-term behaviour of butt fusion welds in MDPE pipe systems. As such the presentation of results has been divided into three separate chapters. The first chapter on the results provides the basic data on the influence of axial misalignment, pipe size and welding conditions on the performance of butt fusion welds in MDPE pipes. The second chapter is on the failure analysis, which includes observations on the crack initiation and propagation path study of circumferential butt weld failures and fracture surface examinations in terms of both macro and micro features of both weld and pipe failures. In the final chapter on the results, the changes in density, crystallinity, number and weight average molecular weight and oxidation induction time of the pressure tested and untested 63mm pipes at various times at 79°C are presented.

In each of the chapters, the presentation of results is followed by the discussion. This concentrates upon specific areas of behaviour which promotes an understanding of the mechanical performance of PE pipeline and the processes leading to instances of premature and potentially hazardous failures. Models are considered to explain the reported observations.

It is hoped that the lifetime data on the aligned and misaligned butt fusion welds under both fatigue and stress-rupture conditions will contribute to useful engineering design information for polyethylene pipelines in the water and chemical process industries. Whilst the failure analysis and the influence of elevated temperature testing on the material property should yield an insight into the material behaviour from the material science point of view.

Field Survey Before the presentation of fatigue performance data, it is instructive to consider the results of a field survey which was carried out to assess the magnitude of the axial misalignment in the butt welds made during the installation of MDPE pipelines. The misalignment measurement in the field survey was made using purpose built equipment on site at six locations, five of which were installing 125mm SDR11 pipe, the sixth 90mm SDR11 pipe. Of the 53 butt welds examined, three had axial misalignments in the ranges 15-20 per cent of the nominal wall thickness, the rest had axial misalignments of less than 10 per cent, see figure 4.0. This preliminary survey thus shows that axial misalignment of 15-20 % of the nominal wall thickness can occur in practice.

4.1.0 The Influence Of Axial Misalignment On The Fatigue Performance Of Butt Fusion Welds

The majority of fatigue tests on aligned and variously controlled misaligned butt fusion welds have been assessed on the blue pigmented Rigidex 002-50 medium density polyethylene in SDR11 of three different pipes sizes; 63, 90 and 125mm tested at three different pressure ranges (ΔP); 6.5, 8.0 and 9.5 bar (corresponding to hoop stress range, $\Delta\sigma_h$ of 3.29, 4.05 and 4.81Mpa respectively). However, for 63mm pipe systems, an initial feasibility study was carried out on black Rigidex 002-60 high density polyethylene pipe at one pressure range, ΔP=9.33 bar ($\Delta\sigma_h$=4.73MNm^{-2}). Throughout this chapter 63mm pipe systems in Rigidex 002-50 MDPE is regarded as the base data to which other pipe sizes and grades are compared.

All the fatigue tests were carried out with nominal duration time of six seconds for both a set maximum internal gauge pressure and minimum zero gauge pressure to give a frequency of five cycles per minute (.083Hz). The applied wave form was of trapezodial type; however, it was not identical for each of the three different pipe sizes. The rate of pressurisation was different depending on the pipe size and pressure range. This

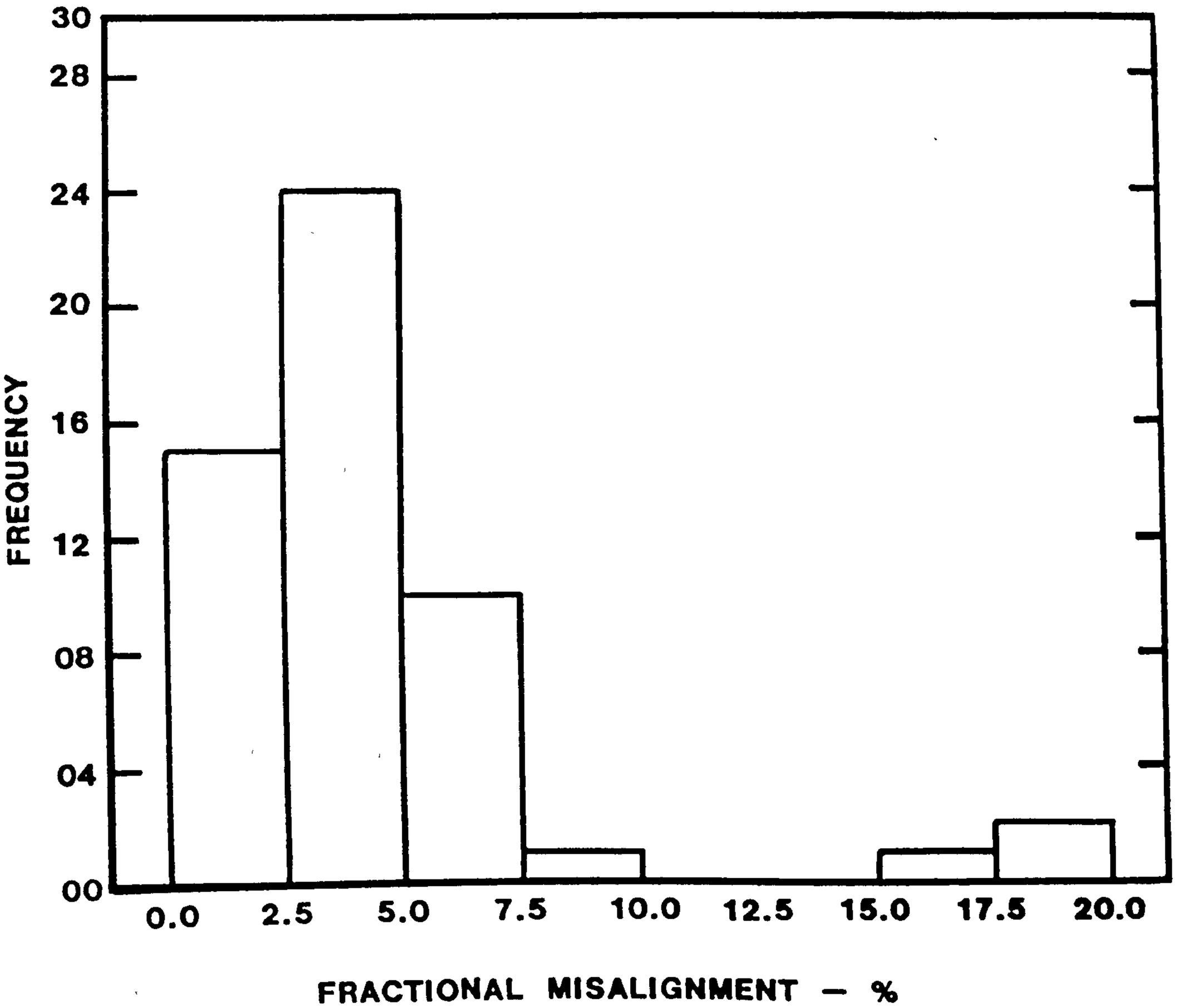

Fig. 4.0 Histogram of the on-site measured axial misalignment in 90 and 125mm polyethylene pipe systems.

was inherent in the nature of the experimental set-up of fatigue testing systems over which there was no accurate control. The values of rate of pressurisation are given in the table 3.9(b); in the main the rate of pressurisation was 1.6 times greater at ΔP=9.5 bar and 2 times greater at ΔP=6.5 bar for 63mm pipes compared to 125mm. Tests were carried out in a water environment at a test temperature of 79±1°C; selected and limited tests were also carried out at 69±1°C and 59±1°C.

The sample size (number of test samples) used for each test pressure range varied from a minimum of three to a maximum of eight depending on pipe size. The mean and standard deviation values have been recorded in the tables and also includes individual values. Coefficient of variation is also noted in the tables to indicate the measure of the spread in relative terms by dividing the standard deviation by the sample mean, higher values indicating relatively greater scatter.

(i) 63mm Pipe Systems: Rigidex 002-60 HDPE Table 4.1(a) contains the lifetime as the number of cycles to failure of aligned and controlled misaligned butt welds in 63mm SDR11 pipe tested at ΔP=9.33 bar ($\Delta\sigma_h$=4.73MNm^{-2}) and at a test temperature of 79°C. The data of table 4.1(a) is recast in table 4.1(b), as the mean reduction in performance of the nominally misaligned butt weld compared to the nominally aligned butt weld. The reduction in performance was calculated according to equation 4.0:

$$\frac{\text{mean aligned performance} - \text{mean performance at given misalignment}}{\text{mean aligned performance}} \qquad (4.0)$$

The following general comments can be made on the results of 63mm Rigidex 002-60 HDPE pipe systems:-

(a) All fatigue tested misaligned butt welded pipe samples (18 in total) failed at the butt weld in the circumferential plane or on a plane perpendicular to extrusion

direction or pipe axis. The failure site was located on the circumference of the butt weld where the controlled axial misalignment was greatest. Of the five nominally aligned butt welded samples tested, three failed at the butt weld in the circumferential plane whereas two failed in the pipe. Both these pipe failures were within one outside diameter of the butt welds which constitute a weld failure.

(b) The scatter in the lifetimes of the butt welds was observed to decrease with increasing nominal fractional misalignment (nominal fractional misalignment is the axial misalignment expressed as a fraction of the nominal pipe wall thickness). The coefficient of variation was least (.059) for the maximum nominal fractional misalignment (44%) examined. The coefficient of variation was similar for the aligned and for nominal fractional misalignment of 9% (.277 and .279 respectively). Minimum scatter at 44% fractional misalignment may be indicative of the severity of stress concentration at this magnitude of misalignment.

(c) For nominal fractional misalignments of 9 and 18% the average reduction in performance of 24 and 56 per cent respectively was observed. For a nominal fractional misalignment of 44%, the reduction of 79% per cent was recorded, not a large increase in the reduction in going from 18% to 44% fractional misalignment compared to change in fractional misalignment from 9% to 18%.

(d) The relationship between the nominal fractional misalignment and the number of cycles to failure is shown in figure 4.1 which also includes the curve for Rigidex 002-50 MDPE pipe systems. It clearly demonstrates the influence of misalignment on the pipe systems performance. It is apparent that the performance of Rigidex 002-60 HDPE pipe systems is inferior compared to Rigidex 002-50 MDPE pipe systems.

Table 4.1(a) Number of cycles to failure of butt welds in 63mm SDR11 Rigidex 002-60 HDPE pipe systems tested at 79°C and a frequency of 0.083 Hz.

	Number Of Cycles To Failure			
Nominal Fractional Misalignment, %	00	09	18	44
	19,320 P*	16,410	8,550	5,220
	19,560 P*	17,670	10,380	5,730
	28,890	17,700	11,550	5,760
	33,205	19,260	12,840	5,970
	35,520	21,750	13,530	6,120
		32,040	15,900	6,150
Mean	27,299	20,805	12,125	5,825
s.d.	7,559	5,802	2,565	344
(coeff. variation)	(.277)	(.279)	(.213)	(.059)

Notes: (1) The axial misalignment is expressed as a fraction of the nominal pipe wall thickness.

(2) All the failures were in the butt weld and lay in the circumferential plane bar except those indentified by P*. In the P* cases the failure was in the pipe but within one outside diameter of the butt weld.

Table 4.1(b) Average reduction in the performance of nominally misaligned butt welds compared to the nominally aligned butt weld.

Nominal Fractional Misalignment, %	Average Reduction %
09	24
18	56
44	79

Table 4.1(c) Comparison of Rigidex 002-60 HDPE with Rigidex 002-50 MDPE pipe systems in terms of ratio of mean performance of 002-60 HDPE to 002-50 MDPE.

Nominal Fractional Misalignment, %	Ratio of Mean Performance
00	0.30
09	0.31
18	0.30
44	0.22

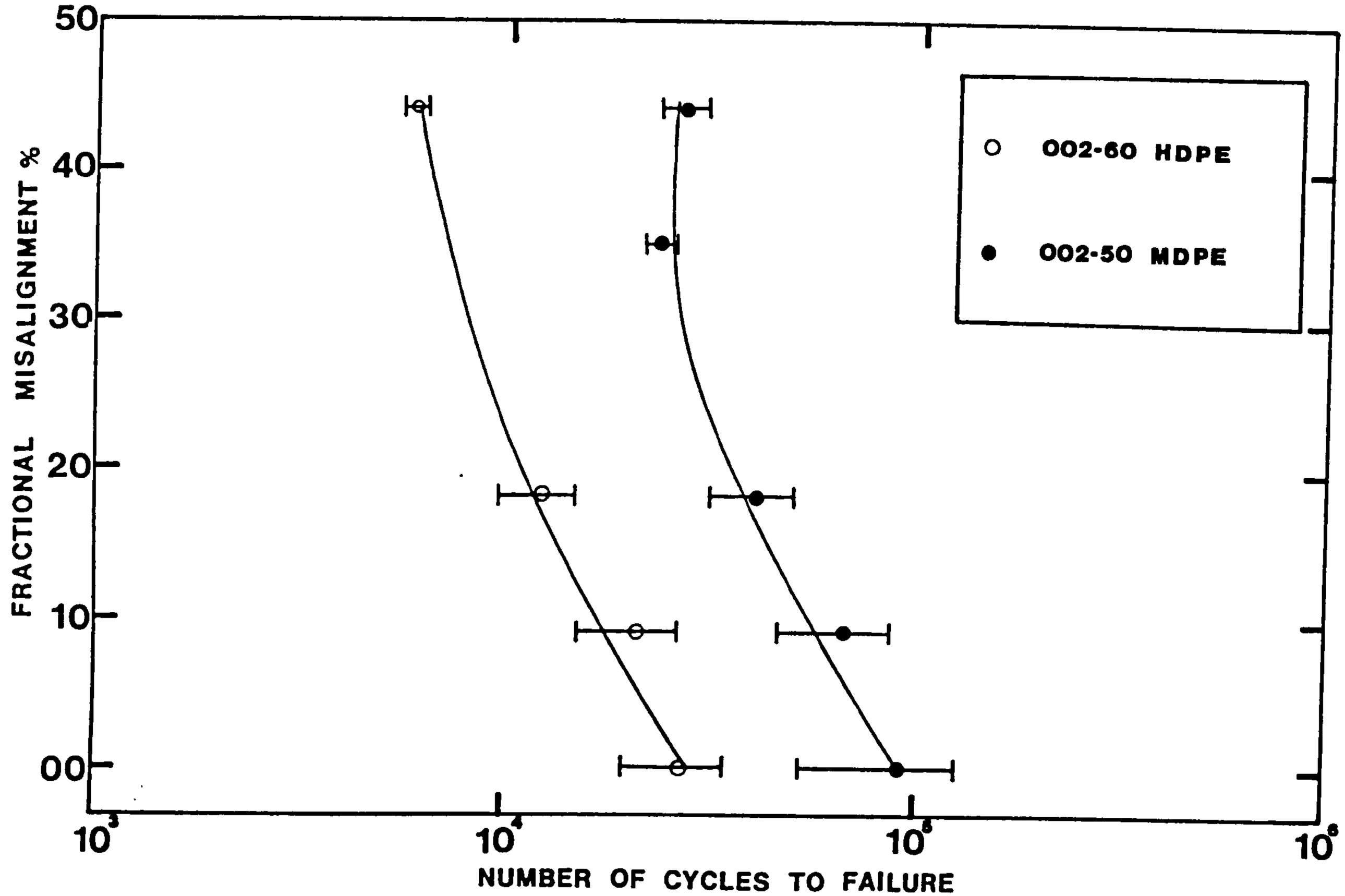

Fig. 4.1 A plot of nominal fractional misalignment versus logarithm number of cycles to failure for 63mm butt welds in Rigidex 002-60 HDPE and in Rigidex 002-50 MDPE pipe systems tested at 79°C.

Rigidex 002-50 MDPE All the lifetime data in the form of number of cycles to failure of the aligned and variously controlled misaligned butt fusion welds tested under three different pressure ranges at 79°C are supplied in tables 4.2. Table 4.5(a) provides the average reduction in performance for the three internal pressure ranges as a function of nominal fractional misalignment; reduction was evaluated in the manner described previously. The influence of misalignment on the lifetime is also exhibited in figure 4.2(a) and 4.3(a). The following observations are made on the lifetime data of 63mm Rigidex 002-50 pipe systems:-

(a) All the misaligned butt welds tested (59 in total) under three different pressure ranges failed in the circumferential fracture plane at the weld where the controlled axial misalignment was introduced. The failure was locally on the circumference of the butt weld. Of the sixteen aligned butt welds tested at three different pressure ranges, fifteen failed at the butt welds of which eleven were in the circumferential plane and four in the axial plane; one aligned butt welded sample did not fail within the allocated testing time. No pipe failures were observed. It would appear that for 63mm pipe systems, the butt weld is therefore the weakest link in the chain for fatigue loading.

(b) For the butt welds tested at a pressure range of 9.5 bar, the coefficient of variation was least (≈0.1) for the large fractional misalignment (35% and 44%) and higher (.4 to .3) for the low fractional misalignment (00 and 09%). This trend was consistent with the Rigidex 002-60 HDPE data. A similar pattern was repeated for butt welded samples tested at ΔP=6.5 bar; however, it was not repeated for the data generated at ΔP=8.0 bar.

The problem of scatter in experimental results is common to most physical tests, and particualarly pronounced in fatigue testing of unnotched specimen because the behaviour of materials under

load is dependent on 'small scale' variables. In the case under consideration, variations in misalignment on the nominally controlled value of misalignment might have caused the spread in the lifetime and also possibly from the variation in notch dimensions, which is created by the rolling of the weld bead onto the pipe surface. Scatter is also expected to increase with the decrease in stress amplitude, that is the smaller scatter at high stress amplitudes is believed to result from shorter initiation periods prior to crack propagation. This was observed only for 18% fractional misalignment.

(c) It is apparent from the table 4.5(a) and figure 4.2(a) that whether one considers the mean lifetime or for that matter the conservative case of minimum lifetime, the performance of the butt weld reduces with increasing fractional misalignment at all three test pressure ranges. For example, the mean lifetime of butt welded samples with a nominal fractional misalignment of 18% was reduced by 81, 54 and 56% at test pressure range of 6.5, 8.0 and 9.5 bar respectively when compared to the aligned butt weld.

For nominal fractional misalignments above 20% and particularly in the range 30 to 45%, the effect of increasing misalignment was small or negligible.

(d) Table 4.6(a) gives the ratio of mean performance at ΔP=9.5 bar to the mean performance at ΔP=6.5 bar and it indicates that for fractional misalignment of 35 and 44% the reduction was greatest at lower pressure range.

(e) For butt welds tested at a pressure range of 9.5 bar the trend in mean reduction in lifetime values with increasing fractional misalignments compared to the aligned weld was similar to that observed for the Rigidex 002-60 HDPE pipes. However, Rigidex 002-50 MDPE was more tolerant to misalignment compared to Rigidex 002-60 HDPE. The performance of Rigidex

002-50 MDPE was on the whole three times better than Rigidex 002-60 HDPE, - see table 4.1(c).

(f) In figure 4.2(a) the performance of various misaligned butt welds is shown on a semi-logarithm plot. The data in figure 4.2(a) has been plotted in two ways. Firstly, the mean value and the range is plotted as the nominal misalignment against the number of cycles to failure. Secondly, the measured maximum misalignment of the butt weld at the failure site is plotted against number of cycles to failure as represented by individual data points. Relationships between the number of cycles to failure and fractional misalignment can best be described by a polynomial of degree greater than or equal to 3 depending on pressure range used, that is in general;

$$N_f = A + B(M_a) + C(M_a)^2 + D(M^a)^3 + E(M^a)^4 + ... \quad (4.2)$$

where N_f is the number of cycles to failure and M_a is the fractional misalignment. A, B, C, D and E are constants. Equation 4.2 can account for the following observations:-

(1) For small misalignment (<20%), pipe systems performance reduces more drastically (the first two terms on the right side, RHS of the equation 4.2 are most important) and

(2) For fractional misalignments above 20%, the effect of increasing misalignment becomes small or negligible (power terms on the RHS of the equation 4.2 become important).

(g) In figure 4.3(a) relationships between axial stress range and number of cycles to failure as a function of various fractional axial misalignment is shown. This plot is preferred over a plot of hoop stress range against logarithm number of cycles to failure because of the predominant failure of butt welds in the circumferential fracture plane.

Table 4.2 Number of cycles to failure of butt welds in 63mm SDR11 Rigidex 002-50 MDPE pipe systems tested at 79°C and a frequency of .083 Hz.

Nominal Fractional Misalignment, %	Number Of Cycles To Failure Internal Pressure Range, bar gauge (corresponding Hoop stress range, MNm^{-2})		
	9.5 (4.81)	8.0 (4.05)	6.5 (3.2)
00	58,290 81,570 60,150 96,090 63,300(A) 132,060 73,620 169,260 Mean ± s.d. 90,668 ± 37,202 (coeff. variation) (.410)	115,560 124,770(A) 136,140(A) 146,880(A) Mean ± s.d. 130,833 ± 13,600 (coeff. variation) (.104)	260,880* 681,390 985,440 >1,200,000 Mean ± s.d. 781,982 ± 407,349 (coeff. variation) (.521)
09	49,980 61,830 53,430 64,440 53,610 82,170 57,060 108,570 Mean ± s.d. 66,386 ± 19,786 (coeff. variation) (.298)	74,280 77,400 80,850 129,870 Mean ± s.d. 90,600 ± 26,317 (coeff. variation) (.291)	577,590 616,380 610,770 >975,000 Mean ± s.d. 694,935 ± 187,493 (coeff. variation) (.270)
18	28,620 39,240 35,040 40,200 37,680 41,790 38,130 61,560 Mean ± s.d. 40,283 ± 9,494 (coeff. variation) (.236)	53,160 58,800 60,390 66,690 Mean ± s.d. 59,760 ± 5,565 (coeff. variation) (.093)	101,250 145,530 152,880 315,720 Mean ± s.d. 178,845 ± 94,056 (coeff. variation) (.526)
35	21,930 21,930 22,710 26,490 Mean ± s.d. 23,265 ± 2,187 (coeff. variation) (.904)	42,510 48,630 49,710 62,430 Mean ± s.d. 50,820 ± 8,364 (coeff. variation) (.165)	68,820 69,060 71,730 84,810 Mean ± s.d. 73,605 ± 7,586 (coeff. variation) (.103)
44	22,590 26,190 24,240 26,760 25,170 28,290 25,500 35,040 Mean ± s.d. 26,723 ± 3,762 (coeff. variation) (.141)	42,030 44,940 51,000 54,210 Mean ± s.d. 48,045 ± 5,555 (coeff. variation) (.116)	80,070 86,100 88,320 90,930 Mean ± s.d. 86,355 ± 4,632 (coeff. variation) (.054)

Notes; A - indicates axial butt weld failure,) - indicates sample did not fail, * - very early failure in the Analysis of table 4.5(a) it has been omitted.

Table 4.3 Number of cycles to failure of pipe to pipe butt welds in 90mm SDR11 Rigidex 002-50 MDPE pipe systems tested at 79°C and a frequency of .083 Hz.

	Number Of Cycles To Failure		
Nominal Fractional	Internal Pressure Range, bar gauge		
	9.5	8.0	6.5
00	82,200(P) 195,390(P) 104,280(A) 213,240(P) 137,160(A) 233,160(P) 192,750(A) 260,790	262,980 444,900 546,810 >647,310	441,630 549,240(P) >1,200,150 >1,116,180
Mean ± s.d. (coeff. variation)	177,371 ± 63,172 (.350)	475,500 ± 164,017 (.275)	>826,800 ± 386,664 (.468)
09	63,600 68,220 73,860 97,740		218,370 224,220 499,560 575,670
Mean ± s.d. (coeff. variation)	75,855 ± 15,181 (.200)		379,455 ± 185,267 (.488)
18	43,050 46,860 47,670 54,000	55,650 66,150 68,820 70,110	212,650 224,550 266,880 363,150
Mean ± s.d. (coeff. variation)	47,895 ± 4,541 (.095)	65,183 ± 6,566 (.101)	266,865 ± 68,254 (.256)
44	23,010 23,130 25,200 25,530		76,800 85,320 86,010 95,730
Mean ± s.d. (coeff. variation)	24,218 ± 1,333 (.055)		85,965 ± 7,741 (.090)

Notes: as per table 4.1 and 4.2

Table 4.4 Number of cycles to failures of pipe to pipe butt welds in 125mm SDR11 Rigidex 002-50 MDPE pipe systems tested at 79°C and a frequency of .083 Hz.

Nominal Fractional Misalignment, %	Number Of Cycles To Failure	
	Internal Rressure Range, bar gauge	
	9.5	6.5
00	>210,000 262,710(P)	>967,350 >978,540 >985,620
Mean ± s.d. (coeff. variation)	>236,355 ± 37,272 (.158)	>977,170
09	85,470 119,400 147,330	417,630 579,750 >957,300
Mean ± s.d. (coeff. variation)	117,400 ± 30,979 (.264)	651,560 ± 276,909 (.425)
18	57,000 70,380 86,700	150,570 214,890 299,100
Mean ± s.d. (coeff. variation)	71,360 ± 14,874 (.208)	221,520 ± 74,487 (.336)
44	24,900 28,710 33,150	63,660 92,010 95,160
Mean ± s.d. (coeff. variation)	28,920 ± 4,129 (.143)	83,610 ± 17,349 (.208)

Table 4.5 Average reduction (%) in the performance of nominally misaligned butt welds compared to the nominally aligned butt welds in (a) 63, (b) 90 and (c) 125mm Rigidex 002-50 MDPE pipe systems.

(a)

Nominal Fractional Misalignment, %	Average Reduction - %		
	Internal Pressure Range, bar gauge		
	9.5	8.0	6.5
09	28	31	27
18	56	54	81
35	74	61	92
44	71	63	91

(b)

Nominal Fractional Misalignment, %	Average Reduction - %		
	Internal Pressure Range, bar gauge		
	9.5	8.0	6.5
09	57		>54
18	73	>86	>68
44	86		>90

Table 4.5(c)

Nominal Fractional Misalignment, %	Average Reduction - %	
	Internal Pressure Range, bar gauge	
	9.5	6.5
09	>50	>33
18	>70	>77
44	>88	>91

Table 4.6(a) Ratio of mean performance at ΔP=9.5 bar to mean performance at ΔP=6.5 bar for variously misaligned butt welds in 63, 90 and 125mm Rigidex 002-50 MDPE pipe.

Nominal Fractional Misalignment, %	Pipe Diameter, mm		
	63	90	125
00	.12	.21	.24
09	.10	.20	.18
18	.23	.18	.32
35	.31	-	-
44	.31	.28	.35

Table 4.6(b) Ratio of mean performance in 90 and 125 to mean performance of 63mm pipe systems.

Nominal Fractional Misalignment, %	90mm			125mm	
	Pressure Range, bar			Pressure Range, bar	
	9.5	8.0	6.5	9.5	6.5
00	1.96	3.63	>1.06	>2.6	>1.25
09	1.14	-	0.55	1.76	0.94
18	1.19	1.09	1.49	1.77	1.24
44	0.91	-	1.00	1.08	0.97

Table 4.6(c) Ratio of mean reduction in performance in 90 and 125mm pipe systems to 63mm pipe systems.

Nominal Fractional Misalignment, %	90mm		125mm	
	Pressure Range, bar		Pressure Range, bar	
	9.5	6.5	9.5	6.5
09	2.04	>2.00	>1.78	>1.22
18	1.30	>0.84	>1.25	>0.95
44	1.21	>0.99	>1.24	>1.00

Table 4.7 Ratio of weld bead height, d to pipe wall thickness, t and weld bead height to weld bead width, w for aligned butt welds in 63, 90 and 125mm Rigidex 002-50 MDPE pipe systems.

Pipe Diameter	Inside Weld Bead		Outside Weld Bead	
mm	d/w	d/t	d/w	d/t
63	.624 ± .161	.648 ± .092	.456 ± .050	.558 ± .064
90	.431 ± .113	.403 ± .090	.376 ± .032	.363 ± .034
125	.453 ± .140	.310 ± .041	.437 ± .017	.313 ± .025

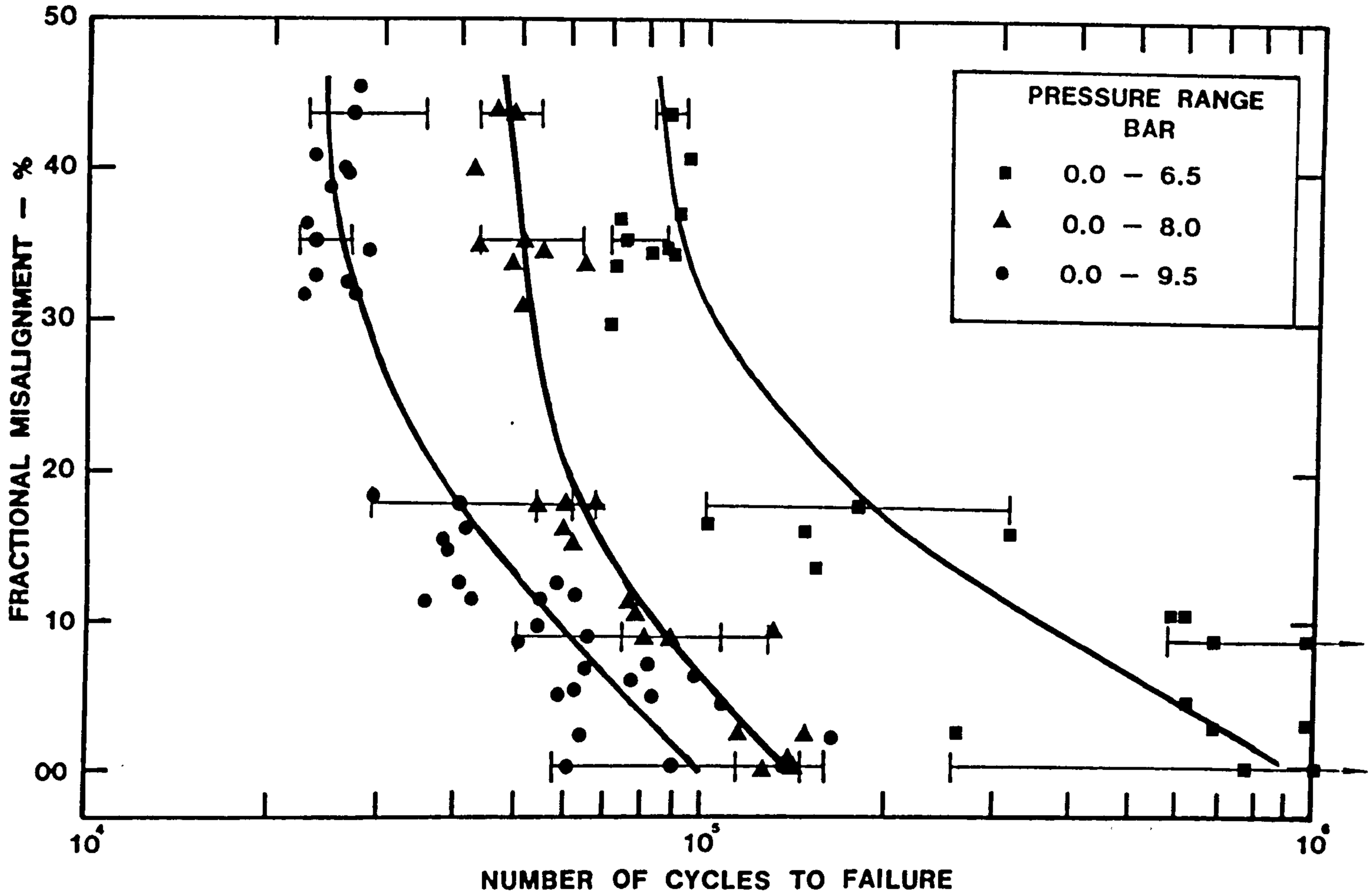

Fig. 4.2(a) Nominal/measured fractional misalignment versus logarithm number of cycles to failure for butt welds in 63mm SDR11 Rigidex 002-50 MDPE pipe systems.

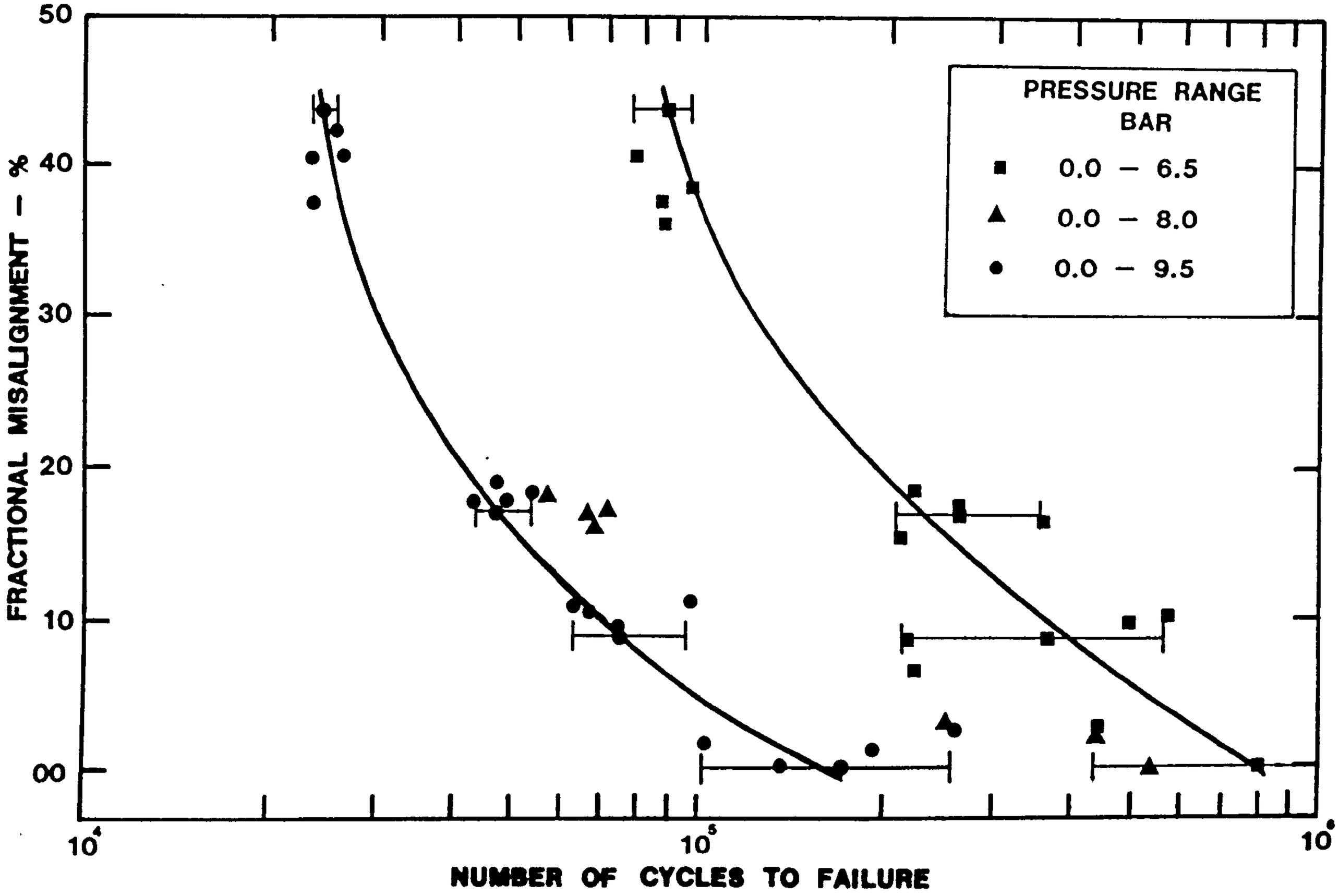

Fig. 4.2(b) Nominal/measured fractional misalignment versus logarithm number of cycles to failure for butt welds in 90mm SDR11 Rigidex 002-50 MDPE pipe systems.

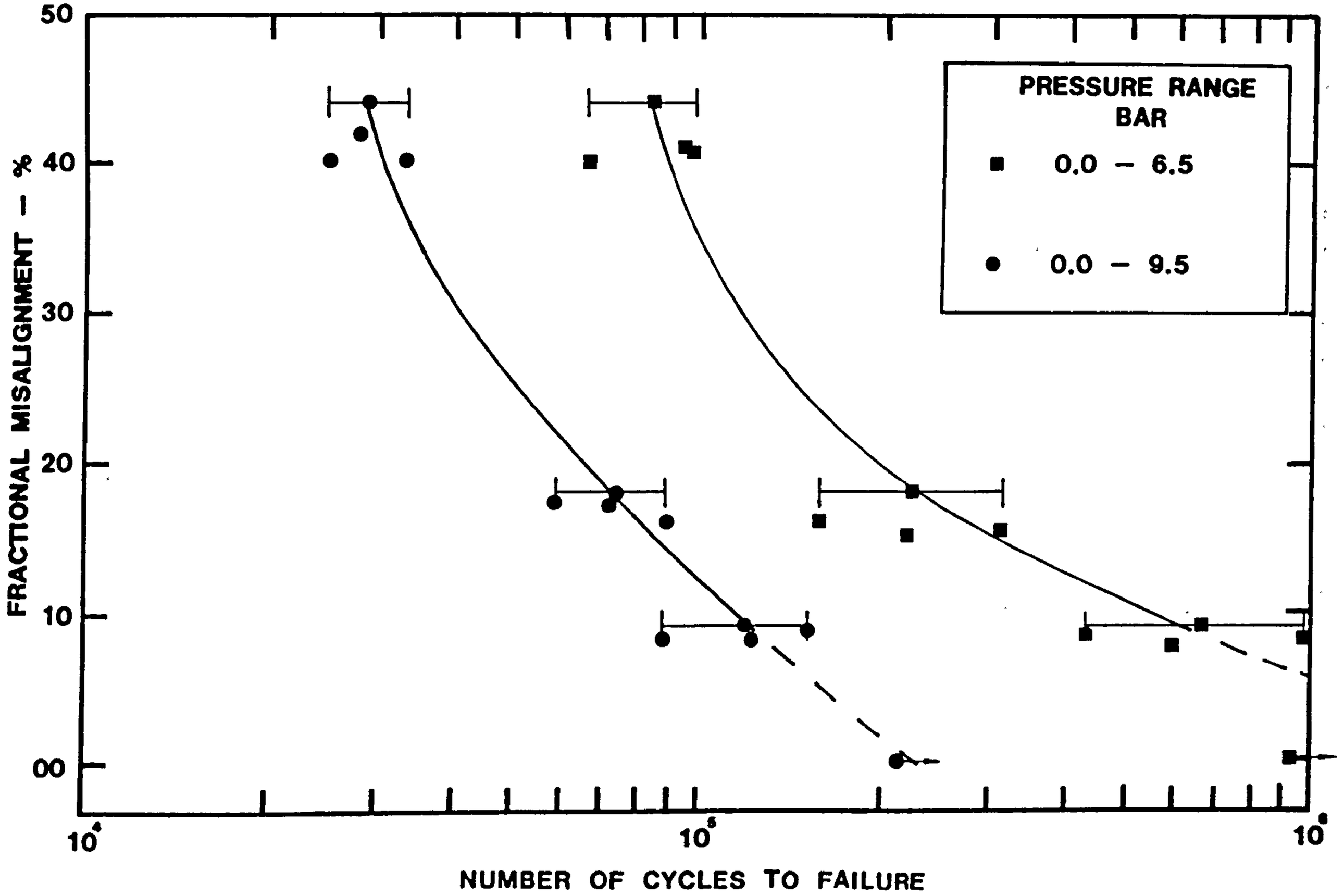

Fig. 4.2(c) Nominal/measured fractional misalignment versus logarithm number of cycles to failure for butt welds in 125mm SDR11 Rigidex 002-50 MDPE pipe systems.

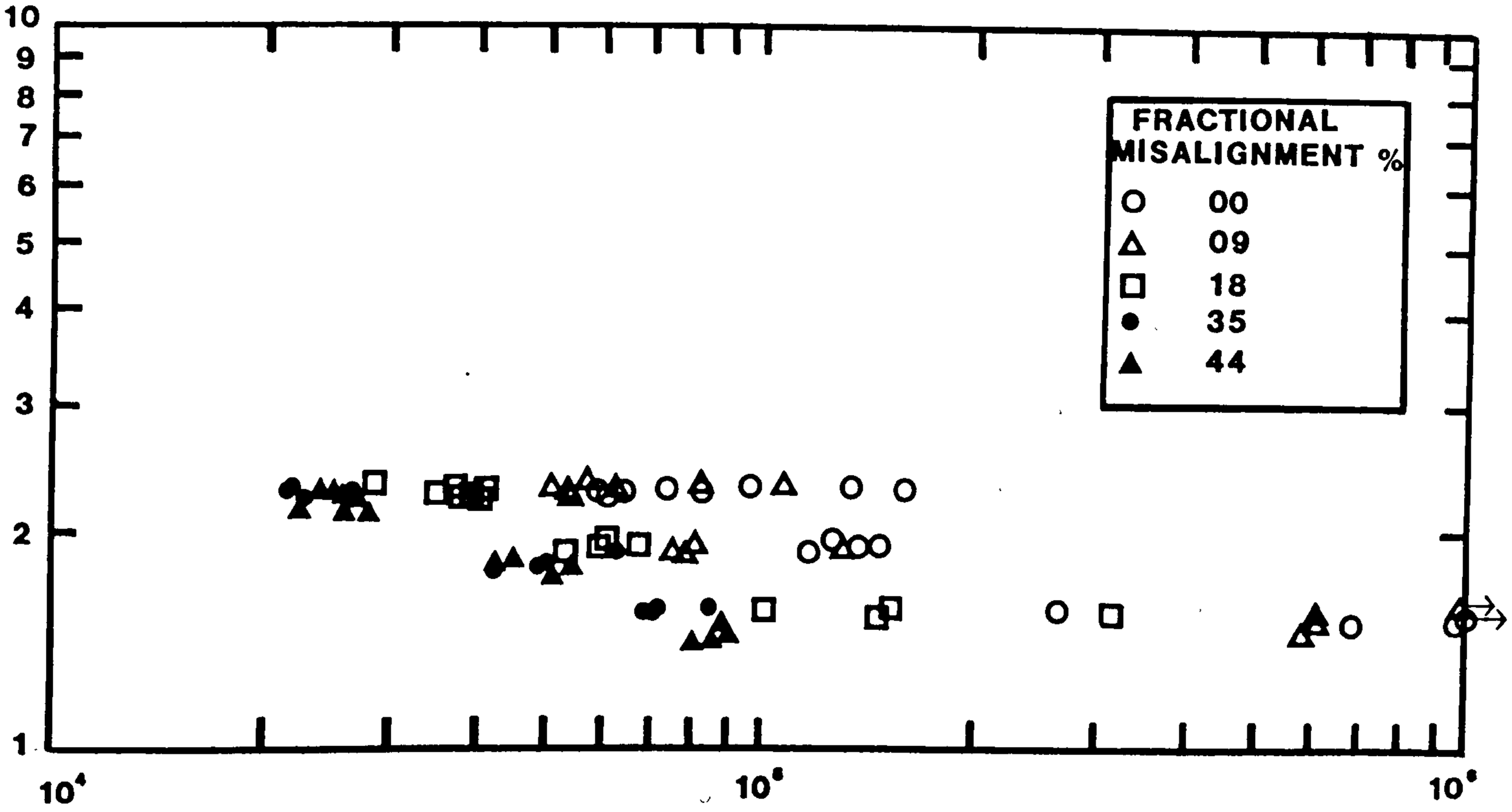

Fig. 4.3(a) Axial stress range versus logarithm number of cycles to failure as a function of fractional misalignment for butt welds in 63mm SDR11 Rigidex 002-50 MDPE pipe systems.

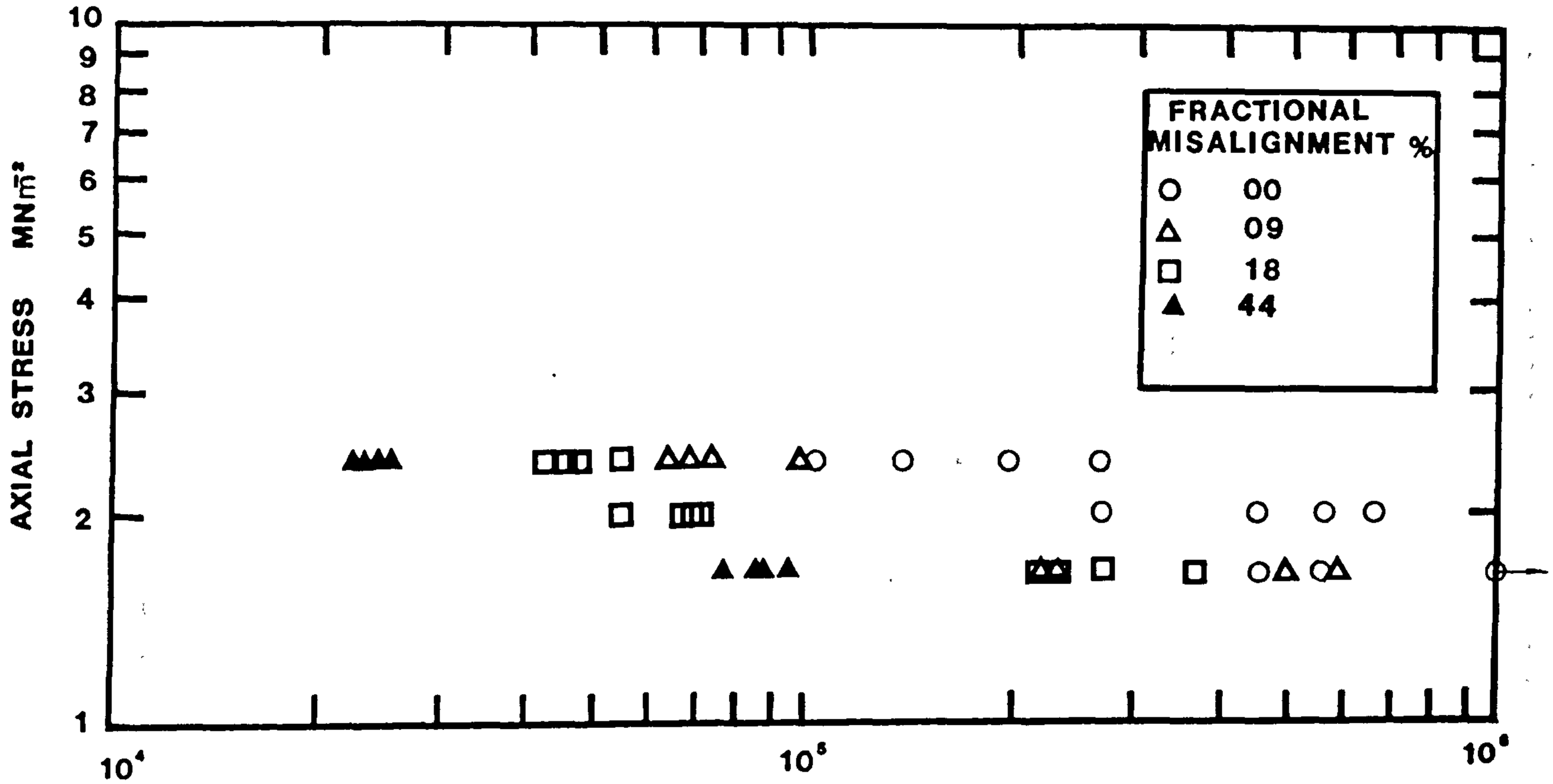

Fig. 4.3(b) Axial stress range versus logarithm number of cycles to failure as a function of fractional misalignment for butt welds in 90mm SDR11 Rigidex 002-50 HDPE pipe systems.

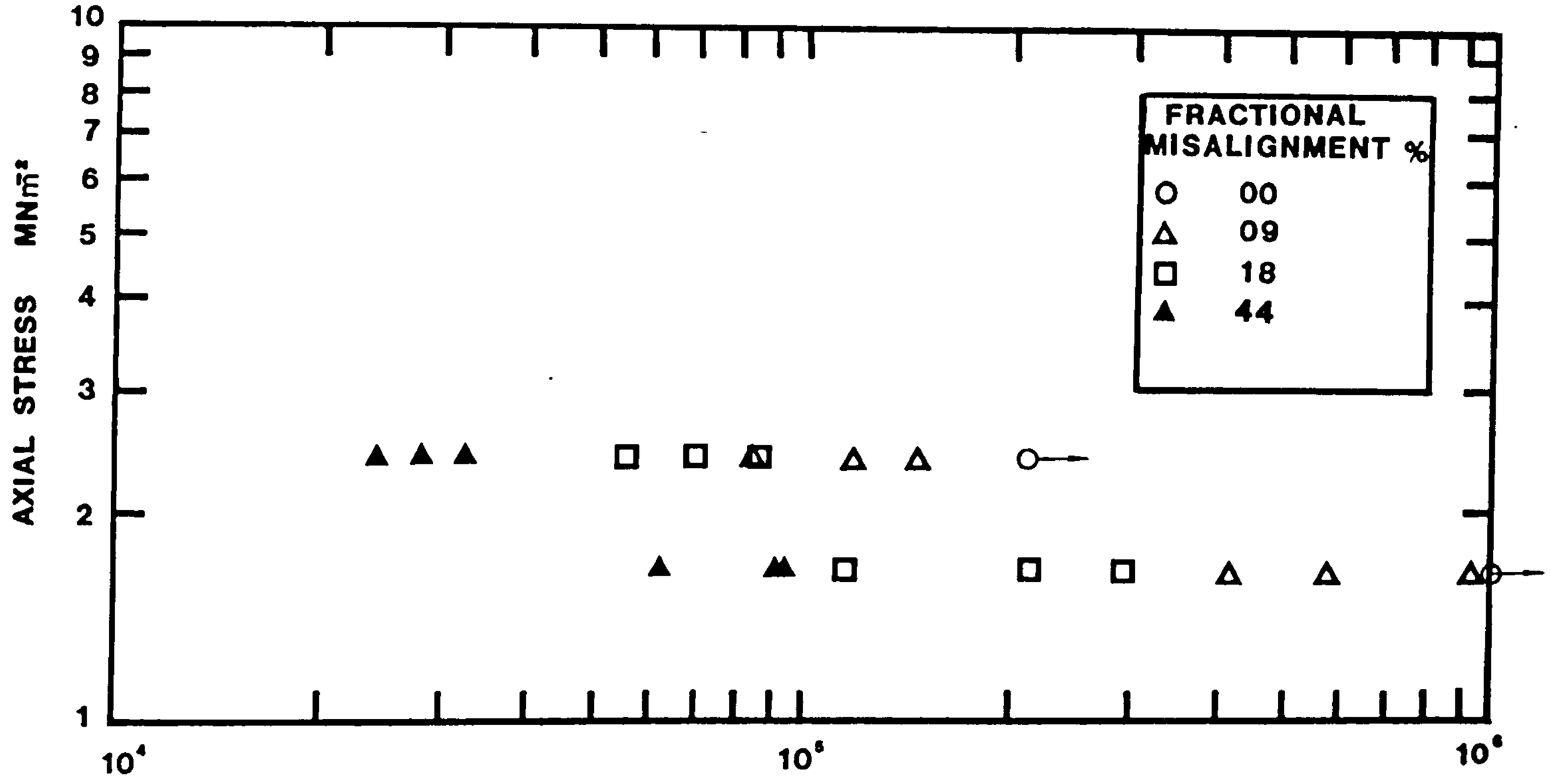

Fig. 4.3(c) Axial stress range versus logarithm number of cycles to failure as a function of fractional misalignment for butt welds in 125mm SDR11 Rigidex 002-50 MDPE pipe systems.

(ii) <u>90mm Rigidex 002-50 MDPE Pipe Systems</u> 90mm pipe systems were tested as a part of an investigation into the influence of pipe diameter on the performance of butt welds. Essentially the tests at ΔP=6.5 and 9.5 bar (corresponding to $\Delta\sigma_h$=3.29MNm^{-2} and 4.81MNm^{-2} respectively) were repeated and selected tests were also carried out at ΔP=8.0 bar ($\Delta\sigma_h$=4.05 MNm^{-2}). The number of cycles to failure of the aligned and controlled misaligned butt welds in 90mm pipe systems tested under the above mentioned pressure ranges at 79°C are given in table 4.3. The average reduction in the lifetime of three differently misaligned butt welds compared to the aligned butt weld are provided in the table 4.5(b). In figure 4.2(b) and 4.3(b) the lifetime data has been displayed in the graphical form. Figure 4.2(b) shows the relationship between the number of cycles to failure and the nominal/measured fractional misalignment, whilst, figure 4.3(b) exhibits the relationship between axial stress range and number of cycles to failures as a function of various fractional misalignment.

The general remarks on the results of 90mm pipe system which can be made are:-

(a) All the misaligned butt welds failed in the circumferential plane at the weld, (in total 28 at three dissimilar pressure ranges as was observed in 63mm pipe systems). However, of the sixteen aligned butt welds tested at three dissimilar pressure ranges, seven failed at the weld of which four were in the circumferential plane and three in the axial plane. Four pipe failures remote from the weld were observed, one pipe failure within one outside diameter of the end cap and three samples did not fail within the allocated testing time. It appears there is a 50% probability that the failure of aligned welds in 90mm pipes will occur at weld or in the pipe whereas in 63mm pipe, circumferential failures were predominant. For aligned butt welds in 90mm pipe, the weld is not always the weakest link in the chain.

(b) The trend in the coefficient of variation is clear and consistent compared to 63mm data. At all three test pressure ranges the coefficient of variation decreases as the fractional misalignment increases and it also increases with decreasing pressure range. For ΔP=9.5 bar, the coefficient of variation decreased from .35 to .06 as the fractional misalignment increases from 00 to 44% and for ΔP=6.5 bar decreases from greater than .42 to .09 for same increase in fractional misalignment.

(c) The ratio of the mean performance of butt welds in 90mm pipe system to 63mm pipe system is displayed in the table 4.6(b). It is apparent from this table that in general while the performance of the variously misaligned butt welds is similar to 63mm pipe systems, the aligned butt weld performance has improved ($\propto$ 2.0 times at ΔP=9.5 bar) compared to aligned butt weld in 63mm pipe. The observed improvement in the aligned butt weld may be attributed in one of the following ways or any combined effect;

(1) If the assumption is made that the performance of an aligned butt weld is sensitive to minor changes in rate of pressurisation then the improved performance of aligned butt welds in 90mm pipe systems may be due to the fact that the rate of pressurisation for 63mm pipe systems was 1.2 and 1.6 times greater compared to 90mm pipe system at ΔP=9.5 bar and 6.5 bar respectively,

(2) If it is assumed that the minor change in rate of pressurisation has no influence in aligned butt welds then the improvement in performance may be attributed to the fact that there is a relative decrease in the bead size compared to pipe wall thickness for 90mm pipe - see table 4.7, which probably decreases the probability of failure at the butt weld and extends the lifetime of aligned butt welds and,

(3) circumferential crack growth rates in 90mm pipe are different from these in 63mm for the aligned butt weld.

(d) The reduction in the performance of misaligned butt welds in 90mm pipe systems compared to 63mm pipe systems as represented by its ratio are cited in the table 4.6(c) which shows that the reduction in performance of 9% fractional misalignment in 90mm pipes is twice as great as in 63mm pipes. The reduction in performance for 18 and 44% fractional misalignment is about one and half times greater than for 63mm pipe size. It seems then for 90mm pipe systems the performance is very sensitive to minor fractional misalignment at the weld.

(iii) 125mm Rigidex 002-50 MDPE Pipe Systems The results of the tests carried out at ΔP=6.5 and 9.5 bar for variously controlled misaligned butt welds at 79°C are included in the table 4.4 in the form of number of cycles to failure. The reduction in the lifetime of the misaligned butt welds compared to aligned butt welds are exhibited in the table 4.5(c). All the values in the table 4.5(c) are recorded as greater than since the aligned butt weld failures were not observed at the weld within the allocated testing time.

Figure 4.2(c) indicates the relationship between the fractional misalignment and the number of cycles to failure and figure 4.3(c) the relationship between axial stress range and number of cycles to failure as a function of various fractional misalignments.

The following general observations were made regarding the performance of the 125mm pipe systems:-

(a) All the misaligned butt welds failed in the circumferential plane at the weld (in total 17 at two different ΔP) in common with observations made on 63 and 90mm pipe systems. None of the aligned butt welds had failed within the allocated testing time, surpassing the mean lifetime of 63mm

pipe system at ΔP = 9.5 bar and equal to the 63mm pipes at ΔP=6.5 bar

(b) The trend in the coefficient of variation is similar to the one anoted for the 90mm pipe systems; the coefficient of variation decreases as the fractional misalignment increases and it also increases at the lower pressure range. For ΔP=9.5 bar the coefficient of variation decrease from .26 to .14 and at ΔP=6.5 bar it decreases from .43 to .21 for fractional misalignment increase from 9 to 44%.

(c) The ratio of the mean performance of butt welds in 125mm pipe systems to 63mm pipe systems are given in table 4.6(b). It shows that

(1) The performance of highly misaligned butt welds (44%) is similar to 63mm pipe systems,

(2) For fractional misalignment of 9 and 18%, the performance has almost doubled compared to 63mm pipe system at ΔP=9.5 bar and at ΔP=6.5 bar it has not changed significantly,

(3) The aligned butt weld performance has improved compared to aligned butt welds in 63mm pipes, the magnitude of which is uncertain since no failures were observed within the allocated testing times. The observed improvement in the aligned butt welds may be attributed to the similar reasoning put forward for 90mm pipe systems - see section 4.1.2, note (c). Table 4.7 gives the ratio of weld bead height to the pipe wall thickness in the aligned butt weld and it seems that this value for 125mm is half that of the 63mm pipe.

(d) The ratios of the reductions in the misaligned butt weld performance in 125mm pipe systems to the reductions in misaligned butt weld performance in 63mm pipes are indicated in the table 4.6(c). It shows that reductions in the performance of all the misaligned butt welds at two ΔP are greater than

those observed for 63mm pipe systems. It appears that with an increase in pipe diameter the performance is sensitive to minor axial misalignments.

4.2.0 The Influence Of Temperature On The Fatigue Performance Of Aligned And Misaligned Butt Welds In 63 And 90mm Pipe Systems

(i) Rigidex 002-60 HDPE A number of butt welds having a nominal fractional misalignment of 44% in 63mm pipe systems were tested over a pressure range of 9.33 bar ($\Delta\sigma_h$=4.73MN$_m^{-2}$) and at a test temperatures of 59 and 69°C in order to establish the temperature dependence relationship which would provide some guide to its likely performance at lower temperatures. The number of cycles to failure of the misaligned butt welds tested under the above mentioned conditions are given in table 4.8. All the misaligned butt welds failed in the circumferential plane at the weld, similar to the failures observed at 79°C.

A plot of logarithm mean number of cycles to failure against reciprocal of absolute temperature, an Arrhenius plot, is shown in figure 4.4(a) based on the mean lifetime of 44% fractionally misaligned butt welds tested at ΔP=9.33 bar and at 79, 69 and 59°C. The prediction of lifetime obtained from the Arrhenius plot is discussed in section 4.5.2.

(ii) Rigidex 002-50 MDPE Pipes A selected number of aligned and misaligned butt welds, with 18% fractional misalignment, in 63 and 90mm pipes were tested at 59 and 69°C under a test pressure range of 9.5 bar ($\Delta\sigma_h$=4.81MN$_m^{-2}$). The lifetime data in the form of number of cycles to failure for these butt welds are given in the table 4.9. None of the aligned butt welds in 63 and 90mm pipes had failed at 59°C within the allocated testing time. All the other failures in the aligned and misaligned butt welds recorded in the table 4.9 failed at the butt weld in the circumferential plane, similar to the failures noted at 79°C.

Table 4.8 Fatigue performance of nominally 44% fractional misalignment butt weld in 63mm Rigidex 002-60 HDPE pipe at 59 and 69°C.

	Number Of Cycles To Failure	
Test Temperature °C	69	59
	12,090	42,930
	13,830	42,780
	19,350	51,480
	22,710	54,030
	22.830	61,560
		63,120
Mean ± s.d.	18,162 ± 4,988	52,650 ± 8,766
(coeff. variation)	(.275)	(.167)

Table 4.9(a) Fatigue performance of nominally aligned and nominally 18% fractional misaligned butt welds in 63 and 90mm Rigidex 002-50 MDPE pipe at (a) 69°C and (b) 59°C.

(a)

Nominal Fractional Misalignment, %	Number Of Cycles To Failure	
	Pipe Outside Diameter, mm	
	63	90
00	104,040 168,750 240,240 296,220 353,130 433,410 449,490	331,560 1,118,040 >1,155,000 >1,155,000
Mean ± s.d. (coeff. variation)	292,183 ± 130,226 (.446)	>939,900 ± 405,934 (.432)
18	83,010 99,960 118,200 134,850	103,980 112,950 131,220 135,540
Mean ± s.d. (coeff. variation)	109,005 ± 22,436 (.206)	120,923 ± 14,948 (.124)

(b)

Nominal Fractional Misalignment, %	Number Of Cycles To Failure	
	Pipe Outside Diameter, mm	
	63	90
00	>750,000 >750,000	>750,000
18	340,650 354,060	434,250 601,470

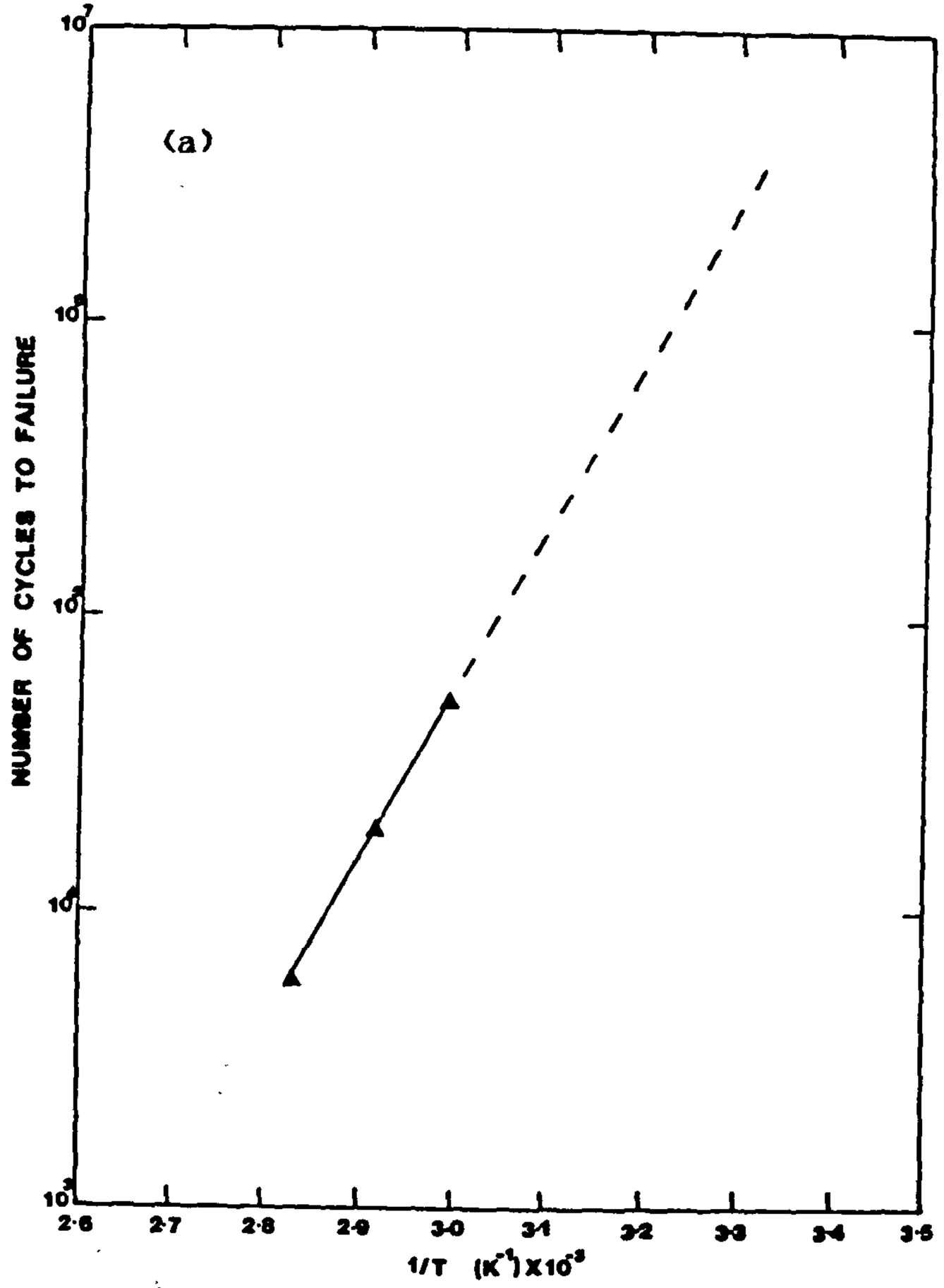

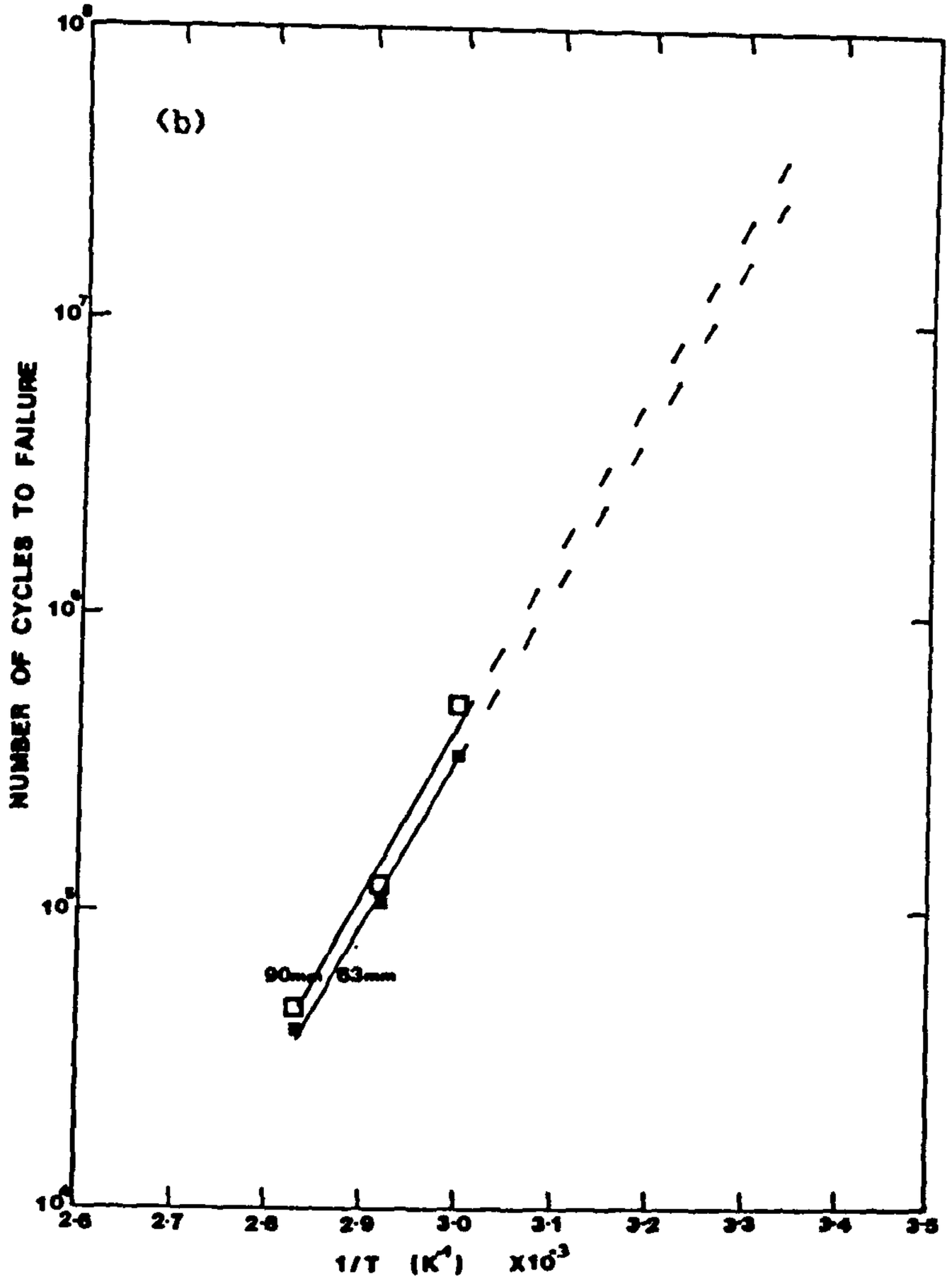

Fig. 4.4 Dependence of number of cycles to failure on the reciprocal of absolute temperature for the butt weld having nominal fractional misalignment of (a) 44% in 63mm Rigidex 002-60 HDPE and (b) 18% in 63 and 90mm SDR11 Rigidex 002-50 HDPE.

A plot of logarithm number of cycles to failure, logarithm N_f against reciprocal of absolute temperature is shown in figure 4.4(b) based on the mean lifetimes at three test temperatures for butt welds having 18% fractional misalignment. The curves for aligned butt welds are omitted because of insufficient data.

4.3.0 The Influence of Axial Misalignment On The Stress-Rupture Performance of Butt Fusion Welds

Pipe systems described in the section 4.1.0 were also assessed under stress-rupture conditions at 79°C but only at one pressure. The chosen pressure corresponded to a hoop stress which lay just below the knee in the material manufactures stress-rupture curve and it also corresponded to the maximum pressure used under fatigue, thus enabling the comparison of stress-rupture and fatigue to be made at the one pressure. Tests at other pressures and temperatures were not possible since the expected lifetime, especially of Rigidex 002-50 MDPE, exceeded far beyond the time limit for the project.

The sample size for the stress-rupture tests varied from a minimum of four to a maximum of eight depending on pipe diameter. In a similar manner to the presentation of the fatigue performance data, the tabulation of the stress-rupture lifetime data records the individual values, mean, standard deviation and coefficient of scatter.

(i) <u>63mm Rigidex 002-60 HDPE</u> Table 4.10(a) contains the lifetime in terms of testing time to failure of aligned and controlled misaligned butt welds in 63mm SDR 11 pipe tested at a constant gauge pressure of 9.33 bar (σ_h=4.73MN_m^{-2}) at 79°C. Table 4.10(b) gives the reduction in performance of nominally misaligned butt welds compared to the nominally aligned butt welds; the reduction is calculated according to equation 4.1. The following points can be made on the results of 63mm Rigidex 002-60 HDPE pipe systems:-

Tables 4.10(a) Stress-rupture lifetimes of butt welds in 63mm SDR11 Rigidex 002-60 HDPE pipe tested at 9.33 bar and at 79°C.

	Time To Failure, Hours.			
Nominal Fractional Misalignment, %	00	09	18	44
	69.9	67.2	31.7	13.9
	80.8	75.6	39.1	14.6
	137.9(P)	76.7	47.1	16.4
	147.9	76.8	55.5	19.2
	151.9(P)	91.2	55.8	19.5
	178.5	-	74.6	30.0
	254.9	-	-	-
Mean ± s.d. (coeff. variation)	138.4 ± 85 (.419)	77.5 ± 8.6 (.111)	50.6 ± 15 (.300)	18.9 ± 5.9 (.311)

Table 4.10(b) Average reduction (%) in the performance of nominally misaligned butt welds compared to the nominally aligned butt weld.

Nominal Fractional Misalignment, %	Average Reduction %
09	44
18	63
44	86

Table 4.10(c) The ratio of mean testing time to failure under stress-rupture to mean testing time to failure under fatigue.

Nominal Fractional Misalignment, %	The Ratio Mean Testing time to failure
00	1.52
09	1.12
18	1.25
44	0.97

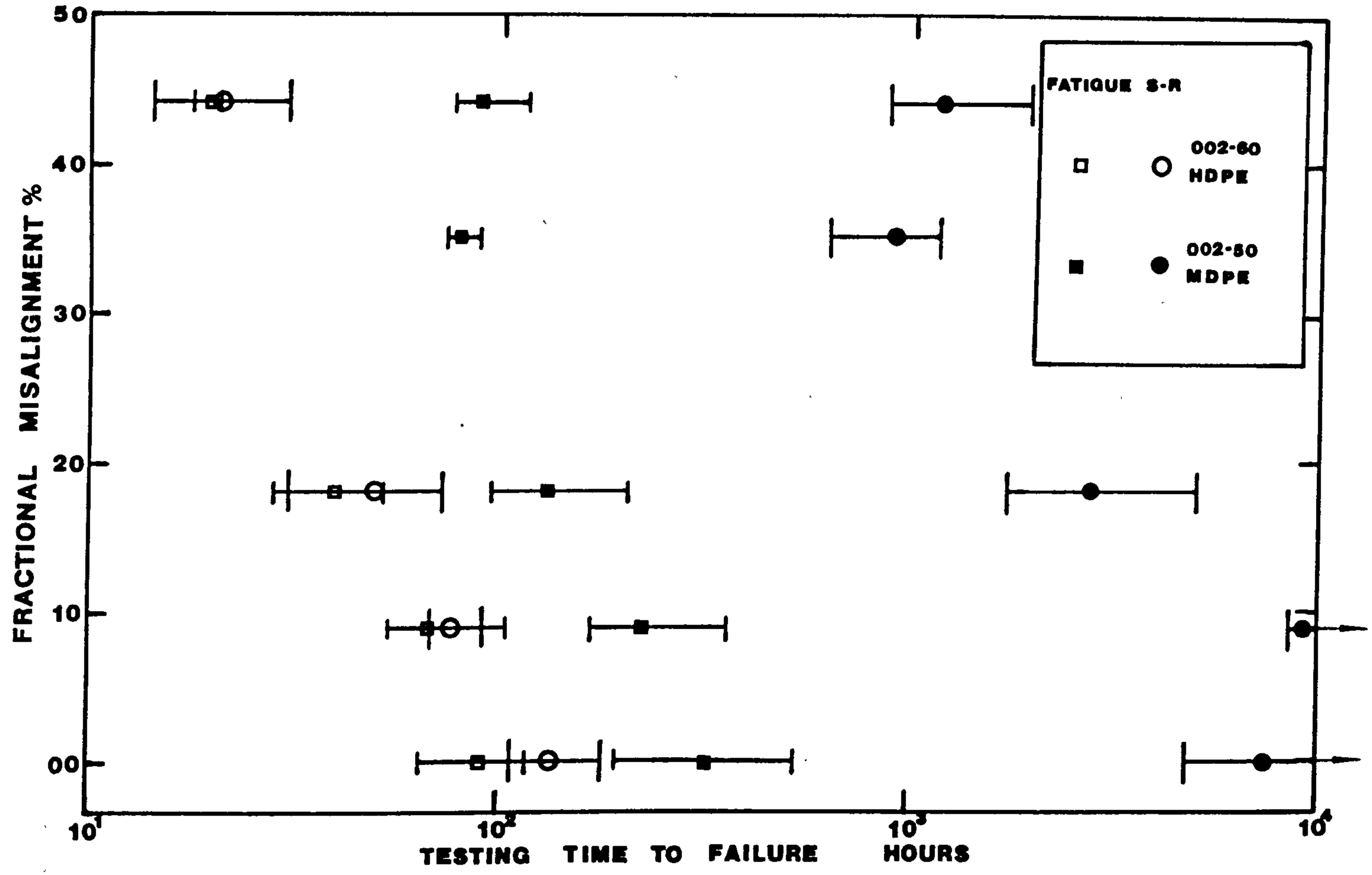

Fig. 4.5(a) Influence of fractional misalignment on the total testing time to failure under stress-rupture and fatigue for 63mm SDR11 Rigidex 002-60 HDPE and Rigidex 002-50 MDPE pipe.

(a) All stress-rupture tested misaligned butt welded pipe samples (17 in total) failed at the butt weld in the circumferential plane as was observed under fatigue. Of the seven nominally aligned butt welded pipe samples tested, three pipes failed remote from the butt weld, the remainder failed at the weld in the circumferential plane. Pipe failures had a similar lifetime to aligned butt welds.

(b) The coefficient of scatter was greatest for the nominally aligned butt welds and was surprisingly least for nominally 9% misaligned butt welds. The coefficient of scatter was on the whole greater than those recorded under fatigue, perhaps indicating that the notches under stress-rupture are not as sensitive.

(c) In terms of total testing time to failure, aligned butt welds under stress-rupture were marginally superior compared to under fatigue. An average increase in the lifetime of 52% was noted, whereas there was no significant increase in the stress-rupture performance of misaligned butt welds compared to under fatigue - see table 4.10(c) and figure 4.5.

(d) For nominal fractional misalignents of 9 and 18% the reduction in performance of 44 and 63% respectively was observed, compared to the aligned welds. This reduction was noticably greater than one observed under fatigue where it was 34 and 56% respectively. For a nominal misalignment of 44%, the reduction of 86% under stress-rupture was recorded compared to 79% under fatigue.

(ii) <u>63mm Rigidex 002-50 MDPE Pipe Systems</u> All the stress-rupture lifetimes of the aligned and variously controlled misaligned butt fusion welds in 63mm SDR11 002-50 MDPE pipes tested under the gauge pressure of 9.5bar (σ_h=4.81MNm^{-2}) at 79°C are supplied in the table 4.11. The following observations are made on these stress-rupture data:-

Table 4.11 Stress-rupture lifetimes of butt welds in SDR11 63, 90 and 125mm Rigidex 002-50 MDPE pipe systems tested at 9.5 bar and at 79°C.

	Time To Failure, Hours.		
Nominal Fractional Misalignment, %	Pipe Outside Diameters, mm		
	63	90	125
00	4,846.3 8,152(P) 4,919.4 8,442(P) >7,227.9 8,915(P) >7,371.5 10,945.6	1,728(P) 2,138(P) 3,267(P) 3,935(P)	>3,251.8 >3,759.2 >3,888.1 >3,896.9
Mean ± s.d. (coeff. variation)	>7,602.5 ± 2,632 (.267)	>2,767 ± 1,015 (.367)	>3,699.0 ± 304
09	8,543.6 8,754.8 9,601.8(P) 12,003.7(P)	2,742.0 3,015.1 3,568.5 3,762.4	2,721.4 3,393.9 >3,147.3 >3,440.3
Mean ± s.d. (coeff. variation)	9,726.0 ± 1,586 (.163)	3,272.0 ± 475 (.145)	>3,176.0 ± 329 (.104)
18	350.5 2,096.7 1,735.9 2,719.6 2,047.5 3,514.1 2,131.1 5,008.1	915.5 1,567.2 1,822.4 2,057.5	907.7 1,129.7 1,166.4 1,193.3
Mean ± s.d. (coeef. variation)	2,836.0 ± 1,121 (.395)	1,591.0 ± 493 (.310)	1,099.0 ± 130 (.118)
35	632.9 899.6 936.2 1,169.0		
Mean ± s.d. (coeff. variation)	909.0 ± 220 (.242)		
44	858.0 1,151.5 874.0 1,436.1 936.1 1,901.7 1,143.7	311.2 318.8 328.8 371.6	222.1 235.4 310.2 333.4
Mean ± s.d. (coeff. variation)	1,186.0 ± 375 (.316)	332.6 ± 27 (.081)	275.0 ± 55 (.200)

Table 4.12 The ratio of mean stress-rupture performance of butt welds in Rigidex 002-60 HDPE to mean stress-rupture performance of butt welds in Rigidex 002-50 MDPE pipe systems.

Nominal Fractional Misalignment, %	The Ratio Of Mean Stress-Rupture Performance
00	18.2×10^{-3}
09	08.0×10^{-3}
18	17.8×10^{-3}
44	16.0×10^{-3}

Table 4.13 Ratio of stress-rupture performance in terms of total testing time to total testing to failure under fatigue for ΔP=9.5 bar in Rigidex 002-50 MDPE pipe systems.

Nominal Fractional Misalignment, %	Pipe Outside Diameter, mm		
	63	90	125
00	25	>05	>05
09	04	13	>08
18	21	10	05
35	12	-	-
44	13	04	03

Table 4.14 Ratio of mean performance of misaligned butt welds in 90 and 125mm to 63mm in Rigidex 002-50 MDPE pipes.

Nominal Fractional Misalignment, %	Pipe Outside Diameter, mm	
	90	125
09	0.34	>0.33
18	0.56	0.39
44	0.28	0.23

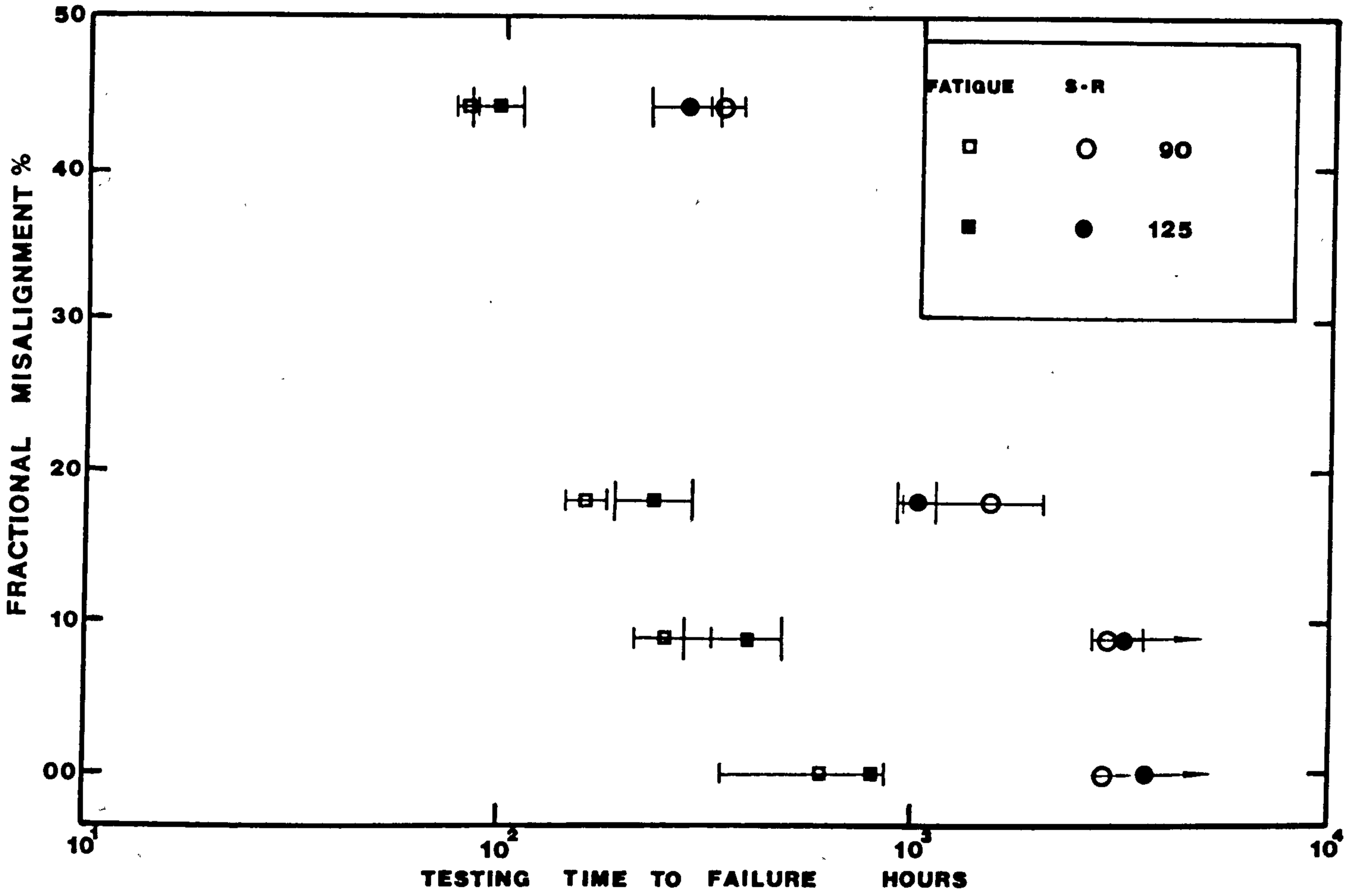

Fig. 4.5(b) Influence of fractional misalignment on the total testing time to failure under stress-rupture and fatigue for 90 and 125mm SDR11 Rigidex 002-50 MDPE pipe.

(a) All the misaligned butt welds (21) in 63mm pipe systems failed in the circumferential plane at the weld, with the exception of two 9% fractional misaligned butt welds, failure occuring locally on the butt weld where the misalignment was introduced. Of the eight aligned butt welds tested, three circumferential weld and three failures in the pipe away from the butt weld were observed. For two samples, the test was stopped after 7000 hours.

(b) The coefficient of variation for the 18 and 44% misaligned butt welds seems to be similar. However, they are all greater than those recorded under fatigue, again indicating that notches may be less sensitive under stress-rupture.

(c) Assuming the mean performance of aligned butt welds is greater than 7700 hours then the reduction for highly misaligned butt welds (18% and above) would be greater than 60%.

(d) The ratio of the mean performance of butt welds in Rigidex 002-60 HDPE to Rigidex 002-50 MDPE are contained in the table 4.12, and it shows that the stress-rupture performance of Rigidex 002-50 MDPE pipe welds is by far the superior, more than 50 times better than Rigidex 002-60 HDPE - see also figure 4.5, whereas under fatigue the performance of the Rigidex002-50 MDPE pipes was only three times better than Rigidex 002-60 HDPE

(e) The ratio of the mean testing time to failure under stress-rupture to fatigue are included in the table 4.13, and it indicates that while the stress-rupture performance in general is improved compared to under fatigue at all the misalignments by more than 12 times, the best improvement in performance is obtained with the aligned butt weld (it is 25 times better than fatigue).

(iii) 90 and 125mm Rigidex 002-50 MDPE Table 4.11 contains the stress-rupture data generated for 90 and 125mm pipes at

various misalignments under a constant gauge pressure of 9.5 bar ($\Delta\sigma_h$=4.81MN_m^{-2}) at 79°C. The general remarks which can be made on the results of the 90 and 125mm pipe systems are:-

(a) In common with the other misaligned butt welds, all the misaligned butt welds in 90 and 125mm (in total 23) pipe systems failed in the circumferential plane at the weld.

In the 90mm pipe systems, all the four aligned butt welds failed in the pipe remote from the butt weld, on average after 2767 hours. In the 125mm pipe systems no failure was observed in any of the four aligned butt welded samples after 3000 hours and the test was discontinued after this time.

(b) The coefficient of variation for 18 and 44% fractional misalignment did not vary much and it decreased with increases in outside diameter from 90 to 125mm.

(c) In terms of total testing time to failure, in 90mm pipe systems the performance under stress-rupture is better compared to fatigue; the relative improved performance decreases with increasing fractional misalignment. The performance is 13 times better under stress-rupture for 9% fractional misalignment and 4 times better for 44% fractional misalignment. The relative improvement in stress-rupture performance also decreases with increase in pipe outside diameter to 125mm, that is for 125mm pipe systems the stress-rupture performance is better by a value greater than 8 times for 9% fractional misalignment and is similar to fatigue testing time for 44% fractional mislaignment - see table 4.13.

(d) There is a distinct difference in the lifetime of misaligned butt welds in 90 and 125mm pipe systems compared to the 63mm pipe systems. The lifetimes in the 90 and 125mm pipe systems have been reduced compared to the 63mm by two thirds in the case of the 44% fractional misalignment, by more than a

half in the 18% fractional misalignment and by a third in the 9% fractional misalignment case. Stress-rupture data seems to indicate there might be a pipe size effect for misaligned butt welds. However, there is no significant difference in the lifetime of misaligned butt welds between 90 and 125mm.

Note that none of the misaligned butt welds in all the three pipe diameters of Rigidex 002-50 MDPE pipe failed below the minimum specified time of 170 hours at 80°C (and at 4MPa - WAA specification 4 - 32 - 04.)

4.4.0 Influence Of Welding Conditions On Fatigue Performance Of Aligned Butt Fusion Welds

A limited study was undertaken on the influence of welding conditions on the fatigue strength of butt fusion welds. The purpose of the study was to identify the welding condition variable which would reduce the performance of aligned butt welds and also to examine the associated failure mode. The welding variables examined were:-

- Heat soak time
- Heat removal time
- The welding pressure

All the other variables were kept to the standard welding conditions listed in the table 3.6. The first two welding variables were examined for both 63 and 90mm aligned welds in Rigidex 002-50 MDPE pipe, while the third one only for the 90mm aligned welds in Rigidex 002-50 MDPE pipe. The welding variables of heat soak time and welding pressure were chosen to alter the weld bead size and heat removal time was chosen to produce "cold" welds. The aligned butt welds produced under these conditions were tested under fatigue at a pressure range of 9.5 bar using 5 cpm with a trapezodial waveform. The results of this examination are contained in the table 4.15.

(1) Effect of Heat Soak Time Since the heating pressure and the heater plate temperature were held constant, the amount of melt formed was solely dependent on the time of heat application. With the decrease in heat soak time to 30 seconds (0.5 times the standard), the weld bead size was made smaller. In the 63mm pipe the ratio of inside weld bead depth to wall thickness (d/t) was .560 (see table 4.16) compared to .648 for the standard weld. Although all the failures were observed at the weld in the circumferential plane for the heat soak time of 0.5 times the standard, the mean lifetime was seen to increase by a factor of 1.7 or an increase of 67% in the lifetime.

An increase in the heat soak time to 180 seconds, 3 times the standard, gave the d/t (inside) ratio of .923 and the mean lifetime was similar to the standard. It seems that the smaller weld bead size tends to improve the performance of aligned butt welds marginally in 63mm pipe systems.

Note that by increasing the bead size, the reinforcement effect is not brought as might have been expected because of the inherent presence of notches between the weld bead and the bore: thus, it is not a straight forward case of increasing effective wall thickness at the weld.

In general, for 90mm pipe systems, a high portion of pipe system failures were observed to be in the pipe remote from the weld; from the total of 27 aligned butt welds produced under different welding conditions, 17 failures were observed in pipe. These pipe failures are denoted by P or P1 in the table 4.15. In some cases, the failure site was removed and the pipe welded. When the sample was placed back under test, it failed again in the pipe remote from the butt weld as denoted by P2 in the table 4.15, perhaps indicating that the 90mm pipes came from a poor batch of production/material. Since a significant number of failures were in the pipe, it makes it difficult to comment on the trend. However, it is apparent that an increase in the heat soak time to 180 seconds in the 90mm pipe system has promoted

circumferential failure at the weld in all the three samples and inside d/t ratio was .595. The heat soak time of 30 seconds gave an inside d/t ratio of .321 and no failures were recorded within 300,000 cycles, surpassing the maximum number of cycles to which the standard weld was subjected. Standard weld beads in 90mm pipe had d/t ratios of about .402.

(ii) Effect of Heat Removal Time The effect of removal time would be dependent upon the time taken for the temperature to fall to a certain value. Therefore, it would be dependent on both the ambient conditions and size and average temperature of the melt at the end of the heating period. Thus a longer removal time must cause a decrease in temperature and therefore an increase in the viscosity of the melt. One would expect then for an extremely high value of heat removal time (24 seconds, four times the standard) to produce a cold joint which would fail rapidly when under test. However, failures in both 63 and 90mm have resulted from slow crack growth. While all the four samples in the 63mm pipe systems failed in the circumferential plane at the weld, in the 90mm pipe all the three samples failed in the axial plane at the weld due to surface defect on the internal bead caused by irregularity in melt flow during welding. The lifetime for the aligned butt welds with heat removal times of 24 seconds was similar to the standard butt welds for the 63mm pipe size and for the 90mm pipe size the mean lifetime was halved compared to the standard aligned weld which had failed in axial plane at the weld.

It is interesting to note that with a heat removal time of 12 seconds (two times the standard) the mean lifetime was increased by 50% compared to the standard weld for 63mm pipe and for 90mm pipe two circumferential failures were recorded with the lifetime similar to 63mm pipe systems. Now, although a heat removal time of 12 seconds and 24 seconds did not reduce the lifetime significantly, it is not recommended to have such high values. The butt welds in the testing programme were produced indoors with the ambient temperature in the range of 18 to 26°C

whereas in the field one needs to take into account the very low temperatures in winter and also the chilling factor of wind which may well produce a cold joint .

(iii) Effect Of Welding Pressure The effect of increasing welding pressure would be to produce a thin melt flow zone and force the most of the softened material into the bead. However, the ratio of d/t does not seem to vary significantly. No failures were observed for butt welds produced under varying welding pressure, so the comment is restricted to the fact that the performance is at least as good as the standard if not better and may be independent of welding pressures examined (0.5 times and 2 times the standard welding pressure).

Table 4.15 Influence of welding conditions on fatigue testing of aligned butt welds in Rigidex 002-50 MDPE pipe.

Welding Condition/ Parameter	Number Of Cycles To Failure	
	Pipe Outside Diameter, mm	
	63	90
Standard	58,290 81,570	82,200(P) 195,390(P)
	60,150 96,090	104,280(A) 213,240(P)
	63,300(A) 132,060	137,160(A) 233,160(P)
	73,620 160,260	192,750(A) 260,790
Mean ± s.d. (coeff. variation)	90,668 ± 37,202 (.410)	177,371 ± 63,172 (.356)
Heat Soak Time 30 secs.	87,390 134,190	>300,000 [139,050(P1)]
	124,890 152,640	>300,000 [215,760(P1)]
		>300,000 [291,030(P1)]
Mean ± s.d. (coeff. variation)	124,778 ± 27,464 (.220)	>300,000 [215,280(P1)]
Heat Soak Time 180 secs.	56,910 71,880	124,620 [84,660(P1)]
	68,430 72,960	134,220
		220,320 [168,000(P1)]
Mean ± s.d. (coeff. variation)	67,545 ± 7,349 (.109)	159,720 ± 52,700 (.330)
Heat Removal Time 12 secs.	61,800 147,030	77,190 137,040(P)
	84,960 >178,620	126,330 303,600(P)
Mean ± s.d. (coeff, variation)	118,103 ± 54,060 (.458)	>161,040 ± 98,548 (.612)
Heat Removal Time 24 secs.	85,260 99,240	67,230(A) 94,260(A)
	87,000 103,050	69,030(A)
Mean ± s.d (coeff. variation)	93,638 ± 8,836 (.095)	69,030 ± 15,113 (.197)
Welding Pressure 0.5 x standard		128,670(P1) 184,680(P2)
		157,860(P1) 232,350(P2)
		188,400(P)
Mean ± s.d. (coeff. variation)		158,400(P1)± 29,868 (.189)
Welding Pressure 2.0 x standard		58,650(P1) 184,680(P2)
		63,180(P)
		141,180(P1) 189,300(P2)
Mean ± s.d. (coeff. variation)		87,670(P1)± 29,868 (.529)

Table 4.16 Ratio of weld bead height, d to pipe wall thickness, t and weld bead height to weld bead width, w for aligned butt welds in 63 and 90mm MDPE pipes produced under different welding conditions.

Welding Condition Parameter	Inside		Outside	
	d/w	d/t	d/w	d/t
63mm, HST=30	.608±.145	.560±.076	.448±.043	.464±.040
63mm, HST=180	.772±.118	.923±.062	.425±.045	.676±.085
63mm, HRT=12	.435±.011	.555±.014	.429±.024	.468±.055
63mm, HRT=24	.509±.026	.617±.044	.521±.130	.487±.062
90mm, HST=30	.367±.011	.321±.007	.393±.038	.295±.021
90mm, HST=180	.480±.072	.595±.014	.438±.035	.497±.014
90mm, HRT=12	.428±.014	.325±.032	.464±.032	.408±.078
90mm, HRT=24	.424±.096	.377±.026	.472±.017	.419±.066
90mm, WP x .5	.413±.006	.460±.026	.360±.002	.361±.031
90mm, WP x 2	.381±.032	.405±.015	.417±.010	.390±.016

Notes: HST = Heat soak time in seconds, HRT = Heat removal time in seconds
WP = Welding pressure.

4.5.0 Discussion: Fatigue And Stress Rupture Performance Of Butt Fusion Welds

Introduction The preliminary field survey to assess the magnitude of axial misalignment occurring during the installation of MDPE pipe has shown that a gross axial misalignment of 15-20% of the wall thickness can occur in practice. The consequence of such grossly misaligned butt welds was perfectly illustrated in the control experiments involving fatigue and stress-rupture testing. The evidence presented in the section 4.1 and 4.3 illustrates clearly that the fatigue and stress-rupture lifetimes are strongly influenced by the presence of small axial misalignments.

From the performance data recorded for two grades of polyethylene and three different pipe sizes in the tables, 4.1 to 4.5 and 4.10 to 4.11 and also from the relationship between fractional mislaignment and lifetime shown in figures 4.1-4.2 and 4.5 it is clear that butt weld lifetime reduces with increasing axial misalignment. For instance, the lifetime of a 9% misaligned butt weld in 63mm SDR11 Rigidex 002-50 pipe is reduced on average by 28% compared to aligned butt welds, whilst that of 18% is reduced by 50%. Even greater reductions were noted for butt welds in 90 and 125mm pipe systems. Such performance data has already provided useful design information for polyethylene pipelines in the water and chemical process industries. The discussion presented here will concentrate upon specific areas of behaviour which promote an understanding of the mechanical performance of polyethylene pipelines and the process leading to instances of premature and potentially hazardous failures at butt fusion welds.

There are two consistent observations which need to be elucidated those being the circumferential failure at the weld and the reduction in lifetime with increasing misalignment at a given test pressure range. Firstly, the fact that plane of fracture for the misaligned butt weld failures (in total 122

under fatigue and 61 under stress-rupture) predominately was circumferential at the weld. Crack propagation was therefore primarily in response to the axial stresses. Secondly, the reduction in the lifetime with increasing magnitude of axial misalignment at a given ΔP implies that the axial stress must increase with the axial misalignment. Thus the effect of axial misalignment is to effectively increase the axial stress.

Amplified Axial Stress An axial stress expression which takes into account axial misalignment is required. Two expressions are considered and their validity is then examined by applying them to the experimental data.

(i) Ory's Equation As mentioned in section 2.2.6, Reinke and Potente (125) quote Ory's (87) work in which the increase in axial stress, σ_a and hoop stress, σ_h due to axial misalignment as defined in figure 2.10(a) can be accounted for by the following equation:-

$$\sigma_a = \frac{P(d - t)}{4t}\left(1 + \frac{3e}{t}\right) \qquad (2.20)$$

$$\sigma_h = \frac{P(d - t)}{2t}\left(1 + 0.2789\,\frac{e}{t}\right) \qquad (2.21)$$

where P = applied internal pressure, d = outside diameter, t = wall thickness and e = axial displacement.

Using equations (2.20) and (2.21) on a SDR11 pipe at two different pressures, the increase in the hoop and axial stress with increasing misalignment, which is expressed as a percentage of nominal wall thickness, is shown in figure 4.6(a). From figure 4.6(a) it is clear that it is the axial stress which responds significantly to axial misalignment, the hoop stress increasing only slowly with increasing axial misalignment.

For instance, for an axial misalignment of 10 per cent of the wall thickness, the increase in hoop stress is only 3% while the axial stress increases by 30%. For the case of axial

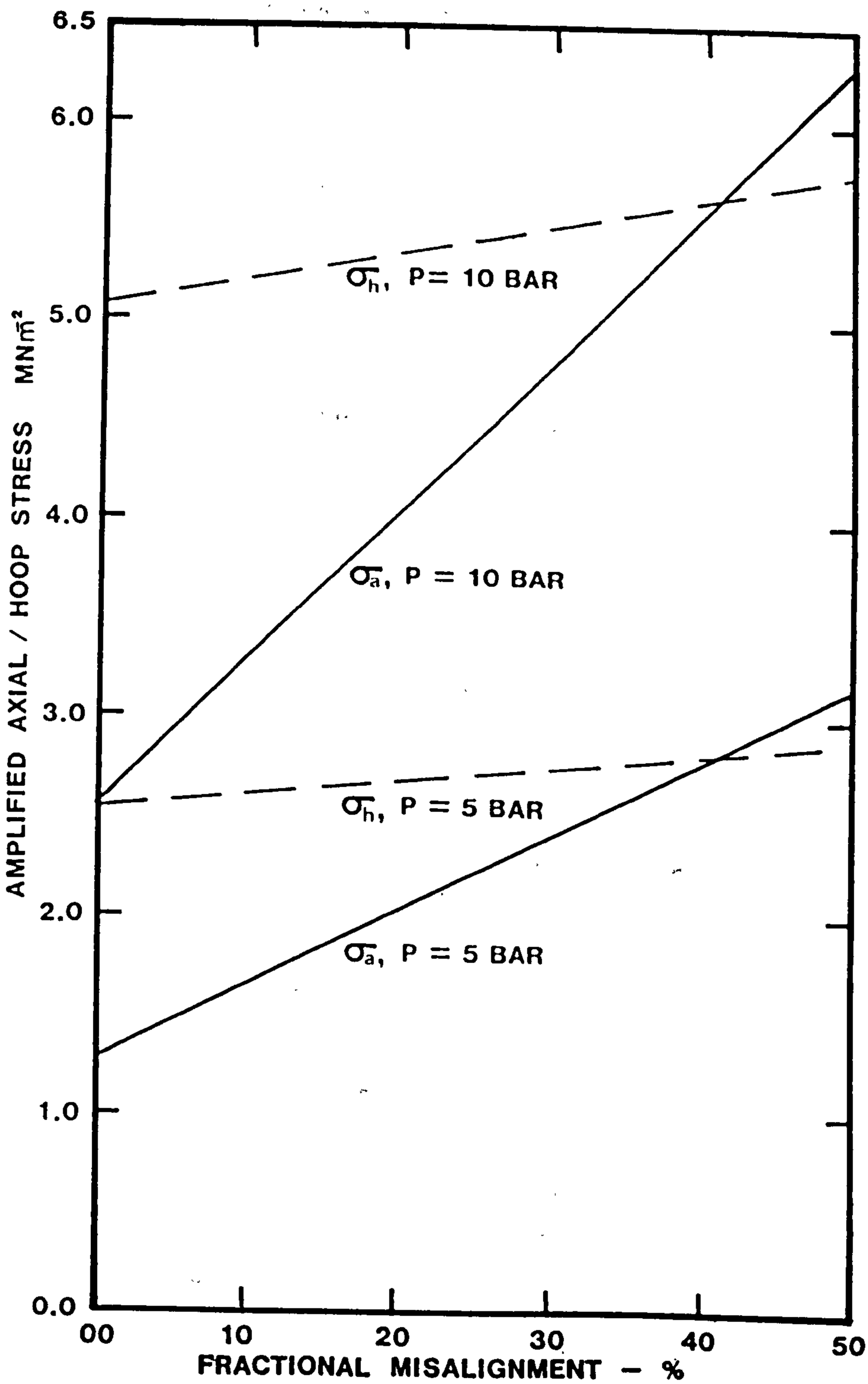

Fig. 4.6(a) Increase in axial/hoop stress due to fractional axial misalignment (e/t) based on Ory's equation (Eq. 2.20 and 2.21) for ΔP=10 bar and 5 bar.

misalignment of 20 per cent of wall thickness the increase in hoop and axial stresses are 6 and 60% respectively over the aligned weld. However, it is also apparent that while axial stress increases with axial misalignment it is still less than the hoop stress up to 44% misalignment. Therefore the axial stress alone is not responsible for initial initiation of misaligned butt weld in reality. This point and the limitation of the approach adopted here will be discussed after the second expression is introduced.

(ii) Nominal Axial Stress At Misaligned Butt Welds

An expression similar to equation 2.21 can be derived in the following manner. The axial or longitudinal stress in the pipe remote from the weld is known, hence the longitudinal force, F_m in the pipe is known and given by (4.1)

$$F_m = \sigma_m A_m \qquad (4.1)$$

where A_m is the area of a perfect annulus.

With the knowledge of F_m and the area of misaligned annulus, A_{mm} that is the offset circles - see figure 4.7(a) the nominal axial/longitudinal stress, σ_{mm} acting on the geometry shown in figure 4.7(a) is given by

$$\sigma_{mm} = \frac{F_m}{A_{mm}} \qquad (4.2)$$

Note the above equation gives a nominal axial stress acting on a misaligned butt weld of the geometry shown in figure 4.7(a). In equation 4.2 A_{mm} was determined numerically using Simpson's rule for each of the offset circles corresponding to each of the magnitudes of misalignment. Hence σ_{mm} was calculated for 9,18,35 and 44% misaligned butt welds and a plot of σ_{mm} verus fractional misalignment was made as shown in figure 4.6(b). The curve 1 in figure 4.6(b) is based on equation 2.20 while curve 2 is based on nominal axial stress and the equation of the line for the curve 2 is

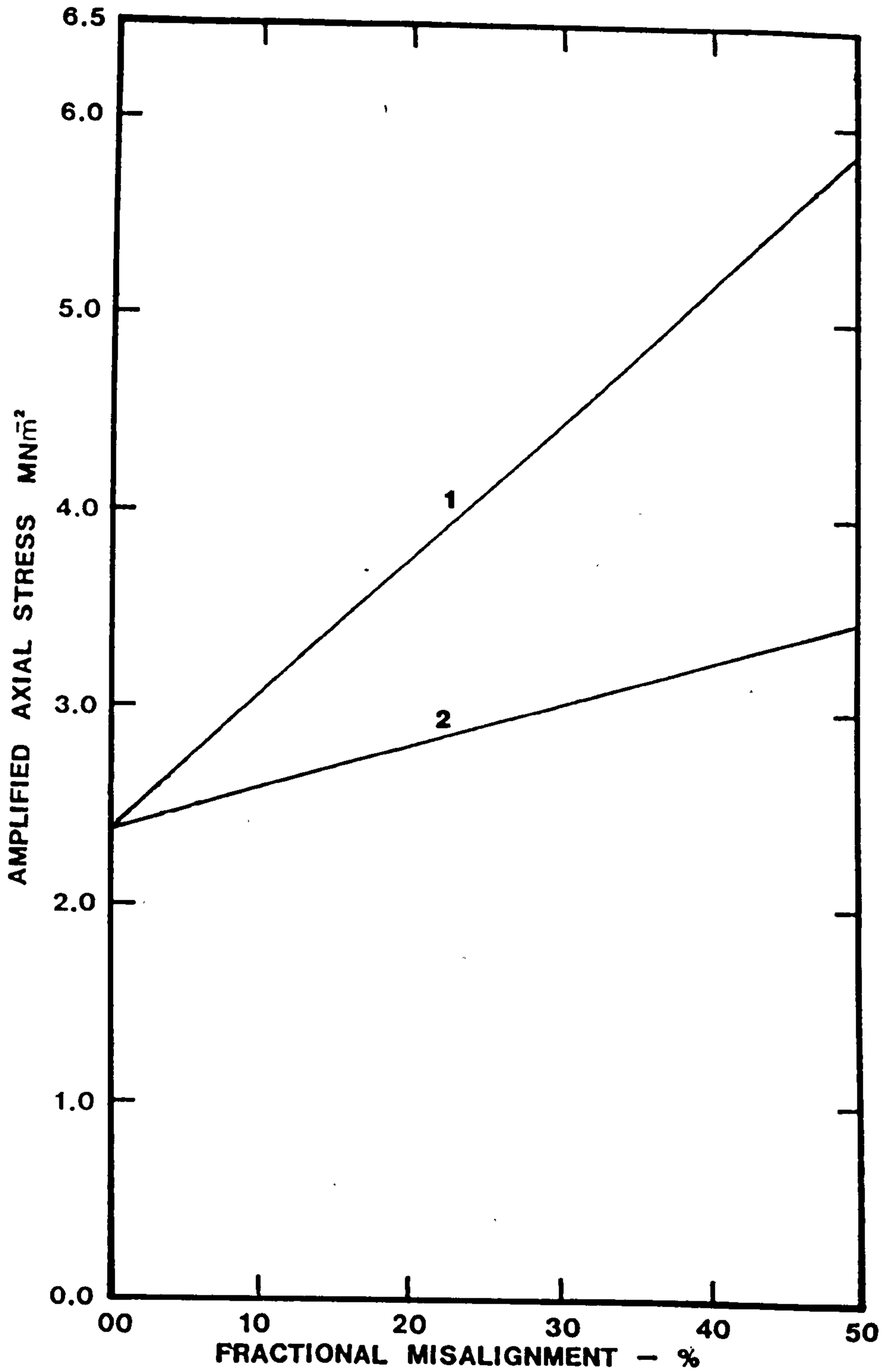

Fig. 4.6(b) Increase in axial stress due to fractional axial misalignment, curve 1 based on equation (2.20) and curve 2 on nominal axial stress at the misaligned butt weld.

$$\sigma_{m} = \frac{P(d - t)}{4t}\left(1 + \frac{e}{t}\right) \qquad (4.3)$$

The difference between equation (2.20)and (4.3) is the constant in front of the term e/t, it is 3 in equation (2.20) and 1 in equation (4.3). It would appear as if the constant 3 in equation (2.20) takes into account the stress concentrator factor whereas equation (4.3) does not. In general, then the increase in axial stress can be given by an expression

$$\sigma_{m} = \frac{P(d - t)}{4t}\left(1 + \frac{Ce}{t}\right) \qquad (4.4)$$

It is acknowledged that the derivation of equation (4.3) is based on a simplistic approach and it is considering the nominal axial stress acting on the misaligned geometry shown in the figure 4.7(a). However, by choosing an appropriate value for constant C in equation 4.4 one can take into account the stress concentration effect due to a staggered weld and also due to notches which are present in reality - see figure 5.9.

The derivation of an equation which takes into account the stress concentration due to staggered butt weld geometry and also the notches using fracture mechanics concepts is beyond the present task. To the authors knowledge the geometry shown in figure 4.7(a) has not been analysied utlising fracture mechanics. However, the circumferential growth from inside circumferential grove in a pipe as shown in figure 4.7(b) has been analysied - see reference 205-208. Such a geometry cannot be modelled to the current problem.

Equation 4.4 is utlised to calculate the axial stress for a range of C values from 0.5 to 4 in order to determine the optimum value for the constant to describe the experimental data for the relationship of :

Logarithm (amplified axial stress) V Logarithm (time to faliure)

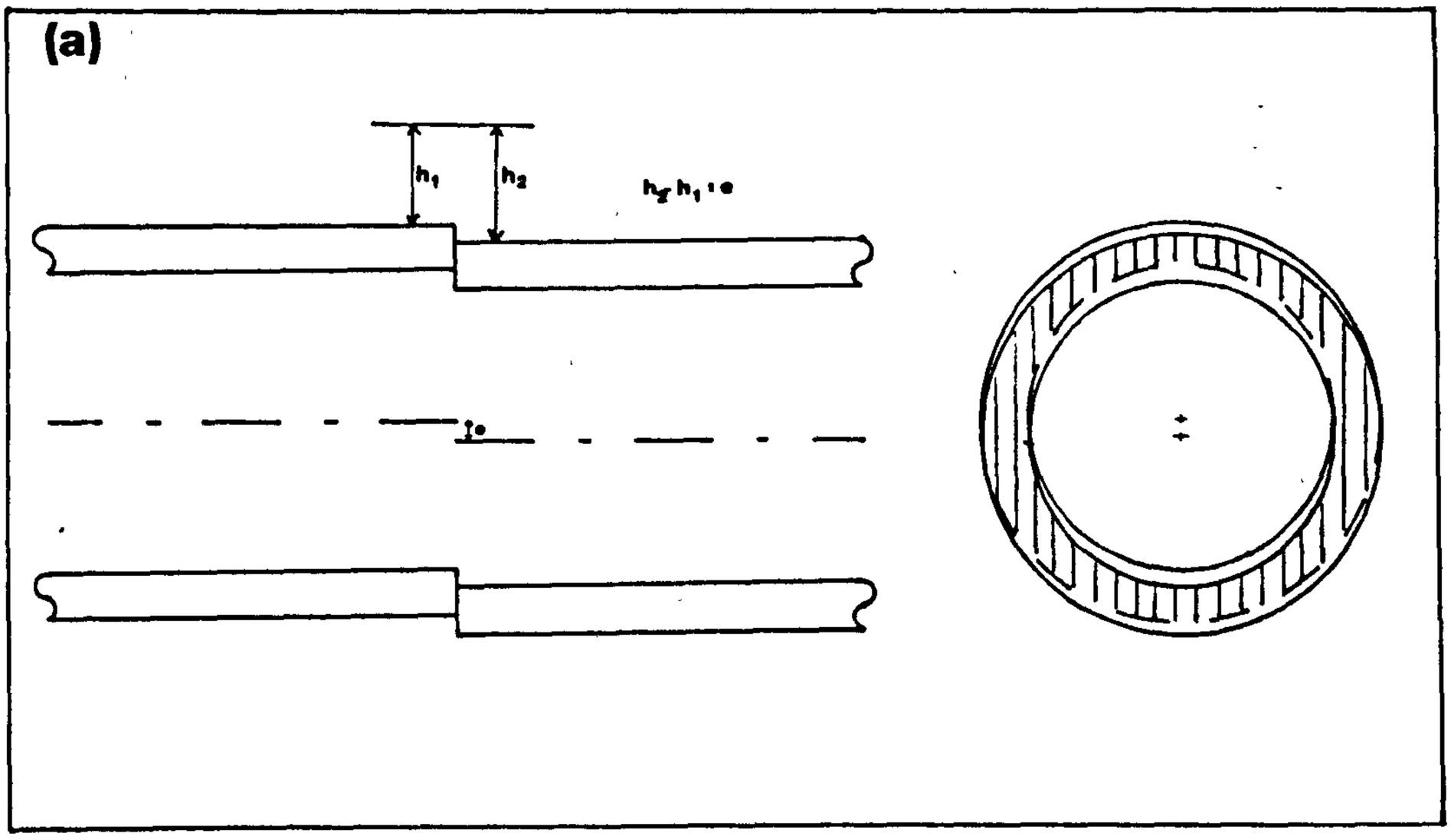

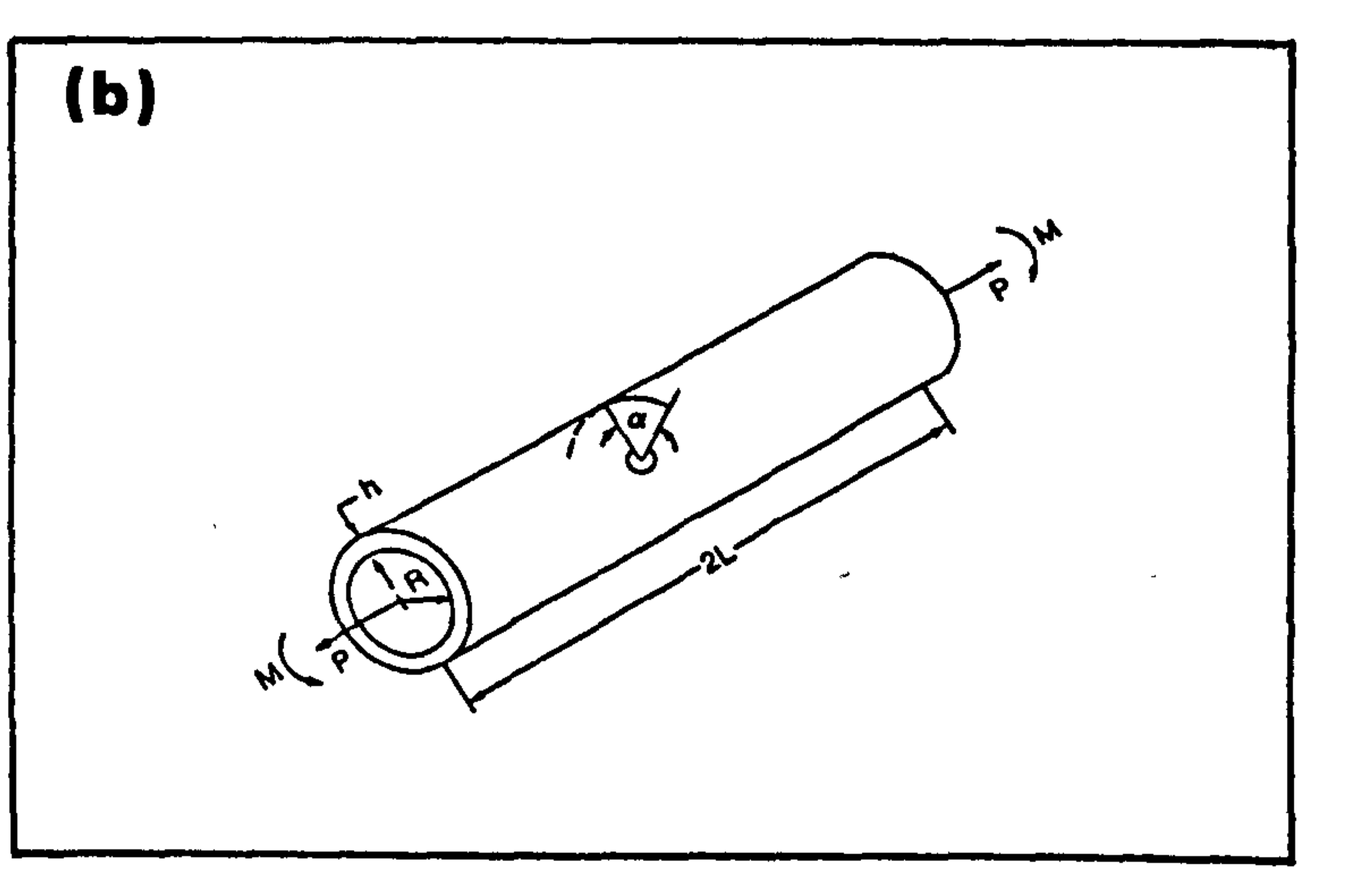

Fig 4.7(a) Misaligned butt weld geometry, (b) circumferential crack in the pipe.

Linear Regression analysis is applied and a correlation coefficient, r, a measure of how well a model accounts for the data is employed in order to ascertain the optimum value of C. All the regression analysis was executed on the computer. Regression analysis assumes the normal distribution for the lifetime and variance to remain constant. If the approach adopted here is valid (use of equation 4.4 to calculate amplified axial stress), then it would enable the plot of axial stress range and lifetime as a function of misalignment shown in figure 4.3 to be converted into one of amplified axial stress range against lifetime such that instead of the four/five curves shown in figure 4.3, the data would fall into one mastercurve.

The bi-logarithmic plot is widely used and is a standard convention to provide the stress-rupture lifetime data of PE pipes. For example, the European Graphical Method and North American Method, whereas the semi-logarithm plot method is the so called Russian method of predicting creep rupture life. In both these presentation methods, it is the pipe hoop stress which is under consideration and time to failure is in hours. In the current form, axial stress was chosen because of the predominate failure of butt welds in the circumferential fracture plane and the time to failure is regarded as the number of cycles to failure in the fatigue case and testing time to failure in hours under stress- rupture conditions.

The fundamental bases on which the logarithm - logarithm plot is based on is the phenomenological creep equation proposed by Sherby (see reference 12)

$$\dot{\epsilon} = A\left(\frac{\sigma}{E(T)}\right)^n \exp\left(\frac{-\epsilon}{KT}\right) \qquad (4.5)$$

Where $\dot{\epsilon}$ is the strain rate, E (t) is the time dependent elastic modulus and n is a constant. If a constant failure strain is assumed this leads to the expression

$$\ln\sigma = \frac{\epsilon_a}{nkT} + \ln E(T) - n^{-1}\ln A + n^{-1}\ln t_f \qquad (4.6)$$

$$\log\sigma = M_1 + M_2 \log t_f \qquad (4.7)$$

Equation 4.6 is a basis for the bi-logarithmic plot which is used in the European Graphical Method and North American Method.

For all the data analysis, amplified axial stress was computed utlising the measured mean outside diameter, minimum local wall thickness at the failure site and measured maximum misalignment at the failure site. The only exceptions were the Rigidex 002-60 MDPE pipe data for both fatigue and stress-rupture case where nominal values were assumed.

4.5.1 Reduction In The Fatigue Performance Of Misaligned Butt Fusion Weld

(i) 63mm Pipe systems The correlation coefficients r for bi-logarithmic, log (amplified axial stress) versus log (number of cycles to failure), using equation 4.4 for a range of C value from 0.5 to 4 to evaluate the amplified axial stress are shown in the table 4.17 for Rigidex 002-60 HDPE and Rigidex 002-50 MDPE data. Rigidex 002-50 MDPE data generated at ΔP=9.5 bar is considered in the table 4.17 and nominal values of misalignment were assumed. It can be seen from the table 4.17 that although the change in r is not significant, the highest r value occurrs when C=3 for both the grades of PE implying optimum value of C=3 is preferred for these data. Rigidex 002-60 HDPE data seems to give a better fit (r=.953) compared to Rigidex 002-50 MDPE (when r=.881).

Figure 4.8 displays the curve for the two grades of PE on a logarithm of amplified axial stress range against logarithm of number of cycles to failure. The amplified axial stress calculated for the plot using equation 2.20. The data obtained from a range of misaligned butt weld tests at one pressure range

Table 4.17 Linear correlation coefficient, r for bi-logarithmic plot using equation (4.4) for C=0.5 to 4.0 to compute amplified axial stress: analysis based on 20 and 35 data points for 63mm SDR11 in Rigidex 002-60 HDPE and in Rigidex 002-50 MDPE pipe systems respectively.

	Linear Correlation Coefficient	
C	Rigidex 002-60	Rigidex 002-50
0.5	.944	.867
1.0	.947	.871
1.5	.949	.875
2.0	.951	.877
2.5	.953	.879
3.0	.954	.881
4.0	.955	.883

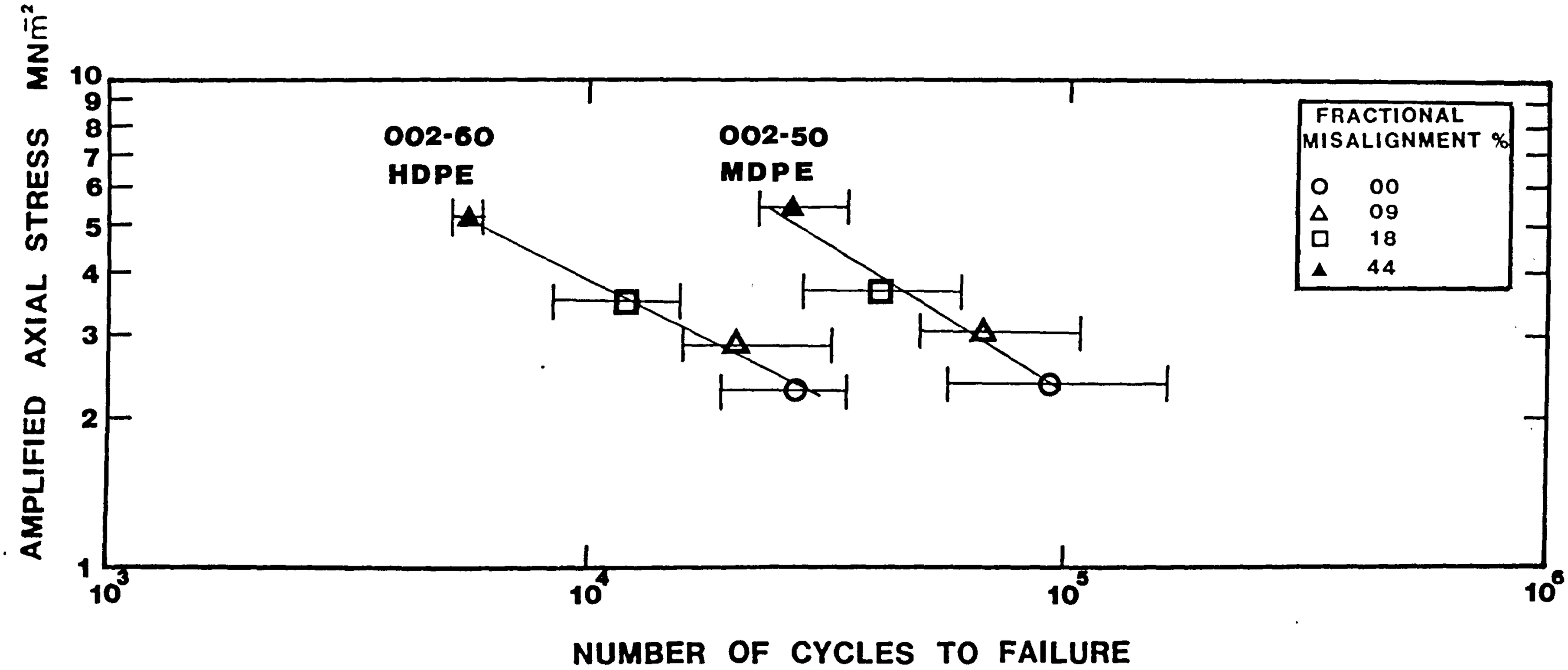

Fig 4.8 Logarithm amplified axial stress versus logarithm number of cycles to failure for 63mm pipe systems in Rigidex 002-60 HDPE and Rigidex 002-50 MDPE.

only nevertheless does fall onto the straight line as expected from the use of amplified axial stress. The gradient of the line for Rigidex 002-60 HDPE is .443 and for Rigidex 002-50 MDPE is .494.

It is apparent that the performance of aligned and misaligned butt welds in Rigidex 002-50 MDPE pipe is superior by a factor of 3 compared to Rigidex 002-60 HDPE. This observation contradicts the anticipated performance since, in general, the fatigue performance of a polymer is expected to improve with increase in molecular weight and crystallinity. For example, De Charantenary et al (192) found the fatigue crack propagation, FCP rate decreased with increasing molecular weight and a fourfold decrease was noted in FCP rates in unpigmented HDPE when percentage crystallinity increased from 47 to 55. Therefore it would appear the Rigidex 002-60 HDPE is inferior to Rigidex 002-50 MDPE because of different use of pigment or some other unknown factor. Note that Rigidex 002-60 grade was withdrawn in mid 1983 and is no longer avalible.

Table 4.18 contains correlation coefficient values for Rigidex 002-50 MDPE pipe systems based on 70 data points generated at three different pressure ranges with five different magnitudes of misalignment. Measured pipe dimensions and misalignment values were used to calculate the axial stress in equation 4.4 for C=0.5 to 4. It shows that r is highest for C=1.5 indicating the optimum value of C=1.5 is preferred for the best fit data.

Figure 4.9(a) gives the bi-logarithmic plot for Rigidex 002-50 pipe systems based on 70 data points. Equation 2.20 was applied to compute the amplified axial stress for consistency purpose with figure 4.8. Note the five curves which were presented in the figure 4.3(a) have merged into one master curve suggesting the approach adopted here is a correct one. The solid line in figure 4.9(a) is the best fit line based on regression analysis of 70 data points generated at ΔP=6.5, 8.0 and 9.5 bar for five

different misalignment with testing times to failure ranging from less than 100 to 4000 hours.

(ii) 90 and 125mm Pipe Systems The correlation coefficients for the logarithm (amplified axial stress) versus logarithm (number of cycles to failure) plot utlising equation (4.4) for C=0.5 to 4 to determine the amplified axial stress are included in the table 4.18. It indicates that for 90mm pipe systems, the optimum value of C=3 is preferred in equation 4.4. Whereas for 125mm pipe system, the optimum value of C is 2.5.

Figure 4.9(b) and (c) display the bi-logarithm plot for 90mm and 125mm data respectively. The amplified axial stress for these plots was determined with the aid of equation (2.20). Note once again the data produced from three/four different magnitudes of misalignment and at least two different pressure ranges fall onto one master curve. 90 and 125mm data tends to have a better fit compared to 63mm. However, the number of data points for 90 was less than half and for 125mm was less than a third of 63mm data.

The gradients of best fit lines shown in figure 4.9(a),(b) and (c) are provided in the table 4.19. The slope is similar for 63 and 90mm data (-.2922 and -.2802 respectively) while it is less for 125mm data (-.3369) by 15% compared to 63mm. Figure 4.10 shows the best fit line for 63, 90 and 125mm data on one plot. There does not appear to be any significant change in the performance of misaligned butt welds with increasing pipe size. However, for 125mm pipe systems a minor improvement in the performance of misaligned butt welds compared to 63mm pipe systems is detectable. These may be due to the fact that rate of pressurisation of the 63mm pipe systems was almost twice that of 125mm.

Whilst little or no change in the performance of misaligned butt welds is detectable with increasing pipe outside diameter, the performance of aligned butt welds noticably increases with

increasing pipe size - see table 4.6(b). In addition, of all the aligned butt welds tested, half in 90 and all the butt welds in 125mm did not fail in the circumferential plane at the weld. The observed improvement in the aligned butt weld may be attributed to one of the following or any combined effects;

(a) Assuming the performance of aligned butt welds is sensitive to changes in the rate of pressurisation then the improved performance of aligned welds in 90 and 125mm may be due to the fact that rate of pressurisation was different to that of 63mm. The rate of pressurisation for 63mm pipe systems was 1.2 and 1.6 times greater compared to 90mm whilst it was 1.6 and 2.0 times greater compared to 125mm at ΔP=9.5 and 6.5 bar respectively. The effect of decreasing pressurisation rate is to decrease the strain rate and thus change the material behaviour. It is well known that with increasing strain rate the Young's modulus and yield strength of polymers increase and material becoming stiffer. A stiffer material usually tends to show less tendency to absorb energy and is less tough.

(b) Assuming the bead size influences the performance of aligned butt welds then the improvement in performance may be attributed to the fact that there is a relative decrease in the bead size compared to pipe wall thickness with increasing pipe outside diameter - see table 4.7. At first sight it might appear that with increasing the bead size one is reinforcing the aligned weld region by effectively increasing the cross-sectional area at that region. However such an effect is not realised because butt welds inherently contain notches, there exists a notch between the weld bead and the pipe surface - see figure 5.9. Thus instead of a large bead reinforcing, a large bead might be acting as a constraint in that region.

(c) The effect of (a) and (b) leads to decrease in the circumferential crack growth rate in 90 and 125mm compared to the 63mm for the aligned butt weld.

Table 4.18 Linear correlation coefficient for bi-logarithmic plot utilising equation (4.4) for C=0.5 to 4.0 in increments of 0.5 to evaluate the amplified axial stress: analysis for Rigidex 002-50 MDPE pipe systems data.

C	Linear Correlation Coefficient		
	Pipe Outside Diameter, mm (Data Points)		
	63 (70)	90 (33)	125 (17)
0.5	.814	.790	.830
1.0	.893	.875	.919
1.5	.909	.905	.954
2.0	.894	.922	.965
2.5	.893	.924	.967
3.0	.876	.923	.964
4.0	.850	.917	.956

Table 4.19 Gradient of the line for the bi-logarithmic plot using equation(2.20) to calculate amplified axial stress.

Gradient Of The Line		
Pipe Outside Diameter, mm		
63	90	125
-.2922	-.2802	-.3364

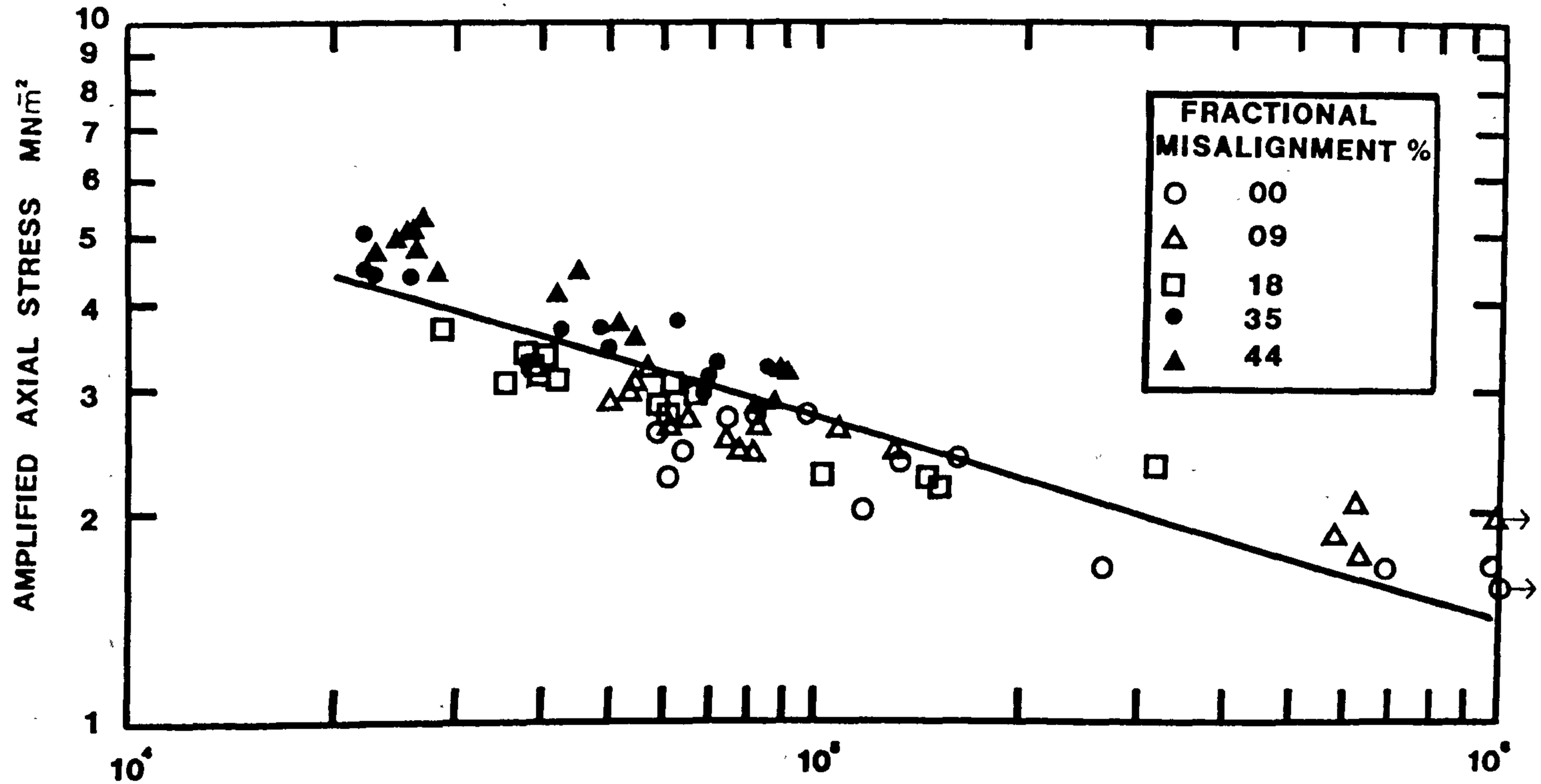

Fig. 4.9(a) Logarithm amplified axial stress versus logarithm number of cycles to failure for 63mm SDR11 Rigidex 002-50 HDPE using equation 2.21 to evaluate amplified axial stress.

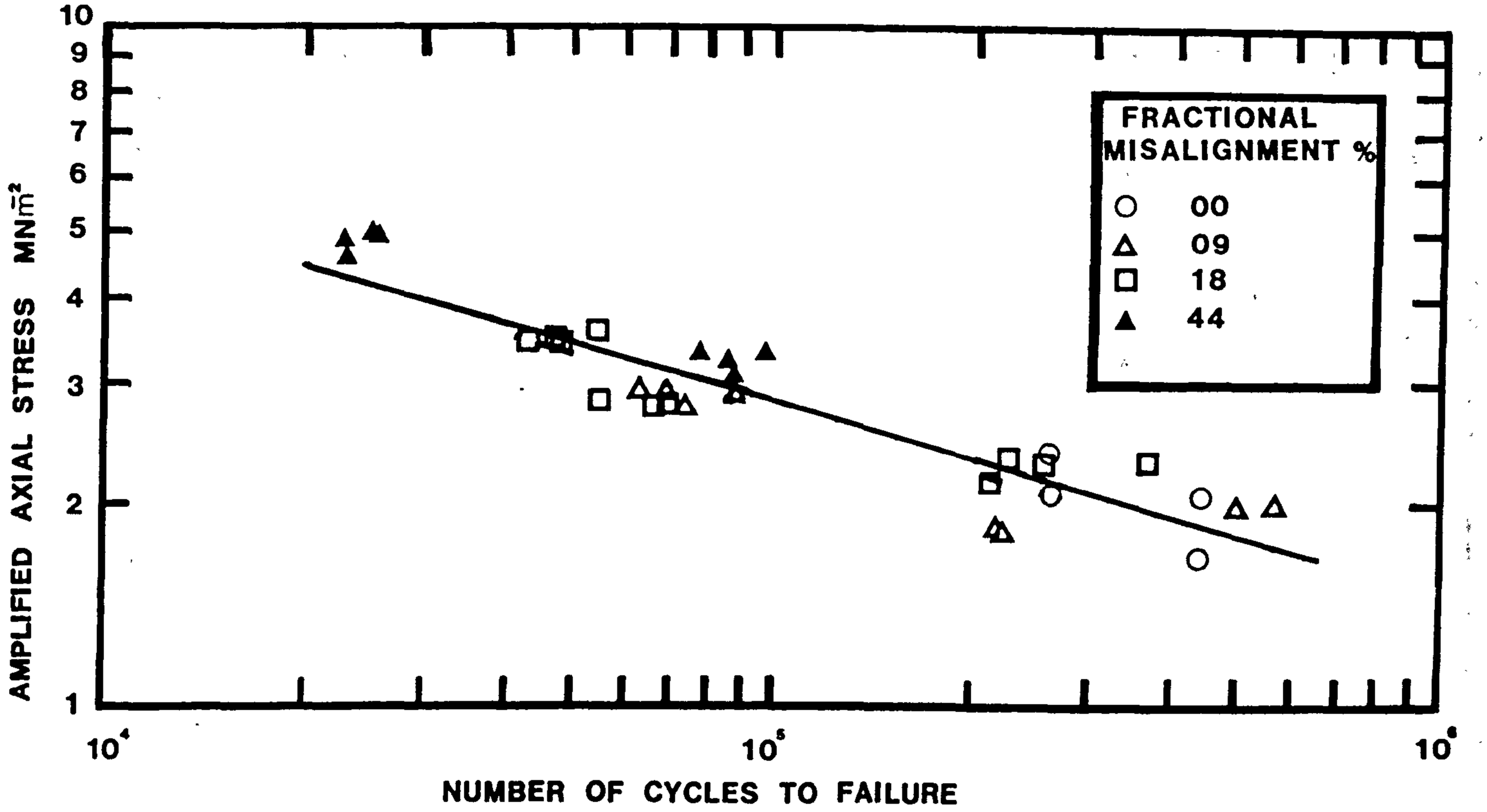

Fig. 4.9(b) Logarithm amplified axial stress versus logarithm number of cycles to failure for 90mm SDR11 Rigidex 002-50 MDPE using equation 2.21 to evaluate amplified axial stress.

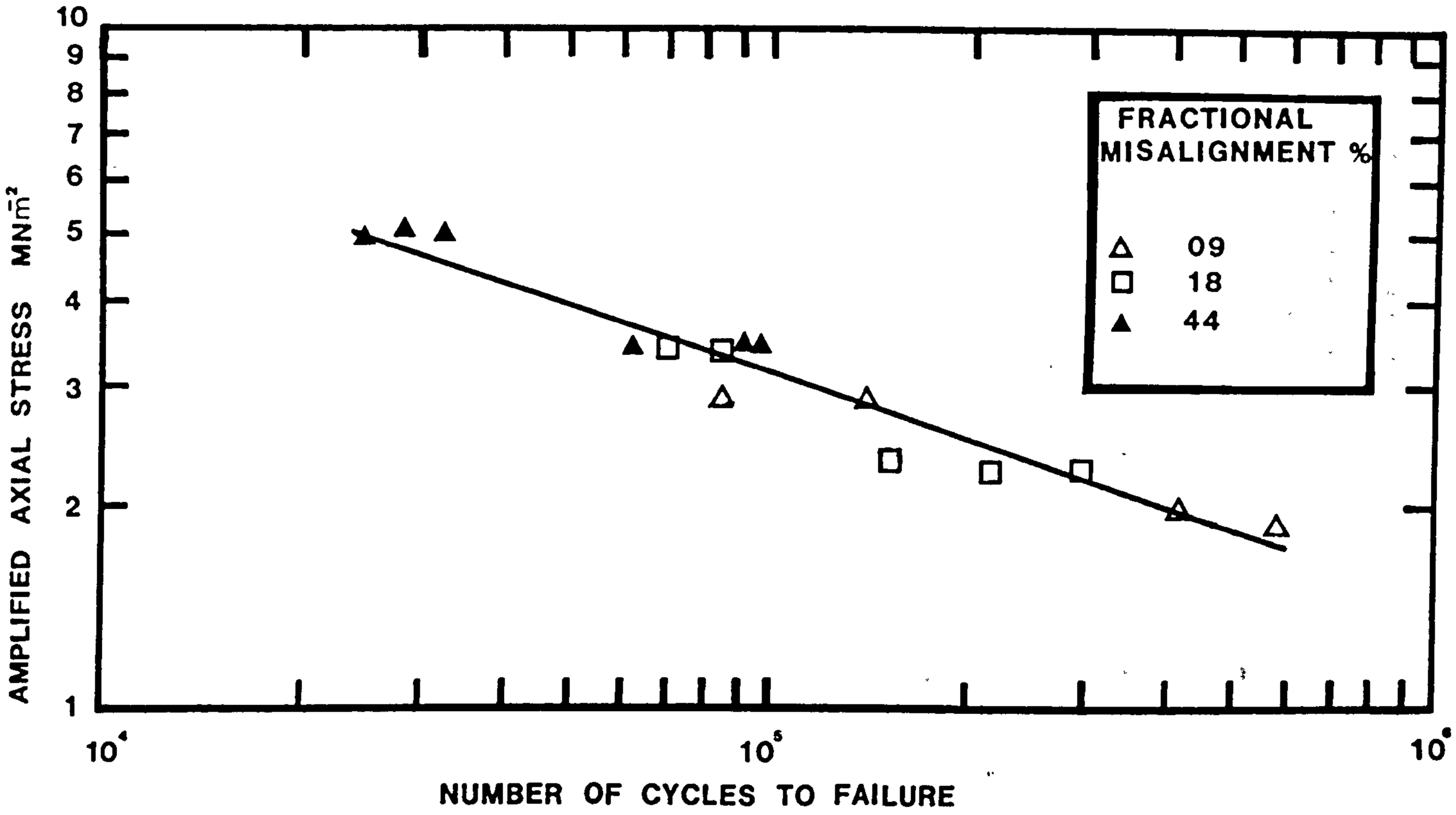

Fig. 4.9(c) Logarithm amplified axial stress versus logarithm number of cycles to failure for 125mm SDR11 Rigidex 002-50 MDPE using equation 2.21 to evaluate amplified axial stress.

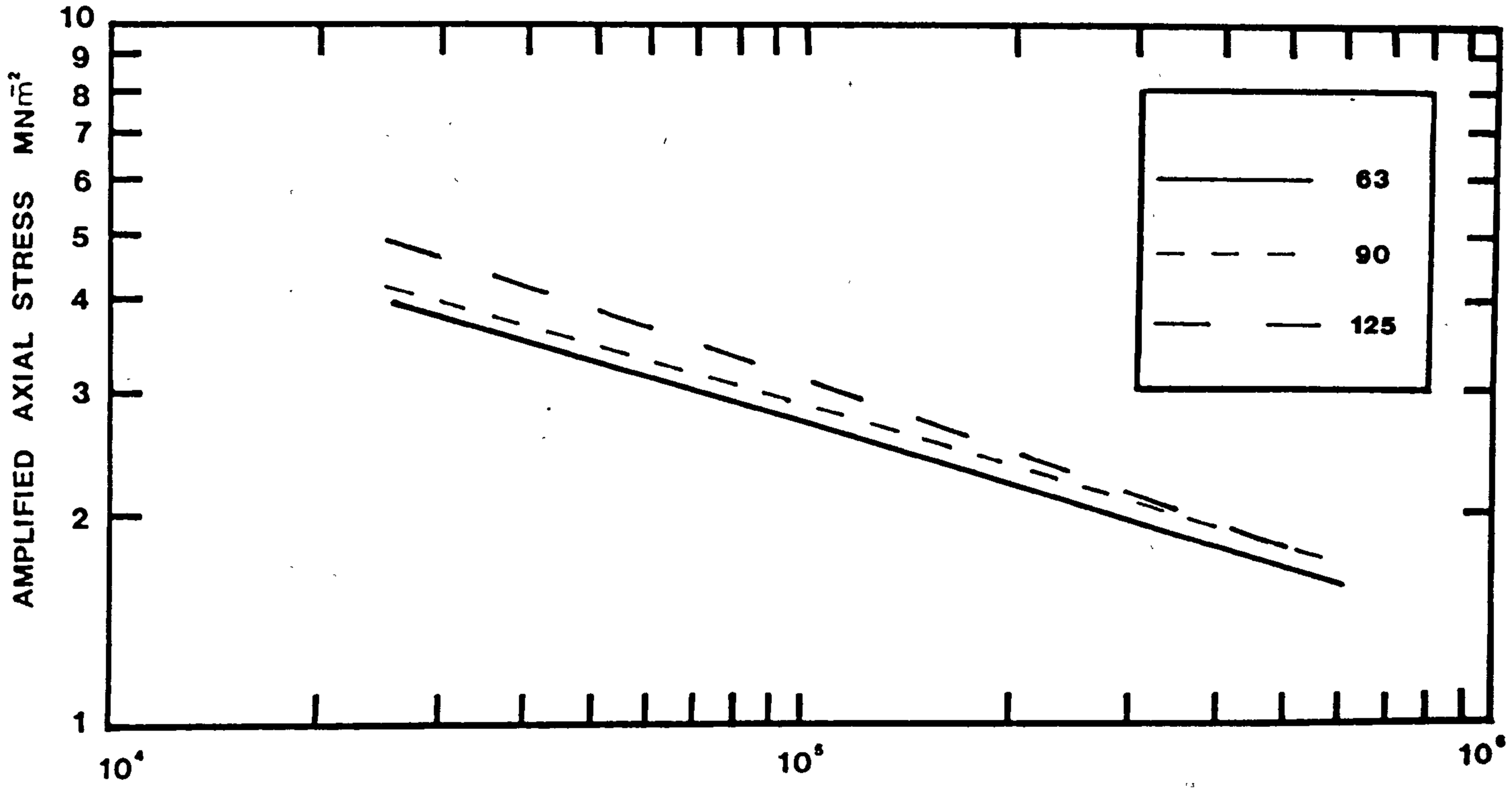

Fig. 4.10 Best-fit line for 63, 90 and 125mm fatigue data, amplified axial stress computation based on equation 2.21.

Equation 4.4 has been applied to model the increase in axial stress due to axial misalignment at the butt weld in 63, 90 and 125mm pipe systems for C values ranging for 0.5 to 4. Optimum values for C in equation 4.4 seems to be specific to pipe diameter. However, since the variation in correlation coefficient was less than 1% to a maximum of 5% for C value in the range 1 to 3, it is concluded C value of 3 and hence equation 2.20 adequately describes all the fatigue data on the bi-logarithmic plot.

4.5.2 The Temperature Dependence Of The Fatigue Performance Of Aligned And Misaligned Butt Fusion Welds In 63 And 90mm Pipe Systems

A selected number of aligned and misaligned butt welds in 63 and 90mm pipe systems were tested at one pressure range and at test temperatures of 59, 69 and 79$_o$C. The aim was to establish the temperature dependence relationship with the lifetimes which would provide some guide to likely performance of butt welds at lower temperatures.

An Arrhenius plot of the performance of 44% fractionally misaligned butt welds in 63mm Rigidex 002-60 HDPE is shown in figure 4.4(a), while figure 4.4(b) gives the same form of a plot for 18% fractionally misaligned butt weld in 63 and 90mm Rigidex 002-50 MDPE pipe. The curves for aligned butt welds are omitted since none of the aligned butt welds at 59°C had failed and besides, for 90mm pipes, there was only one butt weld failure in the circumferential plane at 79°C. However, the lifetimes are provided in the table 4.9.

Considering the Arrhenius plot for misaligned butt welds only, and assuming the relationship between the logarithm of number of cycles to failure and reciprocal of absolute temperature is linear, then extrapolating the best straight line based on the regresion analysis prediction of performance to lower

temperatures can be made. The best fit line shown in figure 4.4(a) and (b) is based on the mean number of cycles to failure with correlation coefficients of 1, .997 and .987 for 63mm Rigidex 002-60 HDPE, 63mm Rigidex 002-50 MDPE and 90mm Rigidex 002-50 MDPE pipe system respectively. The gradients for these lines are similar; 5621, 5489 and 6048 respectively. The slope of the line on an Arrhenius plot is proportional to activation energy, hence the activation energy for the three pipe systems under consideration is similar as one would have expected since material was similar.

The prediction of performance at lower temperatures is made here purely to provide some form of a guideline and since the temperature dependence was only examined at three temperatures with an interval of 10°C, too much importance should not be attached and data should be used with caution. For 44% misaligned butt weld in 63mm Rigidex 002-60 HDPE pipe, extrapolating the best straight line to one decade beyond the lifetime at 59°C it predicts that at 39°C the number of cycles to failure will be about 700,000 or total testing time of 2333 hours (14 weeks). It is normally not advisable to extrapolate the straight line beyond one decade but for the purpose of an estimate in order to gauge some idea of its performance at 20°C, the line when extrapolated, predicts number of cycles to failure of about 9,000,000 or a total testing time of 30,000 hours (1250 days or 3.5 years). The above exercise shows that a butt weld in Rigidex 002-60 HDPE having 44% fractional misalignment subjected continuously to pressure ranges of 9.33 bar ($\Delta\sigma_h$ = 4.73MN_m^{-2}) at a frequency of 5cpm using a trapezodial wave form may fail in about 3.5 years time, falling well short of minimum design lifetime of pipe system of 50 years which include a safety factor of 1.3 or 2.

In the case of 18% misaligned butt welds in 63 and 90mm Rigidex 002-50 MDPE, the predicted number of cycles to failure for these systems at 39°C are about 4.1×10^6 (1.5years) and 7.5×10^6 (≈3years) respectively. whereas the predicted number of cyles

to failure at 20°C are approximately 52x10^6 (≃20 years) and 120x10^6 (≃46 years) respectivley. Therefore, if a butt weld having a misalignment of magnitude 18% of the pipe wall thickness in SDR11 63 and 90mm Rigidex 002-50 MDPE pipe were subjected continuously to a pressure range of 9.5 bar at 5 cpm using the trapezodial waveform then they may fail in about 20 years and 46 years time respectively. This again falls short of minimum design life of pipe system of 50 years.

The above prediction although based on limited test temperatures illustrates that a grossly misaligned butt weld will reduce the lifetime below the 50 years design lifetime of pipe systems. Hence care must be taken to align the butt weld and minimise the misalignment to below 10% of the pipe wall thickness.

4.5.3 Reduction In The Stress-Rupture Performance Of Misaligned Butt Fusion Welds

Stress-rupture performance data is analysed in two main ways. Firstly, the reduction in the stress-rupture performance of misaligned butt fusion welds is analysed using the same criteria as in the fatigue case. Equation 4.4 is employed to model the increase in axial stress for C values in the range of 0.5 to 4 for the representation of data in the form of logarithm of amplified axial stress versus logarithm of time to failure. Secondly, the comparison of the stress-rupture performance to the fatigue performance at an equivalent maximum stress and the same temperature is considered. Note that these two forms of analysis are made possible because all the misaligned butt welds in the three pipe diameters under the stress-rupture conditions had failed in the circumferential plane at the weld in the brittle manner similar to that observed under fatigue.

Amplified Axial Stress

(i) 63mm Pipe Systems Table 4.20, contains the correlation coefficient, r, for bi-logarithmic plots employing equation 4.4 to compute the increase in axial stress due to axial misalignment for C = 0.5 to 4. The correlation coefficient is high, but has remained constant for Rigidex 002-60 data at .915 and for Rigidex 002-50 data at .872 in the range of C = 2.0 to 3.0. The failure of r to respond to change in C value infers that the analysis is not sensitive enough to detect the changes or that it may be due to the fact that nominal dimensions of pipe and nominal value of axial misalignment were assumed in the determination of σ_a.

Table 4.21 provides correlation coefficient values for 63mm Rigidex 002-50 pipe systems where the amplified axial stress was determined using measured dimensions of pipe and measured misalignment. It shows r is highest for C = 3 and compared to values recorded in table 4.20 r changes with C.

Figure 4.11 shows the stress-rupture plot for the two grades of polyethylene. The stress-rupture curve for Rigidex 002-50 MDPE pipe lies well to the right of Rigidex 002-60 HDPE pipe. The performance of misaligned butt welds in MDPE is better by a factor of 50 compared to HDPE. This seems to contradict the Muller and Gaube (91,113) observation who indicated the stress-rupture performance increased with increasing molecular weight and increasing density. The reason for the inferior performance of HDPE compared to MDPE might be due to the different use of pigment, since the performance of a given grade of MDPE is also specific to the use of pigment.

(ii) 90 and 125mm The correlation coefficient values for the analysis of limited 90 and 125mm data are given in table 4.21. Since the analysis involves only 10 data points, it is not surprising that there is no significant change in r with C. However there is a trend in r values and it appears that the

Table 4.20 Linear correlation coefficient, r for bi-logarithmic plot using equation (4.4) for C=0.5 to 4.0 to compute amplified axial stress: analysis for stress-rupture data based on 21 and 23 data points for 63mm SDR11 in Rigidex 002-60 HDPE and in Rigidex 002-50 MDPE pipe systems respectively.

	Linear Correlation Coefficient	
C	Rigidex 002-60	Rigidex 002-50
0.5	.915	.868
1.0	.915	.870
1.5	.915	.871
2.0	.915	.872
2.5	.915	.872
3.0	.915	.872
4.0	.914	.870

Table 4.21 Linear correlation coefficient for bi-logarithmic plot utilising equation (4.4) for C=0.5 to 4.0 in increments of 0.5 to evaluate the amplified axial stress: analysis for stress-rupture butt welds in Rigidex 002-50 MDPE pipe systems data.

C	Linear Correlation Coefficient		
	Pipe Outside Diameter, mm (Data Points)		
	63 (23)	90 (11)	125 (10)
0.5	.804	.953	.977
1.0	.882	.967	.982
1.5	.898	.968	.983
2.0	.905	.967	.984
2.5	.909	.967	.984
3.0	.909	.966	.984
4.0	.909	.965	.985

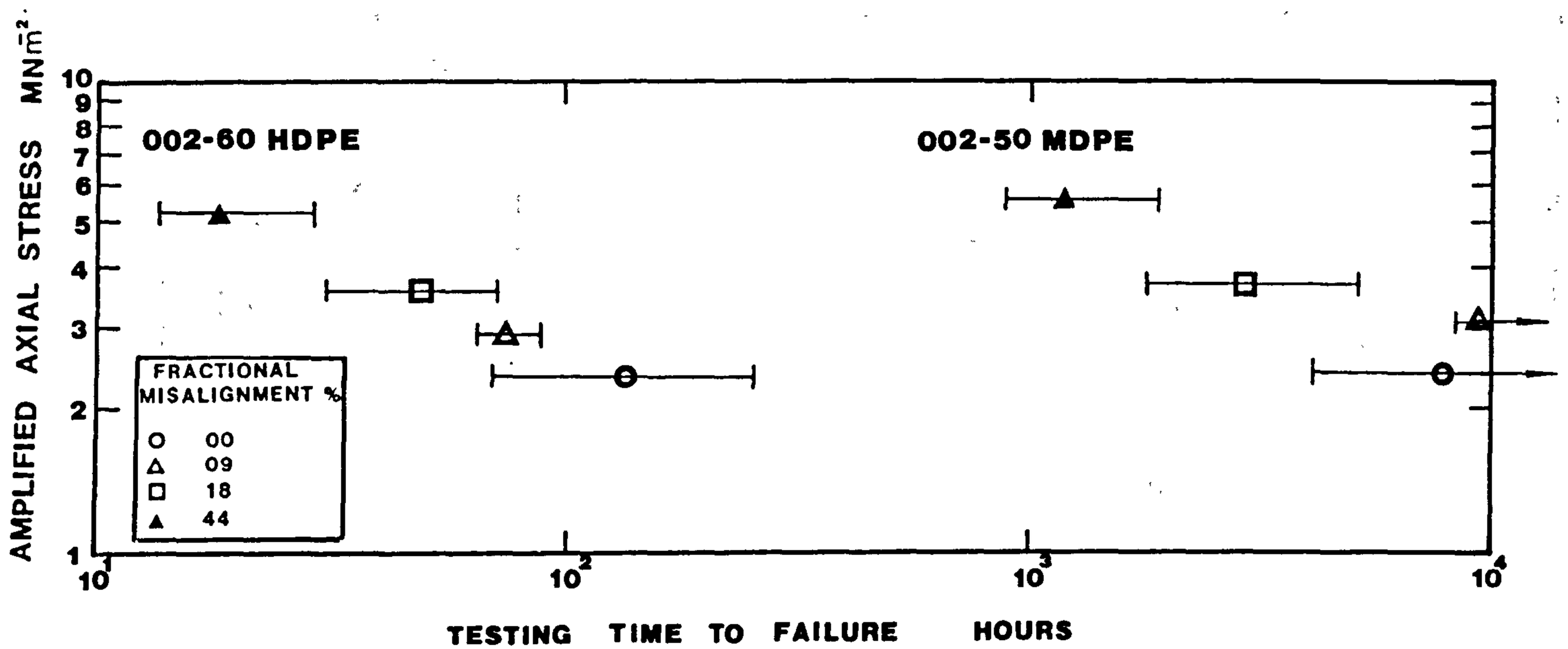

Fig. 4.11 Logarithm amplified axial stress versus logarithm time to failure for 63mm SDR11 Rigidex 002-60 HDPE and Rigidex 002-50 MDPE pipe systems.

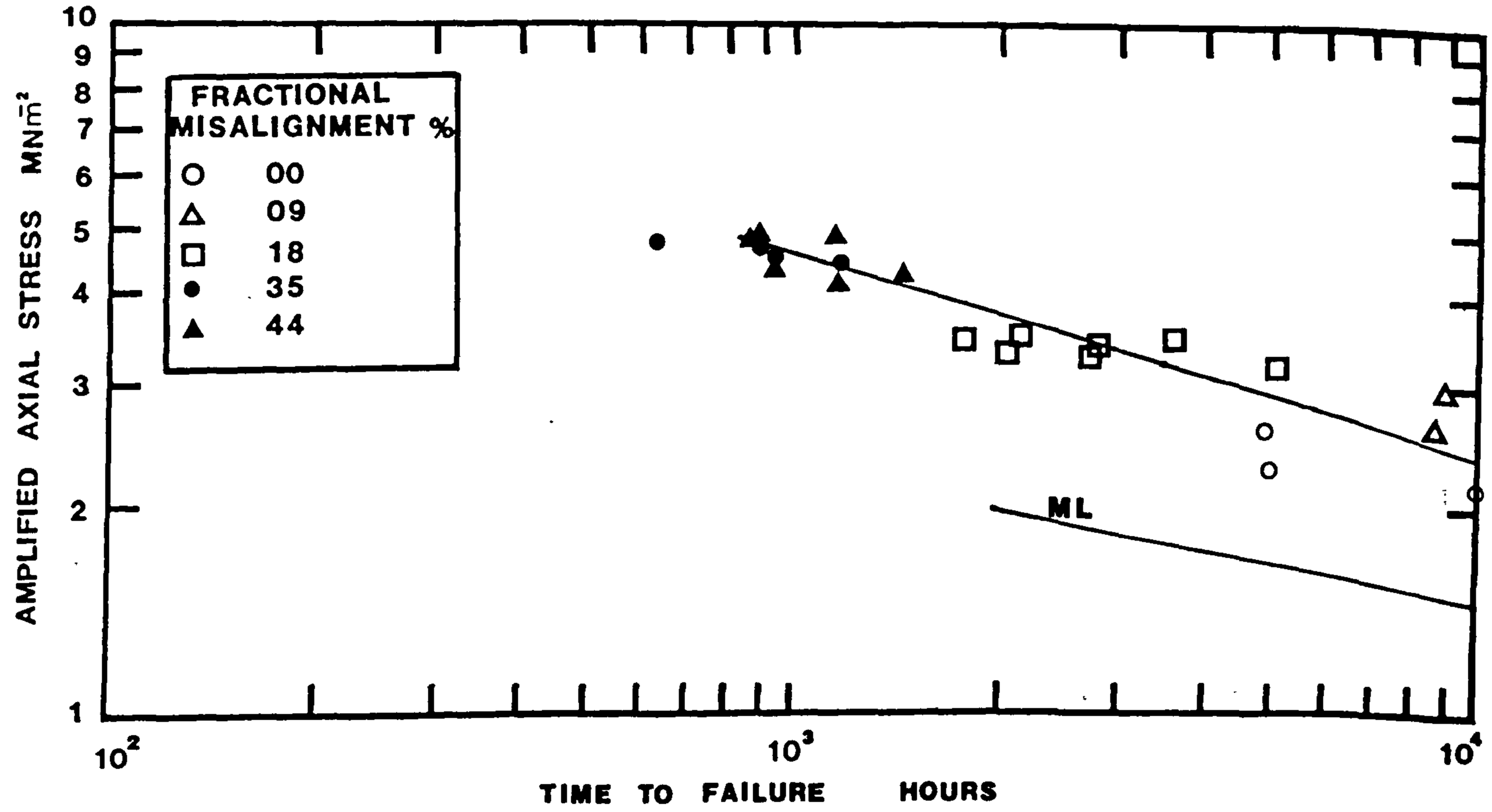

Fig. 4.12(a) Logarithm amplified axial stress versus logarithm time to failure for 63mm SDR11 Rigidex 002-50 MDPE pipe systems.
ML = Pipe manufacture's line (After Ref.3).

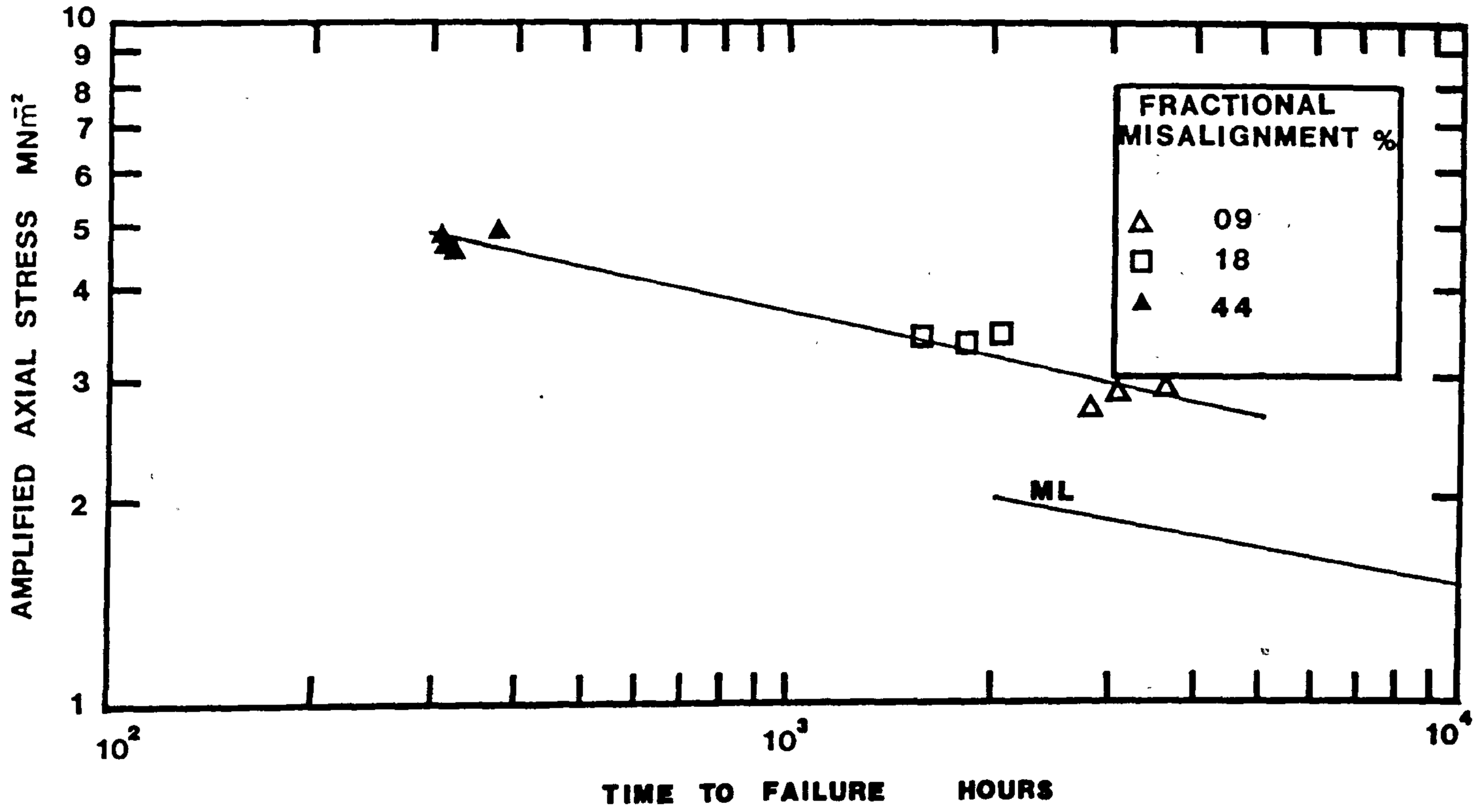

Fig. 4.12(b) Logarithm amplified axial stress versus logarithm time to failure for 90mm SDR11 Rigidex 002-50 MDPE pipe systems.
ML = Pipe manufacture's line (After Ref.3).

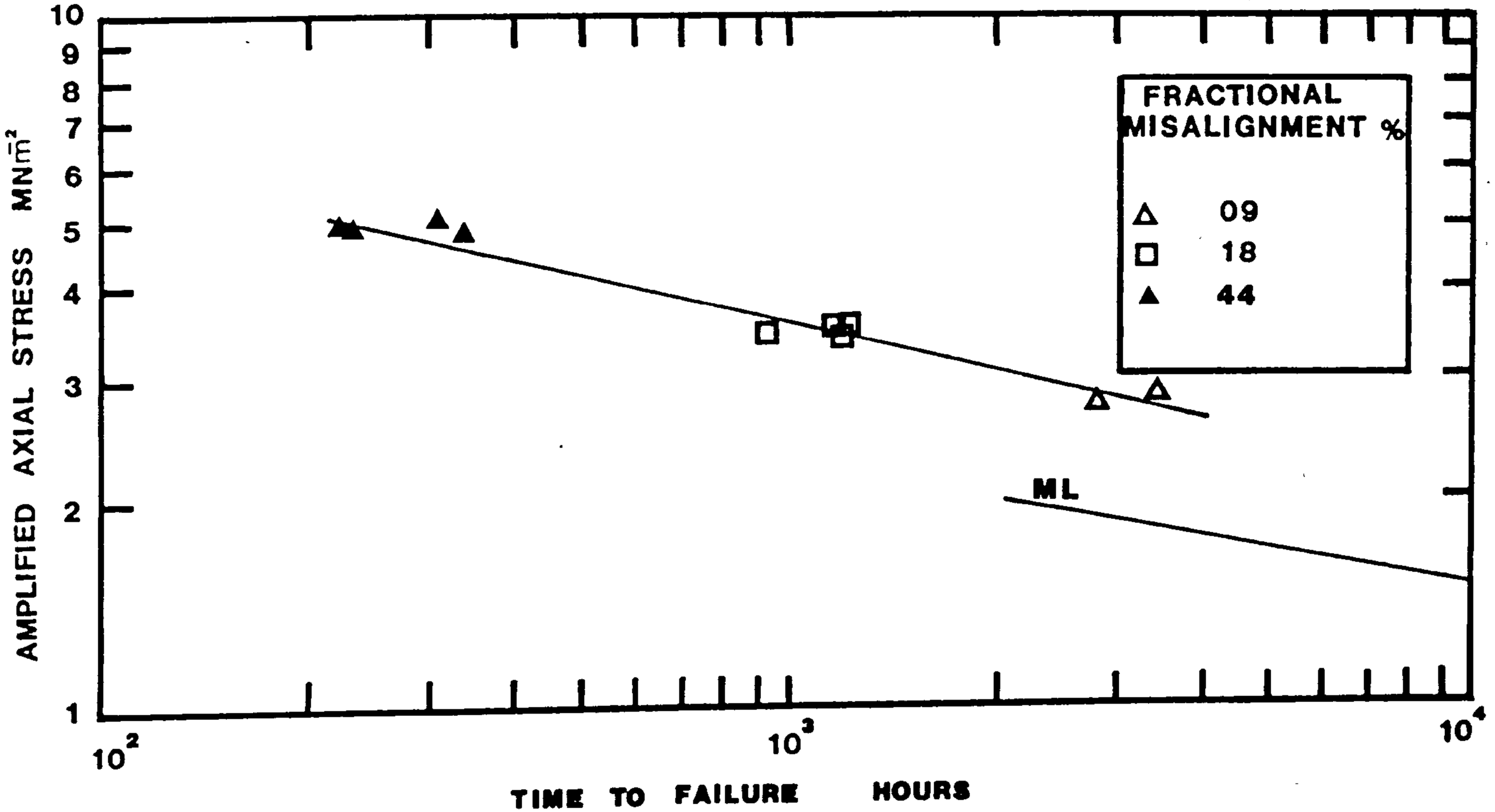

Fig. 4.12(c) Logarithm amplified axial stress versus logarithm time to failure for 125mm SDR11 Rigidex 002-50 MDPE pipe systems.
ML = Pipe manufacture's line (After Ref.3).

optimum value of C is 1.5 for 90mm stress-rupture data, the analysis tends to confirm that the approach of amplified axial stress is correct one.

Figure 4.12 displays the bi-logarithmic plot which shows the curves for 63, 90 and 125mm stress-rupture data. It indicates that the stress-rupture performance of misaligned butt welds tends to decrease with increasing pipe outside diameter to 90 and 125mm. For example for 18% misaligned butt welds the lifetime in 90 and 125mm pipe is reduced by half compared to 63mm performance. In contrast to the effect noted under fatigue, stress-rupture results seem to show that there might be a pipe diameter effect. However, there is no substantial difference in the lifetime of misaligned butt welds between 90 and 125mm.

Stress-rupture curves for all the three pipe sizes in figure: 4.12(a), (b) and (c) are to the right of the manufactures line, thus implying that performance of misalignment butt welds met the manufactures specification and were well within the standard minimum specified time of 170 hours at 80°C and at 4MPa. To take full advantage of the improved grade of pipe material it should be realised that the misalignment must be kept below 10%

None of the aligned butt welds in 90mm and 125mm pipes had failed and only three out of eight in 63mm. This implies pipe to pipe aligned butt welds are not a source of weakness if manufacturer's recommeded conditions of temperature and pressure are used and pipes are aligned correctly. It also confirms the general observation made by the research workers (49, 73, 95, 88) in the field of pipe testing that under stress-rupture the samples do not fail at the weld but in the pipe itself.

Comparison Of Stress-Rupture Performance To Fatigue

Comparison of stress-rupture performance to fatigue is made in two different ways:

(a) Performance is defined by total testing time, t, since in practice it is the total testing time to failure that is normally recorded for service failures.

(b) since the applied wave form under fatigue was a trapezodial type, a pseudo stress-rupture or cyclic stress-rupture lifetime t_f can be defined as

$$t_f = N_f t_{max} \qquad (4.8)$$

where N_f is the number of cycles to failure and t_{max} is the maximum time under the load - see figure 4.13. This concept has been utilised to allow comparisons to be made between stress-rupture and fatigue data (see reference 99,108,109). If $t_{sr} \simeq t_f$, then butt welds exhibit no substantial weakness under fatigue. If however, $t_{sr} >> t_f$, the reverse is true. t_{sr} is the stress-rupture lifetime and for stress-rupture $t_{sr} = t$; for fatigue $t = N_f t_c$ where t_c is the cyclic time.

Finally an attempt is made to predict the fatigue performance from stress-rupture lifetimes assuming cumulative damage principles. An equation similar to that quoted by Staple (99) can be used to predict number of cycles to failure:

$$N_f = \left(\frac{t_{sr}}{(t_{max})_{\tau,\sigma}}\right) \qquad (4.9)$$

(i) <u>Rigidex 002-60 HDPE Pipe</u> Table 4.22 contains the ratios of t_{sr}/t and t_{sr}/t_f, whilst figure 4.14 displays the stress-rupture and fatigue performance of misaligned butt welds in terms of t, t_f and t_{sr}. It shows that in terms of total testing time to failure, aligned butt welds in Rigidex 002-60 HDPE pipe under stress-rupture are marginally better (1.5 times) compared to under fatigue, while there was no change in the stress-rupture performance of misaligned butt welds compard to under fatigue. Comparison of stress-rupture performance to fatigue in terms of a practical parameter, t indicates that for Rigidex 002-60 HDPE tested at a maximum pressure of 9.33 bar shows there

does not seem to be any fatigue weakness. This seems to imply at high stress, fatigue may not be a serious problem for Rigidex 002-60 HDPE. However when stress-rupture performance is compared to fatigue in terms of a more fundamental parameter, t_r a fatigue weakness is exposed in both aligned and misaligned butt welds.

(ii) Rigidex 002-50 MDPE Pipe The ratio of t_{mr}/t and t_{mr}/t_r for 63, 90 and 125mm Rigidex 002-50 MDPE pipe systems are provided in the table 4.23. The curves in terms of t, t_r and t_{mr} for stress-rupture and fatigue performance of misaligned butt welds are shown in figure 4.15. The table 4.23 indicates that whether one considers t or t_r, fatigue weakness in Rigidex 002-50 MDPE is clearly shown; stress-rupture performance is superior to fatigue by more than an order of magnitude.

The aligned and 9% fractionally misaligned butt welds tend to show a severe fatigue weakness compared to 20% and above misaligned butt welds. With increasing pipe diameter to 90 and 125mm, highly misaligned butt welds (18-44%) suggest that the intensity of fatigue weakness is decreasing. Although the comparison of stress-rupture to fatigue is made at one pressure, it is apparent from table 4.23 one needs to consider misalignment and fatigue critically when designing pipe systems.

On the question of fatigue weakness, one can only speculate that under fatigue the crack propagation mechanism, is highly active and responsive compared to under stress-rupture for a given maximum stress. The crack tip blunting mechanism might not be operating as effectively under fatigue as it does under stress-rupture.

Table 4.22 Comparison of stress-rupture lifetime to fatigue for 63mm SDR11 Rigidex 002-60 HDPE pipe systems.

Nominal Fractional Misalignment, %	t_{sr}/t	t_{sr}/t_f
00	1.5	4.2
09	1.1	3.1
18	1.3	3.4
44	1.0	2.7

Table 4.23 Comparison of stress-rupture lifetime to fatigue for three pipe systems in Rigidex 002-50 MDPE.

Nominal Fractional Misalignment, %	t_{sr}/t			t_{sr}/t_f		
	63	90	125	63	90	125
00	25	05	12	82	14	-
09	44	13	08	126	39	28
18	21	10	05	44	29	16
35	12	-	-	34	-	-
44	13	04	03	36	12	10

Table 4.24 Comparison of predicted number of cycles to failure to experimental observed number of cycles to failure.

Nominal Fractional	Npredict/Nexpt			
	Rigidex 002-60	Rigidex 002-50		
	63	63	90	125
00	4.1	67	>13	>15
09	3.0	117	32	46
18	3.3	50	28	15
35	-	32	-	-
44	2.6	36	12	10

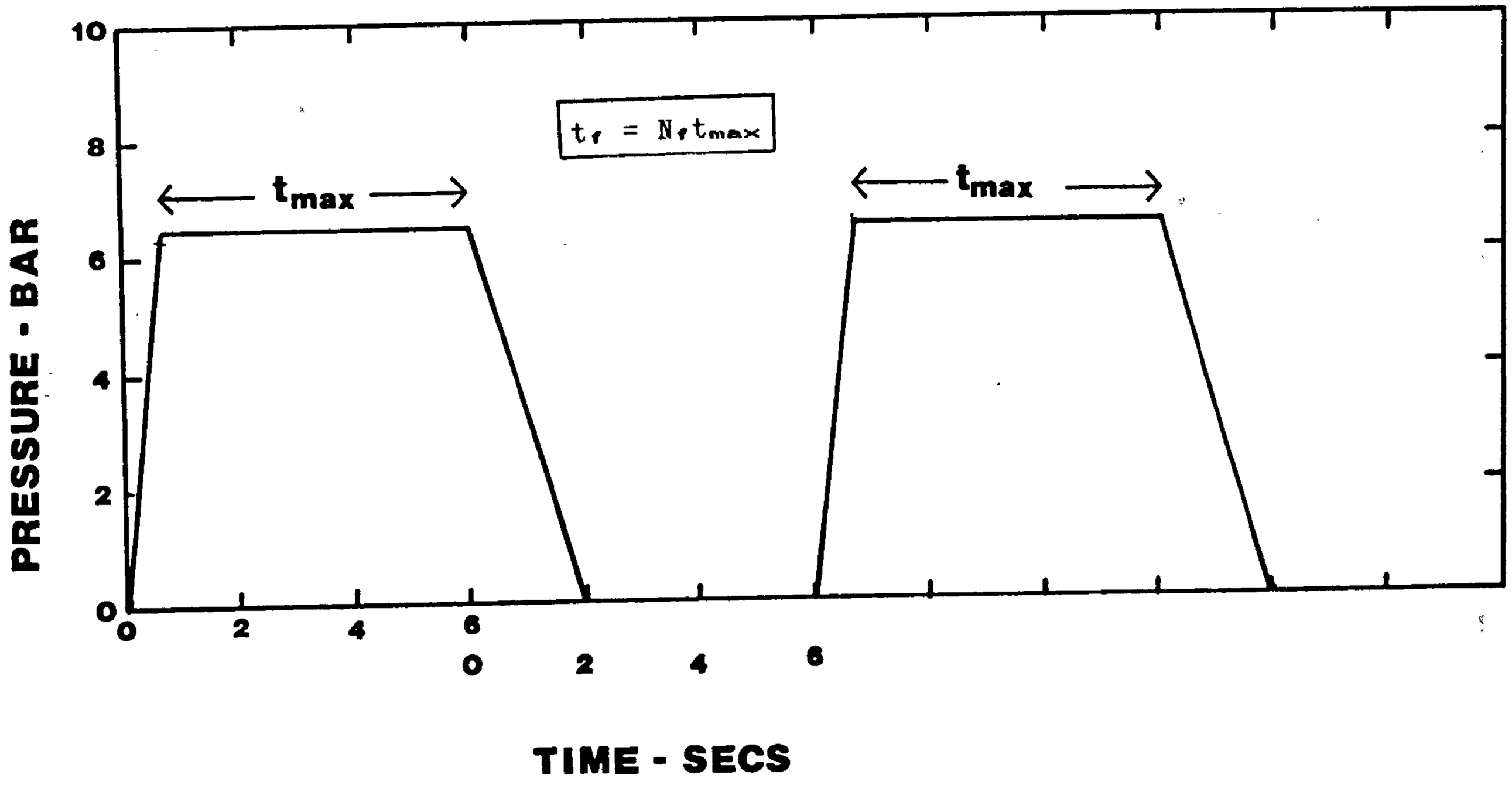

Fig. 4.13 Definition of $t_{fatigue}$.

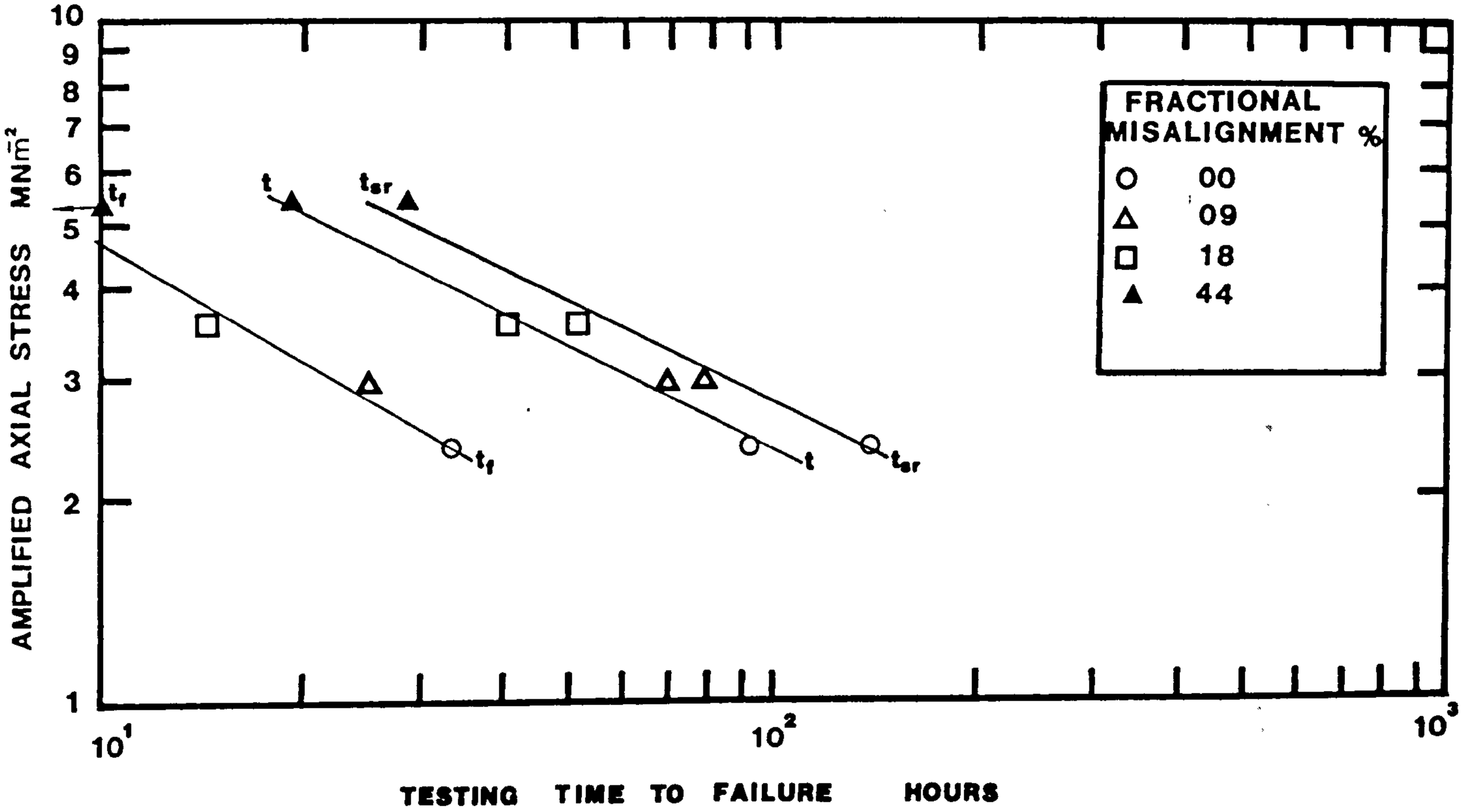

Fig. 4.14 Comparison of fatigue and stress-rupture data in terms of t, t_f and t_{SR} for 63mm SDR11 Rigidex 002-60 HDPE pipe systems.

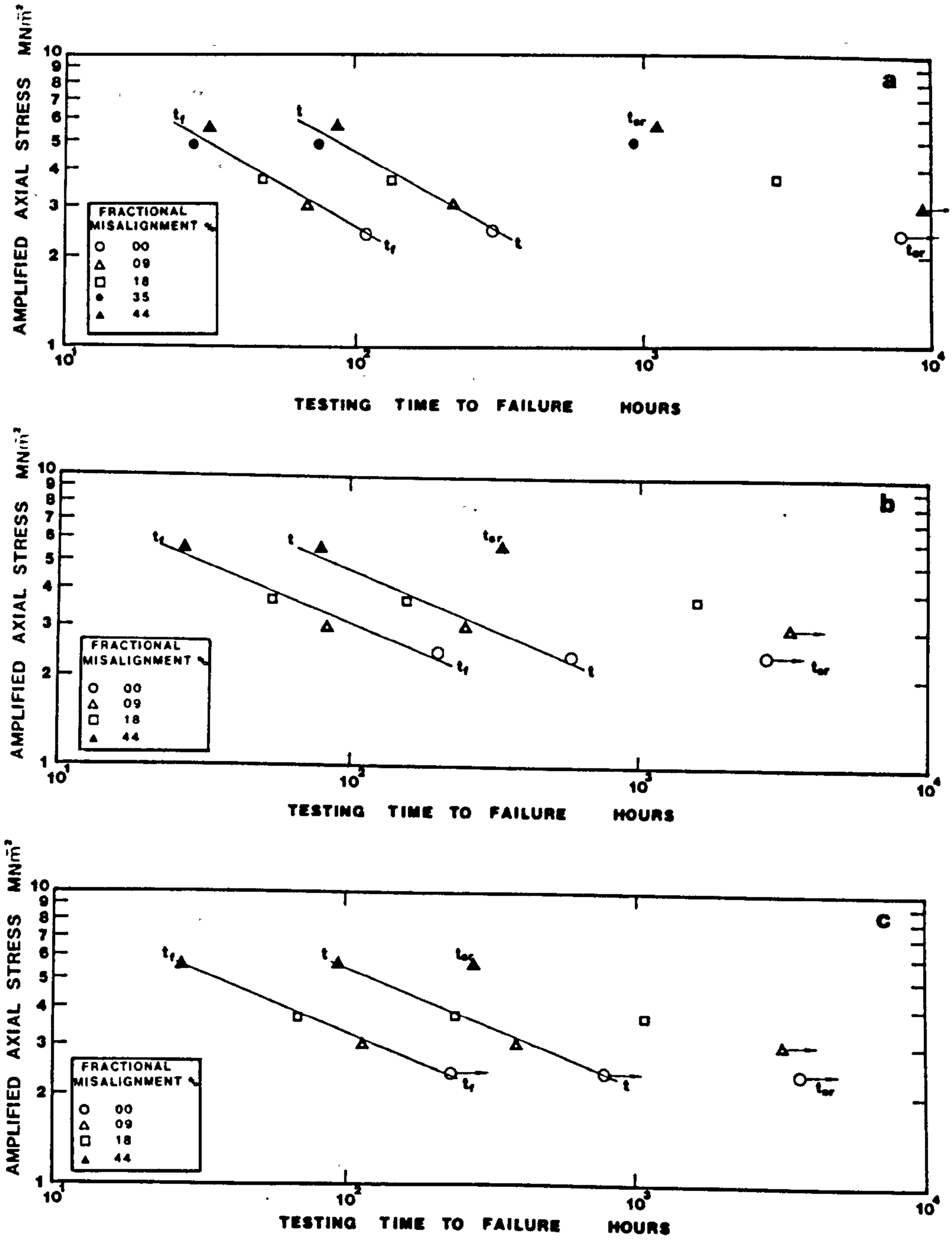

Fig. 4.15 Comparison of fatigue and stress-rupture data in terms of t, t_f and t_{SR} for SDR11 Rigidex 002-60 HDPE pipe systems in (a) 63, (b) 90 and (c) 125mm pipe systems.

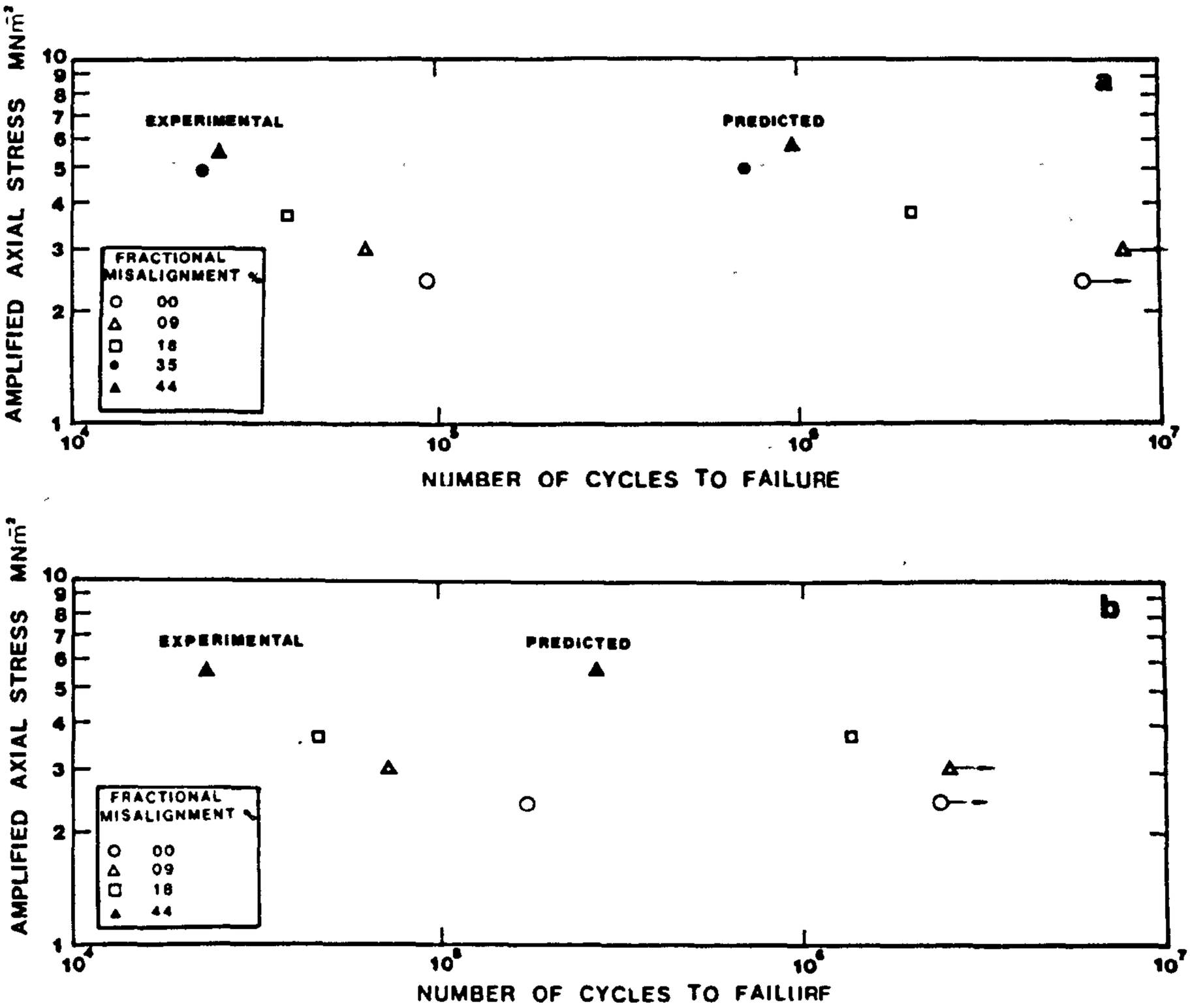

Fig. 4.16 Comparison of observed t_f and predicted t_f for (a) 63, (b) 90 and (c) 125mm SDR11 Rigidex 002-50 pipe systems.

4.5.4 The Influence Of Welding Conditions On The Fatigue Performance Of Aligned Butt Fusion Welds

The independent effect of three welding variables, heat soak time, heat removal time and welding pressure were investigated in 63 and 90mm Rigidex 002-50 MDPE pipes to indentify the variable which would reduce the performance of aligned butt welds. The results of this examination are highlighted in table 4.15. Of the three variables considered some variation in performance with the first two variables was detectable.

(i) Heat Soak Time The effect of decreasing the heat soak times was to increase the performance of aligned butt welds in 63 and 90mm pipes. Since the heating pressure and the heater plate temperature were held constant, the amount of melt formed, and hence the weld bead size, was solely dependent on the time of heat appliction. Decreasing the heat soak time decreases the weld bead size - see table 4.16. The increase in the performance may be due to a decrease in the weld bead size and supports the hypothesis that the weld bead instead of reinforcing the welded region could be acting as a constraint. With a large weld bead produced due to longer heat soak time, one would anticipate that the failure of a butt weld would not occur, since the effective cross-sectional area at the weld has been increased. Hence with large beads, the reinforcement effect might have been expected. However, the geometry of butt welds is such that it contains notches between the weld bead and pipe surface - see figure 5.9. These notches are inherent in the butt weld (see next chapter).

The nature of butt welding is such that when pipe ends are being butted and fused together under pressure, the viscous melt has to flow out. The melt then rolls onto the pipe wall which is at a much lower temperature than the viscous melt thus preventing the rolled melt from fusing onto the pipe wall. Hence the notches which are circumferential or at an angle to the longitudinal direction are inherently present in the weld. Thus

the effect of a small weld bead (decreasing heat soak time) is to act as less of a constraint and retard the rate of crack growth. Note all the butt welds produced with heat soak times of 180 seconds (large bead) in 90mm pipe failed in the circumferential plane at the weld with the average performance of 159,720 cycles to failure, whereas all the butt welds produced with heat soak times of 30 seconds (small bead) in 90mm pipes did not fail after 300,000 cycles.

The effect of a change in the heat soak time may have also influenced the residual stress distribution at the weld. However, since the fatigue testing was carried out at 79°C with samples initially conditioned for 24 hours at 79°C partial or complete relaxation of residual stresses would have occurred. The changes in the residual stresses due to the testing of pipes at elevated temperature (80°C) has been measured by Schonfild and Wintergerst (135), where it was noted that residual stresses relaxed. More recently Bhatnagor and Broutman (193) investigated the effect of annealing on residual stresses in polyethylene pipes and showed that annealing time and temperature altered the residual stress distribution in pipes and these stresses can be completely removed by annealing at temperature between 100°C and 120°C for a time of approximately one hour.

(ii) Heat Removal Time The effect of heat removal time depends upon the time taken for the temperature to fall to a certain value. Therefore it would be dependent on both the ambient conditions, and the size and average temperature of the melt at the end of the heating period. Thus a longer removal time must cause a decrease in temperature and therefore an increase in viscosity of the melt. Hence it was expected that for extremely high values of heat removal time (24 seconds) a cold joint would be produced which would fail instantaneously when under test. However, failures in both 63 and 90mm pipes resulted from a stable crack growth with an average number of cycles to failures of 93,638 and 76,840 respectively. Note that

all the four samples in 63mm pipe systems failed in the circumferential plane at the weld and in the 90mm pipe all three samples failed in the axial plane at the weld, initiating from a flaw on the internal weld bead. Axial failures at welds have been observed by John (72) who recently carried out stress-rupture tests on butt welds in 90mm SDR 11 MDPE pipes made at low environmental temperatures (-20°C) which could be regarded as an equivalent of large heat removal time. He also recorded that the lifetime of these butt welds exceeded the minimum specified time of 170 hours at 80°C.

Although heat removal times of 12 seconds and 24 seconds did not reduce the lifetime significantly, it is not recommended to have such high values. The butt welds in the testing programme were produced indoors with the ambient temperature in the range of 18 to 26°C whereas in the field account of very low temperature in winter and also chilling factor needs to be considered, and which may well produce a cold joint.

(iii) Effect Of Welding Pressure No failures were observed for butt welds produced under varying welding pressures, so it is difficult to deduce the effect of welding pressure on the performance of aligned welds. However, it can be remarked that the performance is at least as good as the standard if not better than the standard butt weld or independent of welding pressure examined. The size of the weld bead did not change with the welding pressure.

Despite an extreme change in the welding variable, - 50 to 100% change in heat soak time and welding pressure, there was no significant change in the lifetime of aligned welds compared to those recorded when misalignments of 10-44% were introduced. This indicates that provided the butt weld is aligned, fatigue performance is tolerant to a wide range of the welding conditions examined, whereas fatigue performance is very sensitive to changes in misalignment. The observation of fatigue performance being almost independent of welding

conditions inspected tends to confirm the findings of Atkinson and co-workers (41-44) and Malguarnera and Earles (45), who had considered extensive welding conditions and found that the short term welding factor did not change significantly; it was in the range .95-.98 most of the time. Wolters and Venema (73) found the stress-rupture lifetime of the butt welds produced under a range of welding conditions to be independent of the welding conditions examined, thus confirming the short term testing data cited above.

The fatigue performance of butt welds to be almost independent of the welding conditions examined may alternatively be interpreted as such that the welding conditions examined produced a flow speed of melt which was above a minimum so that no improvement was possible (63) (see theory of butt fusion section 2.2.3). However, it is noted that the welding conditions examined were not extensive and that the welds were produced in laboratory conditions. Adherence to the recommended welding conditions is still considered vital in order to obtain good welds in the field.

CHAPTER - 5 FAILURE ANALYSIS

5.1.0 Crack Initiation And Propagation Path Studies Of Circumferential Butt Weld Failures

(i) Examination The aligned and misaligned butt welds which failed in the circumferential plane at the weld were sectioned (longitudinal), polished and etched in chromic acid. The etched surface was sputter coated and examined with a light optical microscope to observe the crack propagation path in relation to the melt flow zone, MFZ. MFZ is defined here as the region where the melt was formed and made to flow during the fusion process. MFZ is discernible and has a distinct boundary as shown in figure 5.1.

Figure 5.2 shows schematically the three types of crack propagation path in relation to the MFZ which were observed in the circumferential butt weld failures. In the type I, the crack initiated from the region between inner weld bead and pipe bore. The crack then propagates outside MFZ up to half or greater than half the wall thickness after which it continues to propagate through the MFZ until final rupture through the weld bead. The total path length is approximately the sum of the pipe wall thickness and weld bead height. In the type II, the crack initiates from the same location as in the type I but propagates completely outside the MFZ to the point of final fracture underneath the outside weld bead which is on the same side as the inside bead. The total path length in this case is equal to the wall thickness of the pipe. In the type III, the crack initiates again from same location as in the type I but propagates across the MFZ and failure is underneath the outside weld bead which is on the opposite side of the inside weld bead where initiation took place. The total path length in this case is less than the wall thickness of the pipe when the butt welds are grossly misaligned (44%).

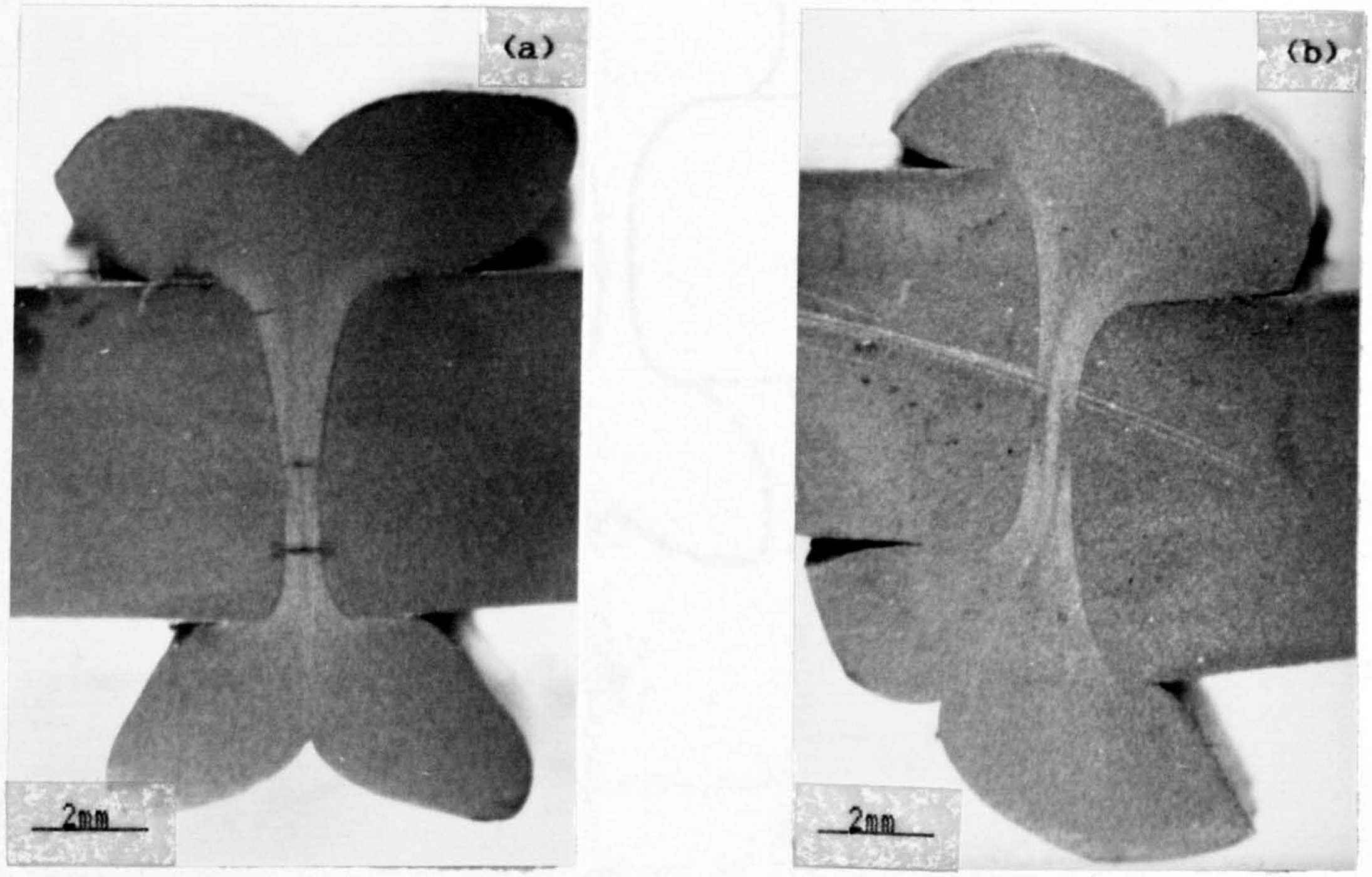

Fig. 5.1 Low magnification optical photomicrograghs of the etched surface of (a) nominally aligned and (b) nominally 44% misaligned butt weld in 63mm SDR11 Rigidex 002-50 MDPE pipe.

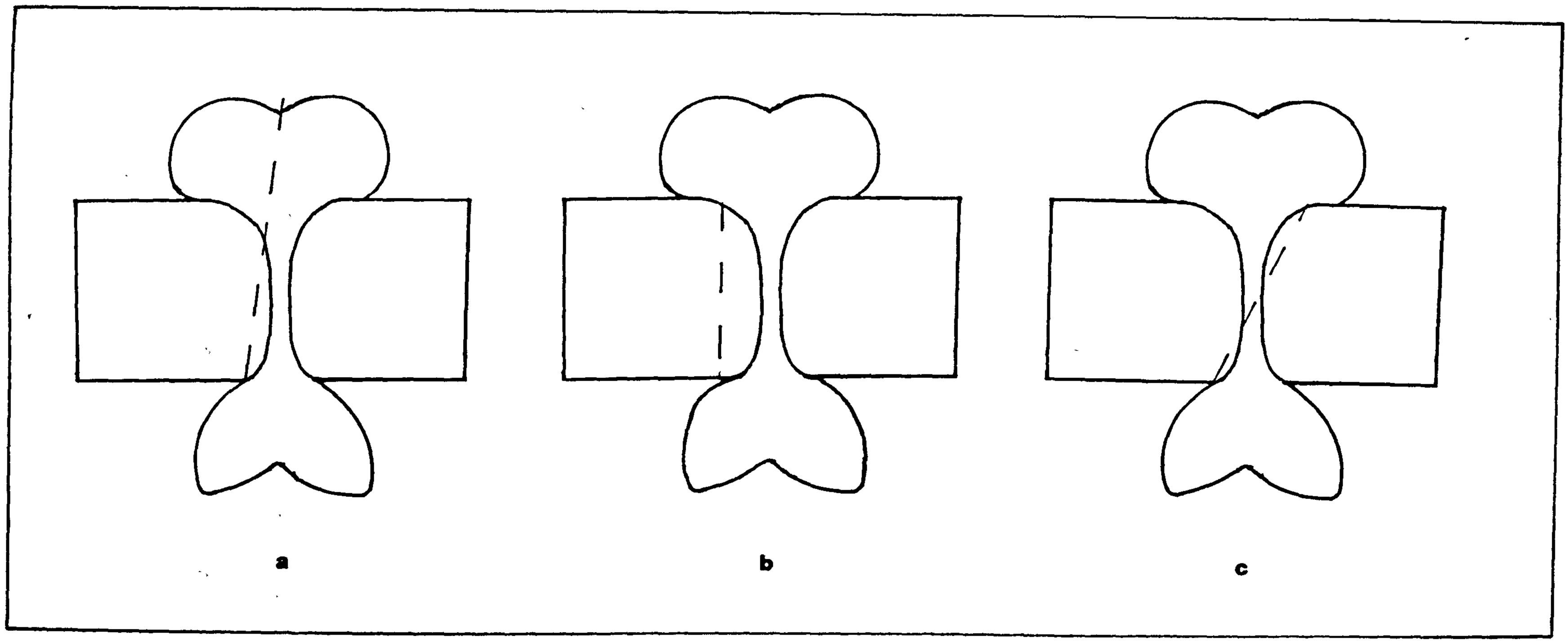

Fig. 5.2 Schematic of three different types of crack propagation path by which aligned and misaligned butt welds failed in the circumferential plane;
(a) Type I, (b) Type II and (c) Type III.

The type I was found to be the most common by which the overwhelming majority of the aligned and misaligned butt welds failed in 63, 90 and 125mm SDR11 Rigidex 002-50 MDPE pipe and also the highly misaligned (18% and 44%) butt welds in Rigidex 002-60 HDPE subjected to fatigue. The type II failure was found to be in the nominally aligned and nominally 9% misaligned butt welds in the 63mm Rigidex 002-60 HDPE pipe systems. One aligned and one 9% misaligned butt weld in 90mm and one 9% misaligned butt weld in 125mm Rigidex 002-50 MDPE pipes also failed in this manner. The type III failure was only associated with the nominally 44% misaligned butt weld failures in 63, 90 and 125mm Rigidex 002-50 MDPE pipes subjected to stress-rupture loading.

Figure 5.3 shows a series of low magnification optical photomicrographs of etched surfaces of failed nominally aligned and misaligned butt welds in 63mm SDR11 Rigidex 002-60 HDPE pipe systems. It can be seen that nominally aligned and nominally 9% misaligned welds failed by the type II path while 18% misaligned welds failed by the type I path.

Figure 5.4 shows a series of low magnification optical photomicrographs of etched surfaces of failed nominally aligned and various misaligned butt welds in 63mm SDR11 Rigidex 002-50 MDPE pipe systems while figure 5.5 shows it in 90mm SDR11 Rigidex 002-50 MDPE pipe systems. All these failures were of the type I path.

Circumferential failure of the butt welds under stress-rupture were also examined. None of the aligned butt welds in 90 and 125mm pipe systems under stress-rupture had failed and only three out of eight aligned butt welds in 63mm pipe systems had failed in the circumferential plane at the weld. These three failures were of the type I. All the 9% and 18% misaligned butt welds in the three pipe diameters failed in the circumferential plane at welds by the type I and the type II manner, while all the 44% fractionally misaligned butt welds in 63, 90 and 125mm pipe systems failed by the type III route. Representative low

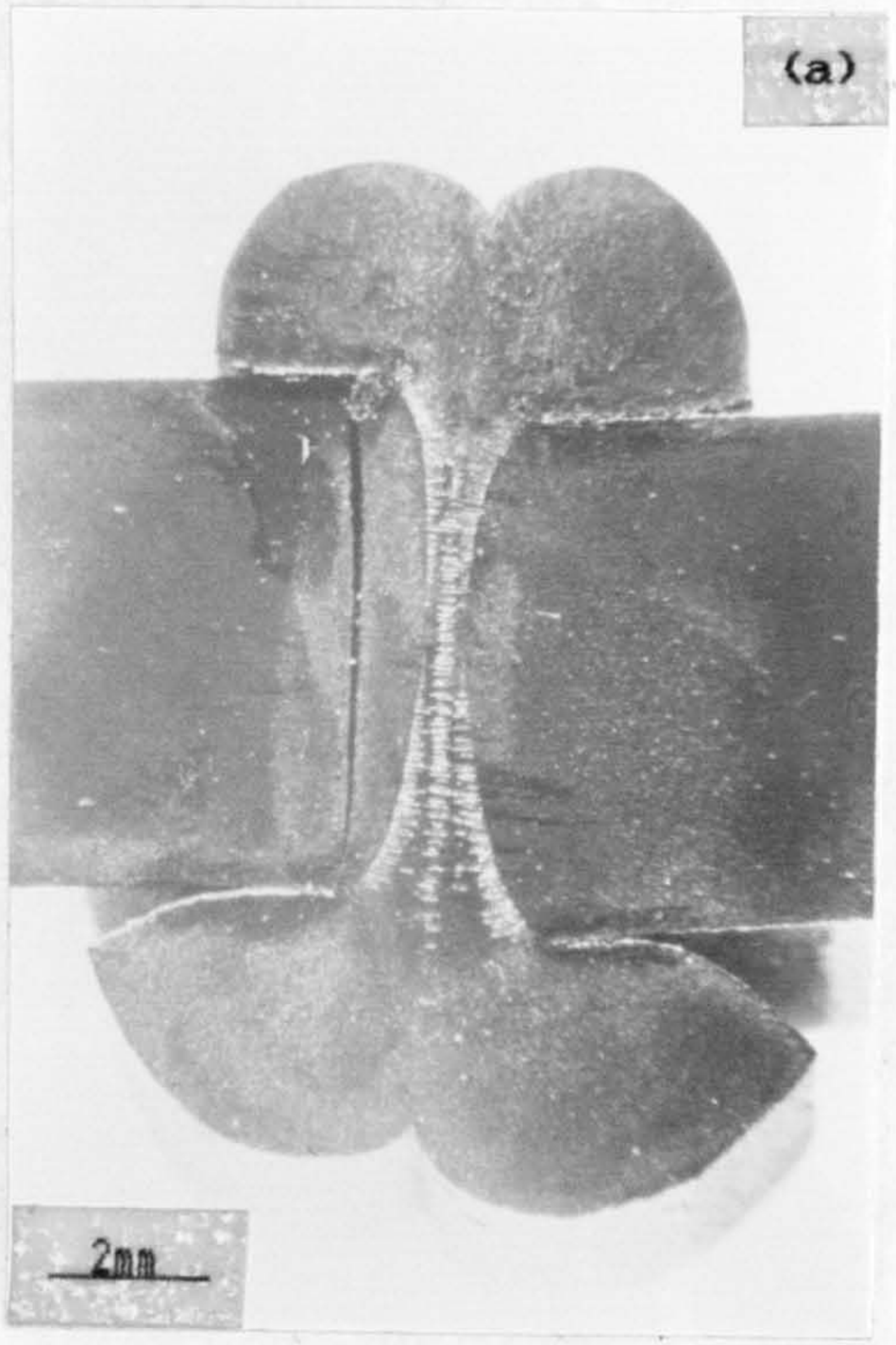

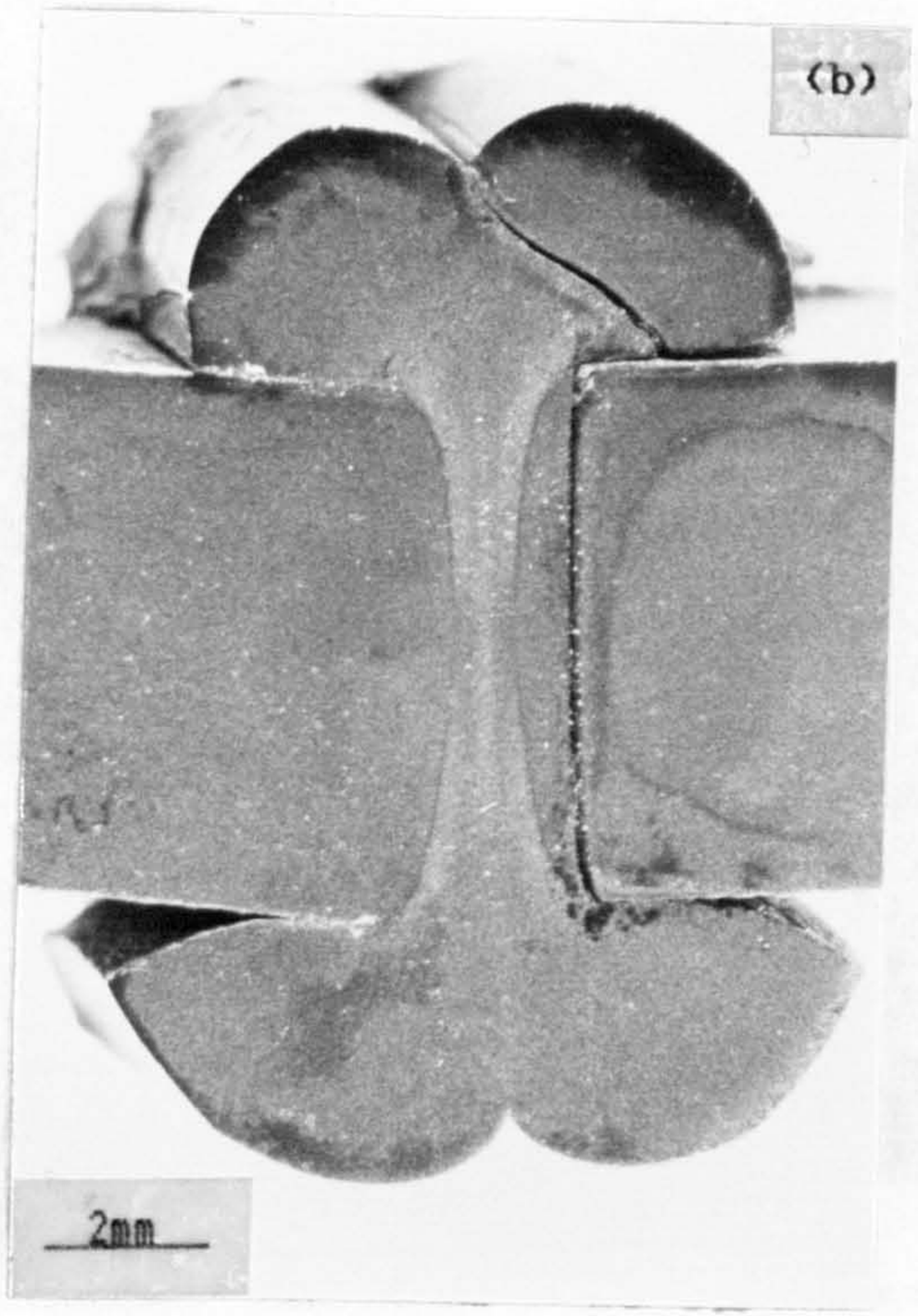

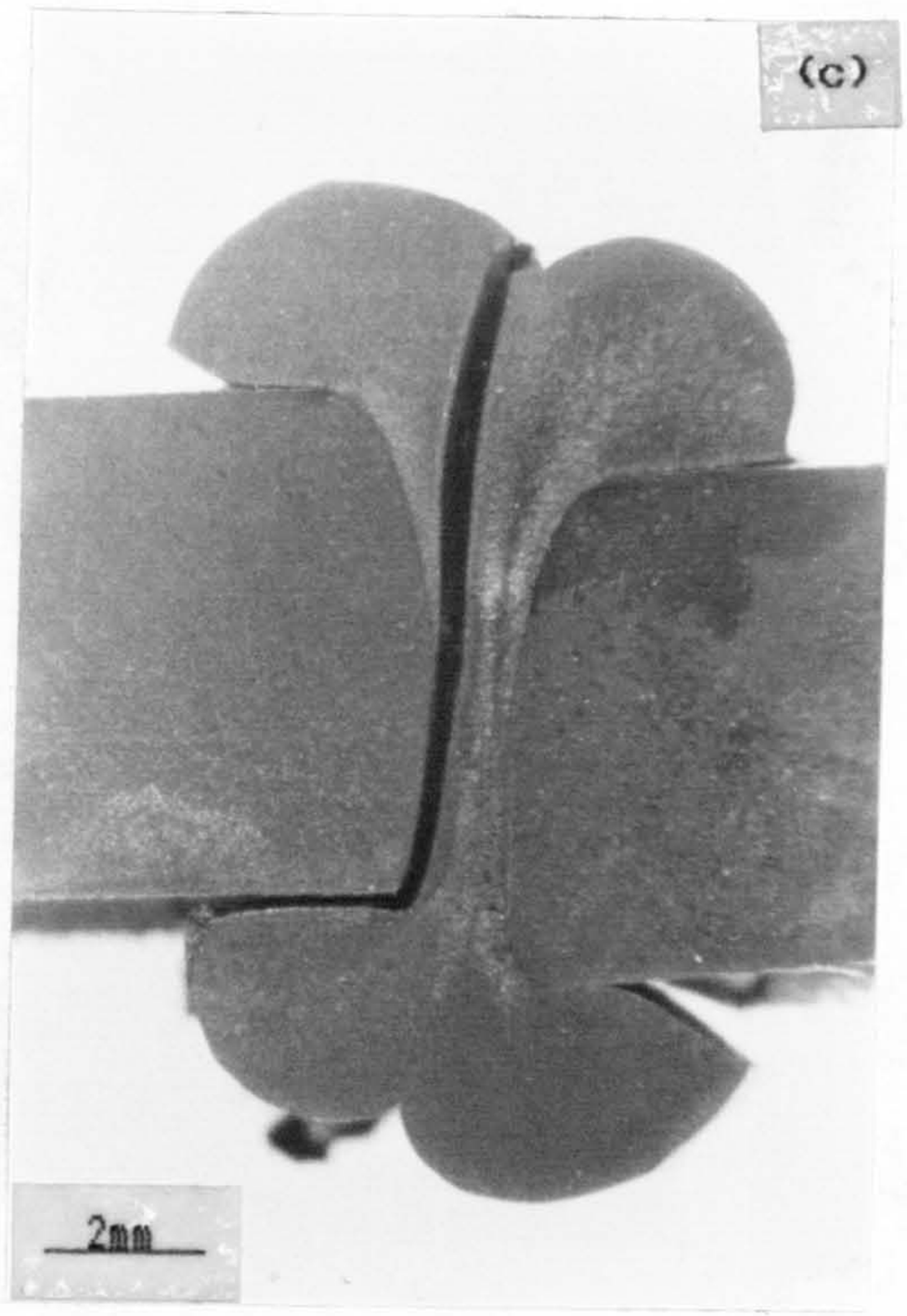

Fig. 5.3 Low magnification optical photomicrograghs of the etched surface of (a) nominally aligned and (b) nominally 9% and (c) 18% misaligned butt weld failures in 63mm SDR11 Rigidex 002-60 HDPE pipe.

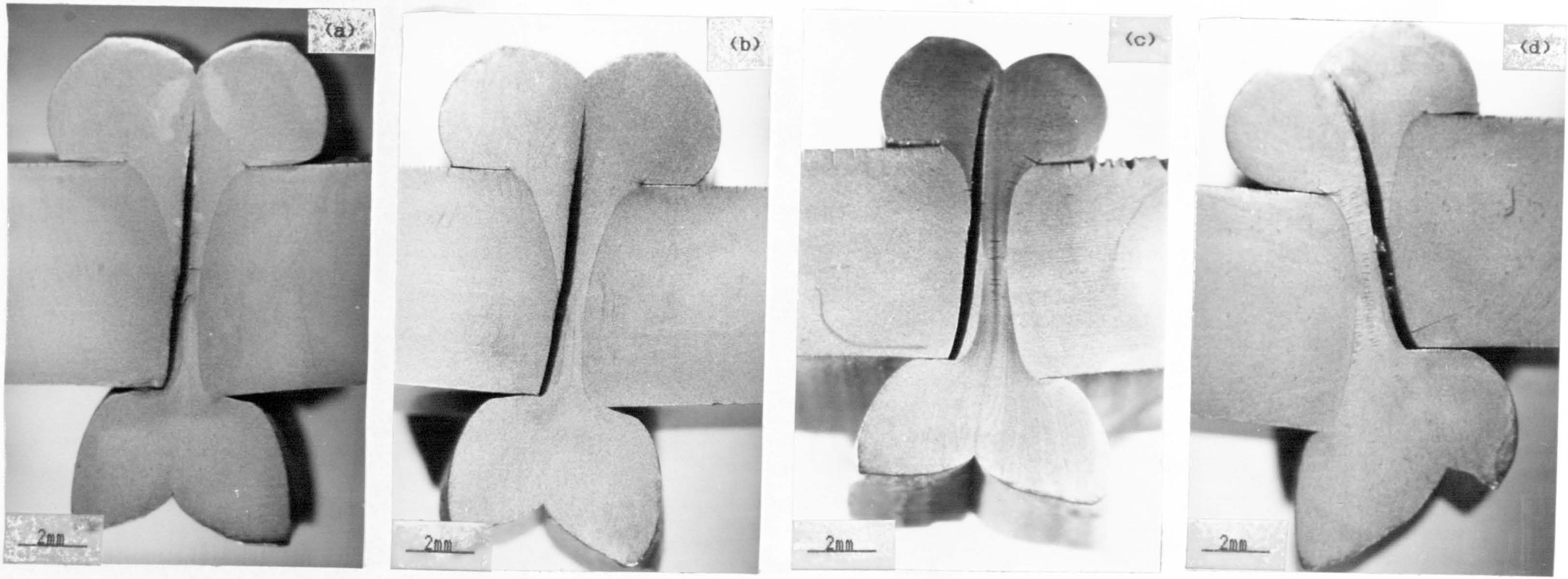

Fig. 5.4 Low magnification optical photomicrograghs of the etched surface of (a) nominally aligned and (b) nominally 9% (c) 18% and (d) 44% misaligned butt weld failures in 63mm SDR11 Rigidex 002-50 MDPE pipe.

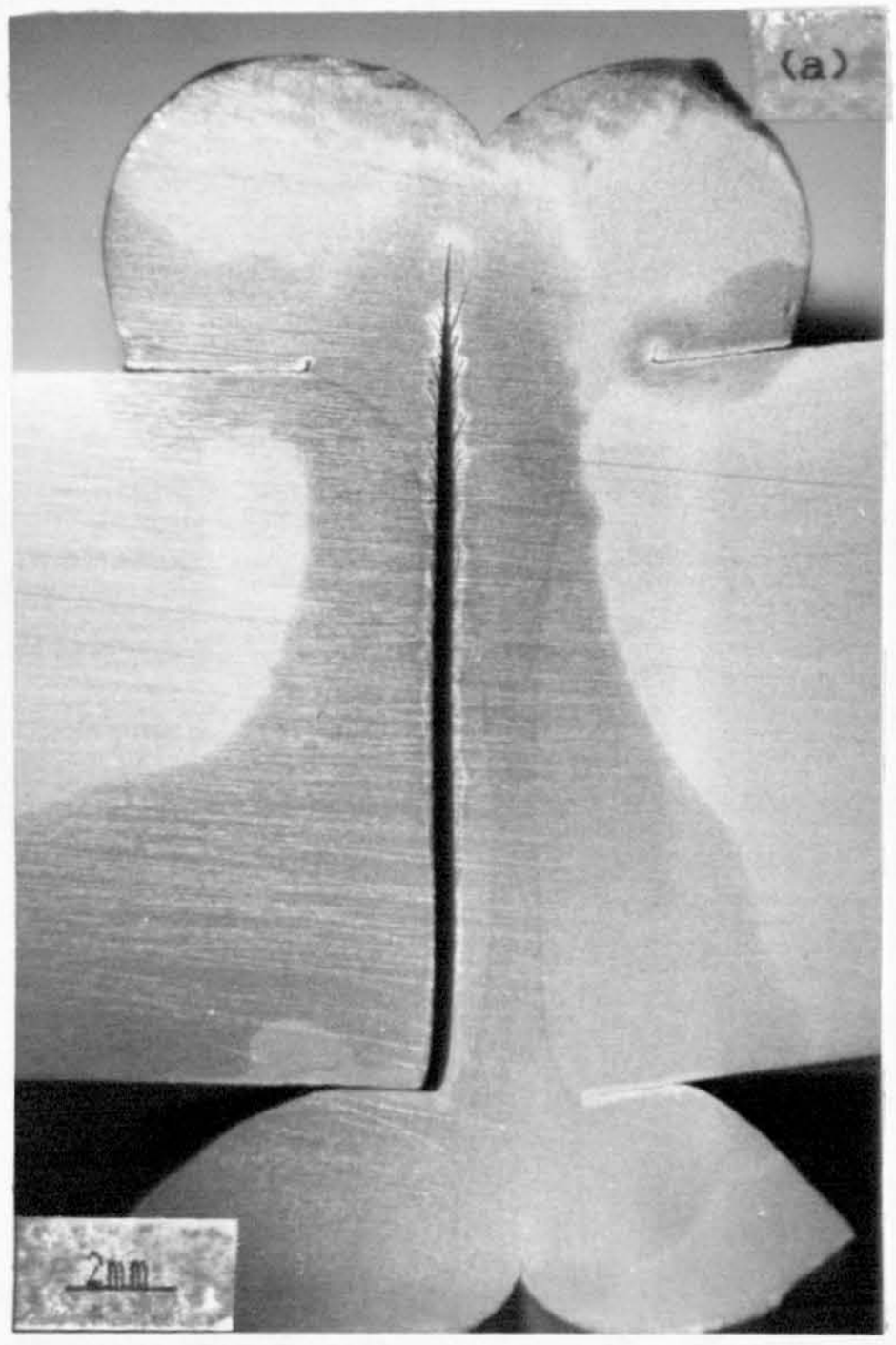

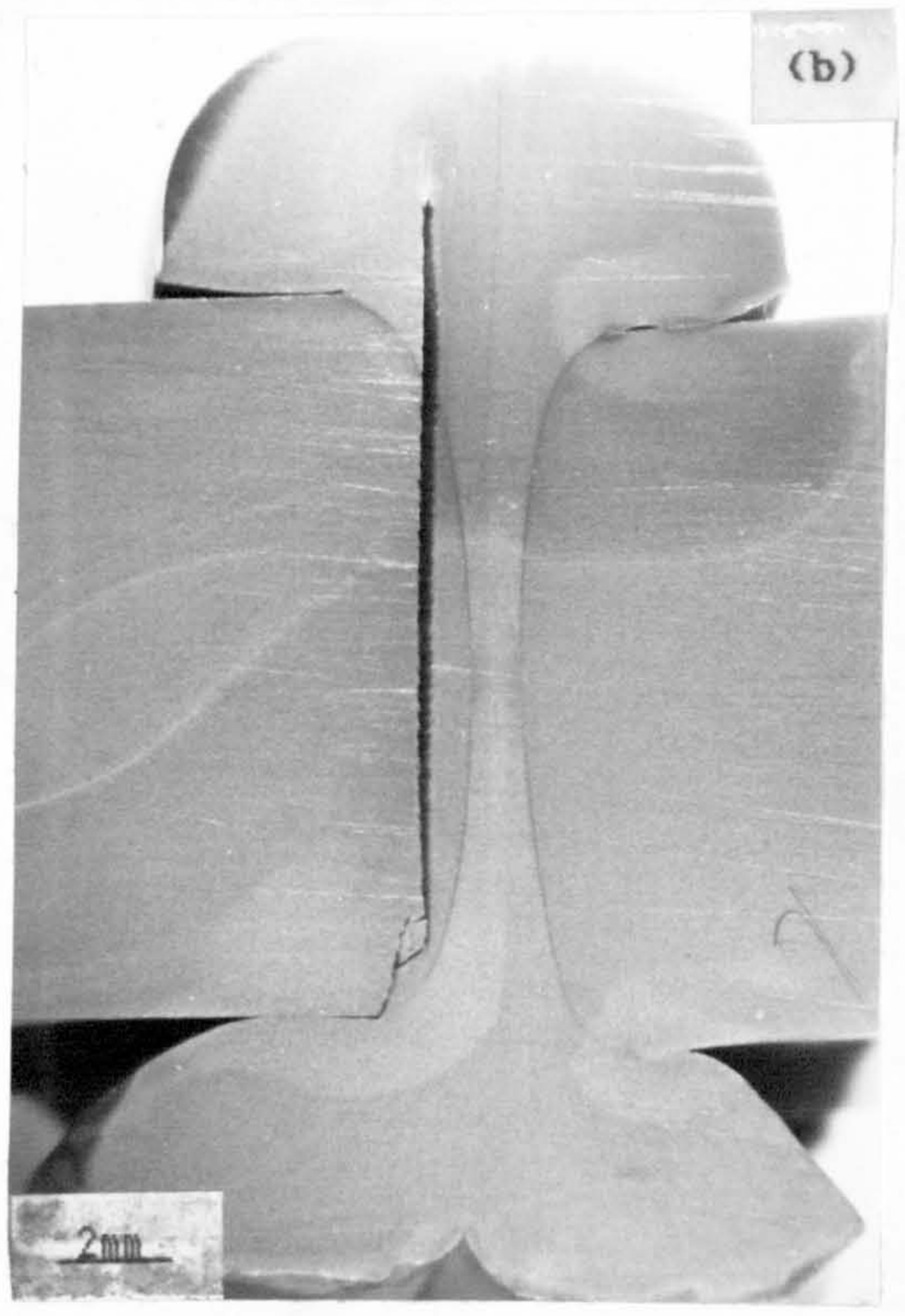

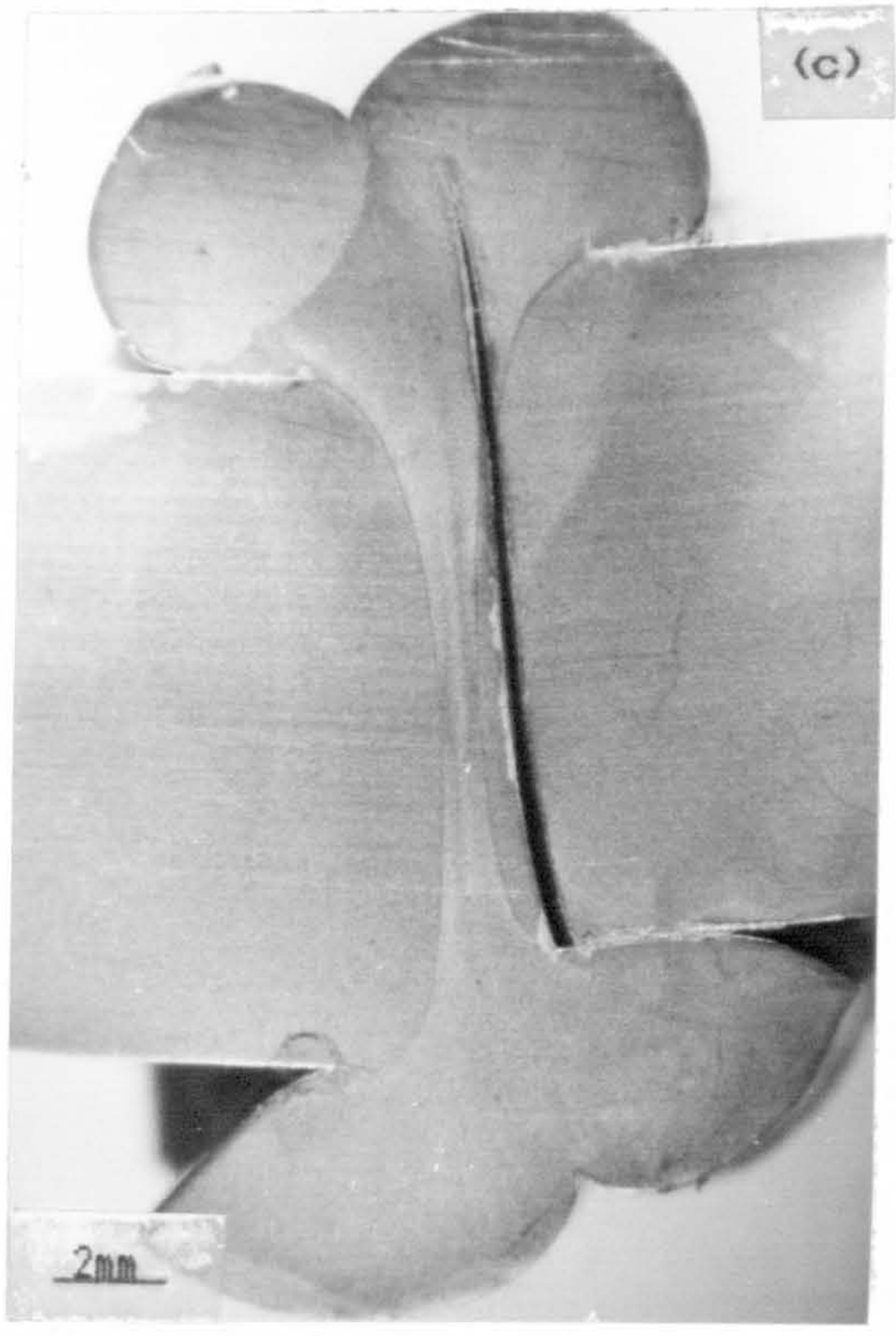

Fig. 5.5 Low magnification optical photomicrograghs of the etched surface of (a) nominally aligned and (b) nominally 9% and (c) 18% misaligned butt weld failures in 90mm SDR11 Rigidex 002-50 MDPE pipe.

magnification optical photomicrograph of etched surface of failed misaligned butt weld failures under stress-rupture conditions of the type I to III are shown in figure 5.6.

It is clear from these photomicrographs that the crack invariably initiated from the notch between the pipe bore and the weld bead. In the type I failure, it then traversed outside the boundary of the MFZ up to half or greater than half the wall thickness after which it continued to propagate through the MFZ until final rupture through the weld bead. It appears that the crack propagation is insensitive to the MFZ to the extent that the initial crack growth does not take place in the MFZ and nor does it propagate along the boundary between the MFZ and the surrounding material.

It is interesting to note two observations germain to circumferential failure;

(a) The examination of axial failures at the weld obtained under fatigue in 63 and 90mm revealed the growth of circumferential cracks taking place from the notch between the inner weld bead and pipe bore - see figure 5.16.

(b) 63mm SDR11 DuPont Blue Aldyl 322, a different grade of MDPE known to have a different weld bead geometry was butt welded on Fusion Plastics Butt Welding Machine. Five aligned butt welds in this grade of pipe were tested at ΔP=9.5 bar and 5 cpm at 79°C; the lifetimes are provided in the table 5.1. All the five aligned butt welds failed at the weld in the circumferential plane. The crack propagation path is shown in the figure 5.7. These weld failures also initiated from the inner weld bead region.

(ii) Removal Of The Internal Weld Bead To examine if the circumferential failure in the aligned welded samples in 63mm SDR11 Rigidex 002-50 MDPE pipe samples had initiated from the notch described above, the internal weld bead was machined off

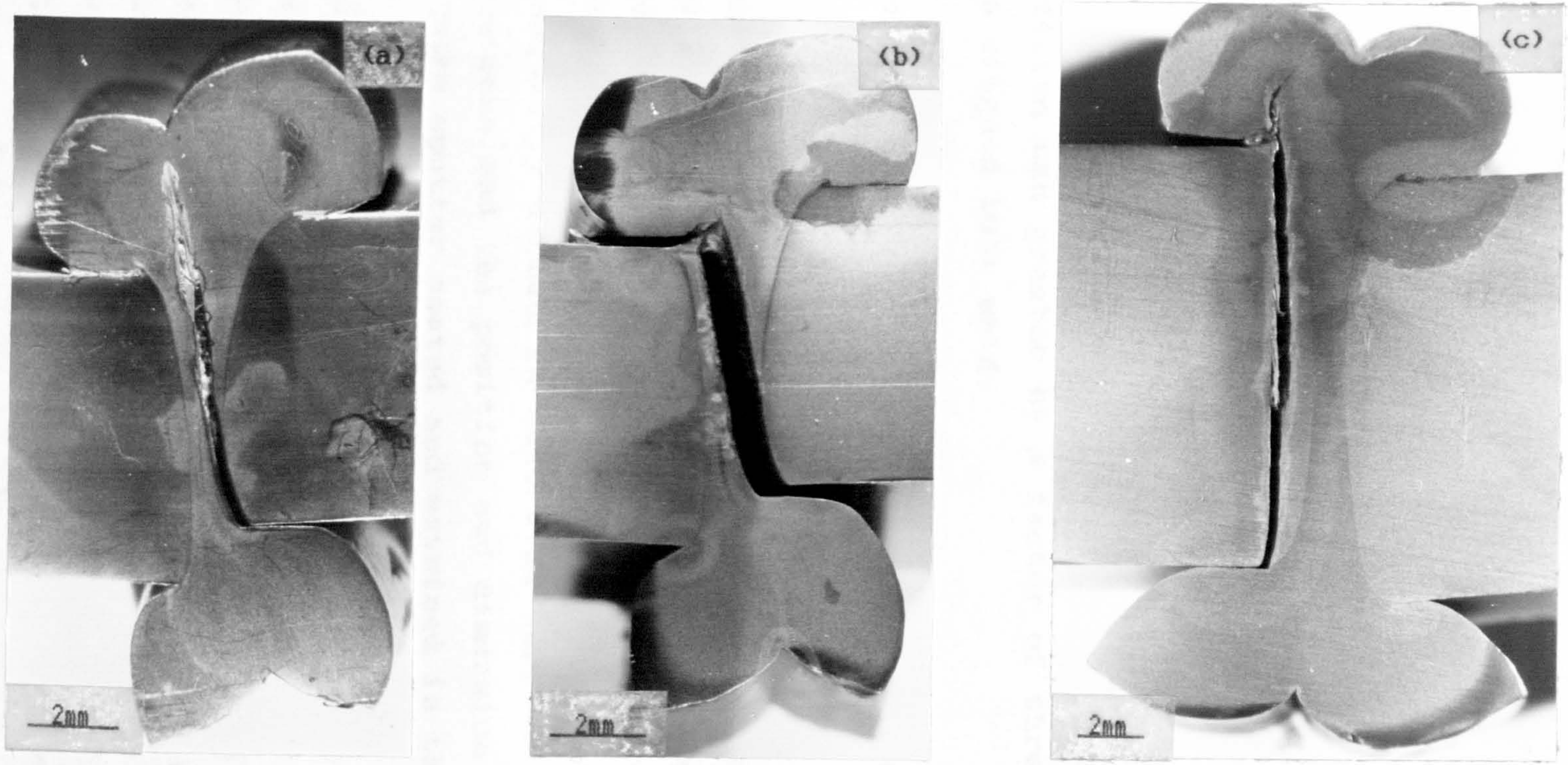

Fig. 5.6 Low magnification optical photomicrograghs of the etched surface of (a) nominally 18% and (b) 44% misaligned butt weld failures in 63mm SDR11 and (c) 18% misaligned butt weld failures in 90mm SDR11 Rigidex 002-50 MDPE pipe under stress rupture condition.

eight samples and in four samples internal and external beads were machined off. These samples were fatigue tested at a presssure range of 9.5 bar with a freqency of 5 cpm at 79°C. The results of these test together with the lifetimes of a straight pipe having no butt weld are given in the table 5.2. The following points emerge from this examination:

(a) All the aligned butt welded samples with the internal weld bead removed failed in the pipe away from the butt weld, (see Fig. 5.8), clearly indicating that the notch is responsible for the observed circumferential failure of the aligned butt welds and the weak link in the chain is not the welded region.

(b) Removing the internal weld bead enhanced the fatigue lifetime of the weld as no weld failures were observed. The mean lifetime was greater by a factor of three compared to the standard aligned butt weld.

(c) Removal of both the internal and external weld bead has led to pipe of an improved quality.

(iii) Notch Dimensions An attempt was made to characterise the dimensions of the notches in aligned and misaligned butt welds in Rigidex 002-50 MDPE pipe systems. Longitudinal sections of butt welds in 63. 90 and 125mm SDR11 pipes were cut, polished and subsequently etched in saturated chromic acid to reveal the melt flow zone and the position and dimension of the notch. The samples were sputter coated and examined in the SEM.

The notch which initiated failure at the butt fusion welds for circumferential failures is formed as the weld bead rolls over onto the pipe. Figure 5.9 shows a series of scanning electron micrographs of the notches in nominally aligned and nominally 44% misaligned butt welds in 63, 90 and 125mm pipe systems. The dimensions of the notch are outlined in the table 5.3. At each combination of pipe diameter and nominal fractional misalignment, data from typically five different welds was used

Table 5.1 Number of cycles to failure of butt welds in 63mm SDR11 DuPont's Blue Aldyl 322A pipe tested at 79°C and a frequency of 5 cpm.

Number Of Cycles To Failure	
	44,850 59,700 69,750 92,750 119,520
Mean ± s.d (coeff. variation)	77,328 ± 29,339 (.380)

Table 5.2. Number of cycles to failure of standard aligned butt welds and of aligned butt welds with internal bead removed in 63mm SDR11 Rigidex 002-50 pipe tested at ΔP=9.5 bar with a frequency of 5 cpm and at 79°C.

Number Of Cycles To Failure			
Standard Butt Weld	Internal Weld Bead Removed	Internal & External Weld Bead Removed	Straight Pipe
58,290	80,550(P)	228,150(P)	240,420
60,150	142,380(P)	253,740(P)	271,950
63,300(A)	153,210(P)	277,740(P)	298,950
73,620	234,000(P)	348,150(P)	358,380
81,570	247,380(P)		>600,000
96,090	424,050(P)		>600,000
132,060	438,390(P)		>600,000
160,260	>552,720		>716,790
Mean	90,668	284,085	276,945	>460,811
s.d.	37,202	168,207	51,608	186,922
(coefficient of (variation)	(.410)	(.592)	(.186)	(.406)

Notes: All the standard butt welds failed at the butt weld in circemferential plane except one denoted by A where failure was in butt weld but the crack was in the axial direction
P denotes failure of the pipe remote from the butt weld.

Table 5.3 Dimensions of the notches in the aligned and misaligned butt welds in 63, 90 and 125mm SDR11 Rigidex 002-50 MDPE pipe.

Nominal Fractional Misalignment %	Pipe Diameter, mm					
	63		90		125	
	Notch Length µm	Notch Tip Radius µm	Notch Length µm	Notch Tip Radius µm	Notch Length µm	Notch Tip Radius µm
00	1105 (±104)	<1	1289 (±97)	<1	1835 (±199)	5 (±2)
09	1153 (±195)	<1	1561 (±336)	<1	2478 (±180)	6 (±3)
18	1232 (±110)	<1	1698 (±441)	<1	2730 (±380)	3 (±2)
44	1320 (±238)	<1	2007 (±131)	<2	2657 (±84)	5 (±2)

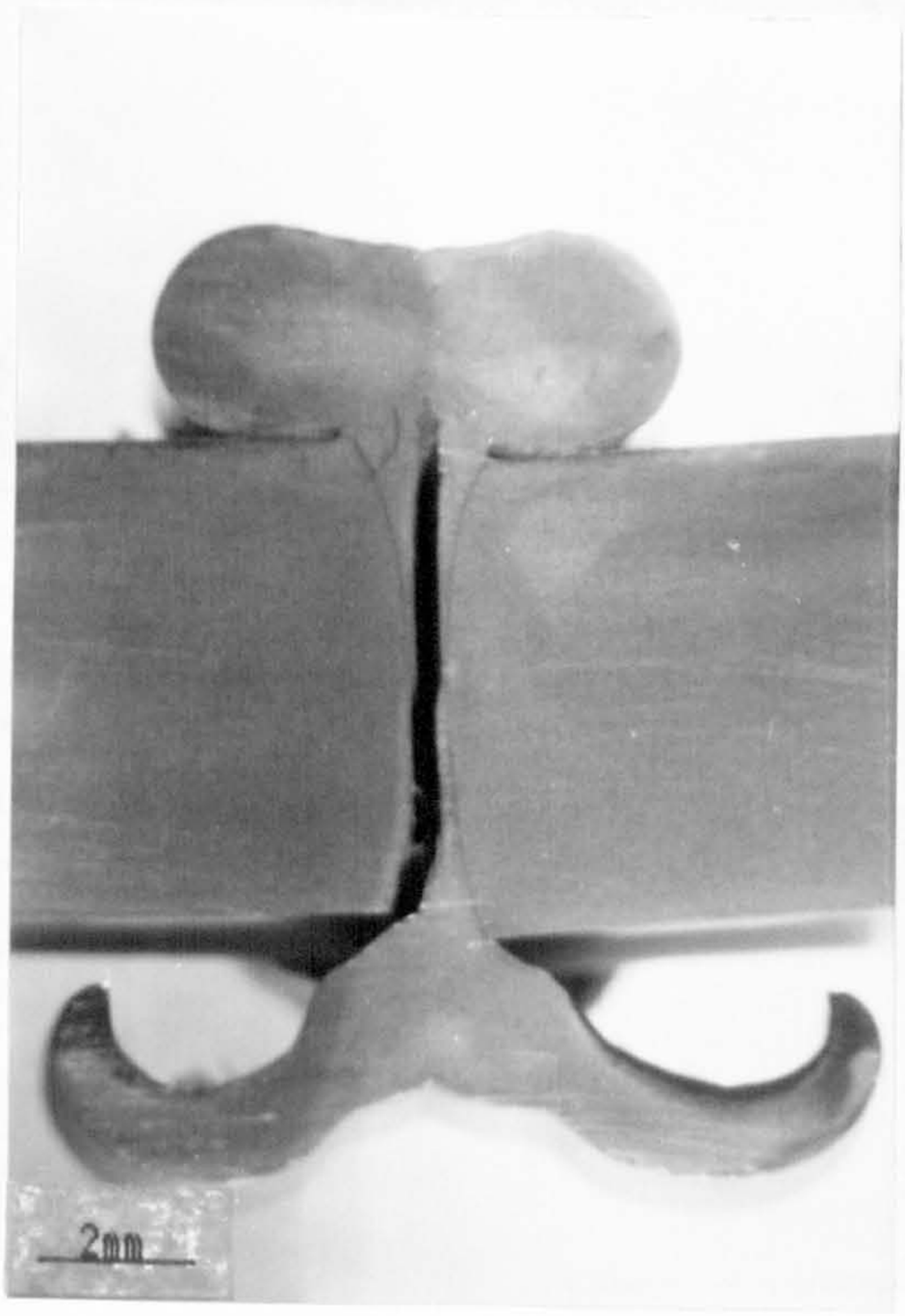

Fig. 5.7 Low magnification optical photomicrograph of the etched surface of a nominally aligned butt weld failure in 63mm SDR11 DuPont Blue Aldyl 322A.

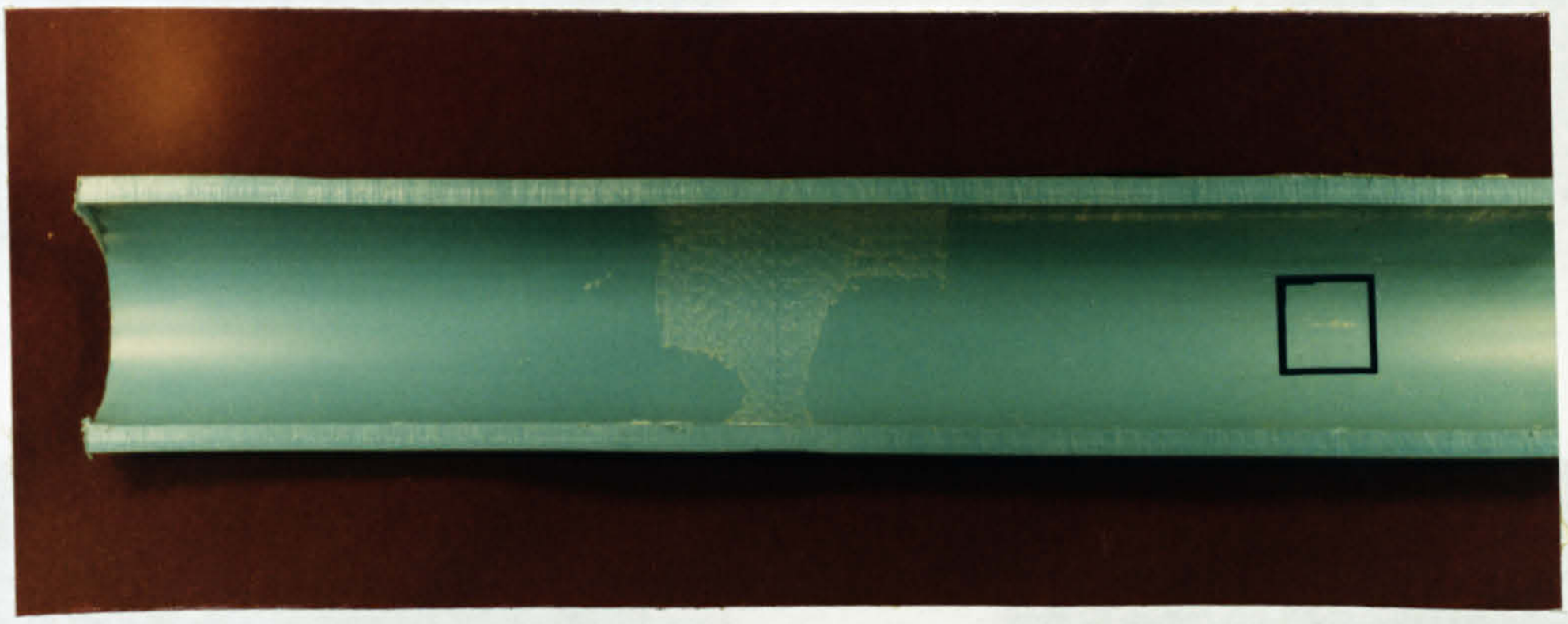

Fig. 5.8 Photomicrograph showing the pipe failure remote from the internal weld removed region.

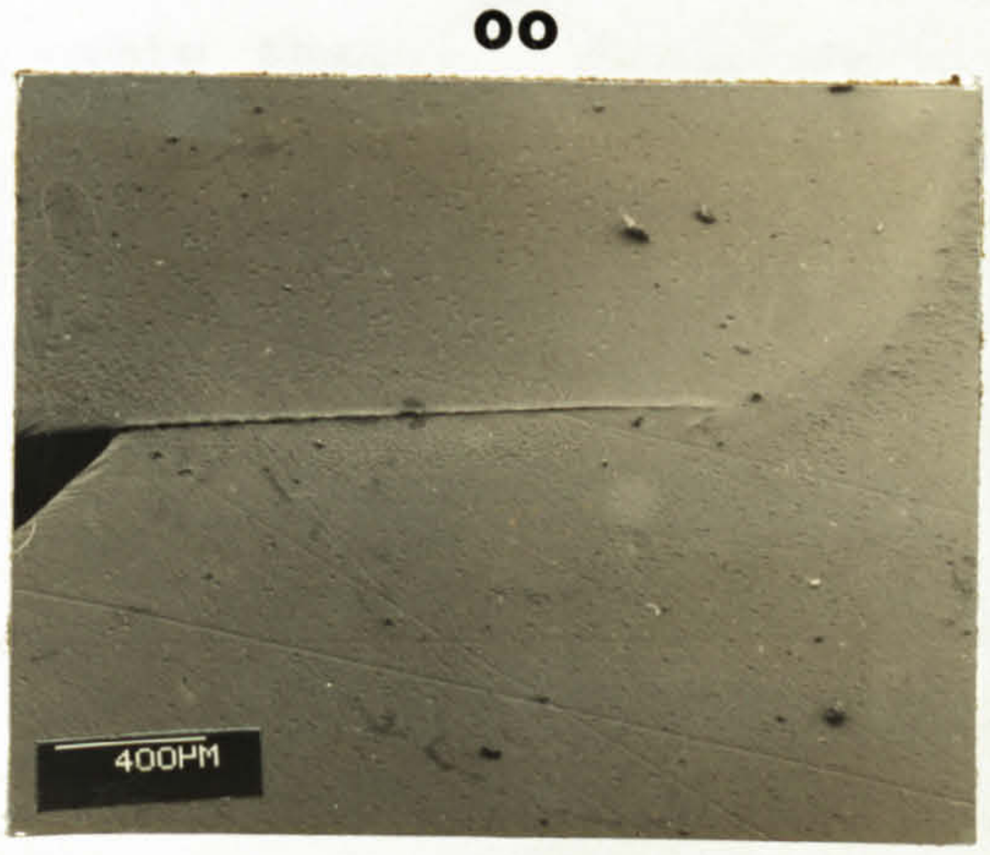

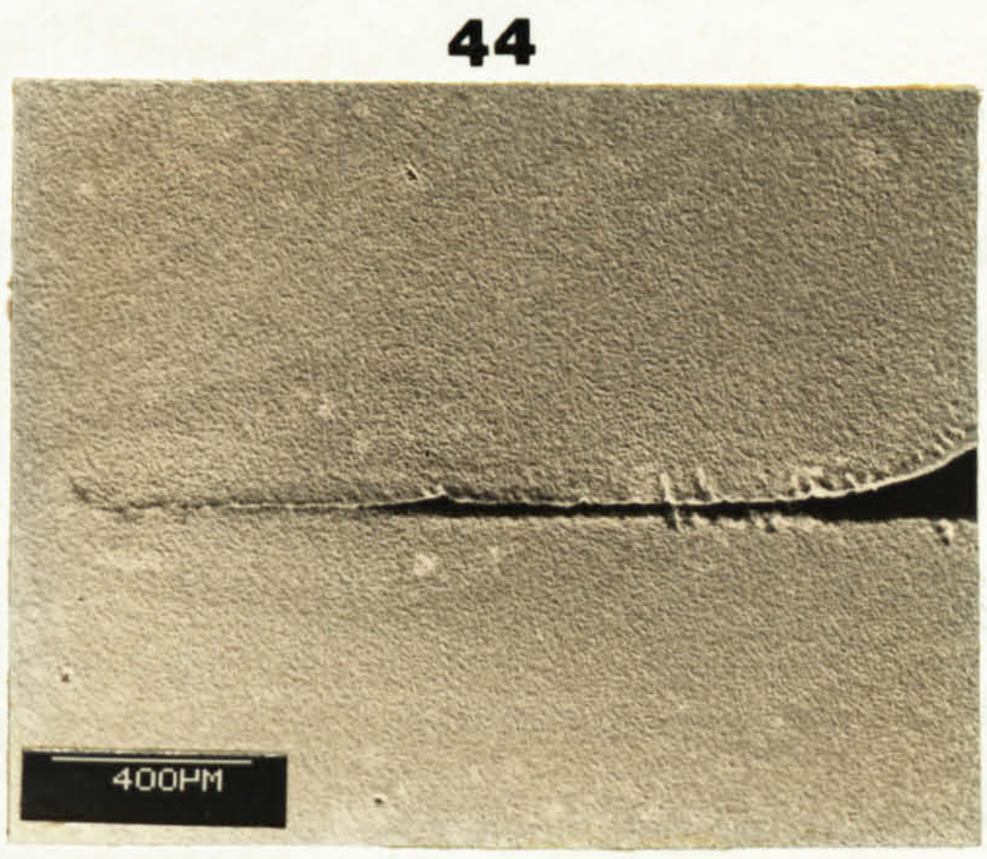

a

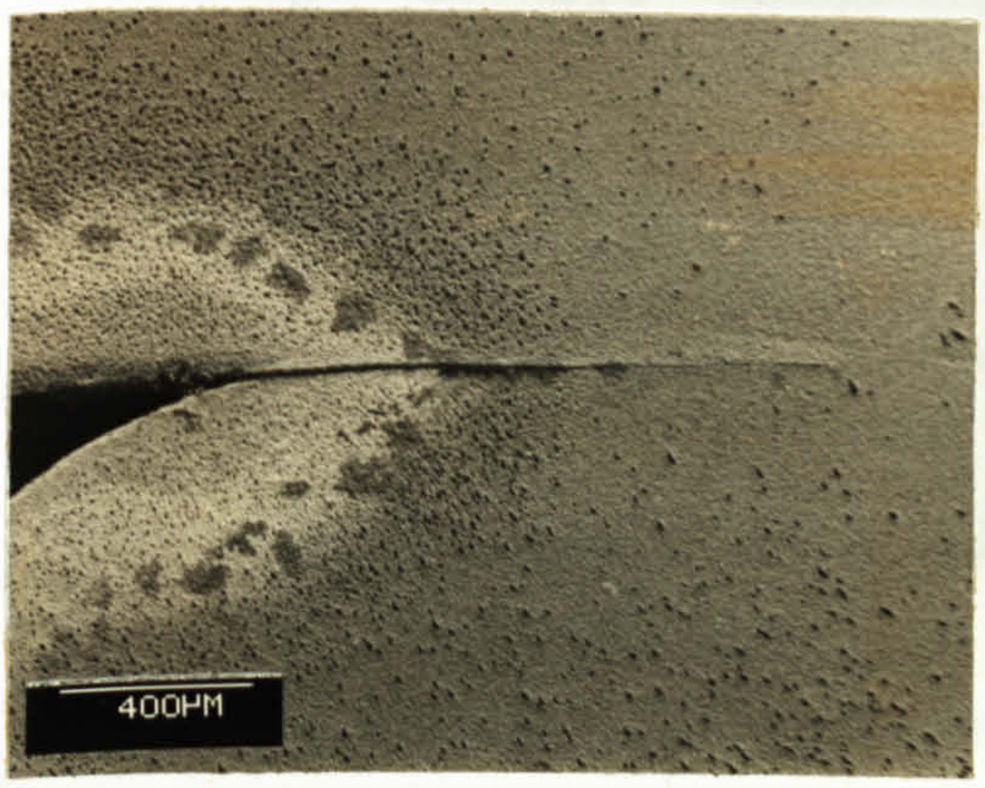

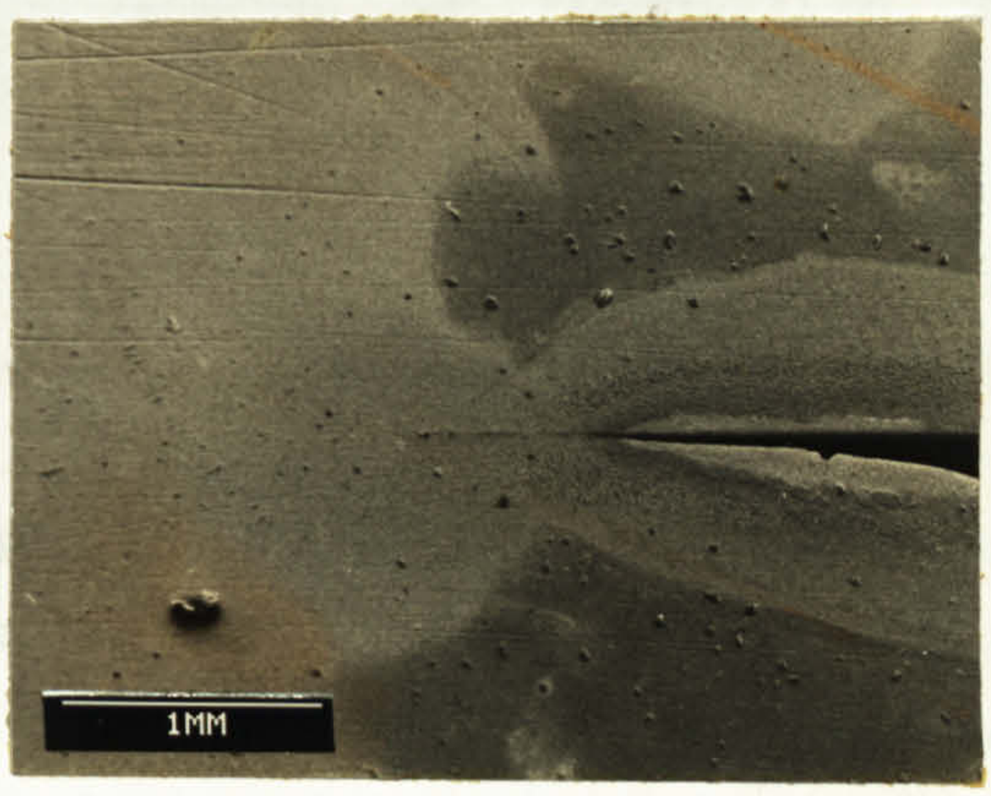

b

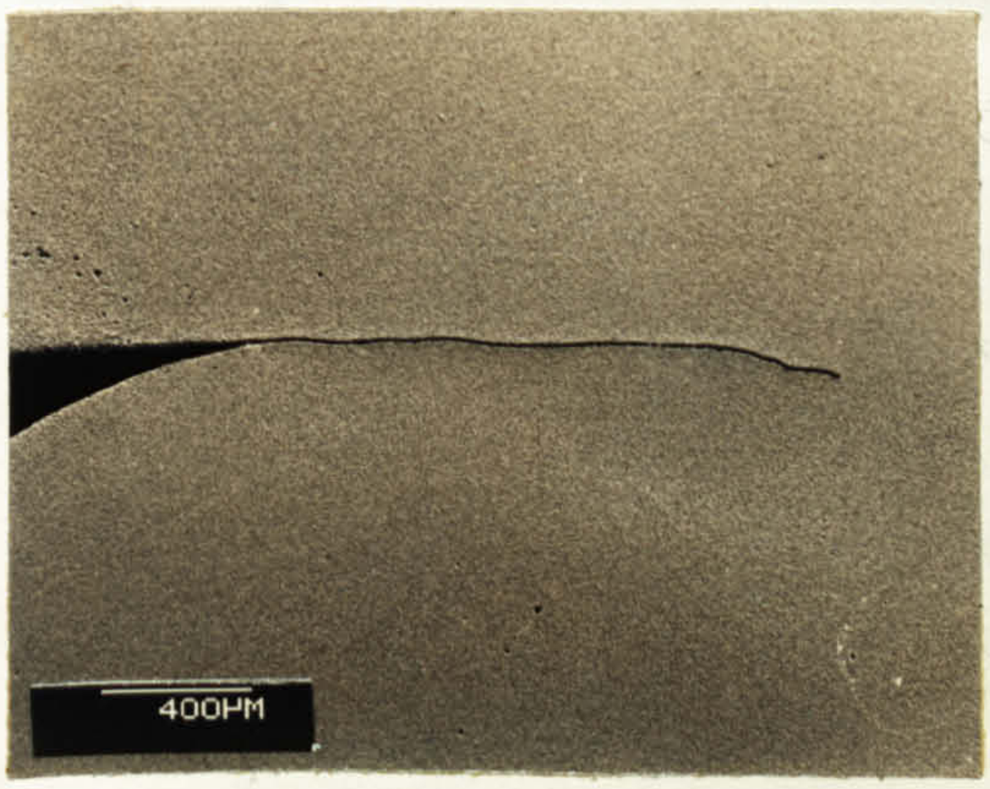

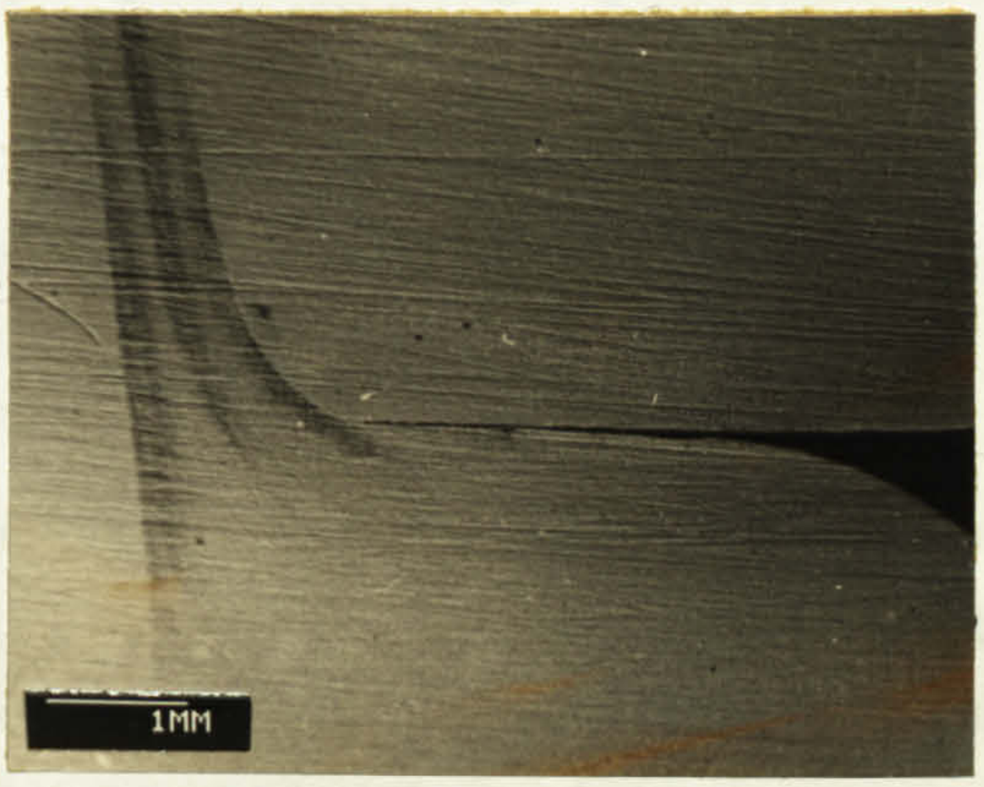

c

Fig. 5.9 Scanning Electron micrographs of the inner weld bead region showing the notches present in nominally aligned and nominally 44% misaligned butt welds in (a) 63, (b) 90 and (c) 125 mm SDR11 Rigidex 002-50 MDPE pipe.

to calculate the average notch length and notch tip radius; the standard deviation is also included. It can be seen from this table that:-

(a) For both the 63 and 90mm pipes the notch tip radius was always small (less than 1μm). For the 125mm pipe the notch tip radius was measurably larger (3 to 6μm).

(b) For each pipe diameter there was a tendency for notch length to increase with misalignment. For the 90 and 125mm pipe the notches at 44% nominal misalignment were typically 50% longer.

(c) At all misalignments the effect of increasing pipe diameter is to extend the notch size.

5.2.0 Fractography: Macrofeatures

(i) Fracture Surfaces Of Circumferential Weld Failures Fracture surfaces of a number of circumferential weld failures in the aligned and misaligned butt welds in 63, 90 and 125mm Rigidex 002-50 MDPE pipe systems tested under fatigue and stress-rupture conditions at 79°C were examined using a stereo light microscope and representative low magnification photomicrographs are shown in figures 5.10 to 5.14.

The general observations which were common to all the fracture surfaces were as follows:-

(a) All the failures were invariably of the brittle type showing no visible sign of any gross straining/deformation. However, stress-rupture failures tended to have some macroductility in the region close to the final rupture. Whitening on all the surfaces was observed, characteristic of crazing and slow stable crack growth. In a few cases in 90mm and 125mm fatigue butt weld failures, there were regions where

the surface was plain and featureless around the initiation region and the final stages of fracture, indicating limited ductility.

(b) Cracks were not initiated from any one point but rather over a local region on the circumference of the butt weld. The low fractional misalignment butt weld failure tended to have greater fracture surface area compared to highly misaligned butt weld fatigue failures. For the stress-rupture failures this trend was also observed but the spread of fracture on the circumference of the weld was seen to be greater at all the misalignments compared to fatigue failure.

(c) Within the first 1-2mm no curved bands were visible, after which curved or arched bands lying perpendicular to the crack direction were evident on the majority of the fatigue failure surfaces. That is, the large scale striations referred to as discontinuous growth bands in the literature were apparent. However, there was no indication of true fatigue striations which are generally considered to be a characteristic of fluctuating loads and represent individual load excursions. It was interesting to note that the discontinuous growth bands were also discovered for stress-rupture failures.

(d) The spacing between these bands varied, depending on the magnitude of the butt weld misalignment and test pressure range. Whereas in the stress-rupture case, the number of bands was fewer and spacing between them was larger at each of the misaligned butt weld failure compared to fatigue.

(e) Longitudinal ridges or tearing ridges lying parallel to the crack growth direction were present at the initiation site and sometimes they were most pronced at the intermediate region or near the final stage of rupture depending on the magnitude of the misaligned butt weld and pipe diameters. These ridges suggest that crack propagation was multiplane to give the fracture surface a rough texture.

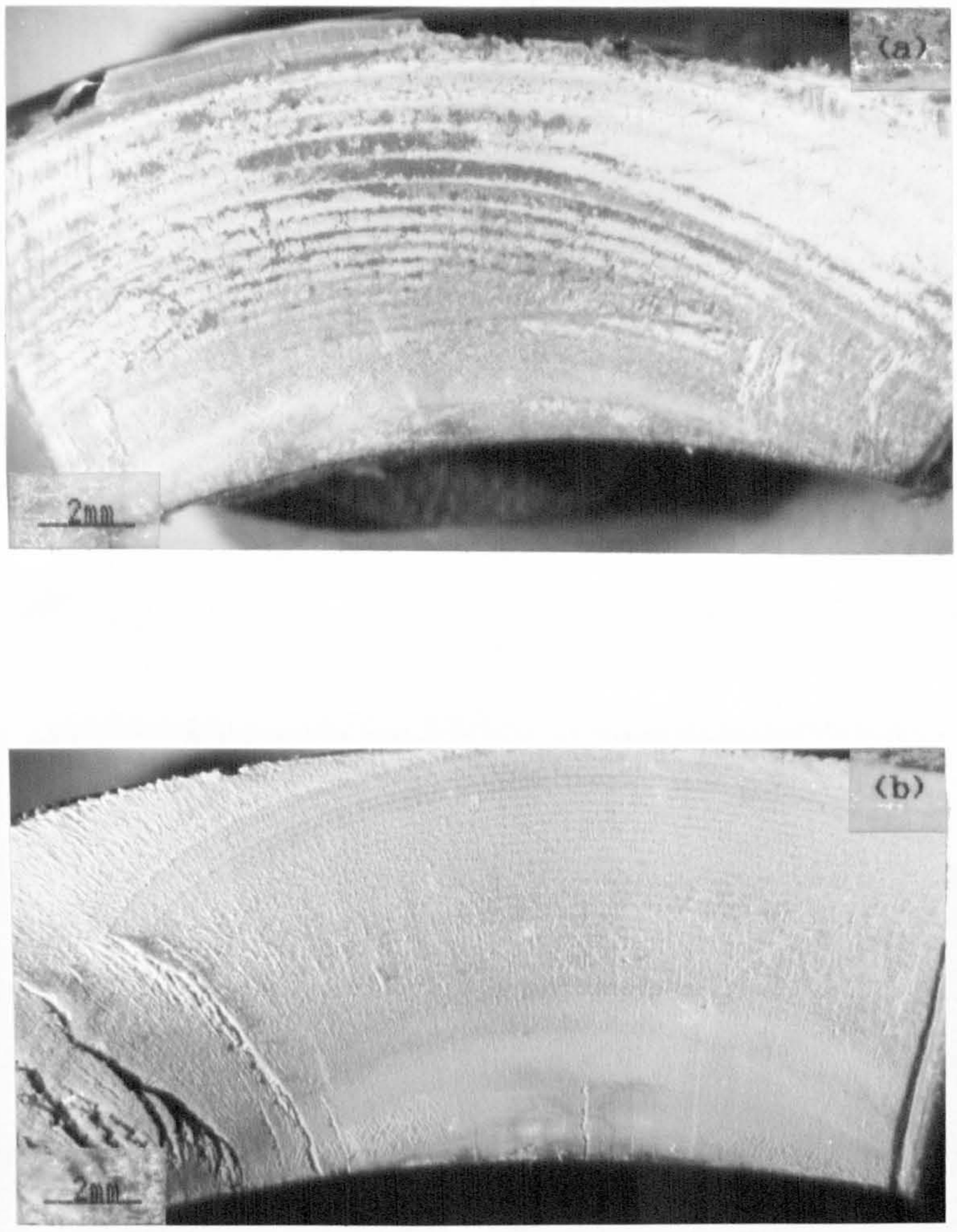

Fig. 5.10 Low magnification photomicrographs of the fracture surfaces of aligned butt weld failures in (a) 63 and (b) 90 mm pipe systems.

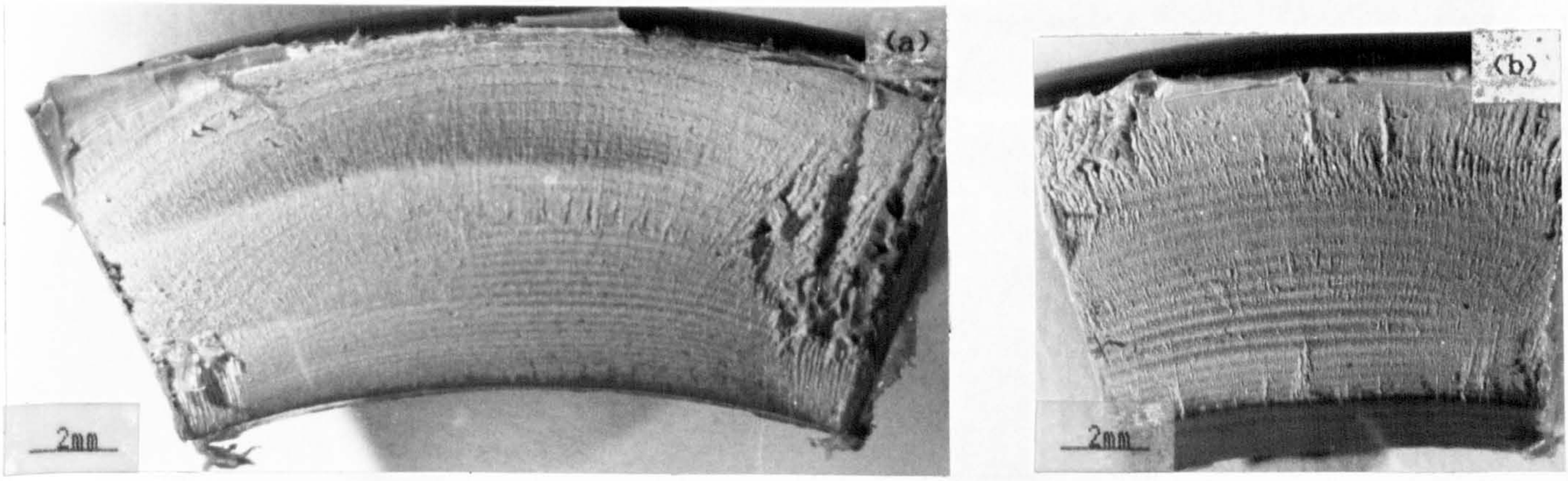

Fig. 5.11 Low magnification photomicrographs of misaligned butt weld fracture surfaces of (a) 9% and (b) 44% tested at ΔP=9.5 bar; (c) 9% and (d) 44% tested at ΔP=6.5 bar in 63mm SDR11 MDPE pipe systems.

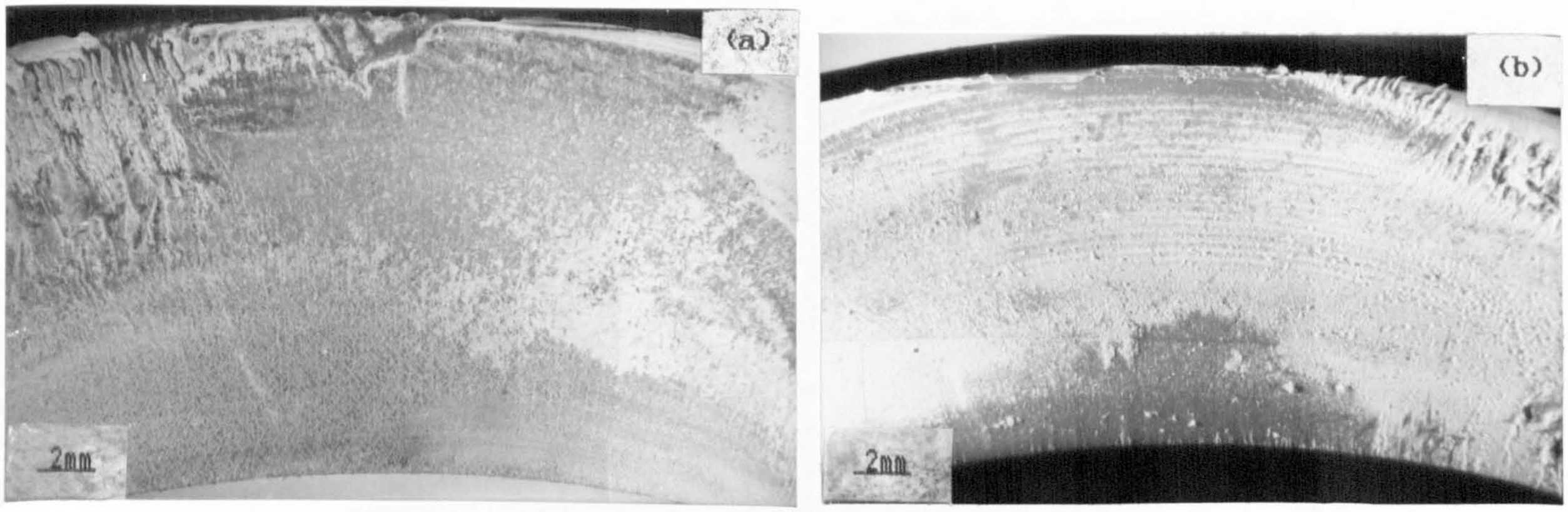

Fig. 5.12 Low magnification photomicrographs of misaligned butt weld fracture surfaces of (a) 9% and (b) 44% tested at ΔP=9.5 bar; (c) 9% and (d) 44% tested at ΔP=6.5 bar in 125mm SDR11 MDPE pipe systems.

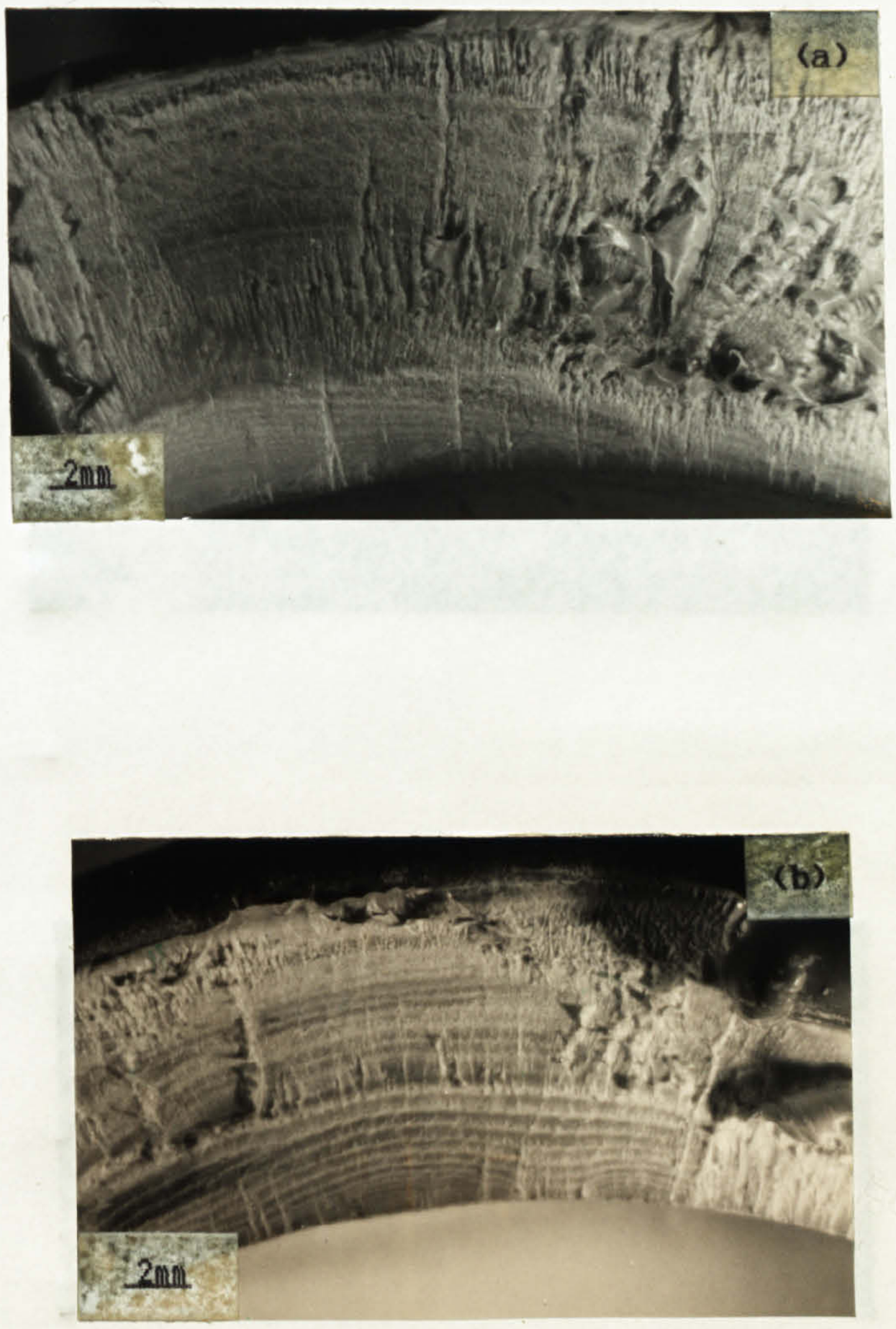

Fig. 5.13 Low magnification photomicrographs of misaligned butt weld fracture surfaces of (a) nominally aligned and (b) 44% misaligned butt weld in 63mm SDR11 MDPE pipe systems tested under stress-rupture condition.

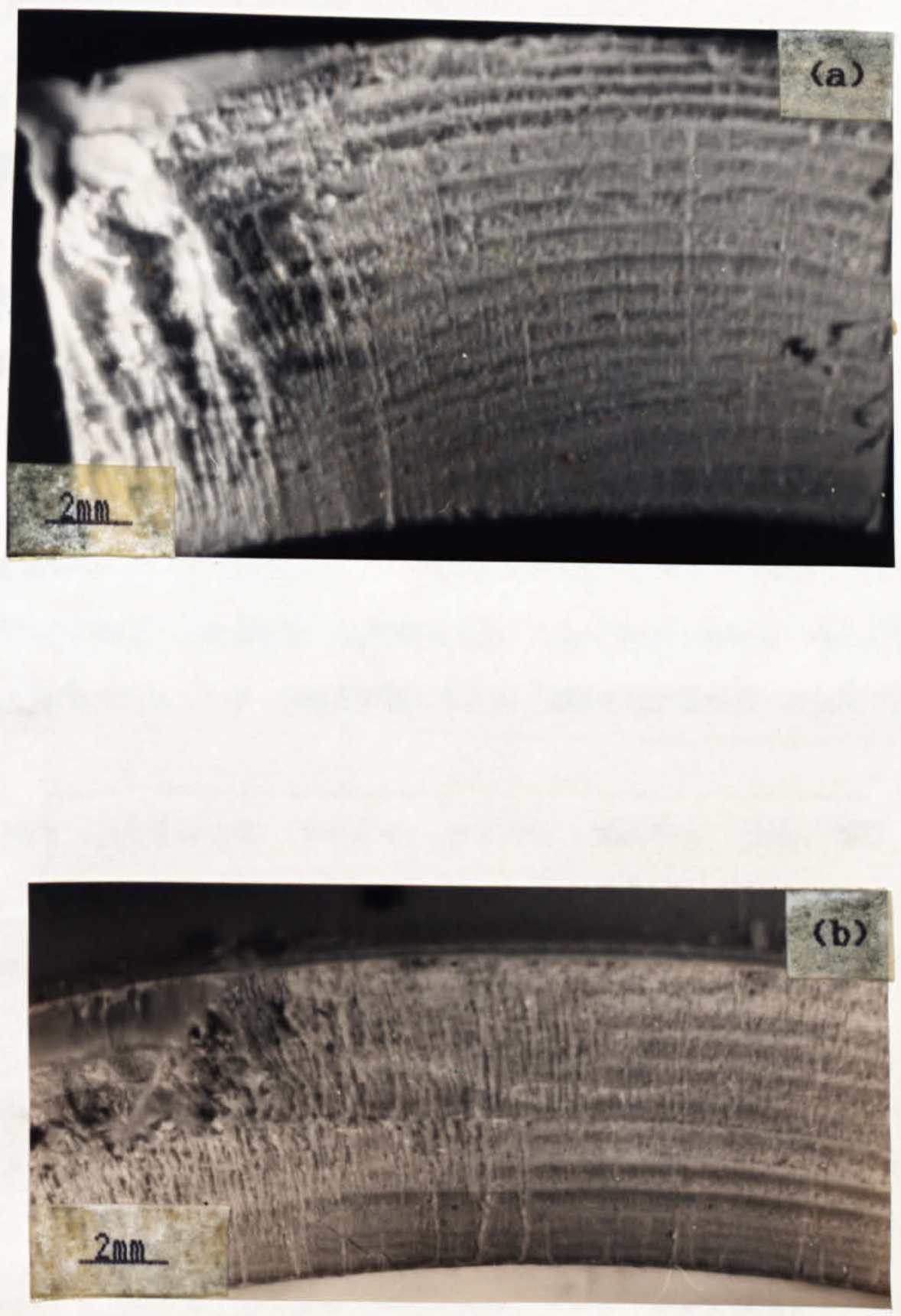

Fig. 5.14 Low magnification photomicrographs of misaligned butt weld fracture surfaces of (a) nominally 9% and (b) 44% misaligned butt weld in 125mm SDR11 MDPE pipe systems tested under stress-rupture condition.

Figures 5.10(a) and (b) shows the fracture surface of aligned butt weld failures in 63 and 90mm pipe systems tested at ΔP=9.5 bar and ΔP=8.0 bar respectively. In most aligned butt weld fracture surfaces in 63mm pipes there was always a greater deposit of scale, obscuring the true nature of the surface. However, the fatigue bands and ridges can be seen.

Figures 5.11 (a) and (b) shows the effect of misalignment in 63mm pipe systems on the fracture surface, while figures 5.11(a) to (d) portray the effect of test pressure range. It is apparent from these low magnification photomicrographs in figure 5.11(a) and (b) that;

(a) the spacing of discontinuous growth bands increases with increasing distance from the initiation site,

(b) a greater number of bands are present for the 9% misaligned butt weld compared to 44% misaligned butt weld,

(c) the relative number of bands also increases with decreasing pressure range. Spacing between the bands probably indicates different crack growth rates and different degrees of stress concentration to which the material has been subjected.

The above observations were also made on 90 and 125mm pipe, although in 125mm discontinuous growth bands were not clearly visible on the fracture surface as shown in figures 5.12(a) to (d).

Figures 5.13 and 5.14 display the fracture surfaces of stress-rupture butt weld failures in 63 and 125mm pipe systems respectively. Figure 5.13(a) is the aligned butt weld fracture surface and (b) is the 44% misaligned butt weld fracture surface in 63mm pipe. Whilst figure 5.14(a) is the 9% and (b) is the 44% misaligned butt weld fracture surface in 125mm pipe. The presence of discontinuous growth bands and longitudinal ridges is evident in all of them. The spacing between the bands tends to increase with increasing distance from the crack initiating

site. Comparison of 5.13(b) to 5.11(b) and 5.14(b) to 5.12(b) indicates that under stress-rupture loading the band spacing is greater compared to under fatigue for highly misaligned butt weld failures.

(ii) Fracture Surfaces Of Axial Butt Weld Failures Figures 5.15(a) to (d) show low magnification optical photomicrographs of axial/longitudinal cracks in the aligned butt welds in 63mm and 90mm pipes while figures 5.16(a) to (d) show the fracture surfaces of these axial failures. It appears that the axial crack was initiated from a surface flaw on the internal bead which was probably caused by local melt disturbance. It is enlightening to note in figure 5.16(a) to (d) that the growth of circumferential cracks initiating from the notch between the weld bead and pipe bore taking place is discerneble. The melt flow zone and weld interface were defined along with, in some cases, evidence of the extrusion flow lines. However, there was a general lack of discontinuous growth bands on the fracture surfaces, only two or three bands were observed on the outskirts of the surface.

(iii) Fracture Surfaces Of Pipe Failures Figures 5.17(a) to (d) displays the fracture surface appearances of pipes in 63 and 90mm diameter which failed under fatigue at ΔP=9.5 bar at 79°C. The majority of pipe failures initiated from the bore, the crack radiating from the initiation site in an elliptical front. The overall fracture surface appearance did not change with pipe diameter. The maximum distance to which the crack spread along the pipe axis was 1½-2½ times the wall thickness for 63mm pipe failure and 1¾-2 times the wall thickness for 90mm pipe failures.

There was no evidence of fatigue striations on the pipe fracture surfaces; however discontinuous growth bands were evident as was observed in the circumferential failures at the weld. The other features which were found to be common on all the pipe failures were lines running parallel with the extrusion direction and

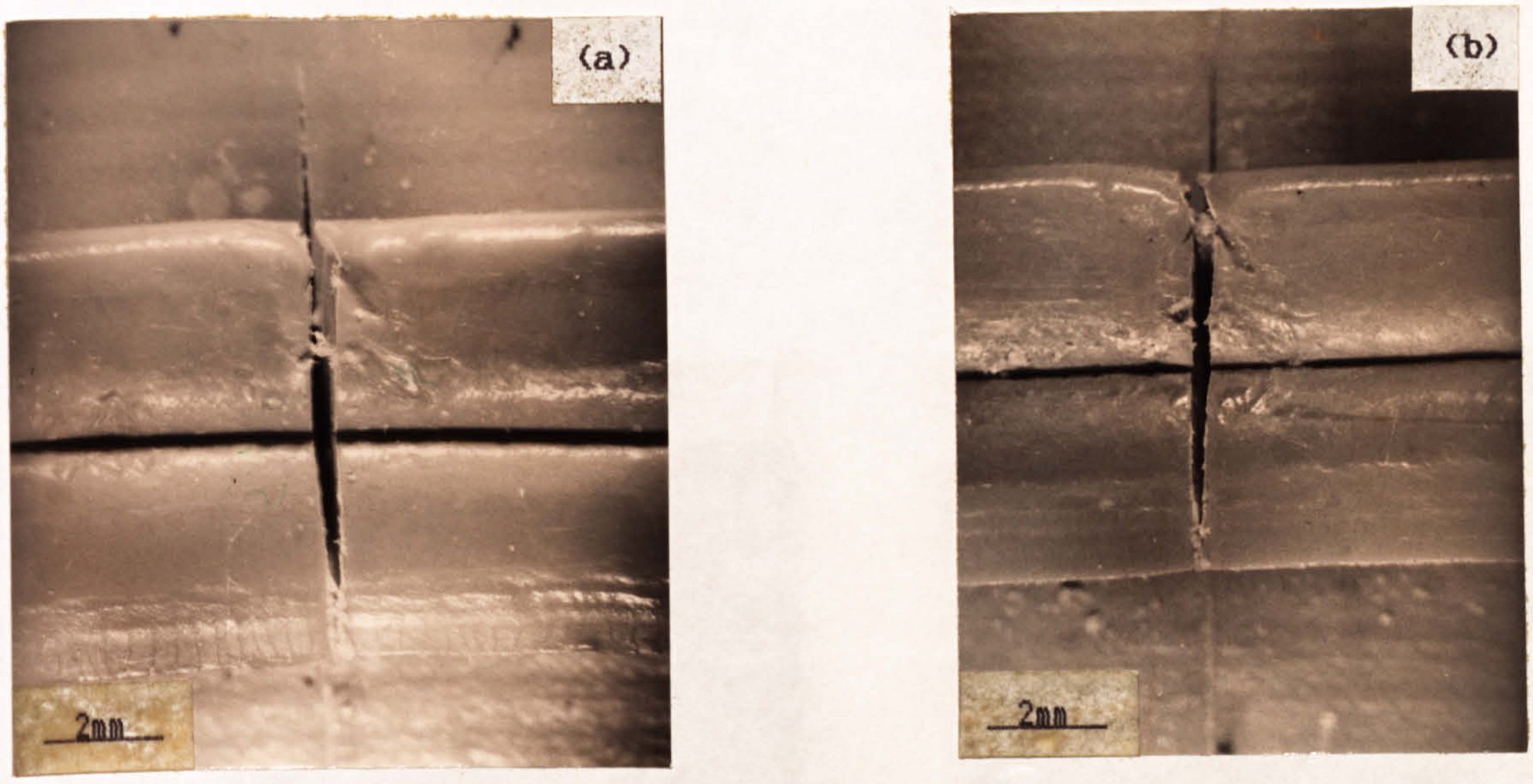

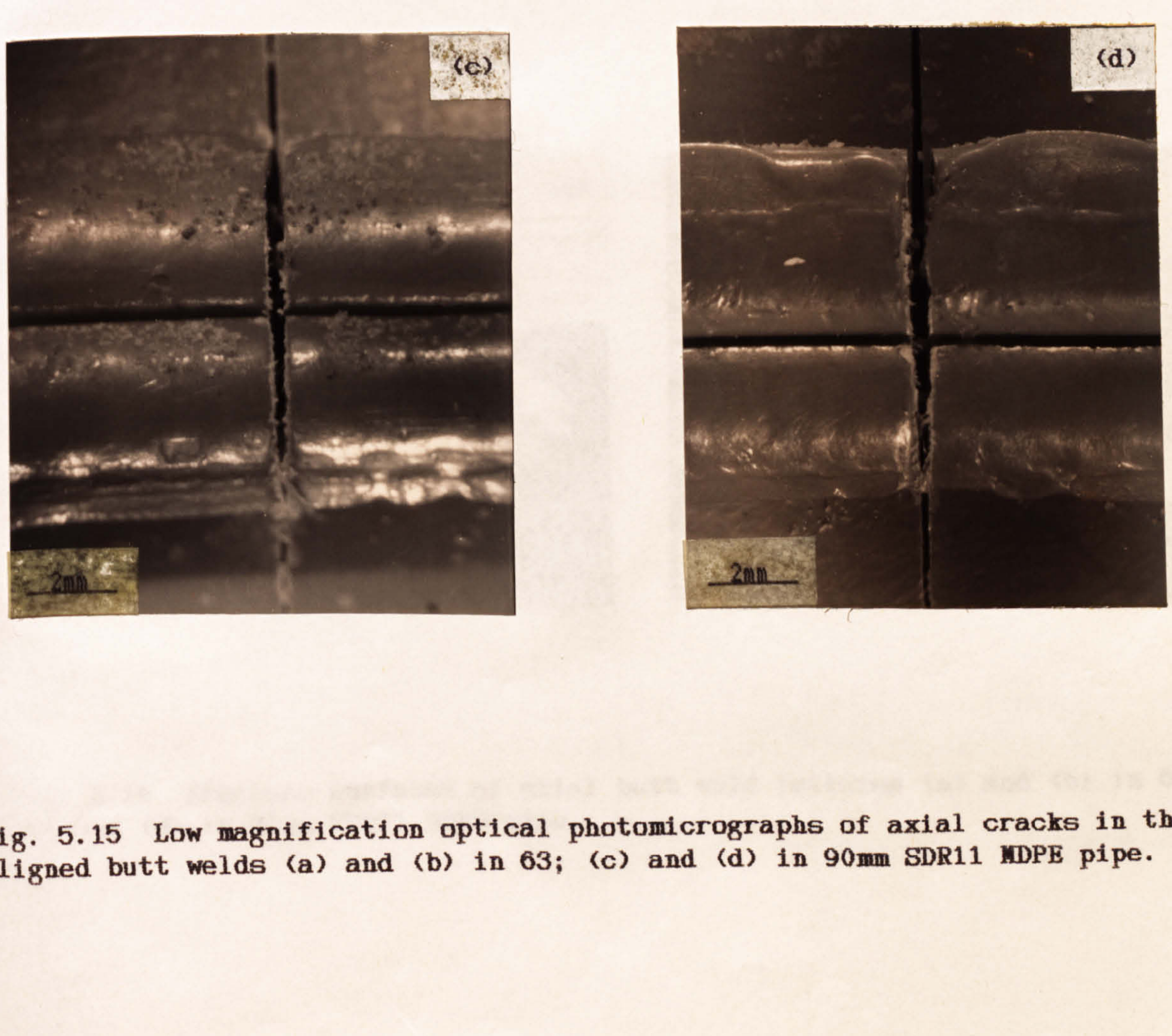

Fig. 5.15 Low magnification optical photomicrographs of axial cracks in the aligned butt welds (a) and (b) in 63; (c) and (d) in 90mm SDR11 MDPE pipe.

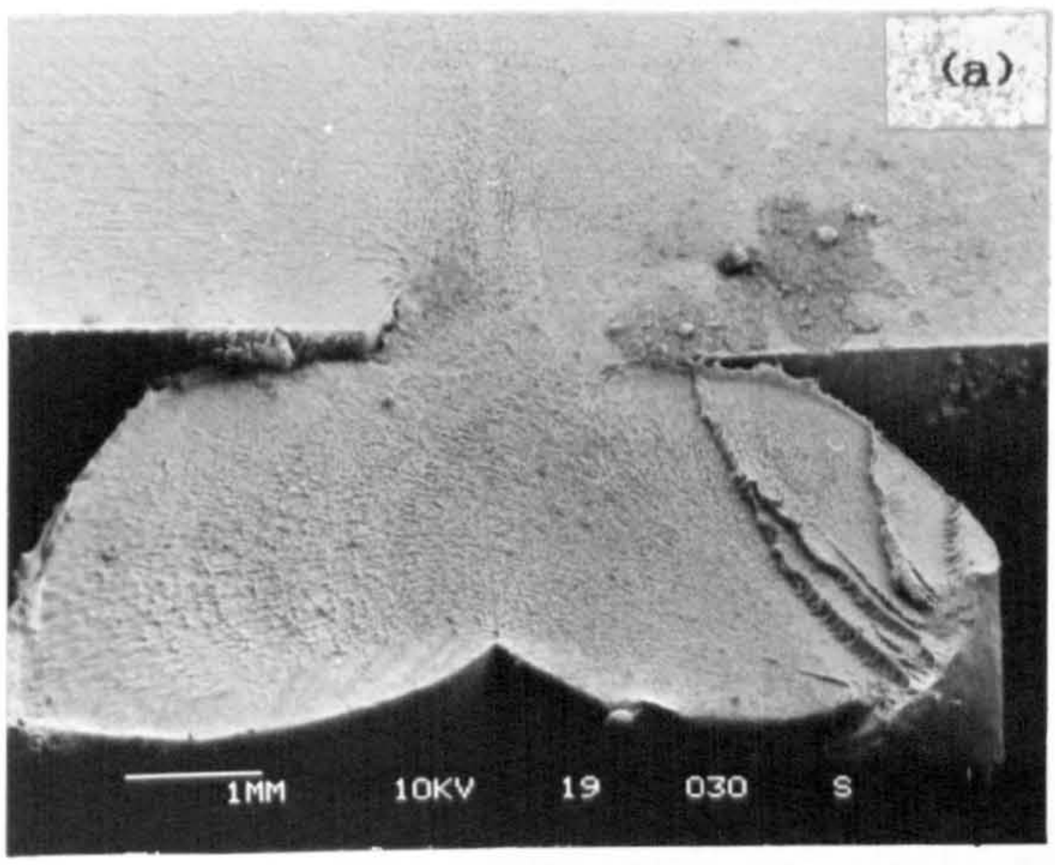

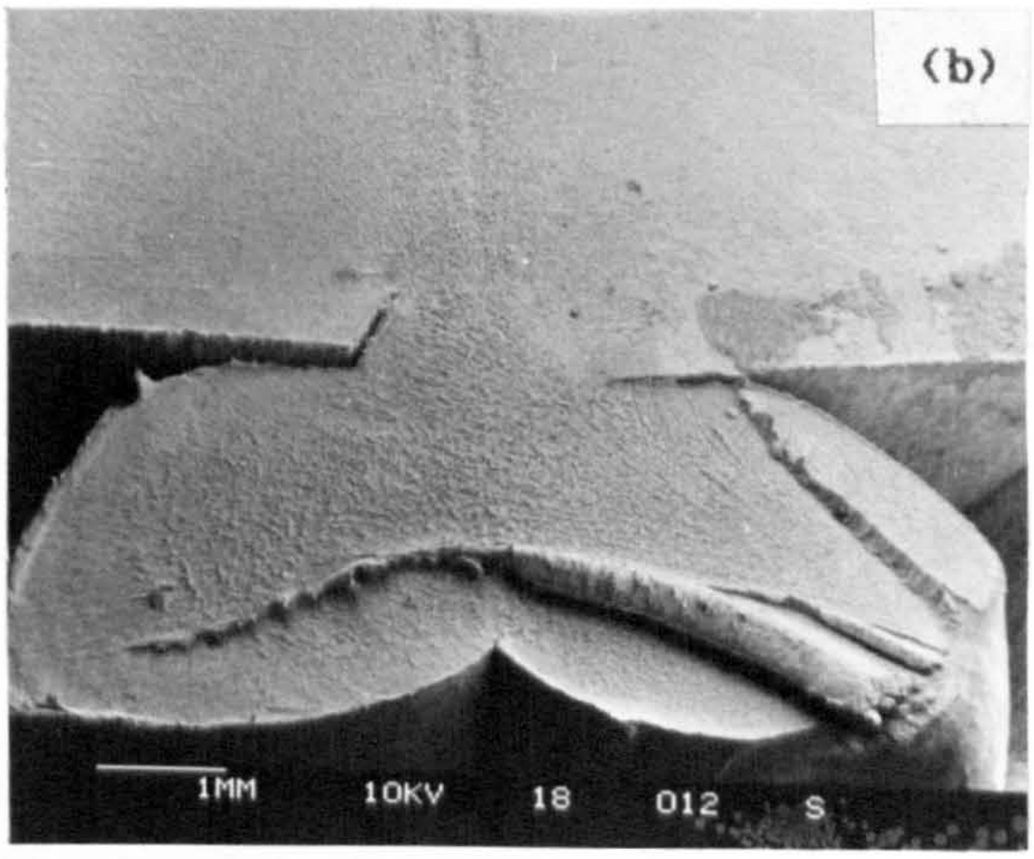

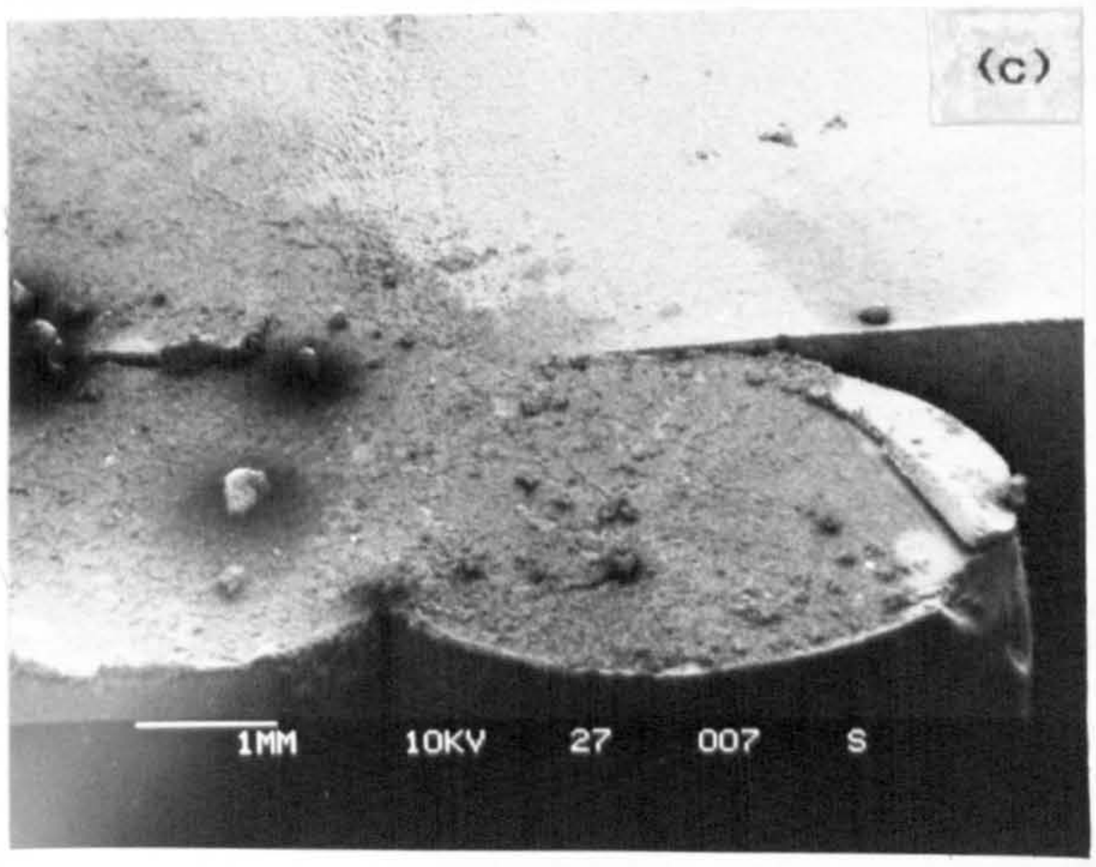

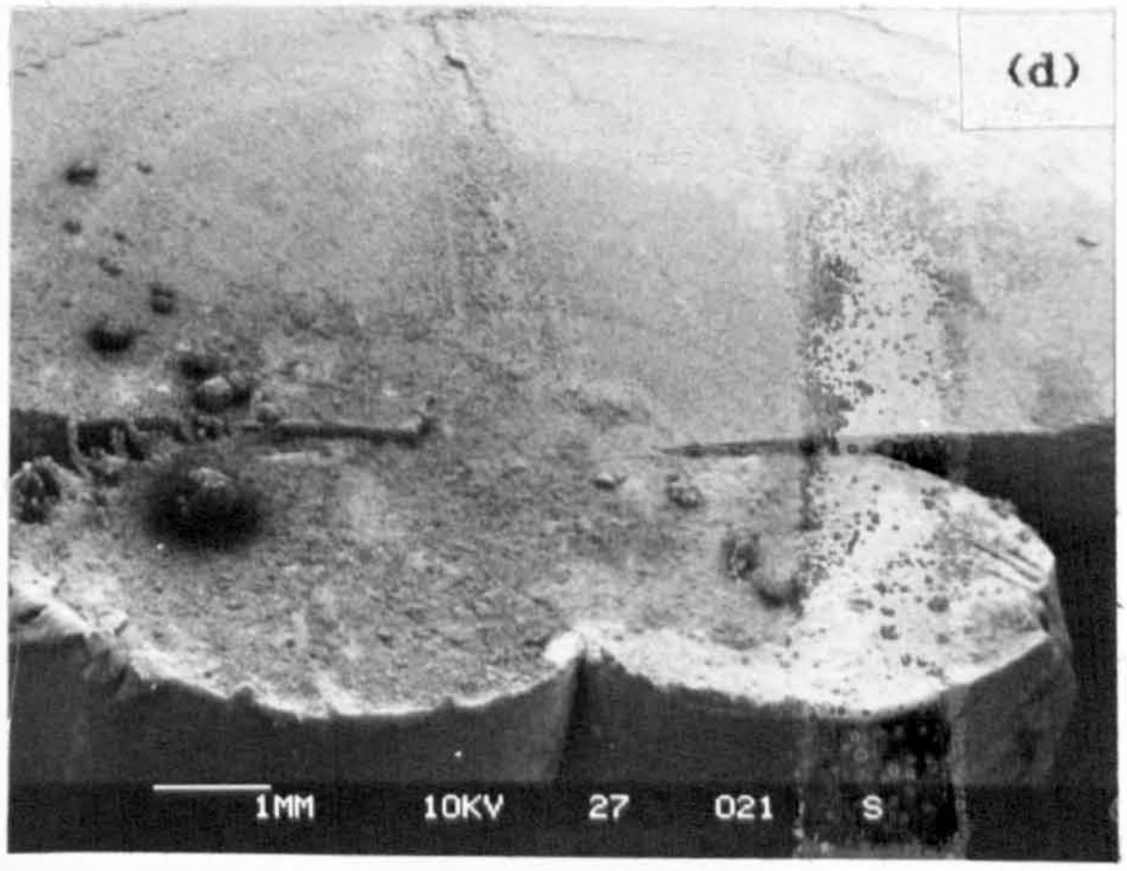

Fig. 5.16 Fracture surfaces of axial butt weld failures (a) and (b) in 63mm; (c) and (d) in 90mm SDR11 MDPE pipe.

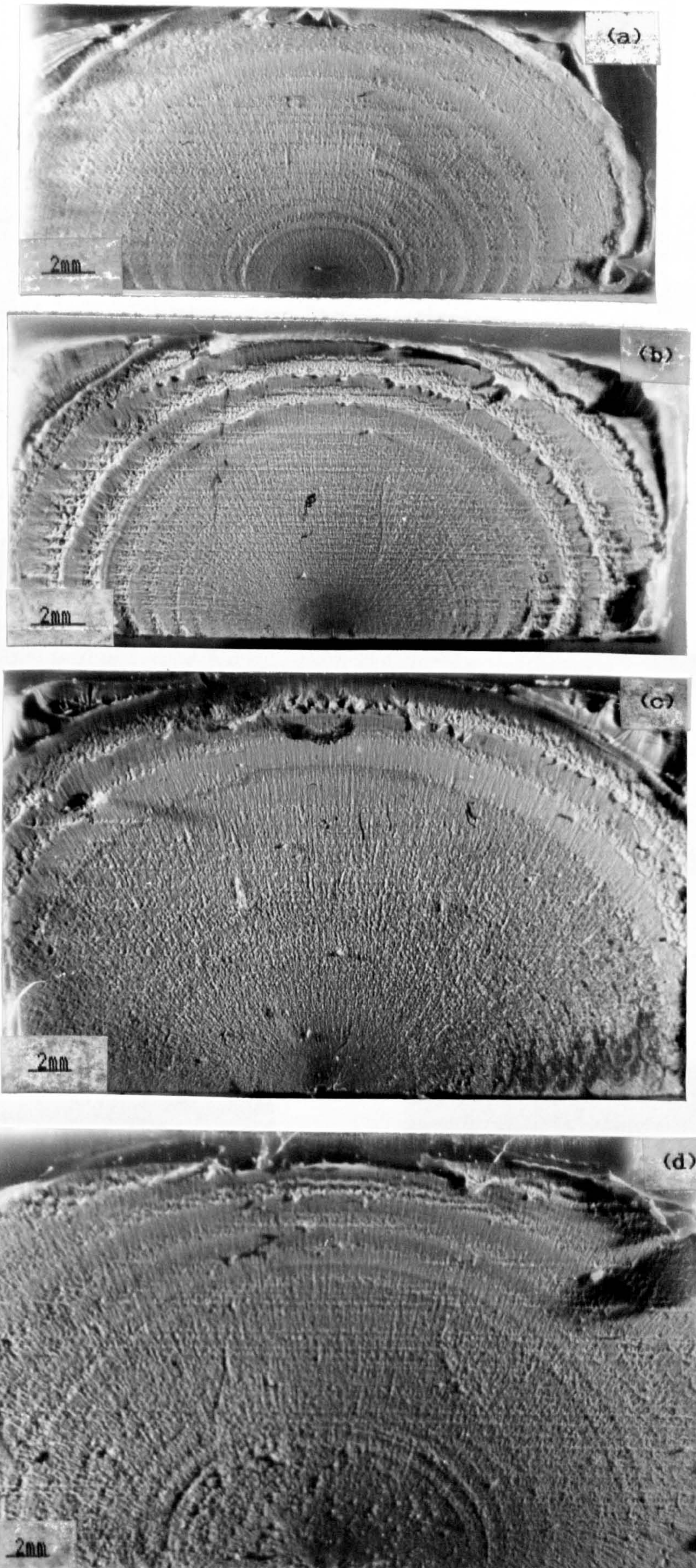

Fig. 5.17 Fracture surfaces of pipe failures (a) and (b) in 63mm and (c) and (d) in 90mm SDR11 pipes tested at ΔP=9.5 bar.

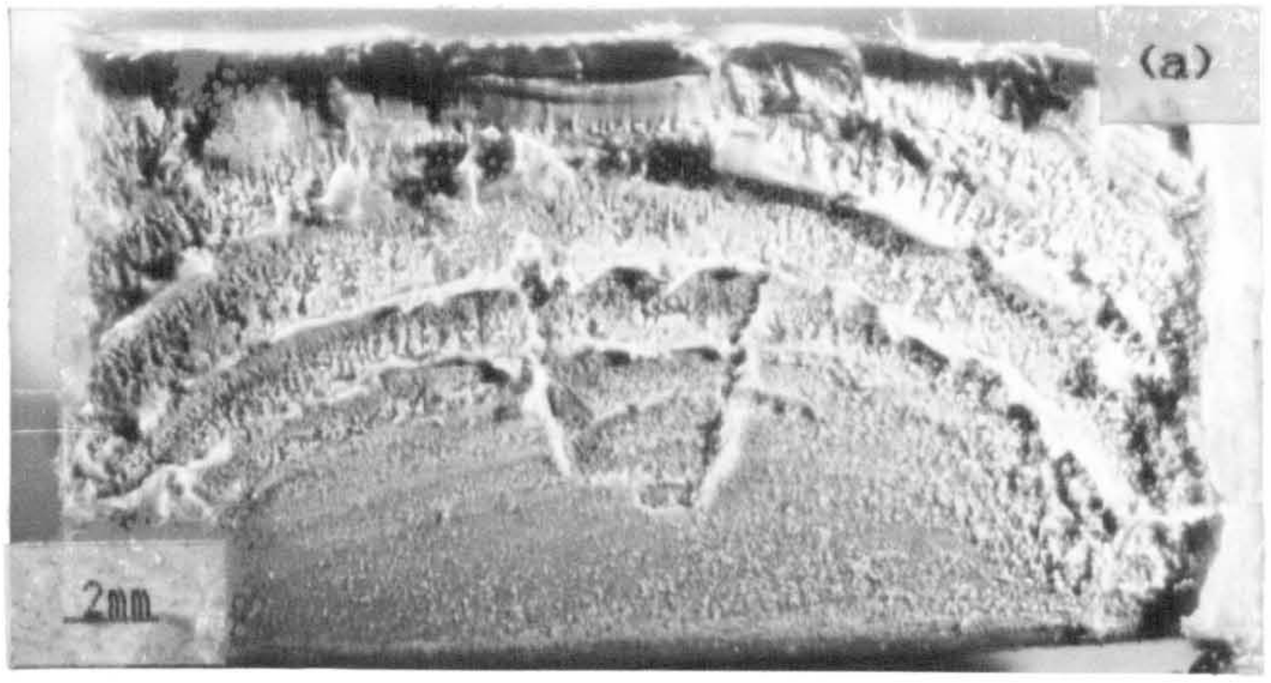

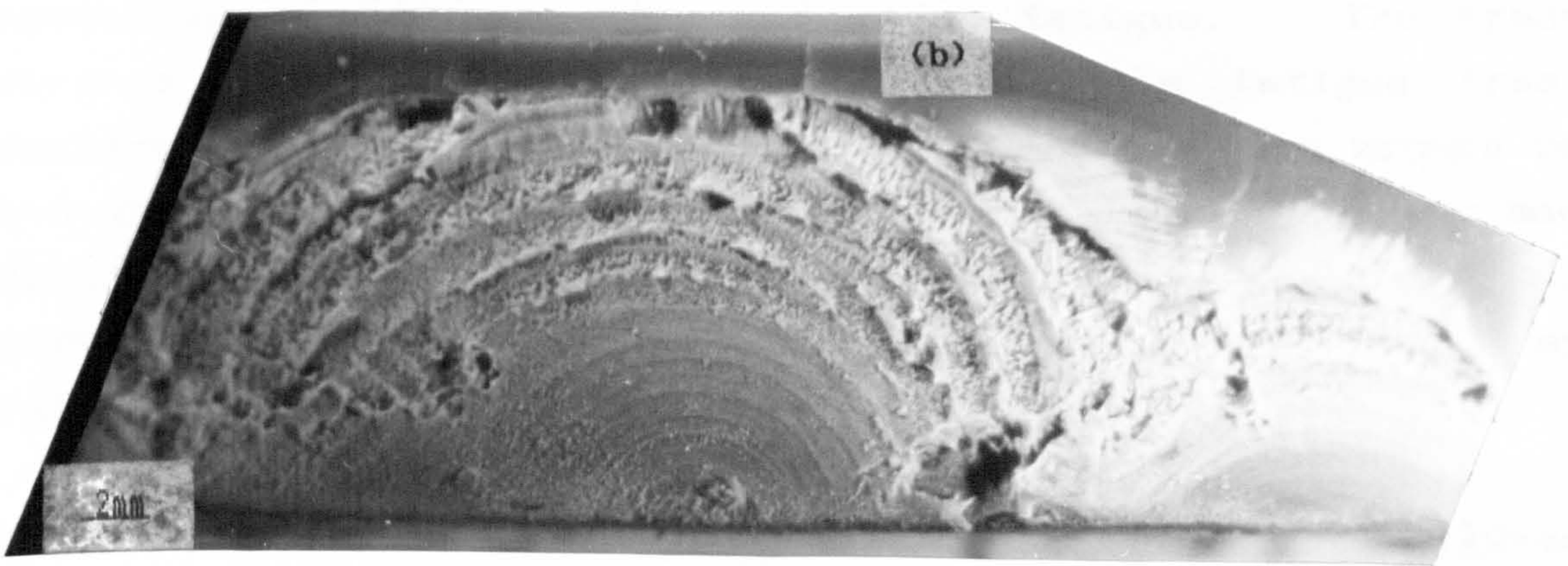

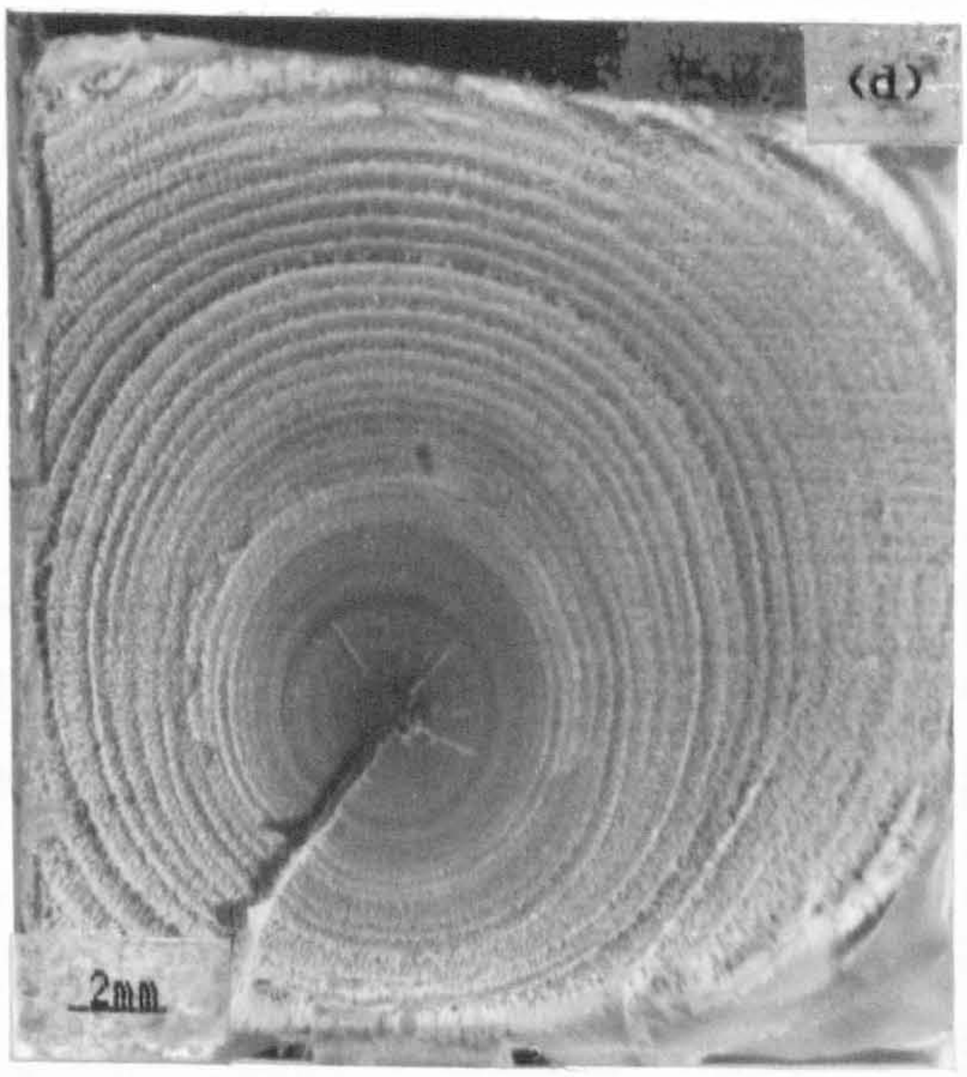

Fig. 5.18 Fracture surfaces of pipe failures (a) and (b) in 63mm and (c) and (d) in 90mm SDR11 pipes tested under stress-rupture condition at 9.5 bar.

small ridges emanating in a radial direction from the source of fracture, that is they were lying perpendicular to the ellipitical front.

All the 63mm pipe failures under stress-rupture loading were noted to initiate from the external surface. These were multiple intiation sites which were adjacent and also about 60mm apart in a straight line. The spreading of fracture along the pipe axis was about 1½-2 times the wall thickness, similar to spreading of fracture observed under fatigue. The fracture surface features were also similar to the fatigue fracture surfaces except that there were fewer discontinuous growth bands and greater spacing between them. It also showed greater macro-ductility on the surface; compare figures 5.18(a) and (b) which portray stress-rupture pipe failures to 5.17(a) and (b) display fatigue fracture.

Figures 5.18(c) and (d) show the stress-rupture pipe failures in 90mm pipe. Pipe failures were seen to initiate from the bore or within 80μm from the bore. The fracture surface of stress-rupture failures in 90mm pipe was not semi-circular as observed under fatigue but rather more elliptical in appearance with the crack front being essentially pinned on the inside wall of the pipe. The spread of fracture along the pipe axis was 1-1¼ times the wall thickness, less than that observed for fatigue failure.

5.3.0 Fractography: Microfeatures

(i) Circumferential Butt Weld Failures Fracture surfaces of circumferential failures of misaligned butt weld failures in 63mm pipe systems were examined in some detail using a scanning electron microscope.

Figure 5.19 shows a low magnification scanning electron micrograph of a fracture surface of a 9% misaligned butt weld tested at ΔP=9.5 bar together with a series of high

magnification of scanning electron micrographs. It clearly depicts the variation in microductility from the initiation site. In general, the microductility seems to increase with increasing distance from the initiation site.

At the initiation site, there does not appear to be any evidence of local drawing or micronecking and microductility which is clearly evident in the latter stages of crack growth. The fracture cannot be classed as truly brittle but quasi-brittle (after Flueler et al (28)) since the formation of fibrils normally resulting from the formation of a craze necessarily involves a local large amount of plastic yielding which increases with crack length. The initial mode of fracture appears to be different from the intermediate stage and outer surface where considerable local yield or micronecking and microductility seems to have occurred. In the latter stages fibril length increases and so do the sizes of holes or voids. Within the voids the interconnecting ligaments holding the fibrils can be seen at latter stages of crack growth.

Comparison of figures 5.19(a) to (d) and figures 5.20(a) to (d) shows that the effect of increasing misalignment is to increase relative microductility at each of the stages from the crack initiation site. Microvoid size at the initiation site is 1-3μm for 9% misalignment and is 3-9μm for 44%. These macrovoids increase to 10-20μm for 9% misalignment and greater than 20μm for 44% misalignment by the approach to final rupture. Comparison of figures 5.19(a) to (d) and figures 5.21(a) to (d) shows the effect of decreasing pressure range (ΔP=6.5 bar) is to decrease the relative microductility.

Figures 5.22 and 5.23 display the fracture surface of nominally aligned and 44% misaligned butt weld failures under stress rupture. It is apparent from the low mangification scanning electron micrographs figure 5.22(a) and figure 5.23(a) that microductility increases along the crack growth direction and

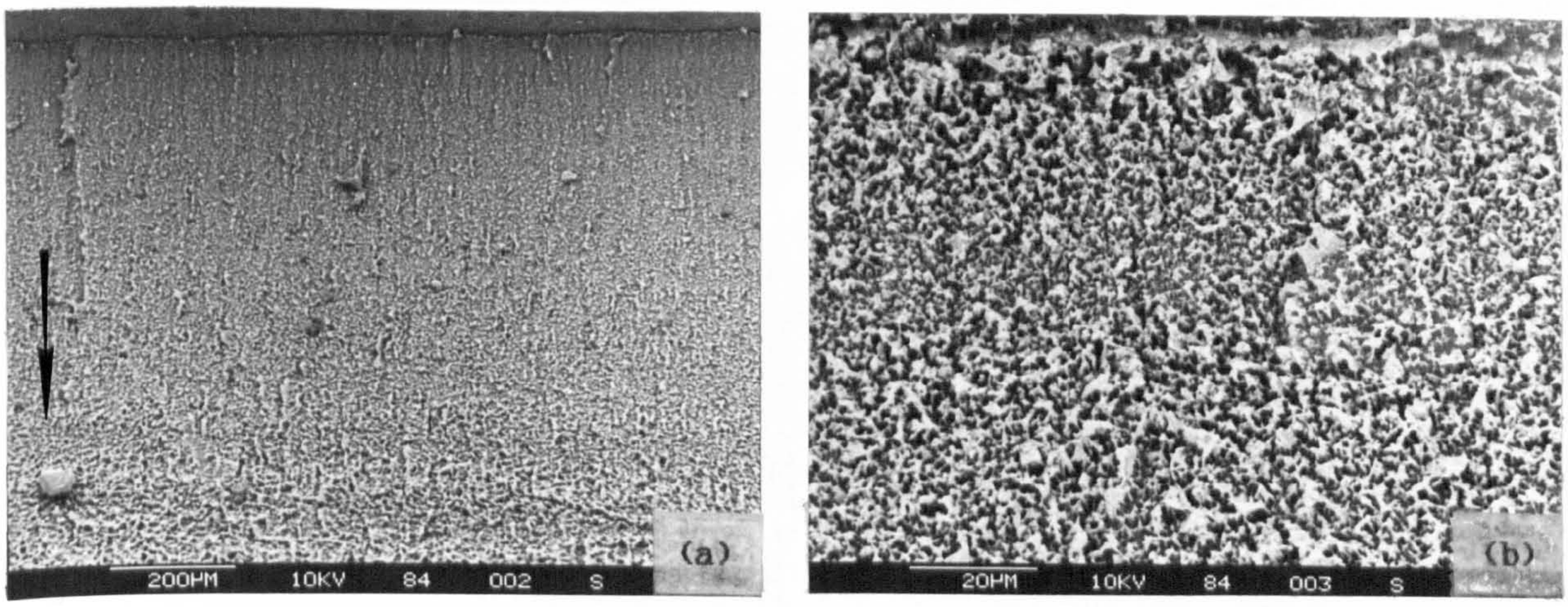

Fig. 5.19 SEM micrographs of fracture surface of 9% misaligned butt weld tested at ΔP=9.5 bar; (a) low magnification and high magnification region of (b) initiation site, (c) intermediate distance and (d) on approach to the final stages of rupture.

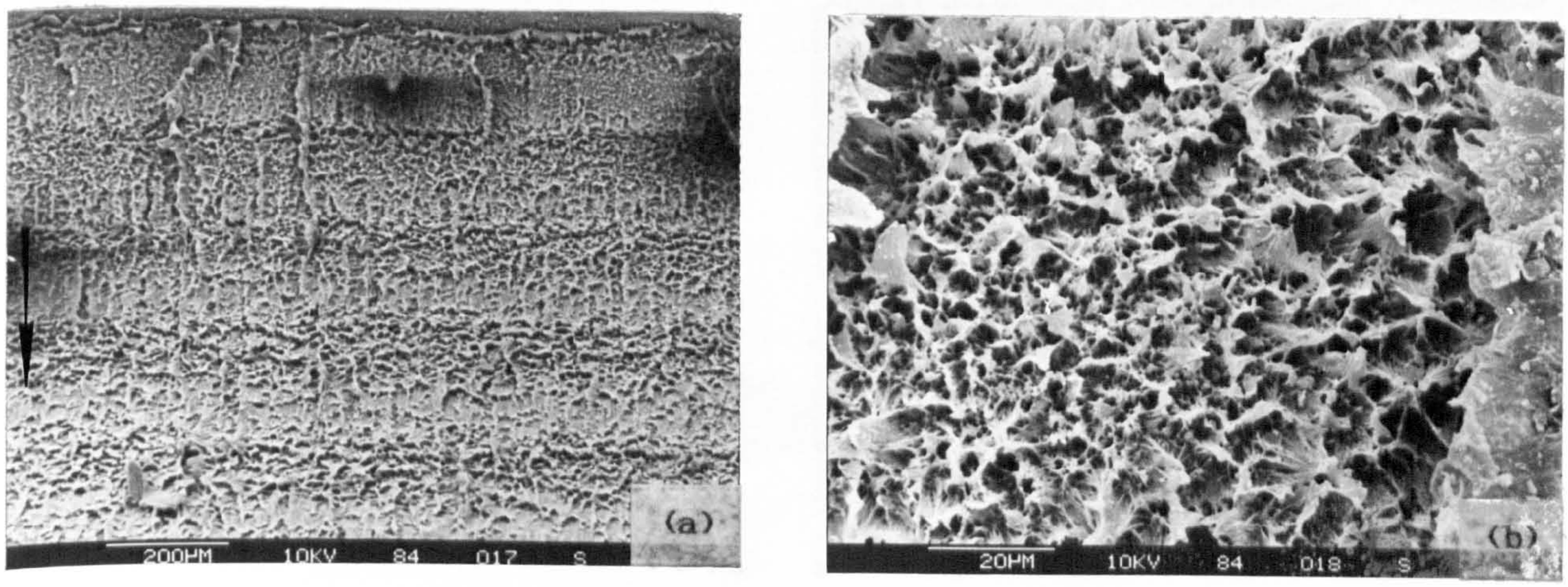

Fig. 5.20 SEM micrographs of fracture surface of 44% misaligned butt weld tested at ΔP=9.5 bar; (a) low magnification and high magnification region of (b) initiation site, (c) intermediate distance and (d) on approach to the final stages of rupture.

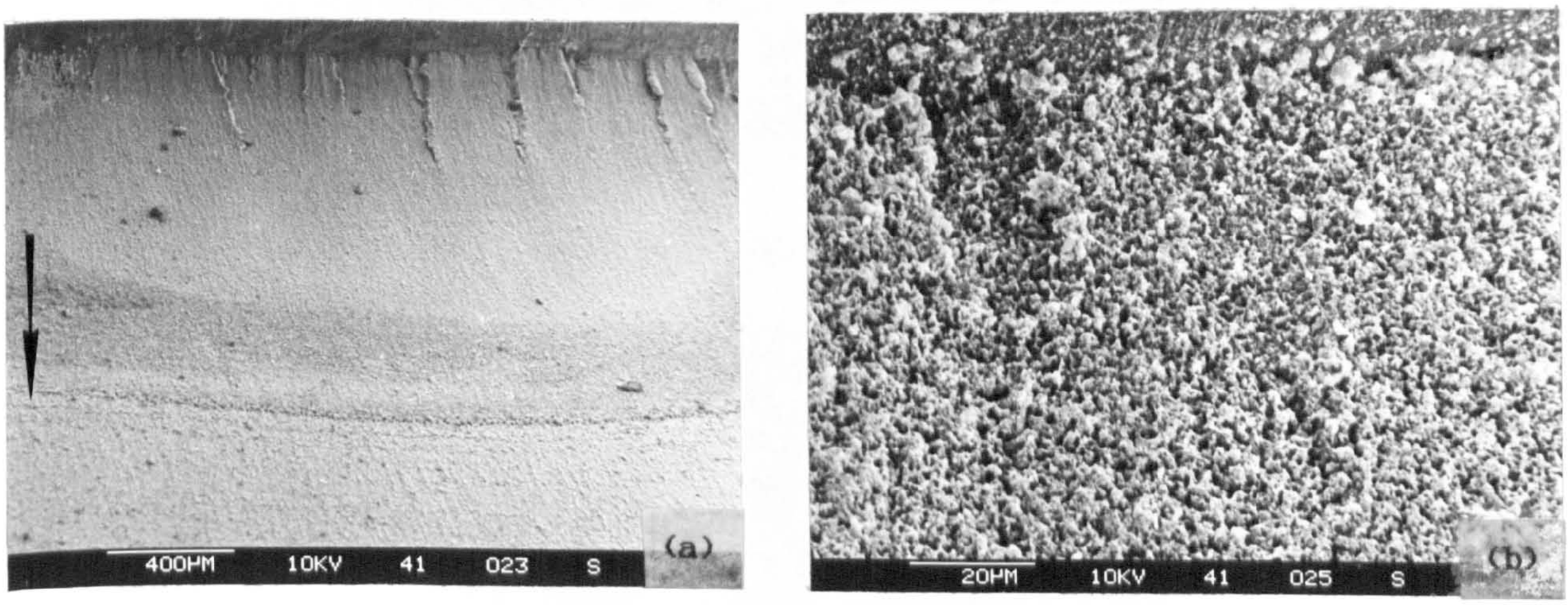

Fig. 5.21 SEM micrographs of fracture surface of 9% misaligned butt weld tested at ΔP=6.5 bar; (a) low magnification and high magnification region of (b) initiation site, (c) intermediate distance and (d) on approach to the final stages of rupture.

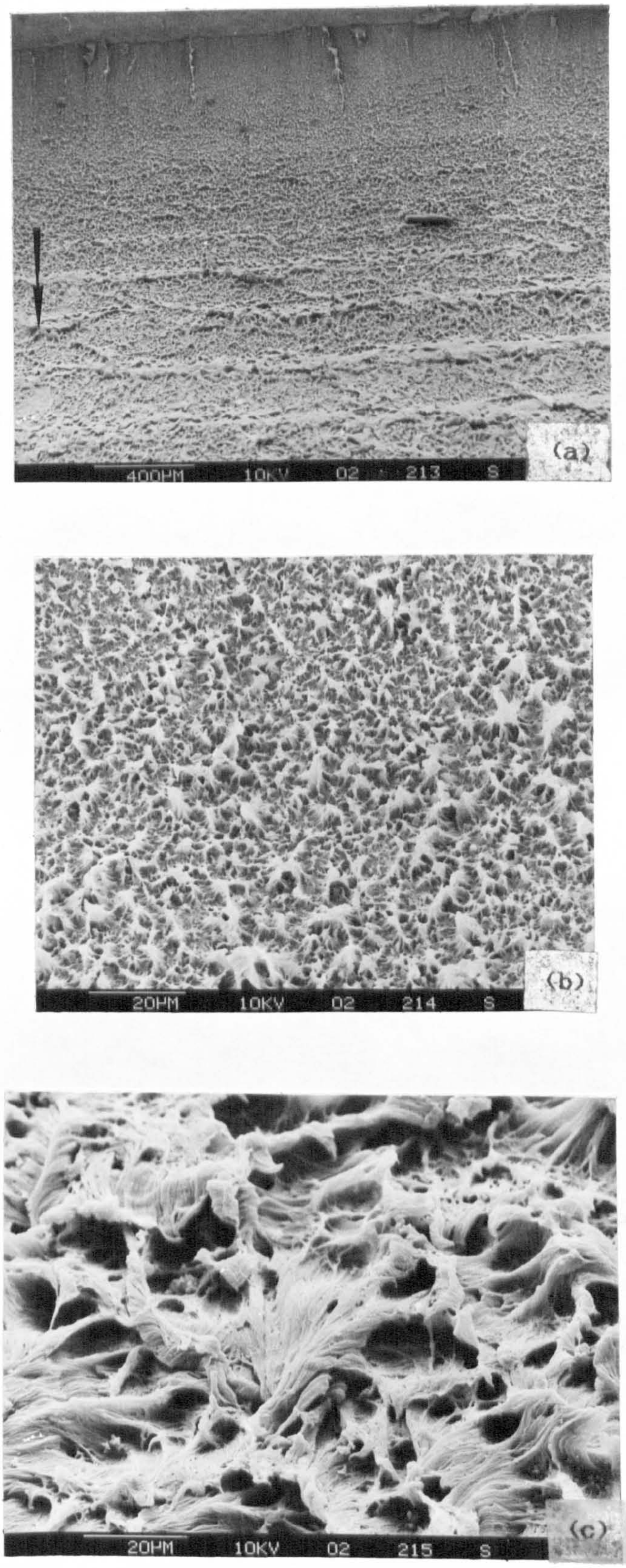

Fig. 5.22 SEM micrographs of fracture surface of aligned butt weld tested under constant pressure of 9.5 bar; (a) low magnification and high magnification regions of (b) initiation site and (c) on approach to the final stages of rupture.

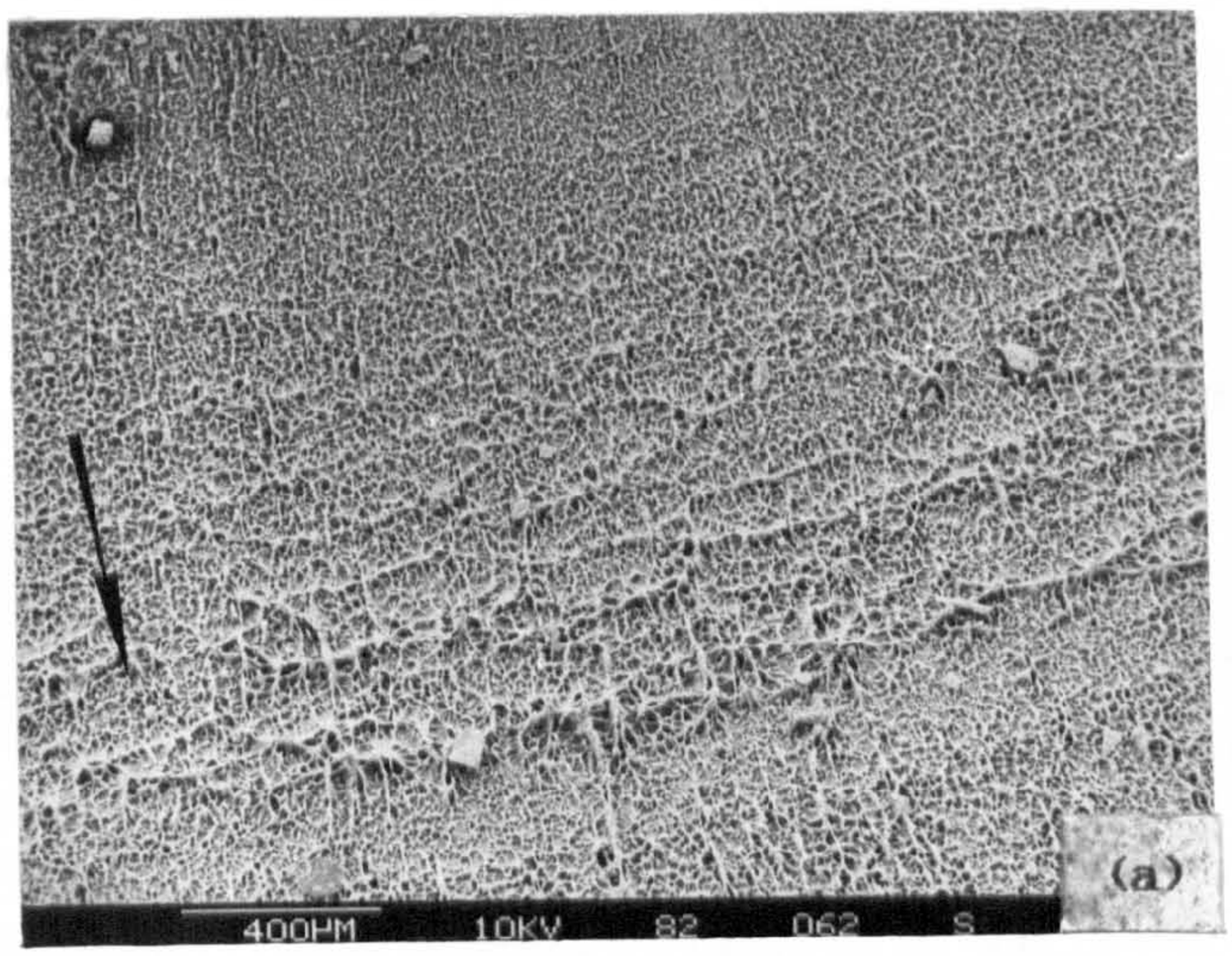

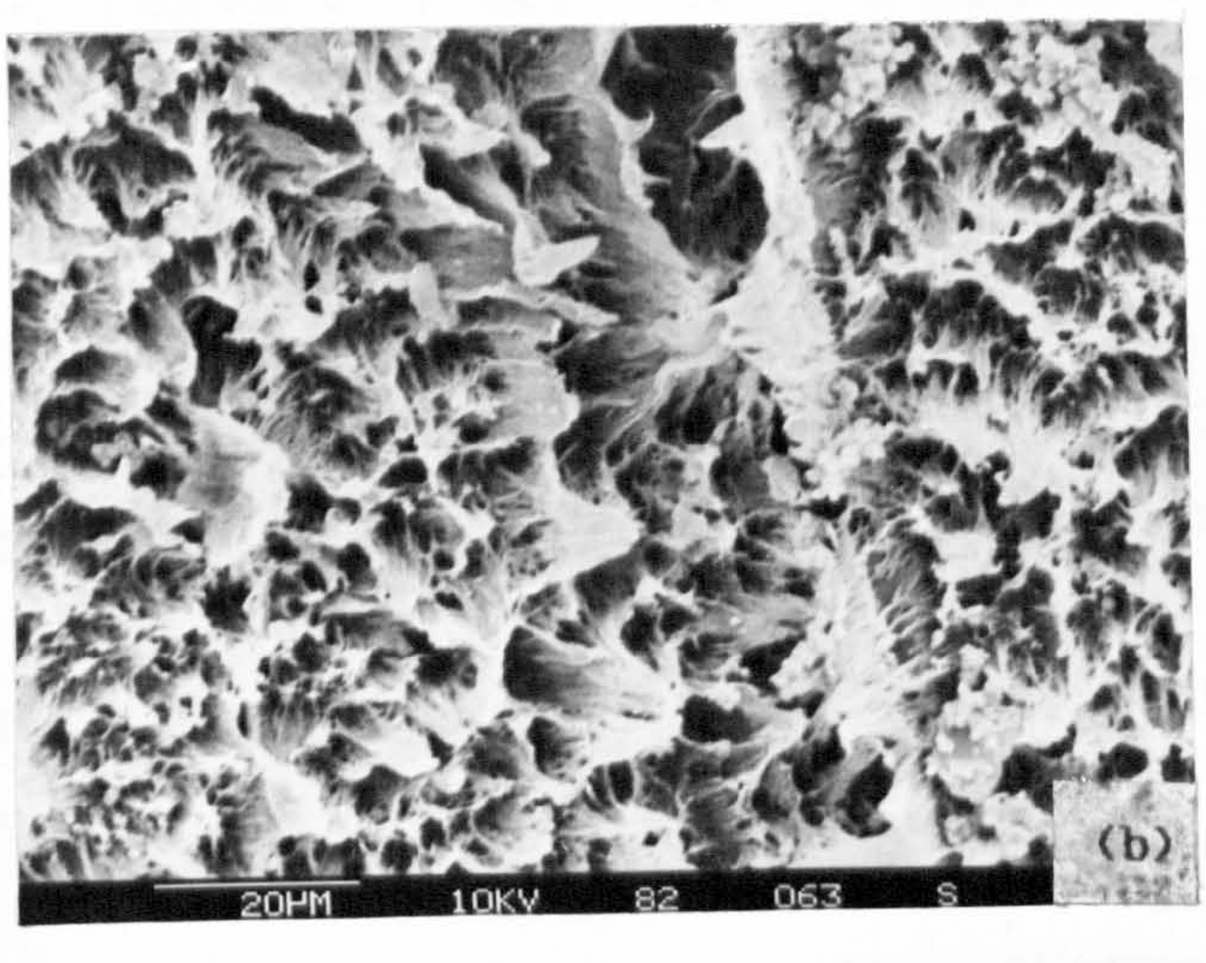

Fig. 5.23 SEM micrographs of fracture surface of 44% misaligned butt weld tested under constant pressure of 9.5 bar; (a) low magnification and (b) high magnification region of initiation site.

also appears to reach at an early stage in the crack growth direction compared to the fatigue fracture surface at a given misalignment. At the initation site the microvoid size is in the range 1-3μm for aligned butt weld failure, while for the 44% misaligned butt weld failure it is 6μm.

(ii) Axial Butt Weld Failures Figures 5.24(a) to (f) portray the fracture morphology of an axial butt weld failure at both relatively low and high magifications at increasing distances from the initation site. Figure 5.24(b) shows the high fibril density near the initation site and fibril length/height is relatively short compared to the region shown in figure 5.24(d) which is the MFZ at the mid-point of pipe wall. The fibril direction at the MFZ is different compared to the surrounding region. In general the fibril texture in the axial butt weld failure surfaces at the initiation site and MFZ is different compared to the circumferential butt weld failure. Figure 5.24(f) shows the discontinuous growth bands in the final approach to the rupture stage. There appears to be alternate regions of where fibrils are present and of featureless regions; this may be representing a stick and slip type of crack growth.

(iii) Pipe Failures Figures 5.25(a) to (c) indicate clearly the typical microfeatures of fracture surfaces observed on pipe failures under fatigue. The overall appearance of pipe failures suggest that the failure mechanism is not dissimilar from that of circumferential failure of the butt weld. Both of them suggest craze formation and slow stable crack growth. The variation in microductility across the surface is apparent in figure 5.25. The initiation site shows relatively greater microductility compared to circumferential failures of 9% misaligned butt weld. The size of fibrils and hole size seems to increase with increasing distance from the initiation site. At the initation region, microvoid sizes are less than 2μm and the intermediate stage it has increased in the range of 6-8μm.

There was no evidence of the presence of fine striations to suggest that fracture occurred due to step-by-step propagation.

Detailed examination of 63mm stress-rupture pipe failures was not possible since the surface was covered with scale debris. However, it can be seen from a low magnification scanning electron micrograph in figure 5.26 that there is a band of width 60-80μm running parallel to the pipe axis on the edge where the external crack was initiated. Elemental analysis of this band revealed it was rich in Calcium, Silicon, Chlorine, Sulphur, Aluminium and Magnesium, whereas, the region away from the bend was rich in Calcium, Silcon, Aluminium, implying that the band had Sulphur and Magnesium.

(iv) Initiation Of Pipe Failures Examination by SEM of the fracture surfaces of pipe failures in 63mm pipe systems tested under fatigue revealed that, 33% of the twelve pipe failures initiated from observable particles and in 90mm pipe systems, 28% of the eighteen pipe failures initiated from particles. Of the two stress-rupture pipe failures in 90mm examined, a particle was found in one of them. Examples of such crack initiators are shown in figures 5.27(a) to (d). No failures were found to be due to macrovoids.

The size of particles and their location with respect to the pipe bore in 63mm and 90mm pipe failures are contained in table 5.4. In the 63mm pipe failures, the initiating particles lay in the size range 120μm to 475μm. In two cases particles were located at the bore while in the other two cases particles were located about 100μm and 200μm away from the bore. In 90mm pipes the size of particles initiation fracture lay in the range of 50 to 570μm. In all the cases particles were located at the bore.

The elemental analysis of the particles indicated that in the majority of cases the initiating particle was Calcium rich and in one case iron was detected.

Table 5.4 Particle size, location and type which were found in the (a) 63 and (b) 90mm pipe failures in Rigidex 002-50 MDPE pipe systems.

(a)

Number Of Cycles To Failure	Particle Size µm	Particle Location	Elemental Analysis
153,210	475	bore	Calcium
253,740	120	bore	Calcium
424,050	412	bore	Calcium
438,390	206	2mm from bore	Iron

(b)

Number Of Cycles To Failure	Particle Size µm	Particle Location	Elemental Analysis
58,650	50	bore	Calcium
87,840	188	bore	Calcium
137,040	438	bore	Calcium
330,600	570	bore	Calcium
1,728Hrs	125	mid-wall	Iron

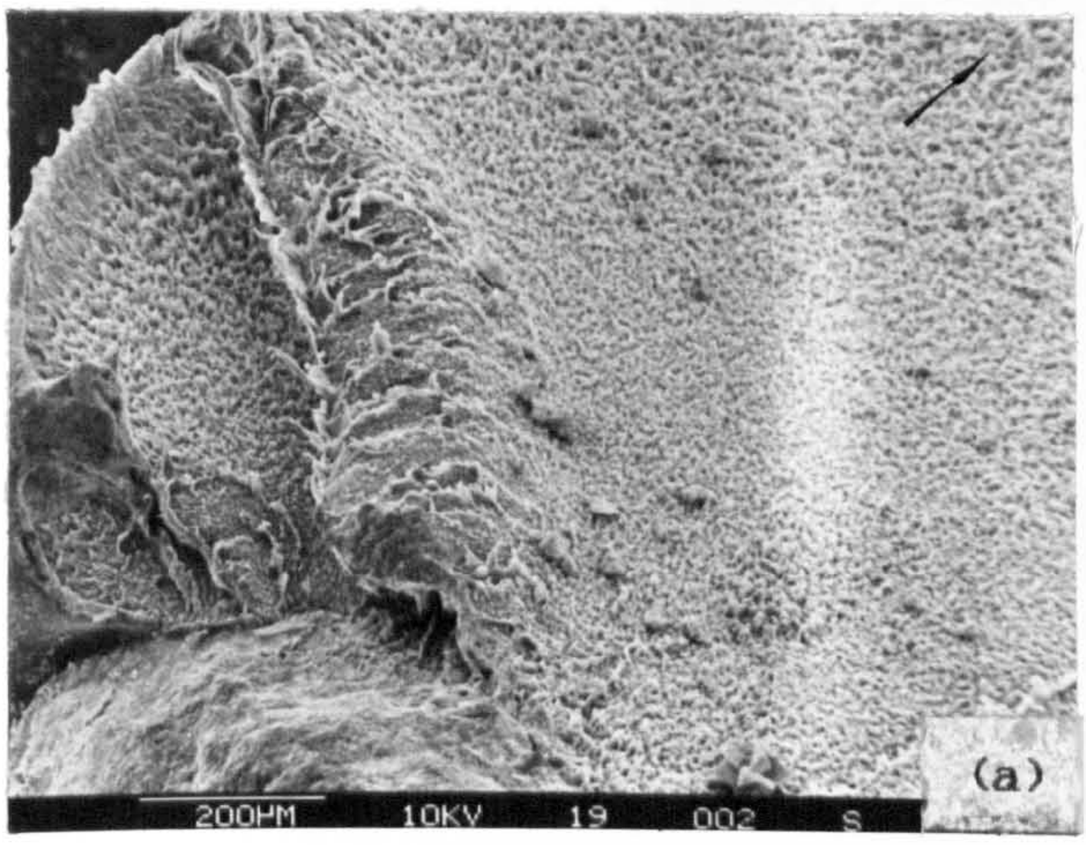

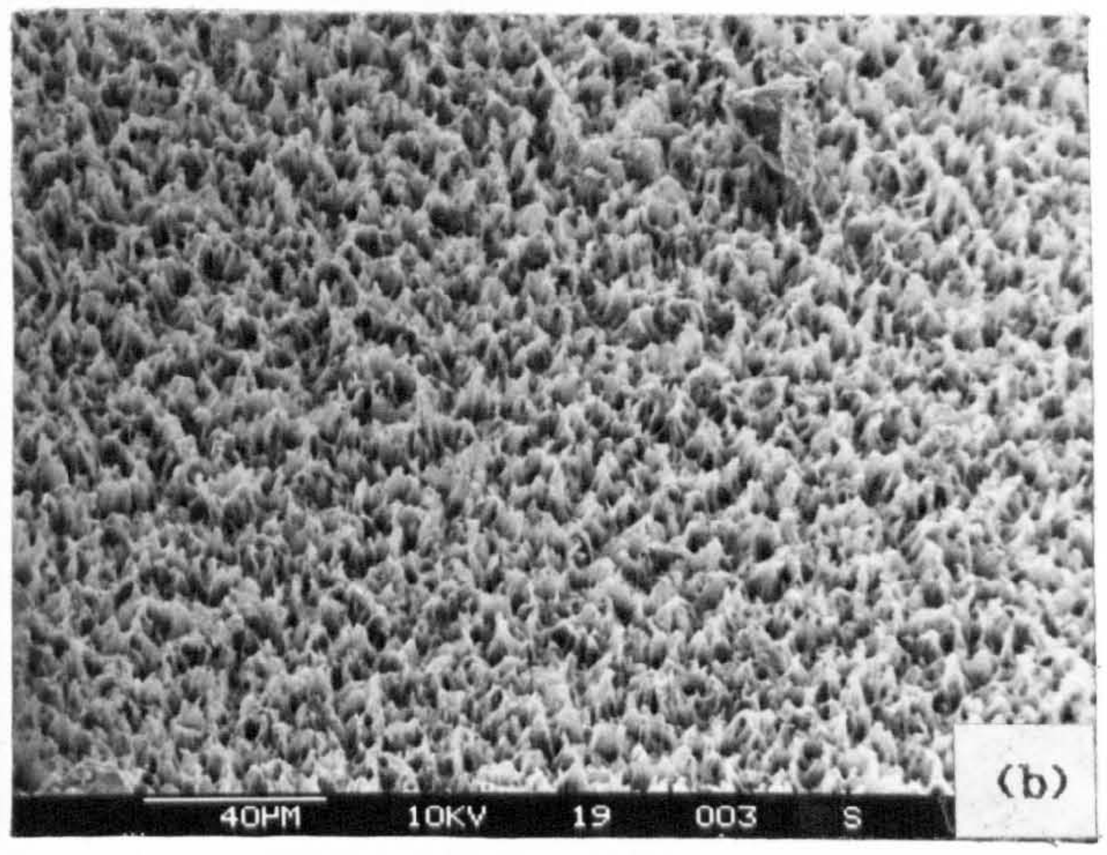

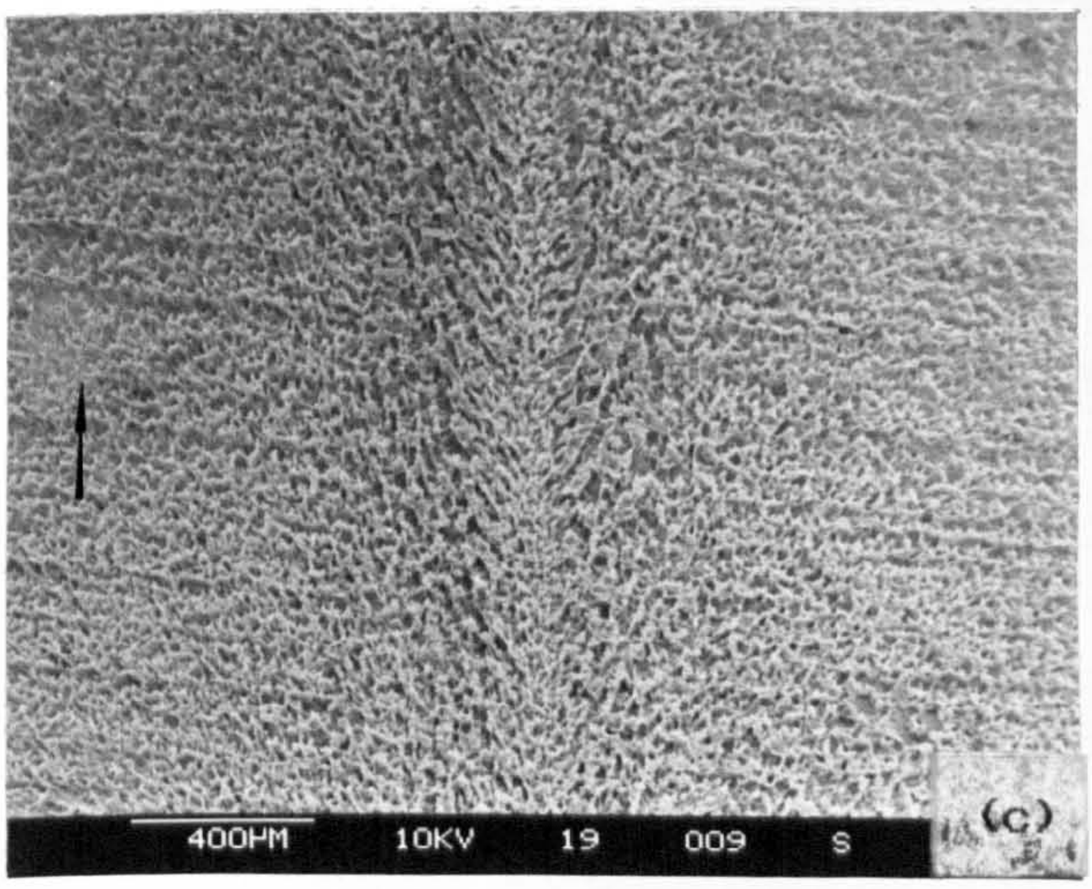

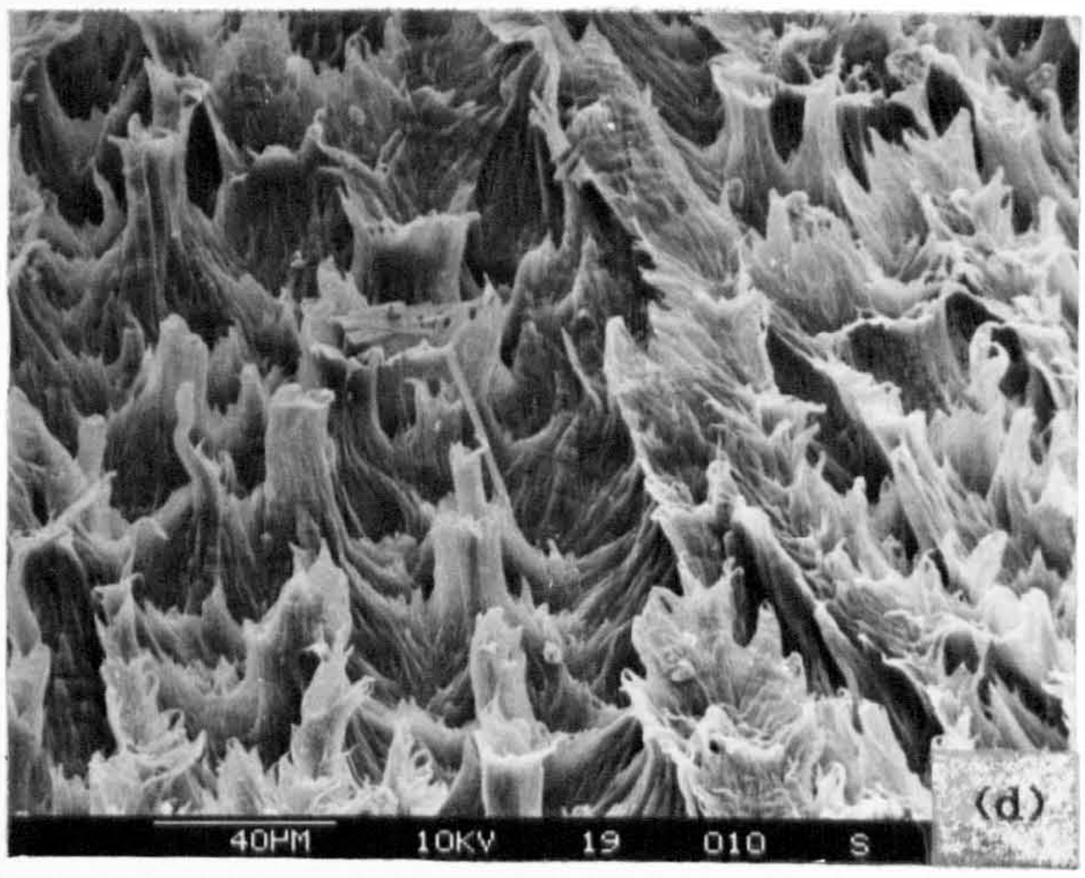

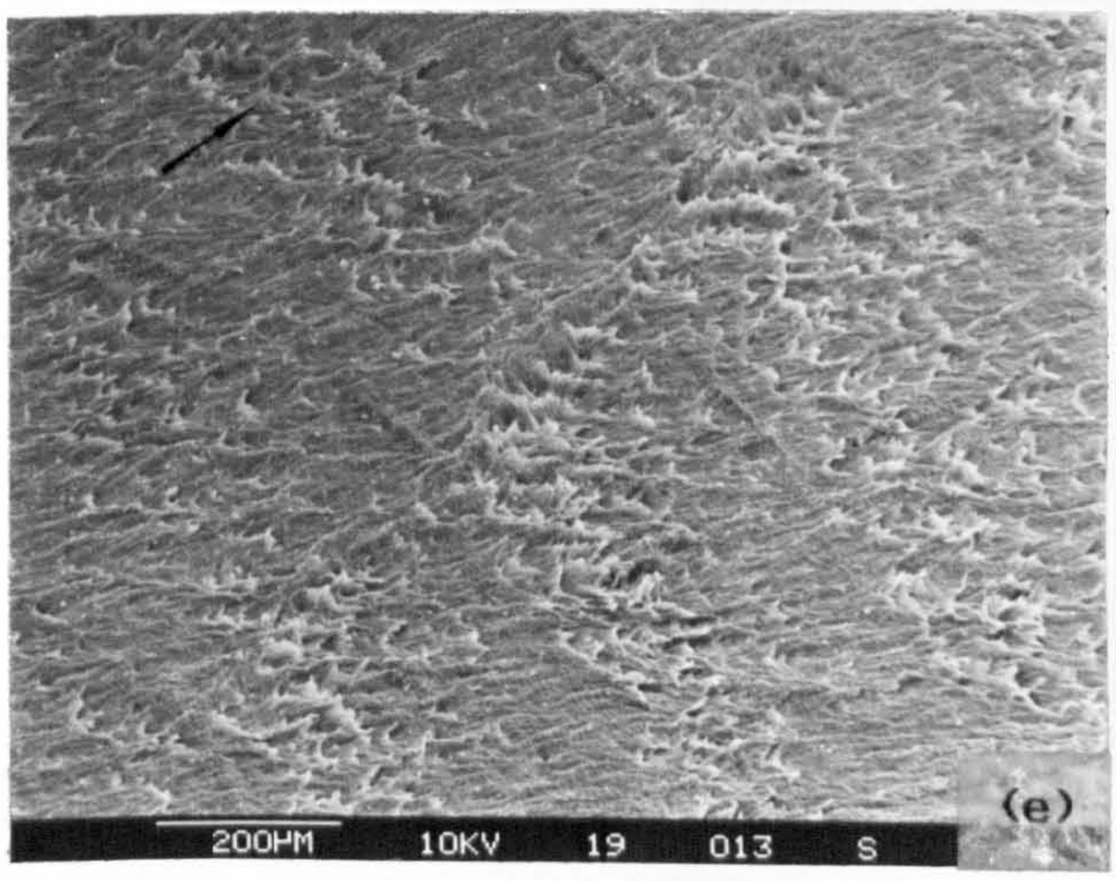

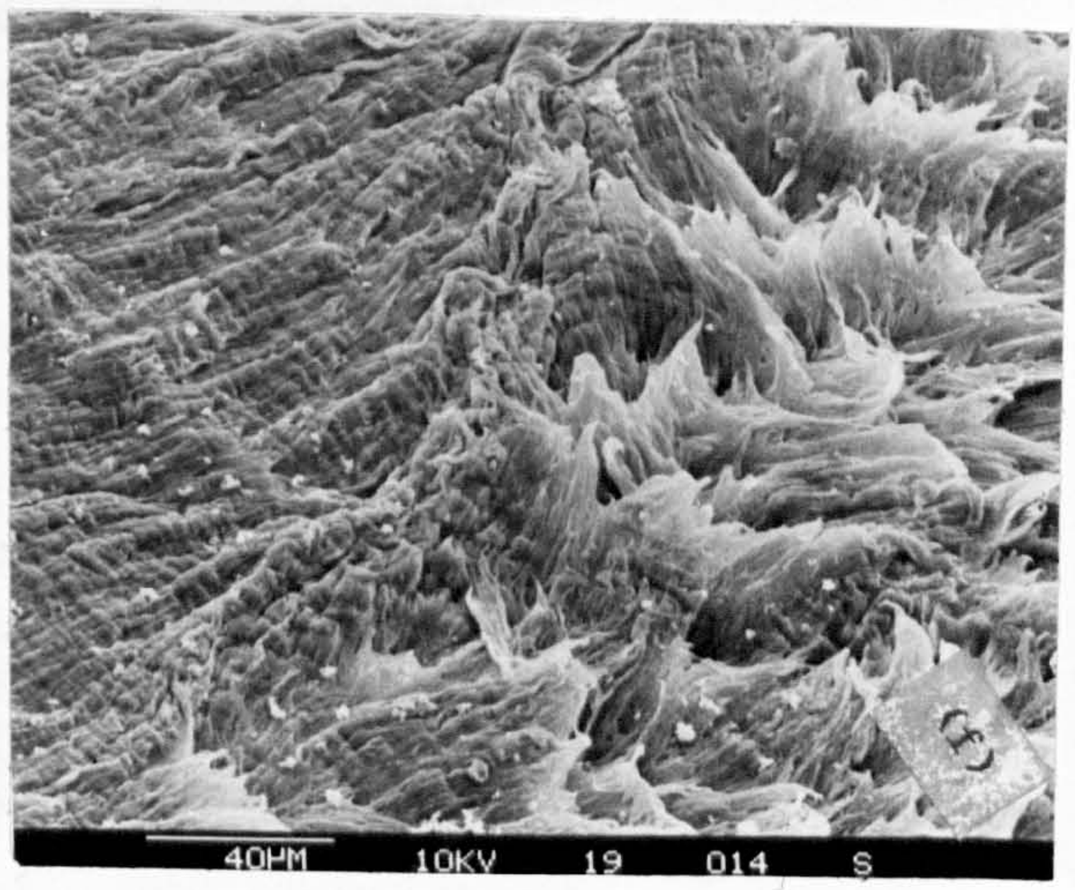

Fig. 5.24 SEM micrographs of fracture surface of axial butt weld failure; (a) and (b) low and high magnification micrographs respectively of initiation site, (c) and (d) low and high magnification micrographs respectively of MFZ at mid-wall and (e) and (f) low and high magnification micrographs respectively of the final stages to rupture.

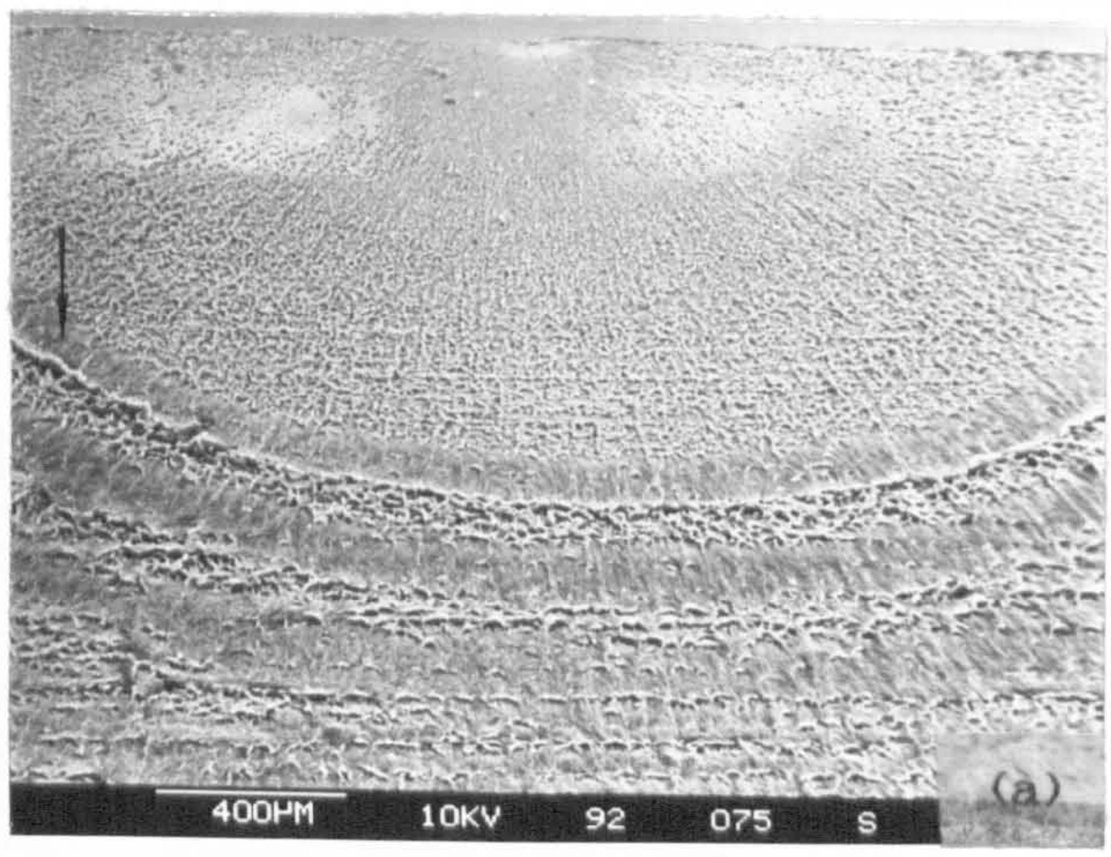

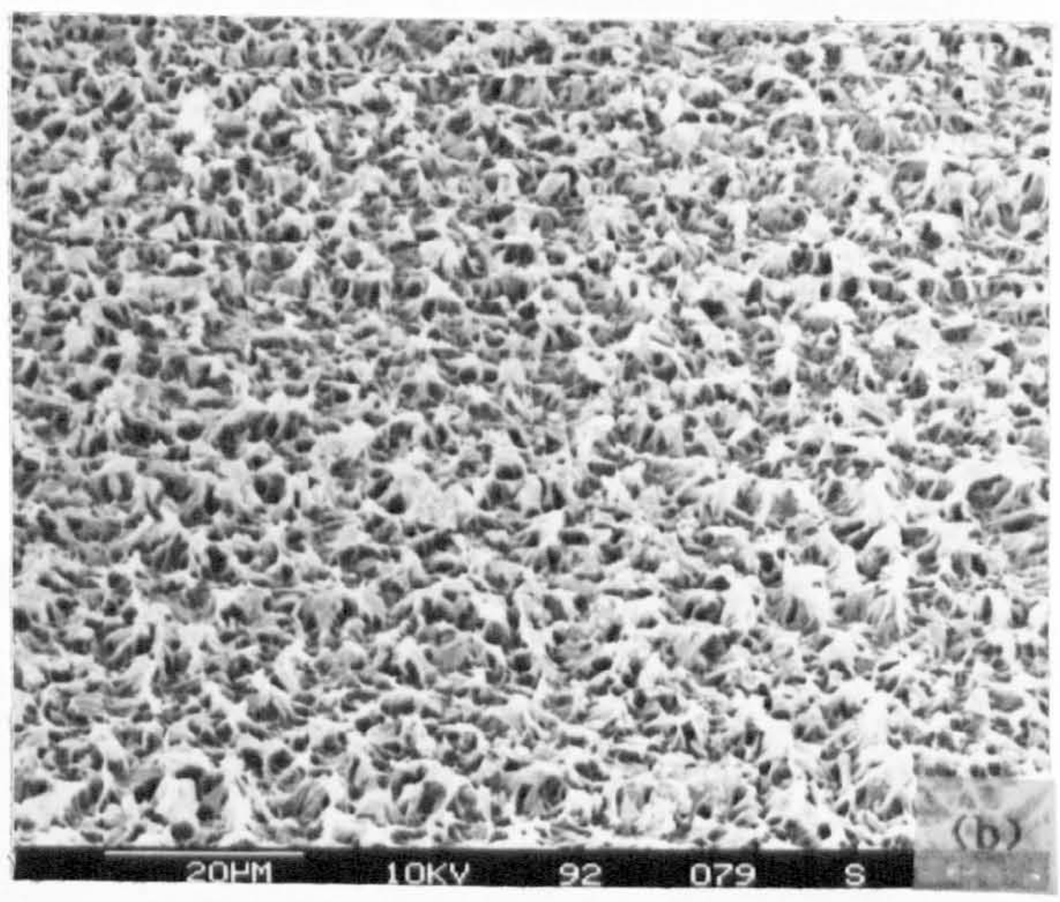

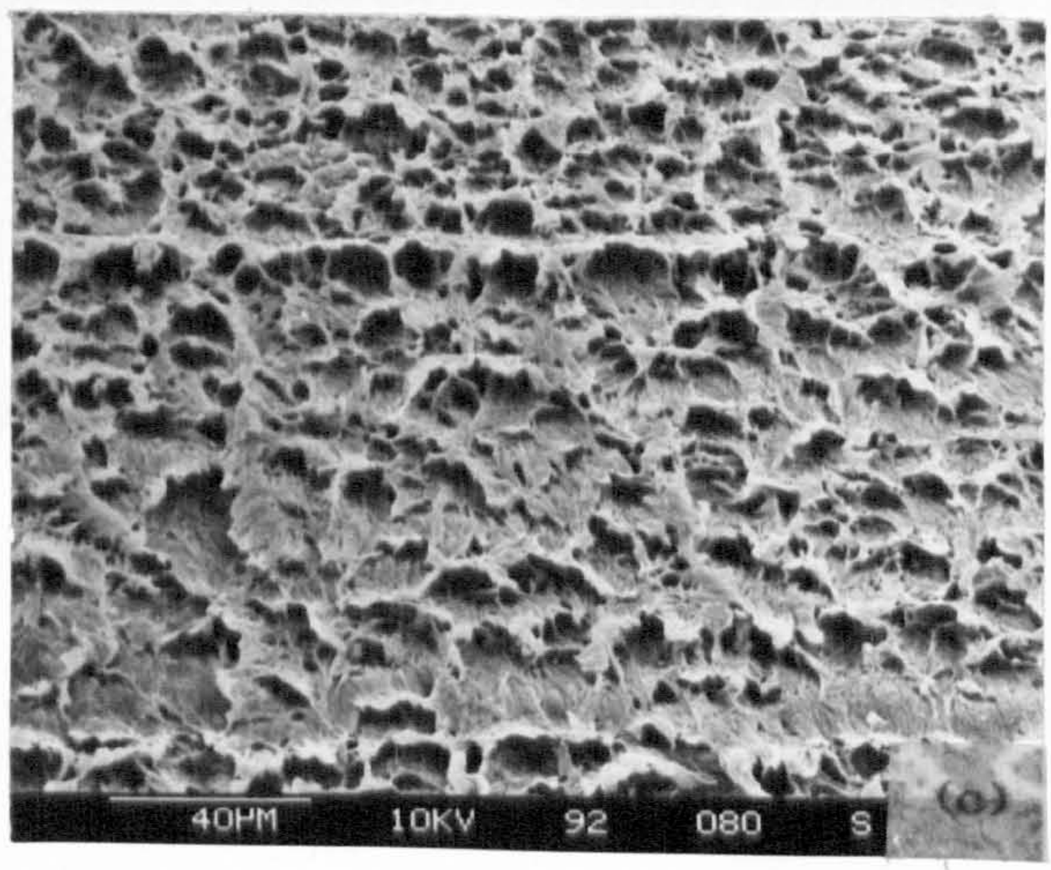

Fig. 5.25 SEM micrographs of fracture surface of pipe failure tested at ΔP=9.5 bar; (a) low magnification and high magnification region of (b) initiation site and (c) intermediate distance from initiation site and mid-wall.

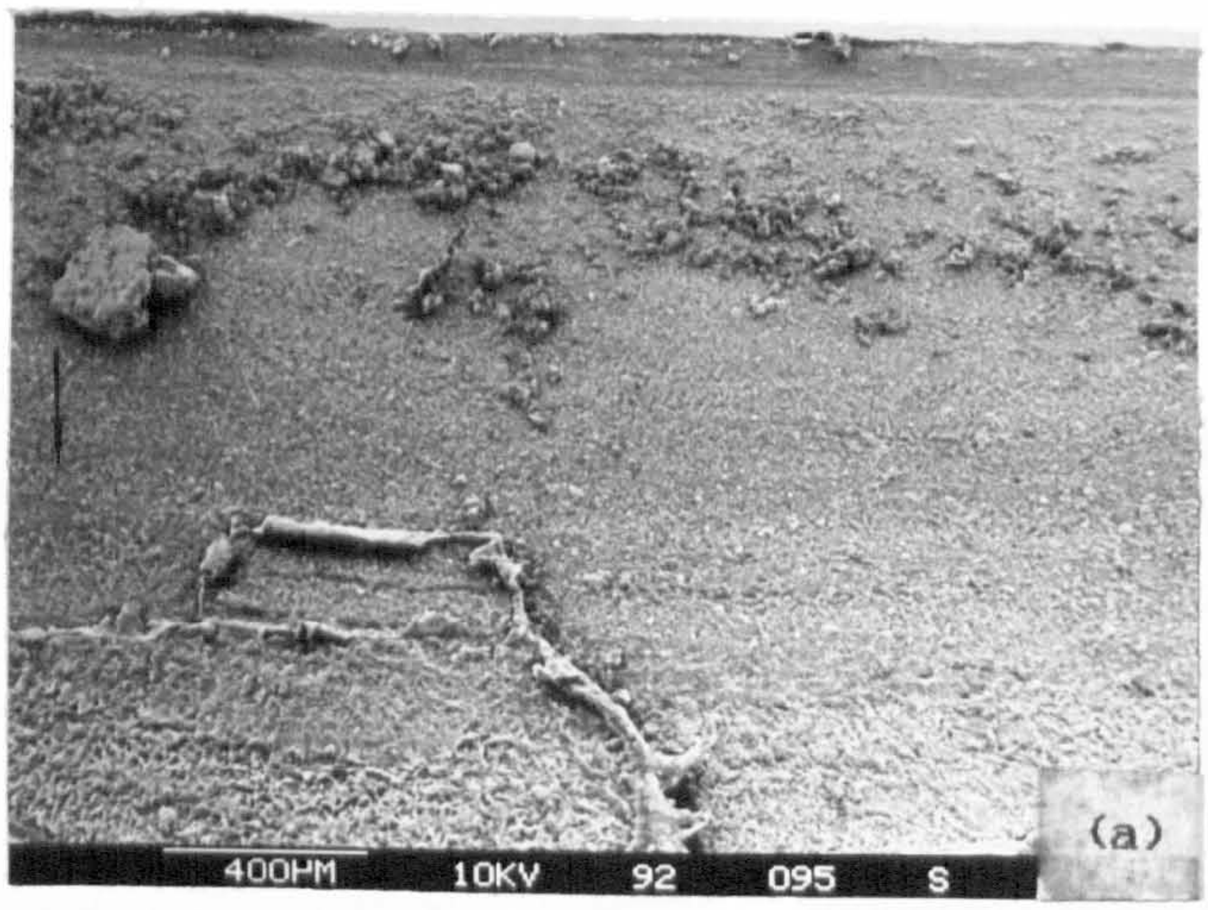

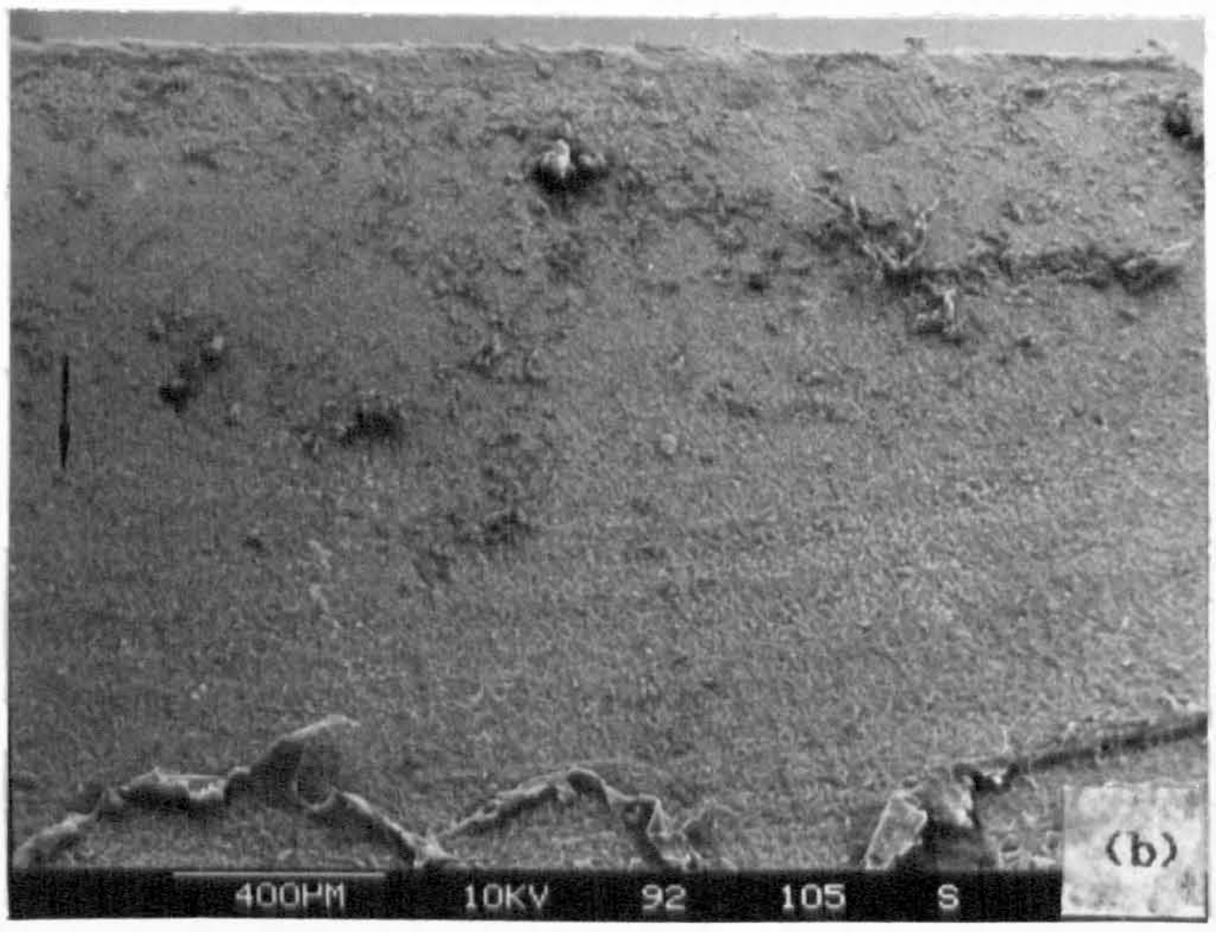

Fig. 5.26 SEM micrographs of fracture surface of pipe failure tested under constant pressure of 9.5 bar.

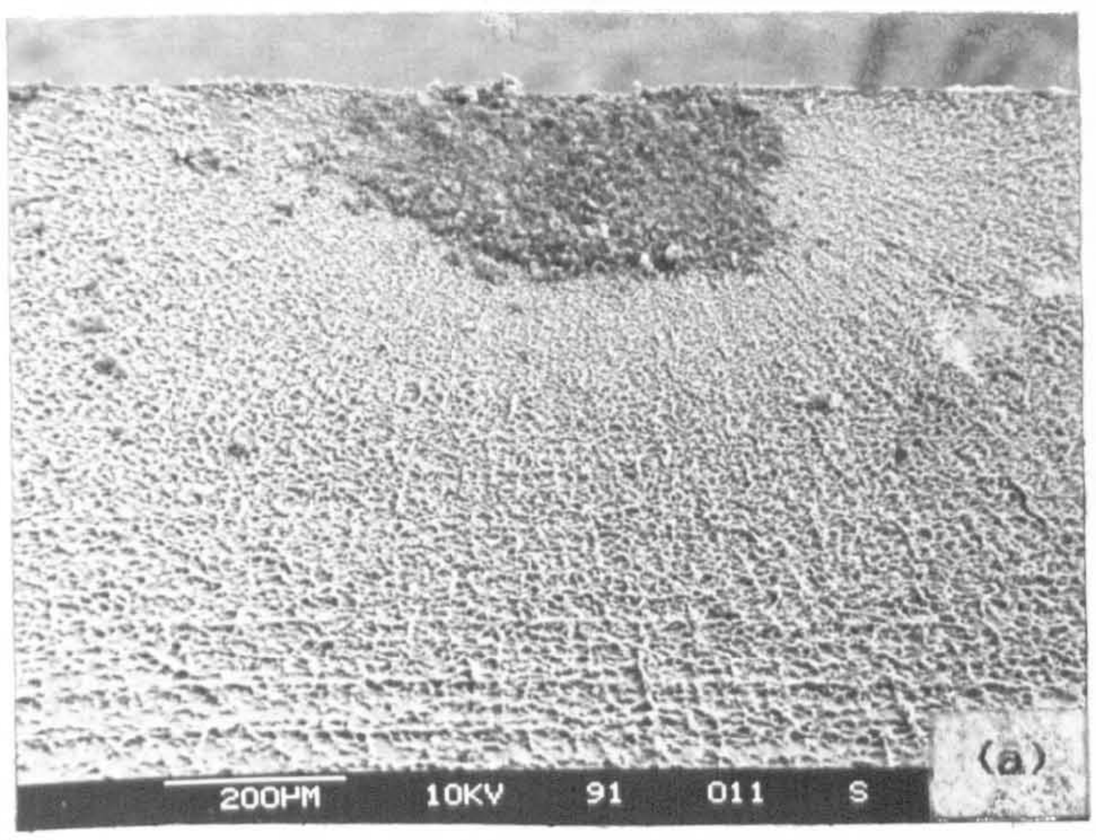

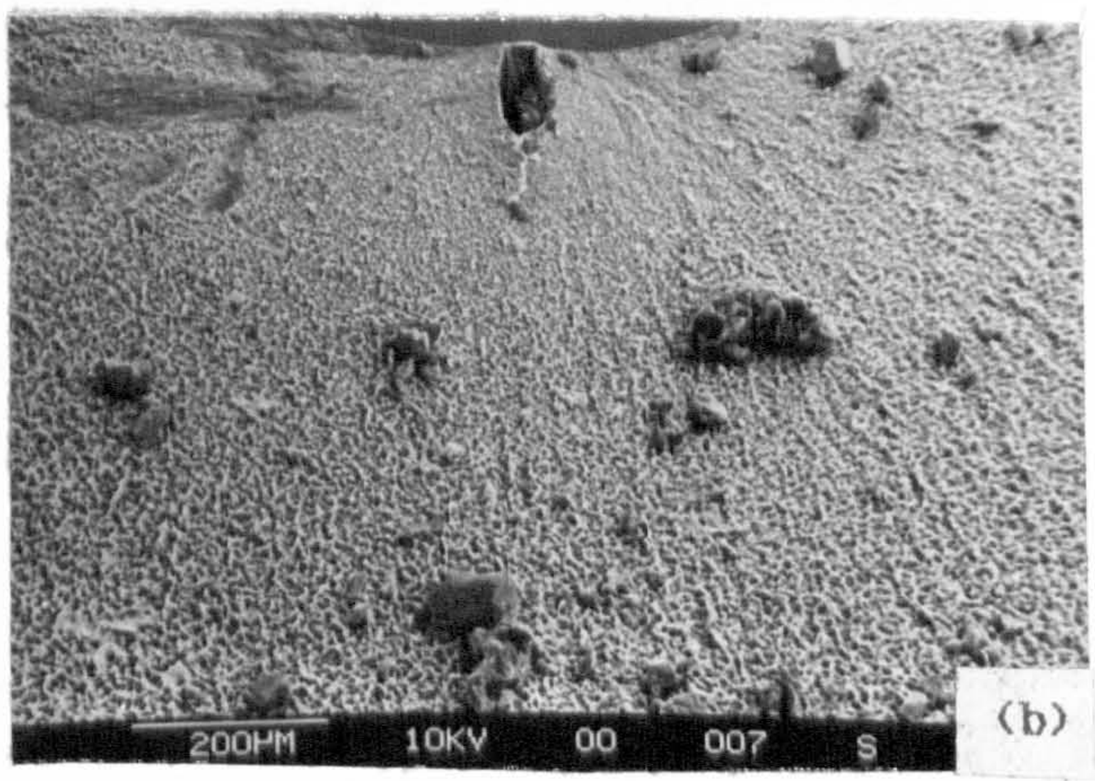

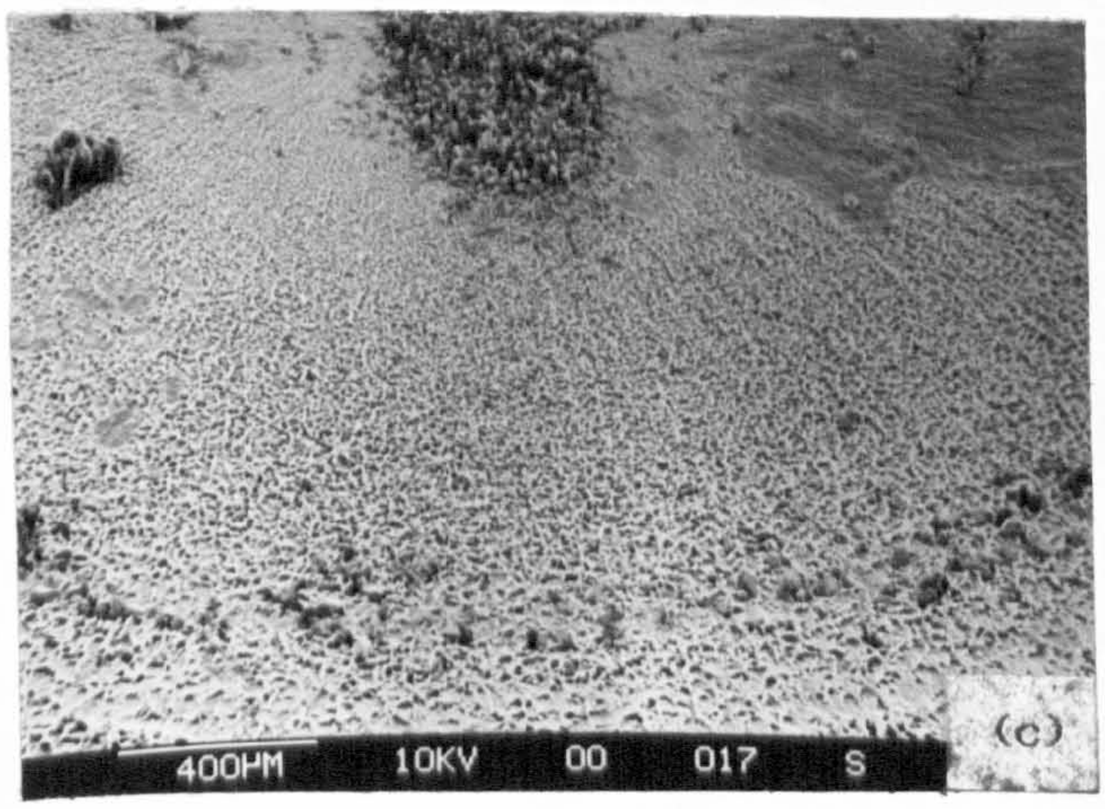

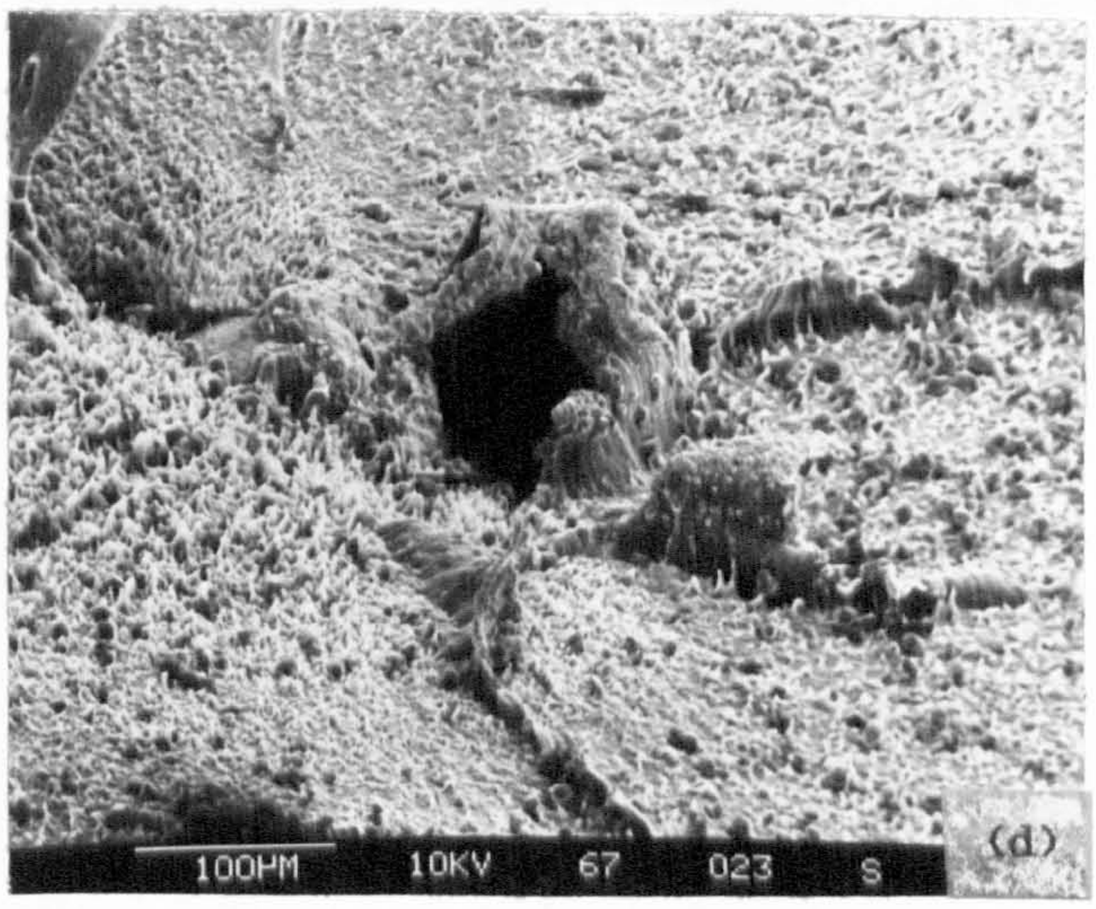

Fig. 5.27 SEM micrographs showing initiating particles (a) and (b) in 63mm; (c) and (d) in 90mm pipe failures.

5.4.0 Discussion: Failure Examination

5.4.1 Crack Initiation And Propagation Path Studies Of Circumferential Butt Weld Failures

The fracture plane of all the misaligned butt weld failures in three pipe sizes under fatigue and stress-rupture was circumferential, the failure occuring locally in the weld where the misalignment was introduced. Figure 5.2 shows schematically the three types of crack propagation path in relation to the MFZ which were observed in the circumferential butt weld failures, whilst figures 5.3 to 5.7 show the low magnification optical photographs of the etched surfaces of variously misaligned butt weld failure sections showing these different types of failure.

It is clear from figure 5.3 to 5.7 that the crack invariably initiated from the notch existing between the pipe bore and the weld bead. It appears that the crack propagation has then proceeded insensitive to the MFZ and no preferred path relative to the MFZ is taken. The crack does not propagate along the boundary between MFZ and the surrounding material which is perfectly illustrated by the type I and II crack propagation paths.

In the aligned butt weld case, the circumferential failure was observed mainly in 63mm pipe systems. The probability of circumferential failures of an aligned butt weld was found to decrease with increasing pipe diameter. This may be due to the fact that the initial circumferential crack growth rate in 90 and 125mm pipe systems may be different. It was noted that the rate of pressurisation of the pipe systems was decreasing with the increase in pipe outside diameter (see table 3.9) thus it is possible that the response of the notch may be slower. The additional factor which may well have hindered the initial circumferential growth is that the bead height to wall thickness ratio (bead size) was decreasing with increasing pipe outside diameter (see table 4.7) Since a notch is present between the

bead and the pipe surface, the weld bead rather than reinforcing could be acting as a constraint in that region. Thus a large bead as found in 63mm pipe systems may well present constraint and hence is conducive to initial crack growth, whereas a small bead in 90 and 125mm pipe systems creates much less of a constraint and hence inhibiting the initial crack growth. Note also the notch tip in a 125mm butt weld was not as sharp as in the 63 and 90mm butt weld. This will also influence the initial crack growth.

It is believed that the circumferential failure can result from lack of fusion as a result of poor welding (73) and also from the change in the microstructure around the welded region (41-44). However, such hypotheses are not applicable here. The evidence for the circumferential butt weld failures to initiate from the notch is overwhelming; firstly, the crack propagation study showed the crack to initiate between the bead and pipe bore, secondly, the circumferential crack growth taking place from the notch was clearly discernible in the axial butt weld failure fracture surfaces - see figure 5.16, thirdly, it was proved conclusively that the notch was responsible for the observed circumferential failure of the aligned butt welds in 63mm pipes in the these butt welds where the internal weld bead was machined off. The failure site for the internal weld bead machined off sample was remote from the weld. The lifetime of the sample with the internal weld bead removed was three times the standard aligned butt weld - see table 5.2.

Circumferential failure of butt welds under stress-rupture conditions have been observed by Diedrich and Gaube (49) and Kashkovskay and Kaigarodov (56) in 100 and 150mm HDPE pipes, while Barker (82) found both the axial and circumferential failure of butt welds in 60 and 63mm HDPE pipes. Diedrich and Gaube have correctly differentiated the two types of failure at the butt fusion weld; circumferential failure as a result of insufficient melt penetration and circumferential failure due to

,

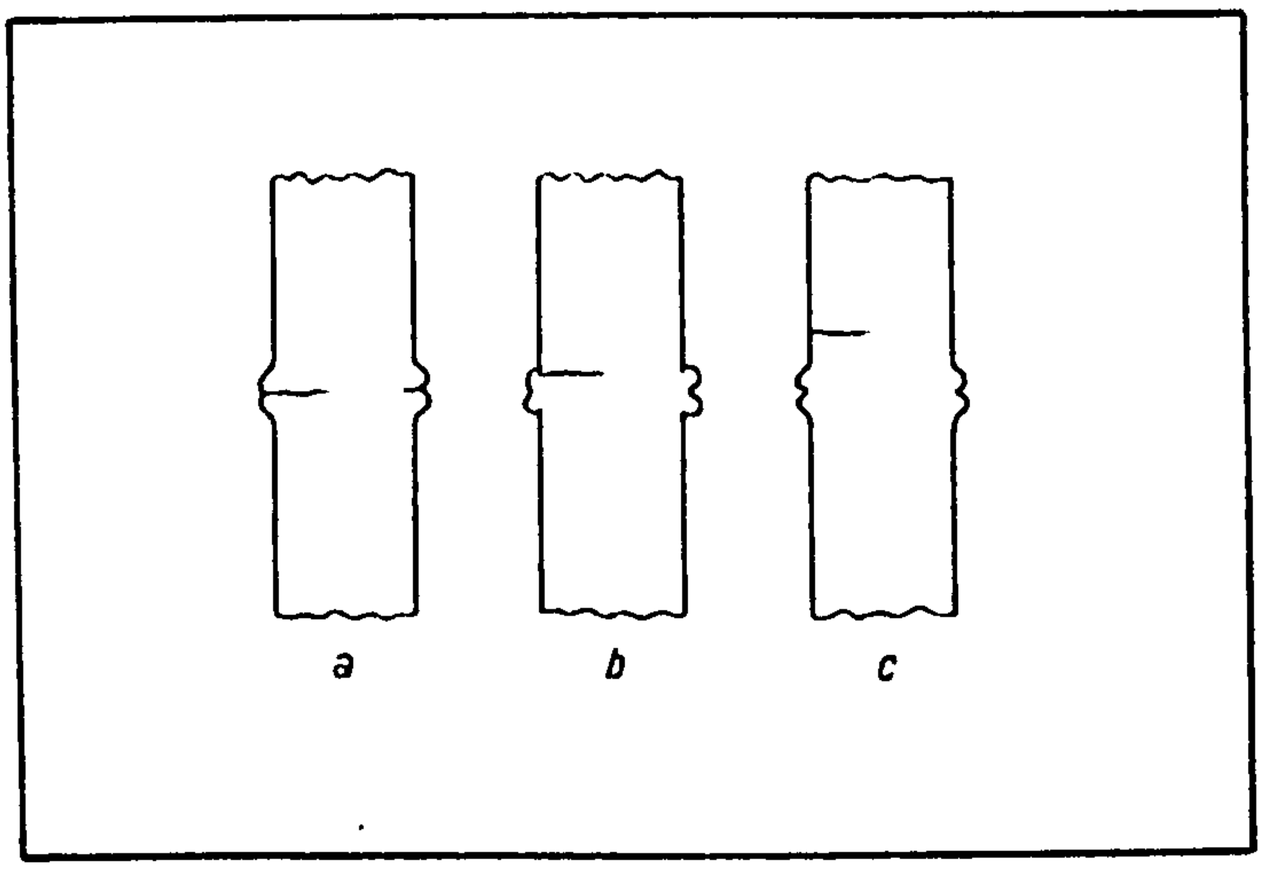

Fig. 5.28 Creep rupture cracks in pressure butt welds with heated tool; (a) cracks on the welding surface, (b) crack starting from notch and (c) crack in the base material.

a notch effect at the weld bead, the location of initiation in both cases is different - see figure 5.28

The geometry of butt welds in both the aligned and misaligned cases is such that it suggests the notch between the weld bead and pipe bore opens initially in response to triaxial stress condition; the hoop, axial and radial components of stress in the pipe. It then changes the orientation and is propagating in response mainly to the axial stress. The notches which are present inherently in the butt weld appear to be somewhat dormant in the aligned butt weld especially in 90 and 125mm pipe systems, whereas in the misaligned butt weld the notch is made active.

It is concluded that if there are any weakness in the aligned butt weld, it is not due to the microstructure of the butt weld but due to the notches which are inherently present in the butt fusion weld. In the misaligned butt weld, the situation is exacerbated by the displacement of the notch into the pipe wall.

5.4.2 Fractography: Macrofeatures

Figures 5.10 to 5.12 and 5.13 and 5.14 show the fracture surface of circumferential butt weld failures under fatigue and stress-rupture respectively. The overall macrofeatures of the brittle fracture were related to the magnitude of misalignment and imposed loading mode. Stress-rupture testing produced fracture surfaces which showed relatively more macro ductility towards the outside region of the fracture surface compared to fatigue failure. Fracture surfaces of axial butt weld and pipe failures are shown in figure 5.16 and figures 5.17 to 5.19 respectively. The main features observed for pipe failures were similar to those observed in the circumferential failure at the weld; the evidence of slow stable crack growth and discontinuous growth bands. The common features observed for both circumferential butt weld failures and pipe failures are discussed below.

Under both modes of testing, failure resulted from slow stable as opposed to fast unstable crack growth. The fracture surfaces of most of the failures under both stress-rupture and fatigue exhibited whitening and relatively smooth surfaces which progressively had a more fibrous texture towards the final rupture region. Whitening of the surface is caused by the microvoids which appear white as the result of light scattering, since they are well below the limit of visual resolution. Under fast unstable crack propagation, fracture surfaces tend to be smooth showing little evidence of any energy absorption process taking place. This was generally absent in most of the fracture surfaces.

The bands on the fracture surface were observed for both the fatigue and stress-rupture failures, which seem to indicate that the mechanism operating under these two conditions is similar. The bands are too large to be caused by incremental extension of the crack during one loading cycle. Instead, they probably correspond to discontinuous crack advance following several hundred loading cycles during which the crack tip remains stationary as described in section 2.3.8. The fatigue fracture sequence that produces the marking together with the model of discontinuous crack propagation mechanism is shown in figure 2.15 after reference (149) and (151). In principle such a model is equally applicable here to describe the formation of the discontinuous growth bands. In the model proposed by Skibo et al (149, 151), the damaged zone ahead of the crack is a single or a few crazes at most developing continuously; however, it is characterised by a decreasing rate with increasing length. When the craze reaches a critical length, the crack advances abruptly across the entire craze and then arrests, with further cycling developing a new craze and the process is repeated. A similar mechanism has also been proposed by De Charentenary et al (192) for HDPE, where it is proposed that the dicontinuous growth bands on the fracture surfaces are formed by the mechanism of large scale void formation in the plastic zone at the crack tip.

The number of bands and spacing between the bands observed on the fracture surface can be related to the stress intensity factor. Several authors (155-190) have used the Dugdale plastic - zone model to describe the craze ahead of the fatigue crack tip and Skibo et al (186) determined the craze length, Rc by measuring the band spacing and deduced the craze surface stress σ_{cs} using equation:

$$Rc = \frac{K_{Ic}^2}{8\pi\sigma_{cs}^2} \qquad (2.35)$$

taking $K_{Ic} = K_{Imax}$ in equation 2.35 can be used then to describe the spacing between the bands. If Rc is regarded as spacing between the bands, then equation 2.35 imply that spacing is proportional to K_{Imax}^2, the spacing will increase with increasing K_{Imax} and hence the number of bands should decrease with the increasing K_{Imax}. This seems to explain the two main observations;

(i) for a given pressure range, the number of bands was found to decrease with increasing misalignment implying the effect of increasing misalignment was to increase the K_{Imax} and

(ii) for a given misaligned butt weld the number of bands increased with decreases in the pressure range, that is K_{Imax} was reduced, therefore spacing between the bands decreases and a greater number were observed. Since the number of bands observed is a function of the pressure range, the fracture surfaces of failed polyethylene pipes could lead to an indentification of the stress level which caused fracture.

The observation that the discontinuous growth bands were not observed in the first 1-2mm from the intiation site could represent the different fracture mode to be in operation in the initial stages. Initially the crack may have opened to the plain strain condition which is made to go through the transition to the plain stress condition by the final progress

of the crack. The change in fracture mode in the final progress of the crack, from stable crack growth exhibiting only localised drawing and fibrillation to one of tearing and macroductility can possibly be a result of the increase in stress at the crack tip with increasing crack depth. At some point the yield stress of the material at the testing temperature is exceeded and the remaining ligament of material fails by yielding and subsequent drawing.

It is not clear as to the absence of discontinous growth bands in butt weld failures of 125mm pipe systems and also axial butt weld failures. It could be that under certain orientations, the stress may induce continuous crack growth. De Charentenary (192) found that a high molecular weight sample (Mw=200,000) of HDPE exhibited a discontinuous propagating mechanism by the presence of several arrest lines whereas low molecular weight HDPE material with Mw not not exceeding 72,000 did not produce a surface with discontinuous growth bands but a continuous propagating mechanism which exhibited extensive microductility. However, since 125mm pipes were of the same grade of MDPE as 63 and 90mm it is assumed to have similar Mw and the lack of discontinuous growth bands may be due to some unknown factor/s.

5.4.3 Fractography: Microfeatures

Figures 5.19 to 5.21 display the variation in microfeatures across the surface for different misaligned butt weld failures under fatigue at two pressure ranges. Figure 5.22 and 5.23 show the micromorphology of fracture surfaces of butt weld failures under stress-rupture loading, whilst figure 5.24 and 5.25 portray the detail seen at high magnification for axial butt weld and pipe failures respectively. The common features observed in all these brittle failures at high magnification are the variations in the microvoid size and micronecking across the fracture surface. For example, in the case of a 9% misaligned butt weld failure, at the initiation site there is little micronecking and microvoids are in the range 1-3μm whereas at

the mid-wall micronecking is clearly apparent and microvoids have increased to 10-20μm.

The observations made in figures 5.19 to 5.25 suggests that the failure micromechanism, which is highly localised and confined to small volumes of material involves:

(i) void nucleation or cavitation,

(ii) growth of the microvoids and fibrillation,

(iii) breakdown or failure of fibrils by micronecking.

These are all the characteristics of crazing. The micromechanism probably entails the initiation of craze/s at the stress concentration (notches in the case of circumferential butt weld failure, surface defects or inclusions or inhomogeneities in the case of axial butt weld and pipe failures) and then entering a period of slow stable growth evidenced by void formation and fibrillation which eventually lad to the breakdown of the final ligament which is unable to support the load. The region ahead of the crack tip will be crazed and process repeated. Initial conditions at the initiation region are predominantly plane strain, and therefore in favour of craze initiation. As the crack approaches the outer surface of the weld or pipe plane stress conditions probably become more important and the fibrillation is lost in some gross yielding and ductility.

There appears to be no evidence for fast crack growth in the final stages of propagation possibly because of the elevated test temperature but also the material fracture toughness may increase to such an extent that yielding becomes the only possible rupture mode. Alternatively, the fast fracture condition may not be realised at the nominal stress level examined, that is the crack length is below the critical crack length for the fast fracture predicament.

Although the observed failure is brittle, craze initiation, growth and breakdown does involve local energy absorption. Since the microductility was evident on the fracture surface, the failure perhaps would be classed more appropriately as quasi-brittle (28). Quasi - brittle mode of fracture has been shown (28) to occur under plane strain conditions in the interior of pipe walls at reduced stresses (below the 'knee' or the stress-rupture curve) and at lower temperatures.

5.4.4 Origin Of Crack Initiating Particles In Pipe Failures.

The size of particles and the type of particles as determined by the elemental analysis which were rresponsible for the pipe failures in 63 and 90mm pipe systems are provided in the table 5.4. In the majority of the cases the initiating particle was Calcium rich and in one case Iron was detected.

Calcium rich particles are most likely to be polymer lubricants which are added to HDPE during processing to improve melt flow properties. When analysing Calcium based particle care was taken to distinguish between an actual inclusion within the pipe material and Calcium Carbonate particles which may have been deposited on the fracture surface near the initiation site, by the water used for testing the pipes. The Iron inclusion found in one case could have originated from the wear of processing equipment or from accidental contamination of the polymer feedstock or may have been present within the polymer granules from the outset.

The initiation particles which failed to produce elemental traces are considered to be Carboniferous in nature. Such material may be unplasticised or degraded polymer, particles or agglomerated pigment or filler or perhaps other forms of organic matter. Note the analysis equipment was unable to detect elements with atomic numbers of sixteen or less.

CHAPTER 6.0 - INFLUENCE OF ELEVATED TESTING TEMPERATURE ON THE MATERIAL'S PROPERTIES

6.0 Introduction

A limited study into the physical and chemical ageing of the pipe material was carried out to identify the effect of elevated temperature testing (79°C) on the structure and hence its influence on the fatigue and stress-rupture performance of butt fusion welded pipe. Two series of tests were undertaken; in the first the specimens were obtained from the surface, centre and bore at the butt weld (MFZ) and 15-20mm away from it (see section 3.1.1 and figure 3.1) of samples subjected to pressure testing times of 200, 2000, and 8000 hours at 79°C. In the second series, the specimens were obtained from the same location as before but from butt welded pipe samples filled with water which were simply left in the water tank at 79°C for the times of 200, 2000, 8000 hours. In the latter case, the sample was not subjected to any stress and it is referred to as a control sample.

The density, DSC, Oxidation Induction Time (OIT), Gel Permeation Chromatography and Infrared, (IR) Specroscopy determination were carried out on the samples described above. The number of specimens used in each of the determinations was three except for DSC and OIT measurements where it was five. The mean values have been tabulated and since the variation in the values was minor, standard deviations are omitted from the table. However, the observed minimum and maximum variation are stated. This study was executed on the 63mm SDR11 Rigidex 002-50 MDPE pipe only.

6.1 Density

Densities of the specimen taken from the locations at the butt fusion weld (MFZ) and 15-20mm away from it through the pipe wall

thickness as a function of time at 79°C are shown in the table 6.1. The following points emerge from the density measurements.:-

(i) As expected the initial density of the untested samples (000 hours) taken 15-20mm away from the butt weld increases from the surface at 937.7 kgm^{-3} through to the bore of the pipe wall at 943.8 kgm^{-3}. This is because the external surface of the pipe was cooled rapidly and the internal surface was cooled slowly during the extrusion of the pipe.

(ii) The density at the butt weld (944.5 kgm^{-3} for 000 hours) was found to be constant through the wall thickness but greater compared to the specimens taken 15-20mm away from it.

(iii) While the above mentioned trends (i,ii) are maintained at all the ageing times, the density of both the control and the sample subjected to pressure testing at 79°C increases faintly with time for the specimens taken at 15-20mm away from the butt weld. The increase in the density after 8000 hours is less than 0.5% of the original value.

6.2 DSC Thermograms

Figures 6.1 and 6.2 display the typical DSC thermograms of the control and pressure tested samples respectively. DSC thermograms of both the control and pressure tested samples at all the ageing times tend to have a small 'hump' at base before the melting peak compared to DSC thermogram of untested sample (000 hours). DSC thermograms of the specimens taken 15-20mm away from the weld were observed to have sharp peaks whereas for the specimens obtained at butt weld/MFZ peaks were slightly broader. The peak melting point and percentage crystallinity were recorded from the DSC thermograms.

Table 6.2 provides the detected change in percentage crystallinity as a function of time for the control and pressure

tested butt welded pipes aged at 79°C. If confirms the trends noted from the density measurement;

(i) Initial percentage crystallinity of the untested samples (000 hours) acquired 15-20mm away from MFZ increases from 42 at the surface to 45 at the bore. However, the percentage crystallinity at the centre and bore was found to be similar.

(ii) Percentage crystallinity at the MFZ (47 for 000 hours) was observed to be constant through the wall thickness but greater compared to the specimens taken at 15-20mm away from it.

(iii) The above trends (i,ii) were maintained with the ageing time, but percentage crystallinity increases with time. An increase of 10% for control and of 17% for pressure tested sample on the original value (at 000 hours) was recorded, a noticeable increase in crystallinity compared to increase in the density.

Table 6.3 gives the peak melting temperature results. Again, similar observations to those mentioned above are apparent at 000 hours. However, the peak melting temperature was not seen to increase with time; it was approximately constant. Note that only one peak in the melting was observed.

Density and DSC thermograms seem to indicate annealing of the pipe material might be taking place at a slow rate which stabilises between 200 and 2000 hours. Increases in crystallinity may have a small effect on the slow crack propagation rate especially those pipes tested at ΔP=6.5 bar.

6.3 Oxidation Induction Time

Table 6.4 contains the OIT of the specimens taken at the MFZ and at a distance between 15-20mm away from the MFZ. Data includes both the control and pressure tested 63mm pipe aged at 79°C. The following remarks can be made on the OIT results:-

(i) For the unaged samples (000 hours), the OIT is more or less constant at about 20 minutes through the wall thickness at the MFZ and 15-20mm away from the MFZ. This indicates that the stabilising system is not significantly used up at MFZ even though it has been subjected to a temperature of 200°C during welding.

(ii) For the control pipe samples, the OIT decreases more rapidly for specimens taken from the surface and bore of the pipe for both the locations; at the MFZ and 15-10mm away from MFZ compared to the core region - see figure 6.3. OIT decreases from an initial value of 20 minutes to about 3 minutes for the surface and bore layer of an 8000 hours aged control pipe samples, while the specimens from the core region decreases to 8 minutes for the same ageing period.

(iii) For the pressure tested pipe samples, the same trend as in the control samples is observed except that the reduction in OIT seems to have been accelerated. The OIT were reduced to only 3 minutes after pressure testing of 2000 hours for the surface and bore layers. While the OIT of the core specimens reduced to 12 minutes for pressure tested samples. This compares to 18 minutes for the control pipe samples.

(iv) The Oxidation Induction Time study shows that the stabilising system is either leached out or used up when samples are aged/tested at 79°C.

6.4 Gel Permeation Chromatography

Table 6.5 gives the number average molecular weight, weight average molecular weight and the Dispersion Ratio of the controlled and tested samples at 79°C.

The results show that there is no significant change in the number average molecular weight or the weight average molecular weight with the time up to 8000 hours. It suggests that there

is no major breakdown of the molecules with time at 79°C for ageing times up to 8000 hours.

6.5 Infrared Spectroscopy

Infrared, (IR) Spectra of the thin layer (4μm thick) removed from the weld bead of untested and the sample subjected to pressure testing of 8000 hours were determined in order to detect the presence of carbonyl groups and hence any degradation of the material. Figure 6.4(a) and (b) are the representative IR spectrum; there was no evidence of any presence of carbonyl group, as the absorption peak at 1700cm^{-1}. which is characteristic of the carbonyl group, was not observed.

IR spectroscopy of the thin layer removed from the surface of the pipe and the bore remote from the butt welded pipe subjected to pressure testing of 8000 hours was also studied. Again, the carbonyl absorption peak was absent from the IR spectrum.

6.6 Fatigue Testing Of Aged Butt Welded Pipes

A limited number of 63mm SDR11 aligned butt welded pipes which were aged at 79°C for 200, 2000 and 8000 hours were fatigue tested with ΔP=9.5 bar at 79°C. Table 6.6 contains the lifetimes in terms of number of cycles to failure of these samples together with lifetimes of the aligned butt welds which were not aged. It shows that the performance of the aged samples tends to be at the upper limit of the unaged samples.

Although no failures were obtained for 2000 hours aged samples and only two samples were tested for ageing time of 8000 hours, it appears as if the ageing time up to 8000 hours does not seem to significantly alter the fatigue performance compared to the unaged sample.

Table 6.1 Density of samples taken from 63mm butt welded pipes in Rigidex 002-50 MDPE pipe as a function of time.

(a) Control Sample at 79°C.

Sample Location	Density, kgm^{-3}			
	Time, Hours.			
	000	200	2000	8000
MFZ Surface	944.9	946.7	947.2	948.0
MFZ Centre	944.8	946.4	946.8	947.6
MFZ Bore	944.5	946.2	946.9	948.1
15-20 Surface	937.7	940.6	941.7	943.1
15-20 Centre	942.9	944.9	945.7	946.0
15-20 Bore	943.8	945.4	946.4	947.4

(b) Sample Subjected to Pressure Testing at 79°C.

Sample Location	Density, kgm^{-3}			
	Time, Hours.			
	000	200	2000	8000
MFZ Surface	944.9	946.6	947.3	948.1
MFZ Centre	944.8	946.0	946.8	947.8
MFZ Bore	944.5	946.8	948.0	948.2
15-20 Surface	937.7	940.8	942.2	943.2
15-20 Centre	942.9	944.8	945.5	946.3
15-20 Bore	943.8	945.7	946.8	947.9

Minimum variation = .1, Maximum variation = .7

Table 6.2 Crystallinity of samples taken from 63mm butt welded pipes in 63mm Rigidex 002-50 MDPE pipe as a function of time.

(a) Control Sample at 79°C.

Sample Location	Crystallinity - % Time, Hours.			
	000	200	2000	8000
MFZ Surface	46.6	46.8	50.0	50.9
MFZ Centre	47.1	48.9	50.0	49.9
MFZ Bore	46.7	47.0	49.7	51.7
15-20 Surface	42.3	46.5	43.0	46.9
15-20 Centre	45.1	51.3	47.8	49.2
15-20 Bore	45.4	50.2	49.9	49.7

(b) Sample Subjected to Pressure Testing at 79°C.

Sample Location	Crystallinity - % Time, Hours.			
	000	200	2000	8000
MFZ Surface	46.6	48.9	48.2	53.9
MFZ Centre	47.1	48.9	50.5	54.5
MFZ Bore	46.7	49.9	47.2	54.8
15-20 Surface	42.3	45.7	44.0	49.5
15-20 Centre	45.1	48.2	52.2	53.7
15-20 Bore	45.4	46.7	50.3	52.9

Minimum variation < 1, Maximum variation = 3

Table 6.3 Peak melting temperature of samples taken from 63mm butt welded pipes in 63mm Rigidex 002-50 MDPE pipe as a function of time.

(a) Control Sample at 79°C.

Sample Location	Melting Peak Temperature - K			
	Time, Hours.			
	000	200	2000	8000
MFZ Surface	400.93	400.89	400.06	400.60
MFZ Centre	400.15	400.93	400.55	400.56
MFZ Bore	400.77	400.93	400.66	401.23
15-20 Surface	397.91	399.16	398.17	398.51
15-20 Centre	399.23	400.22	399.89	399.33
15-20 Bore	400.02	400.06	400.19	400.39

(b) Sample Subjected to Pressure Testing at 79°C.

Sample Location	Melting Peak Temperature - K			
	Time, Hours.			
	000	200	2000	8000
MFZ Surface	400.93	400.14	400.47	401.20
MFZ Centre	400.15	400.12	400.38	400.63
MFZ Bore	400.77	400.58	400.40	401.53
15-20 Surface	397.91	397.73	397.88	398.45
15-20 Centre	399.23	399.63	399.81	400.09
15-20 Bore	400.02	399.79	399.37	399.11

Minimum variation = .27, Maximum variation = .91

Table 6.4 Oxidation Induction Time of samples taken from 63mm butt welded pipes in 63mm Rigidex 002-50 MDPE pipe as a function of time.

(a) Control Sample at 79°C.

Sample Location	Oxidation Induction Time, Minutes				
	Time, Hours.				
	000	200	1000	2000	8000
MFZ Surface	19.5±3.0	15.2±3.0	10.5±0.5	6.8±2.5	2.7±0.2
MFZ Centre	20.8±1.4	25.4±2.8	24.3±0.4	18.1±1.3	8.3±0.8
MFZ Bore	20.1±2.8	16.2±2.3	12.3±0.4	7.0±0.9	5.0±0.3
15-20 Surface	21.2±2.0	12.9±0.6	-	6.2±0.6	3.5±0.7
15-20 Centre	25.0±1.8	24.1±1.2	-	16.5±1.5	6.7±0.8
15-20 Bore	20.7±3.0	17.3±1.6	-	10.5±0.5	6.4±0.7

(b) Sample Subjected to Pressure Testing at 79°C.

Sample Location	Oxidation Induction Time, Minutes				
	Time, Hours.				
	000	200	1000	2000	8000
MFZ Surface	19.5±3.0	16.0±1.3	7.5±1.4	3.0±0.7	1.8±0.6
MFZ Centre	20.8±1.4	25.0±2.2	15.8±3.2	12.0±2.2	3.3±0.4
MFZ Bore	20.1±2.8	15.3±3.5	3.2±1.8	2.2±0.4	0.8±0.8
15-20 Surface	21.2±2.0	13.7±2.4	-	3.7±0.9	0.9±0.2
15-20 Centre	25.0±1.8	26.0±0.9	-	9.7±2.2	3.4±0.8
15-20 Bore	20.7±3.0	14.3±0.3	-	3.8±2.0	0.6±0.1

Table 6.5 Number and Weight Average Molecular Weight of samples taken from 63mm butt welded pipe in 63mm Rigidex 002-50 MDPE pipe as a function of time.

Molecular Weight	Control Sample at 79°C			Sample Subjected to Testing at 79°C		
	Time, hrs			Time, hrs		
	000	200	2000	200	2000	8000
Mn x 10^4	1.82	1.24	1.25	1.32	1.23	1.25
Mw x 10^4	15.70	16.00	16.20	15.40	15.30	15.10
Mw/Mn	8.63	12.90	12.96	11.67	12.44	12.08

Table 6.6 Fatigue performance of butt welds in 63mm SDR11 Rigidex 002-50 MDPE pipe of various ageing times.

Number Of Cycles To Failure			
Ageing Time, hrs			
000	200	2000	8000
58,290	74,340	>120,000	130,410(A)
60,150	134,670	>120,000	133,890
63,300(A)	194,430	>120,000	
73,620			
81,570			
96,090			
132,060			
169,260			

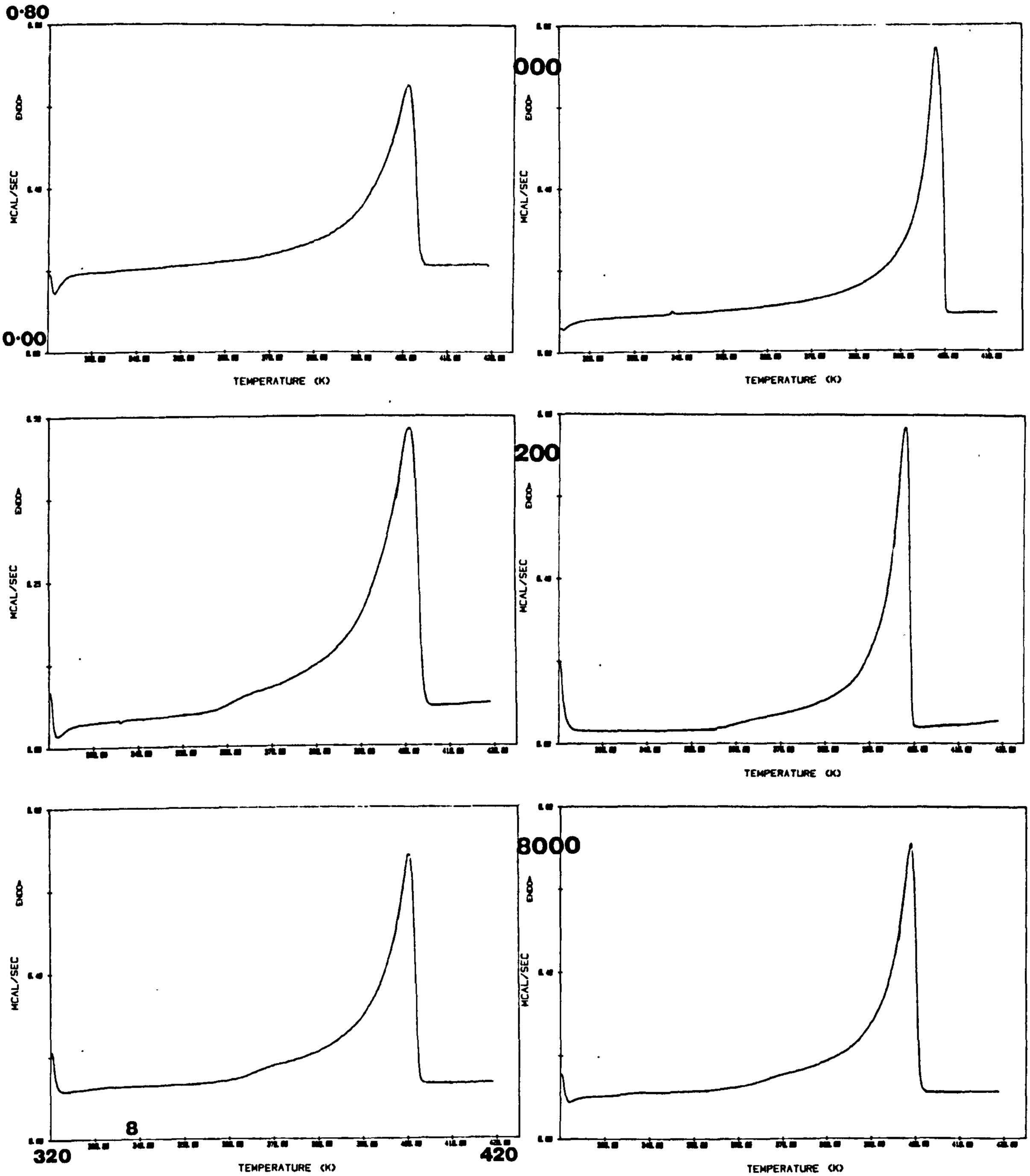

Fig. 6.1 DSC thermograms of surface specimen taken from the butt weld (MFZ) and 15-20mm away from it of the control butt welded MDPE pipe samples aged for 000, 200 and 8000 hours.

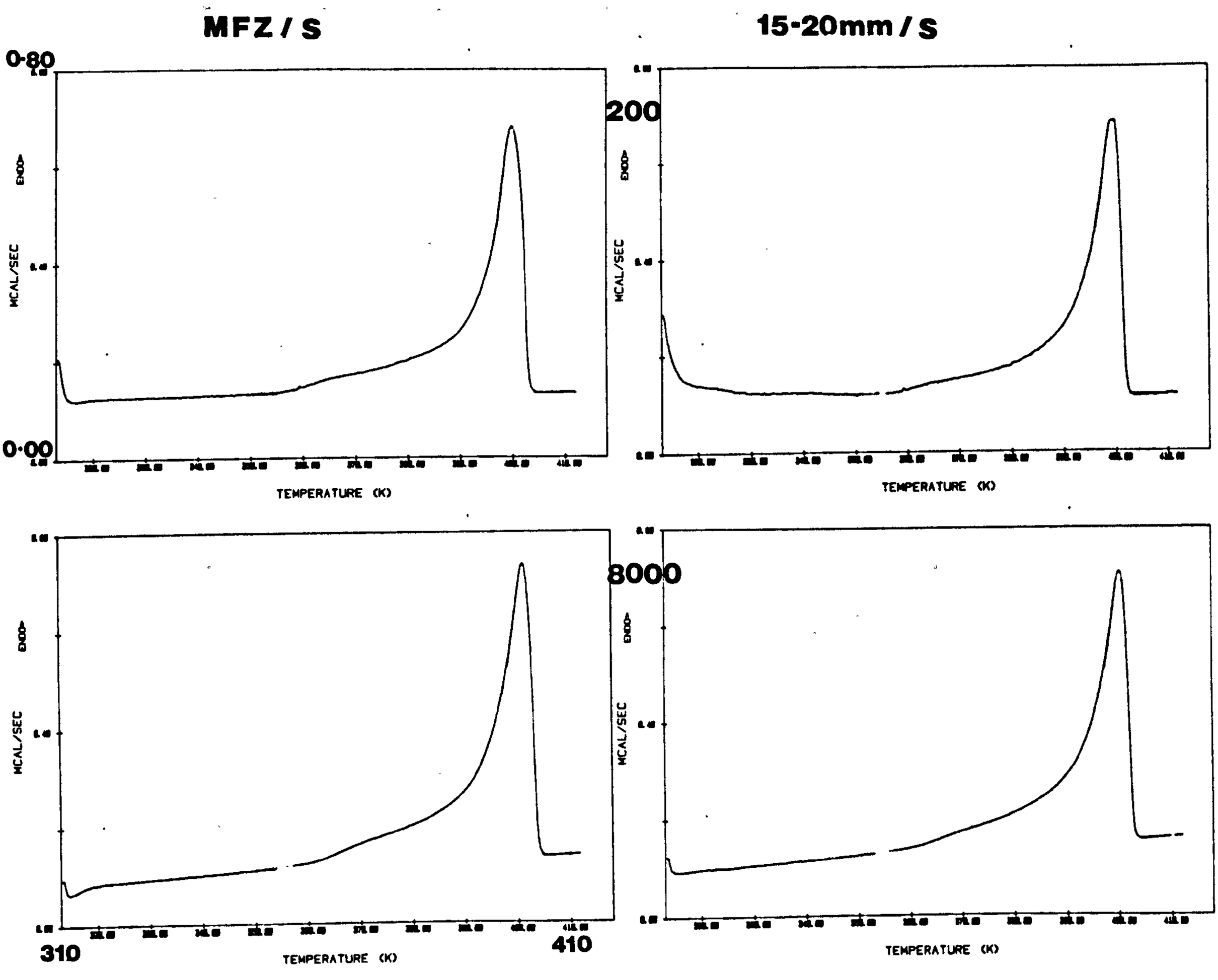

Fig. 6.2 DSC thermograms of surface specimen taken from the butt weld (MFZ) and 15-20mm away from it of the pressure tested butt welds in MDPE pipe sample for 200 and 8000 hours.

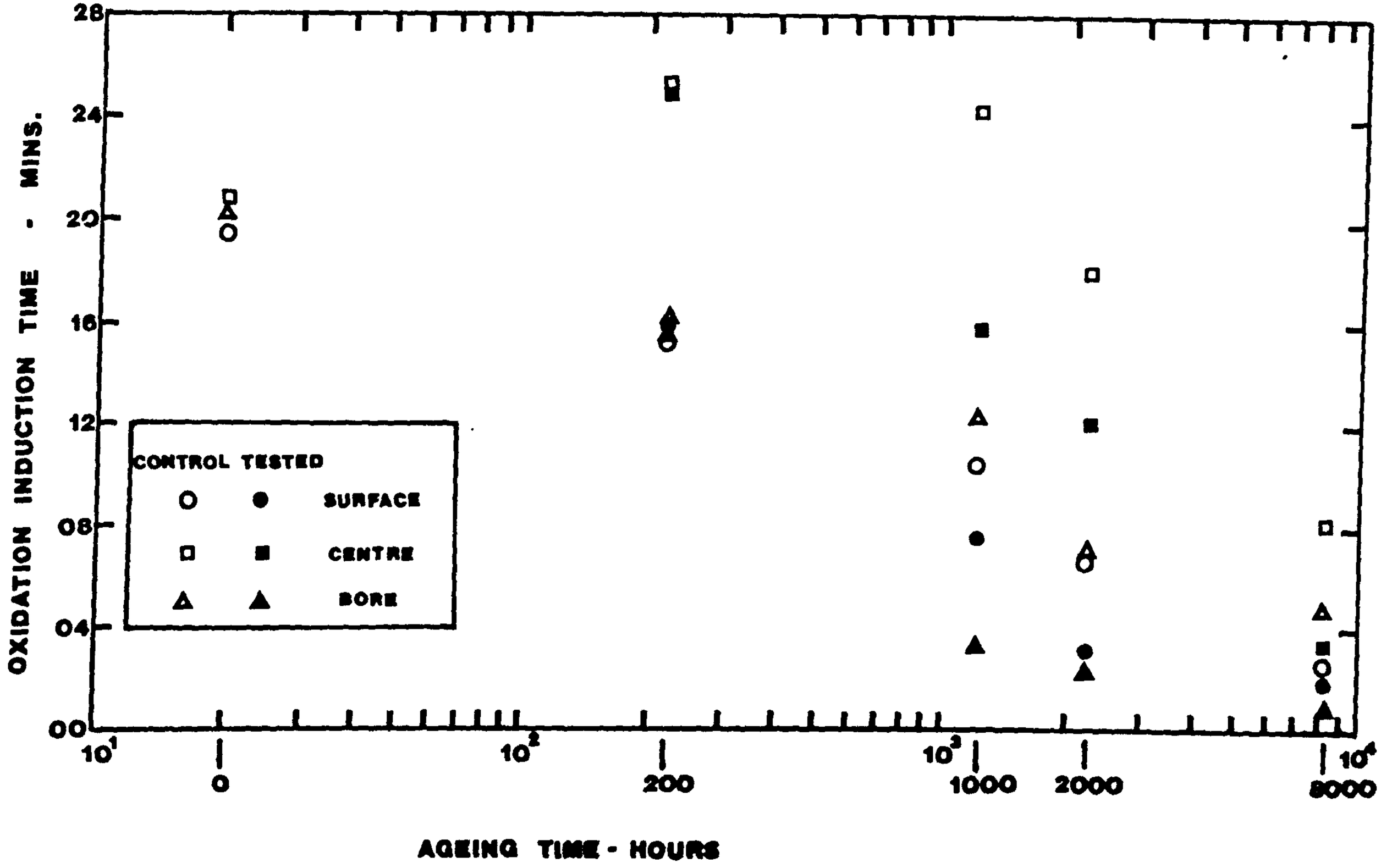

Fig. 6.3 Decrease in Oxidation Induction Time of both the control and pressure tested samples taken from butt welds in MDPE pipe with the ageing/pressure testing time.

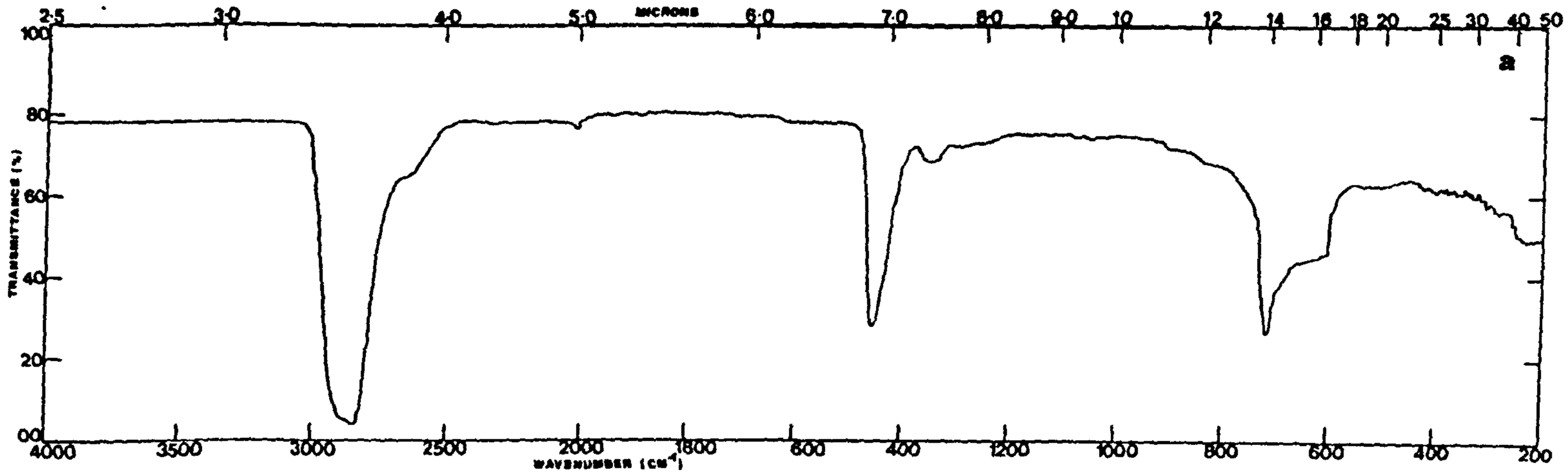

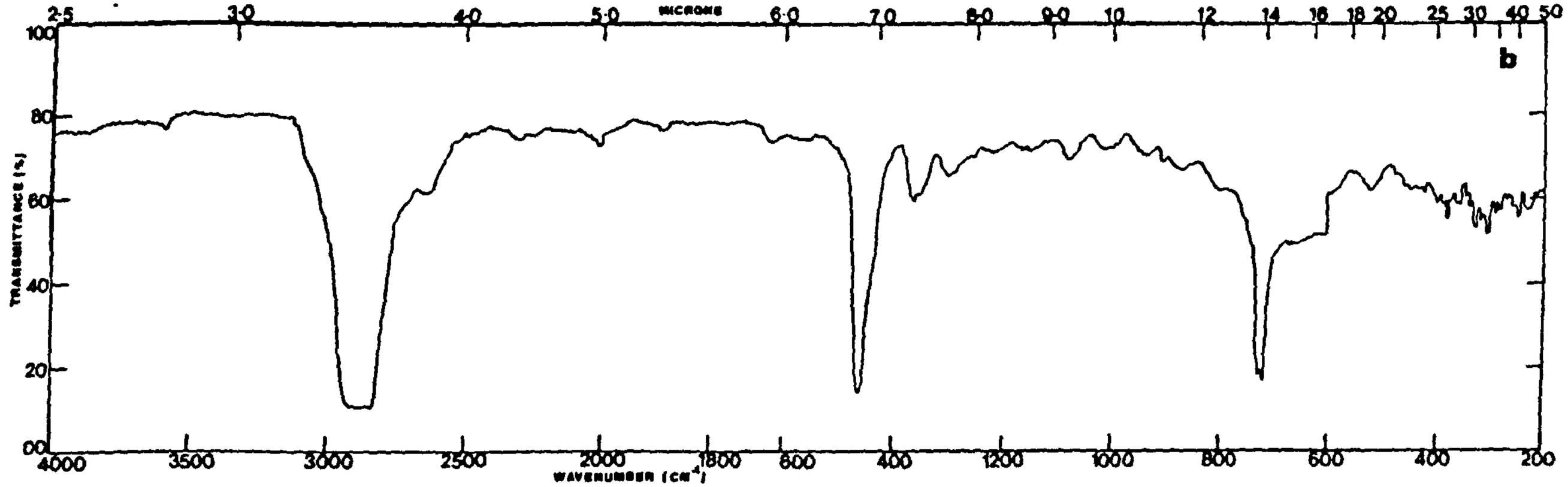

Fig. 6.4 Infrared specturm obtained for the bore skin of MFZ taken (a) from the untested butt welded MDPE pipe sample and (b) from pressure tested butt welded MDPE pipe sample to greater than 8000 hours.

6.7.0 Discussions

(i) Density and Crystallinity Tables 6.1 to 6.3 provide the selected property changes in the material structure with testing time at 79°C for both the umpressurised (control) and pressurised butt welded samples. The properties reported in tables 6.1, 6.2 and 6.3 are density, crystallinity and melting temperatures, respectively. Fine increases in density were recorded with the ageing time, while a noticeable increase in DSC crystallinity was observed with similar trends to those of density with ageing time at 79°C. However, peak melting temperature appears to remain constant.

The increase in density and crystallinity with increasing time seems to suggest a tendency towards a more ordered and stable crystal structure formation. However, this may never be fully realised since at 79°C (≈50° below melting temperature) the thermal motion of the polymer chains is not enough to bring about complete order. It is probably the chains in the disordered region with limited motion attempting to rearrange into three-dimensional order. Note that if a significant ordered structure was formed then the melting temperature would have been raised. As this was not observed it implies only minor changes to the structure.

Changes in crystallinity due to ageing of HDPE pipes at room temperature and due to testing of pipes at elevated temperature have been reported in the literature (13, 133, 135). Improvements in both stress-rupture and fatigue performance have also been reported in the literature (91, 192) with increases in density and crystallinity. Muller and Gaube (91) have shown that the stress-rupture graphs of PE shift upwards with increasing density or differing degree of crystallinity, that is HDPE>MDPE>LDPE, whilst De Charentenary et al (192) found a four-fould decrease in FCP rates in HDPE when crystallinity increased from 47 to 55%. Thus the increase in crystallinity noted in the table 6.2 would be expected to retard the crack

growth rate to some extent under fatigue and stress-rupture for those samples which are tested beyond 2000 hours. Hence any variation in mechanical performance of pipes subjected to longer test times would then be partially explained by changes in above mentioned properties. However, the performance of butt welded samples which were aged at 79°C for 200, 2000, 8000 hours did not significantly increase compared to unaged sample (see table 6.6).

In other words, the density and crystallinity changes observed at 79°C are not of sufficient magnitude to strongly influence the performance.

(ii) Oxidation Indication Times Table 6.4 highlights the oxidation induction times of the control and pressure tested samples as a function of increasing time which have been in a water environment at 79°C. It is apparent that the oxidation induction time decreases with ageing time for the samples obtained from surface, core and bore at the butt weld and 15-20mm away from it. The rate of decrease is rapid and similar for both the surface and bore control samples compared to the core region, whereas, a relatively greater rate of decrease in OIT values of pressure tested butt welded samples is apparent compared to control. Further, the bore region tends to show early deteriation in the OIT compared to the surface.

The decrease in the oxidation induction time suggests that the change in concentration of stabiliser in MDPE may be a result of two processes:

(a) Chemical reactions of the stabilisers, and
(b) physical loss of the stabilisers from MDPE

The loss of the stabiliser through these two possible means is considered.

In order to understand the stabilisers being used up in a chemical reaction one needs to consider mechanism of stabilisation, the aim being to identify the product formation which can be detected. The mechanism of u.v. stabilisation is examined, however the radical formation can equally be obtained under different external energy form, for example stressed chains can also bring about the radical formation. Oxidation of polyolefins is generally assumed to involve a free-radical chain mechanism (210) :

Initiation: $RH \longrightarrow R\cdot + H\cdot$ (6.1)

Propagation $R\cdot + O_2 \longrightarrow RO_2\cdot$ (6.2)

$RO_2\cdot + RH\cdot \longrightarrow ROOH + R\cdot$ (6.3)

Chain branching $ROOH \longrightarrow RO\cdot + \cdot OH$ (6.4)

Termination $R\cdot + R\cdot$ } inert product (6.5)

$RO_2\cdot + R\cdot$ } (6.6)

$RO_2\cdot + RO_2\cdot$ } (6.7)

The propagation reaction (6.2) and (6.3) can be inhibited by free radical scavenger (stabilisers) which destroy the radical produced during stage (6.1).

Inhibition reaction:

$RO_2\cdot + InH \longrightarrow ROOH + In\cdot$ (6.8)

$RO_2\cdot + In\cdot \longrightarrow ROOIn$ (6.9)

It is clear from reaction (6.8) and (6.9), if the stabilisers is used up in the chemical reaction, the resulting product has carbonyl and hydroxyl groups which should be detected in an

infrared spectroscopy analysis. However, since the infrared spectrum of bore skin and surface skin of the sample subjected to 8000 hours (figure 6.4(a) and (b)) showed no carbonyl or hydroxyl absorption peak, it seems to rule this possibility out. The expected absorption peak for C=O stretch is at about $1700cm^{-1}$ and for O-H stretch at $3000cm^{-1}$ and O-H bend at $900cm^{-1}$. In addition, the GPC showed no significant change in Mn and Mw with the ageing time (see table 6.5) indicating no major chain breakdown (degradation) had occurred.

Despite the fact that there is no strong evidence to suggest the loss of stabiliser by the chemical means, it cannot be ruled out. The condition for the reaction described in (6.1) to (6.8) does exist. This is especially true of the pressurised pipe. In the pressurised pipe, the pipe bore is biaxially stressed and dissolved oxygen from the compressed air used to pressurise the sample is present.

The physical loss of stabiliser can occur by two means; volatility loss of stabiliser and extraction due to polymer being into contact with water or organic solvents. The volatility loss can be discounted, as such losses can occur only under processing conditions when the polymer is subject to temperature of above 220°C. It appears that the leaching out of the stabilisers is the likely means which occurs through the diffusion process probably obeying Fick's Law.

Assuming a uniform distribution of stabiliser in the bulk of the polymer, a concentration change at the surface and bore (initial extraction of stabiliser by water) gives rise to concentration gradient which is the driving force of diffusion of stabiliser according to the first Fick Law (6.11) (210)

$$I = -D\frac{(\delta c)}{(\delta x)} \qquad (6.10)$$

$$\frac{(\delta c)}{(\delta t)_x} = D\frac{(\delta^2 c)}{(\delta x^2)_t} \qquad (6.11)$$

where I is the permeation flux, D is the diffusion coefficient and ($\delta c/\delta x$) is the concentration gradient. The diffusion of the stabiliser from the bulk of the polymer into the surface region is thus able to supply the stabiliser where necessary.

It must also be taken into account that the following relationship between solubility and diffusivity of a substance is also valid 210:

$$P = D \times S \qquad (6.12)$$

where P is the permeation constant, D is the diffusion coefficient, and S is the solubility constant. Equation (6.12) implies the diffusion coefficient is inversely proportional to the solubility of the substance in a polymer. Owing to their low solubility in many polymers, stabilisers diffuse to the surface. This phenomenon, which may be regarded as a manifestation of incompatibility and migration ability of the additives in polymers, would be more favourable.

The loss of stabiliser does not have any significant influence on the fatigue performance of butt welds at 79°C as demonstrated by the testing of the 8000 hours aged samples at 79°C, see table 6.6. The obvious consequence of the loss of stabiliser would be that the polymer is not protected against oxidation which could occur during rewelding of the pipes. That is an aged sample which is to be butt welded would be in a danger of oxidation. The performance of such a weld would then be reduced.

CHAPTER 7 - CONCLUSIONS

Fatigue Performance Of Butt Fusion Welds

Fatigue lifetime was found to decrease significantly with increasing axial misalignment at the butt fusion weld in 63, 90 and 125mm MDPE pipe systems. In the butt fusion welds having axial misalignments of 20 per cent of the wall thickness and above, the reduction was greater than 50 per cent compared to the aligned weld. There was no marked change in the performance of misaligned butt welds for the three pipe diameters investigated despite the non-identical rate of pressurisation for each of the pipe systems. However, the performance of the aligned butt welds in 90 and 125mm pipe was noticably better compared to 63mm pipe systems.

The fatigue performance of misaligned butt welds could be explained in terms of amplified axial stresses and in general, the Ory expression for evaluating the increase in axial stress due to mislignment appears to be valid. The improvement in the fatigue performance of aligned butt welds in 90 and 125mm MDPE pipes compared to 63mm MDPE pipes is suggested to be due to the combined effect of rate of pressurisation and bead size.

The temperature dependence of the fatigue performance of aligned and misaligned butt fusion welds in 63 and 90mm MDPE pipe systems suggests that if continuous internal flucatuating pressures under the conditions examined are maintained, the butt fusion welds would not meet the minimum design lifetime of 50 years at a service temperature of 20°C for misalignments greater than 10 per cent of the wall thickness. To take the full advantage of the MDPE grade examined, care must be taken to align the butt weld and minimise misalignment below 10 per cent of the wall thickness.

Stress-Rupture Performance Of Butt Fusion Welds

The reduction in the performance of 20 per cent and above misaligned butt fusion welds was also reduced by greater than 50 per cent compared to aligned welds under stress-rupture conditions for all the pipe diameters examined. Stress-rupture results suggest there might be a pipe size effect; the performance of misaligned butt welds in 90 and 125mm MDPE pipes were more than halved compared to those in 63mm pipe systems. However, there was no substantial difference in the lifetime of misaligned butt welds between 90 and 125mm. All the misaligned butt welds considered in the three pipe diameters surpassed the minimum specified requirement of 170 hours at 80°C.

In terms of total testing time to failure, the aligned and 10 per cent misaligned butt fusion welds were more than ten times better under stress-rupture conditions compared to fatigue for an equivalent maximum hoop stress. Fatigue loading was the most aggressive condition of the two for minor misalignment.

Welding Conditions

Despite extreme changes (-50 to 100 per cent) in the heat soak time, heat removal time and welding pressure, there were not significant changes in the fatigue lifetime of aligned butt fusion welds compared to those recorded when axial misalignments of 9-44 per cent of the wall thickness were introduced. The fatigue performance of aligned butt welds was found to be tolerant to the changes in the welding conditions examined whereas fatigue performance was very sensitive to changes in misalignment.

Failure Analysis

All the misaligned butt welds in the three pipe sizes under both the fatigue and stress-rupture conditions and the majority of the aligned butt fusion welds in 63mm MDPE pipes under fatigue

failed at the weld in the circumferential plain. These were found invariably to initiate from the notch located at the inner weld bead and no preferred crack propagation path was taken in relation to the melt flow zone. It was proved conclusively that the notch created by the internal weld bead rolling onto the pipe bore was responsible for the observed circumferential failure of aligned butt welds in 63mm MDPE pipes by testing of these butt fusion welds where the the internal weld bead was machined off. The failure site for the internal weld bead machined off sample was remote from the weld inferring the material in the melt flow zone does not have any weakness but rather the notch which is inherently present in the butt fusion weld causes the weakness under fatigue.

All the fracture surfaces showed the charateristics of slow crack growth and the majority of them also had discontinuous growth bands. Correlations were found between the spacing of discontinuous growth bands and the magnitude of misalignment and also with the pressure range

Failure mechanisms were found to be highly localised and confined to a small volume of material involving void nucleation or caviation, growth of the microvoid and fibrillation. The failure was not a classical brittle type but rather a quasi-britle type involving local energy absorption.

The Effect Of Elevated Temperature (79°C) Testing Technique

The effect of elevated temperature testing in 63mm SDR11 MDPE pipe was to increase the density and crystallinity signifying a slow annealing process in the material. However, the changes in these parameters were not of a sufficient scale to strongly influence the performance. The main effect of elevated temperature testing in a water environment appears to be the extraction of stabliser from the base polymer as indicated by the rapid decrease in oxidation induction time with the ageing times. The leaching out process is enhanced when the pipe is under pressure.

Future Work

Two other forms of misalignment geometry which could occur in practice are:

(i) pipes of same outside diameters but different SDR are butt welded, giving a constant inside step at the butt weld and

(ii) angular misalignment caused by butt welding coiled pipes.

It would be of great value to determine the performance of these types of butt fusion weld in order to determine which geometry represents the worst case.

The experimental determination of stresses around the butt fusion weld with

(i) varied bead size for a given pipe size,

(ii) weld bead machined off and

(iii) misaligned butt welds using combination of strain gauge and displacement transducers.

Such determination would enable accurate picture of stresses in the butt fusion weld to be built up.

There are lengths of pipes which have been aged to various times, it would be interesting to investigate the variation in short-term mechanical properties across the wall thickness of these aged pipes.

REFERENCES

1 McNally, P.F.
Proceeding of 4th International Conference on Plastic Pipes,
University of Sussex, March 1979, Paper 1.

2 Murphy, J. S.
Proceeding of 6th International Conference on Plastic Pipes,
University of York, March 1985, Paper 32.

3 BP Chemicals Ltd., Rigidex MDPE, Rigidex PC002-50, Data sheet TDS53.

4 Richard, K., Diedrich, G., Gaube, E.
Kunststoffe, 49, 516, (1959).

5 ASTM D 2837 - 76
1977 ASTM Book of Standards Part 34, p390,
American Society for Testing and Materials, Philadelphia, Pa 19103.

6 Gloor, W.E.
Modern Plastics, 36, (1958), 144.

7 Whyman, A.D. and Szpak, E.
SPE Journal, 29, (1973), 74.

8 Zhurkov, S.N.
International Journal of Fracture Mechanics 1, 311, (1965).

9 Larson, F.R. and Miller, J.
Trans ASME 74, (1952), 765.

10 Gladstone, S. Laidler, K.J. and Eyring, H.
The Theory of Rate Processes, McGraw - Hill, New York (1941).

11 Coleman, B.D.
Journal of Polymer Science 20, (1956), 447.

12 Barton, S.J. and Cherry, B.W.
Polymer Engineering and Science volume 19 (8), 1979, 590-595.

13 Barton, S.J. and Cherry, B.W.
Proceeding 4th International Conference on Plastic Pipes,
Sussex University, March 1979, Paper 21.

14 Bragaw, C.G.
Proceeding 5th International Conference on Plastic Pipes,
York University, September 1982, Paper 15.

15 Bragaw, C.G.
Proceeding Plastics Fuel Gas Pipe Symposium, AGA,
New Orleans, 1983, 40.

16 Palermo, E.F.
Proceeding Plastic Fuel Gas Pipe Symposium, AGA,
New Orleans, 1983, 96.

17 Geffroy, R.R. and DeBlieu, I.K.
Proceeding Plastic Fuel Gas Pipe Symposium, AGA,
New Orleans, 1983, 16.

18 Szpak, E. and Rice, F.
Proceeding Sixth Plastic Pipe Symposium, American Gas Association,
Columbus, Ohio, U.S.A., April 1978.

19 Smith,R.A.
Materials In Engineering Applications, Vol.1, December 1978, Part 1.

20 Smith,R.A.
Materials In Engineering Applications, Vol.1, June 1979, Part 2.

21 Marshall, G.P.
Plastics and Rubber Processing and Application,2 (1982), 169-182.

22 Andrews, E.H.
J. Material Science, 9 (1974), 887-894.

23 Williams, J.G.
Fracture Mechanics of Polymers.
Ellis Horwood Limited Publiser, Chichester, 1984.

24 Birch, M.W., Howarth, R. and Marshall, G.P.
Proceeding of 4th International Conference Plastics Pipes,
Sussex University, March 1979, Paper 25.

25 Price, J.B. and Gray, A.
Proceeding of 3rd International Conference Plastics Pipes,
Sussex University, March 1974, Paper 20.

26 Gray, A., Mallinson, J.N. and Price, J.B.
Plastics and Rubber Processing and Application, Vol(1), 1981, 51.

27 Bragaw, C.G.
Proceeding of 4th International Conference Deformation, Yeild and
Fracture of Polymer, Cambridge, April 1979, Paper 1.

28 Flueler, P., Roberts, D.R., Mandel, J.F. and McGarry, F.J.
ASTM STP 736 R.E.Evans (Ed.)
American Society For Testing and Materials, 1981, 15.

29 Freudenthal,A.M.
Proceeding Royal Society, A187, 416, 1946.

30 Weibull, W.
J. Applied Mechanics, 18, 1951, 293.

31 Jayatikala, A. Des and Trustrum, K.
J. Material Science, 12, 1977, 1426-1430

32 Smith, L.A. and Derringer, G.C.
Proceeding Plastic Fuel Gas Pipe Symposium, AGA,
New Orleans, 1983, 25.

33 Derringer, G.C.
SPE 39th ANTEC Proceeding, Boston, May 1981, 71-3.

34 Lusk, D.L.
Polymer Plastic Technology and Engineering, 23,(1), 1984, 69-82.

35 Neumann, J.A. and Bockoff, F.F.
Welding of Plastics, Reinhold, N.Y. 1959.

36 Kaminsky, S.J. and Williams, J.A.
Handbook for Welding and Fabricating Thermoplastic Materials,
Fidelity Press, Boston, 1964.

37 Chasis, D.A.
Plastic Piping Systems, Industrial Press, N.Y., 1976.

38 Anonymous
Thermal and Chemical Welding of Plastic Materials,
Engineering Equipment Users Association, London, 1976.

39 ASTM D3261
Specification for Butt Fusion of PE Plastics, Sch. 40.

40 WRC Specification No 4-32-04
Polyethylene Joints and Fittings suitable for Fusion Jointing of
Pipes

41 Barber, P. and Atkinson, J.R.
J. Material Science, Vol.7, 1972, 1131-1136.

42 Barber, P. and Atkinson, J.R.
J. Material Science, Vol.9, 1974, 1456.

43 DeCourcy, D.R. and Atkinson, J.R.
J. Material Science, Vol. 12.(8), 1977, 1535-51.

44 Atkinson, J.R. and DeCourcy, D.R.
Plastics and Rubber Processing and Application, Vol.1.(4), 1981, 287.

45 Malguarnera, S.C. and Earles, L.L.
ANTEC 1982, 279-282.

46 Bucknall, C.B., Drinkwater, J.C. and Smith, G.R.
Polymer Engineering and Science, Vol.20.(6), 1980, 432.

47 Greig, J.M.
Pipes Pipelines International, 22 No 1, Feb.1977, 16-24.

48 Albrecht, R.
AGA Fifth Plastic Pipe Symposium, Nov.1974, 28.

49 Diedrich,G. and Gaube, E.
Kunststoffe, 60, Feb.1970, 74-80.

50 Diedrich, G. and Kempe, K.
Kunststoffe, 70, Feb 1980, 8.

51 Sucherck, V.J.
Translated Proceeding of 9th IKV Seminar, 1978.

52 Zaitsev, I.K.
Welding Production, Vol.19, No6, June 1972, 20-22.

53 Zaitsev, I.K. and Bukin, E.V.
Welding Production, Vol.20, No 5, May 1973, 18-20

54 Sajzew, K.I. and Zaitsev, I.K.
Zis Mitteilnngen, Vol.19, No3 March 1977, 338-347.

55 Kashkovskaya, E.A., Kaigorodov, G.K. and Petrovski, A.P.
Automatic Welding, Vol.29, No 9, Sept.1976, 21-23.

56 Kashkovskaya, E.A. and Kaigorodov, G.K.
Avt. Svarka, 1975, No8, 23-26.

57 Bukhin, V.E.
Automatic Welding, Vol.25, No1 Jan.1972, 35-37.

58 Kashkovskaya, E.A., Zaitsev, I.K. and Kaigorodov, G.K.
Plast. Massy., No10 1975, 47-8.

59 Menges, G. and Zohren.
Plastverarbeiter, 18(3), 1967, 165.

60 Barton, S.J.
Australian Welding Research, Vol.9. Dec.1980, 26-30.

61 Barton, S.J. and Cherry, B.W.
Welding in the Eighties Proceeding 28th Nat. Welding Cov., Meb.,
Oct.1980, Publ: Milsons Point, NSW 2061, Australia.

62 Potente, H. and Tappe, P.
Materials and Design, Vol.5, No6, Dec/Jan 1985, 273.

63 Potente,H.
Kunststoffe, 67, (1977), 2, 98-107.

64 Voyutskii, S.S.
Autohesion and Adhesion of High Polymers, Interscience Publishers,
1963, John Wiley & Sons, N.Y., London, Sydney.

65 Anandu, J.N. and Karam, H.J.
J. Adhesion, 1,(1969)1, 17-23.

66 Anandu, J.N. and Balwinski, R.Z.
J. Adhesion, 2, (1970)1, 16-22.

67 Anandu, J.N.
J. Ahesion, 2, (1969)1, 31-37.

68 Anandu, J.N. and Dipzinski. J.
J. Adhesion, 2 (1970)1, 16-22.

69 Anandu, J.N.
J. Adhesion 2 (1970)1, 23-29.

70 Menges, G. and Pieschel, D.
Kunststofftech, 13, (1974), 165-170.

71 Briken, F.
Proceeding of 5th International Conference Plastic Pipes,
York University, Sept. 1982, Paper 25.

72 John, P.
Kunststoffe, Vol.72, Nov.1982, 713-715.

73 Wolters, M. and Venema.
Proceeding of 5th International Conference Plastic Pipes,
York University, Sept. 1982, Paper 26.

74 Kolb, K.
Kunststoffe, Vol.66, June 1976.

75 Dziengidewski, E.
Symposium papers and related information on Non-Destructive Testing
of Pipe Systems, Inst. of Gas Tech., Chicago 1976.

76 Kaelble, K.
Physical Chemistry of Adhesion, J. Wiley & Sons (1971).

77 Herrmann, H.
Plastics Pipes Symposium, Frankfurt, Dec.1979.

78 Potente, H. and de Zeeuw, K.
Proceeding of 4th International Conference Plastic Pipes, Brighton, March 1979, Paper 24.

79 Herforth, H.
Plastrevarbeiter, 33, (1982), 5, 14-67, 1469.

80 Hessel, J. and John, P.
Kunststoffe, 74, (1984).

81 Ory, H.
Dunnwandige Drehschalen unter symmetrischer Bellsttung Vorlesung an der RWTH Aachen 1978.

82 Barker, M.B.
PhD Thesis, Brunel University, 1982, Uxbridge.

83 Richard, I.K, Gaube, E. and Diedrich, I.G.
Kunststoffe, Vol.50, June 1960, 3.

84 Gaube, E, Diedrich, G. and Muller, W.
Kunststoffe, Vol.66, Jan.1976, 1.

85 Real, H.
Kunststoffe, Vol.52, April 1962, 6.

86 Vetter, M.
Kunststoffe, Vol.56, April 1966, 14.

87 Menges, u. G. and Ehrbar, J.
Kunststoffe, Vol.53, 1963, 233-243.

88 Vancrombrugge, R.
Plastica, 26, 5, May 1973, 199-207.

89 Gaube, E, Diedrich, G. and Muller, W.
Kunststoffe, Vol.56, Oct.1966, 228.

90 Diedrich, B., Kempe, and Graf, K.
Kunststoffe,Vol.69, 8, Aug.1979, 470.

91 Muller, W. and Gaube, E.
Kunststoffe, Vol.72, May 1982, 297.

92 Marshall, G.P., Taylor, M.D. and Dickinson, A.J.
Proceeding of 5th International Conference Plastic Pipes,
York Unversity, Sept. 1982, Paper 7.

93 Jacobi, H.R.
Kunststoffe, 55, Jan.1965, 39.

94 Lortsch, W.
Kunststoffe, 55, June 1965, 460.

95 Menges, G. and Roberg, P.
Plastverarbeiter, 19, 1968, 936-944.

96 Hucks, R.T.
J. American Water Works Association, 64,(7) 1972, 443.

97 Gotham, K.V. and Hitch, M.J.
Pipes & Pipelines International, 20, Feb 1975, 10-17.

98 Gotham, K.V. and Hitch, M.J.
British Polymer J., 10, March 1978, 47-52.

99 Stapel, J.J.
Pipes & Pipelines International, 22, Part 1 Feb. & Part 2 April 1977.

100 Joseph, S.H.
Proceeding of 4th International Conference Plastic Pipes,
Sussex University, March 1979, Paper28.

101 Joseph, S.H.
Plastics and Rubber Process and Application, Vol.4(4), 1984, 325-330.

102 Joseph, S.H. and Leevers, P.S.
J. Material Science, Vol.20, (4), Jan.1985, 237.

103 Dukes, B.W.
Proceeding of 6th International Conference Plastic Pipes,
University of York, March 1985, Paper 17.

104 Kirby, P.C.
Proceeding of 4th International Conference Plastic Pipes,
Sussex University, March 1979, Paper 26.

105 Fedosoff, F.A. and Szpak, Z.
Engineering Digest, Sept. 1979, 35.

106 Cowley, W.E. and Wylde, L.E.
Chemistry and Industry, No11, June 1978, 371-7.

107 Barker, M.B., Bowman, J. and Bevis, M.
J. Material Science, 15, No1 Jan. 1980, 265-8.

108 Barker, M.B., Bowman, J. and Bevis, M.
Proceeding of 5th International Conference Plastic Pipes,
Leeds University, Sept. 1982, Paper 16.

109 Barker, M.B., Bowman, J. and Bevis, M.
J. Material Science, Vol.18, 1983, 1095-1118.

110 Brydson, J.A.
Plastics Materials, Third Edition, 1975.
Butterworth & Co. (Publisers) Ltd. London: 88 Kingsway, WC2B 6AB.

111 Edited by J.M.Schultz.
Treatise On Materials Science and Technology, Vol.10. Properties of
Solid Polymeric Materials. Part A.
Acedemic Press. 111 Fith Av. N.Y. 1977.

112 Brown, N. and Ward, I.
J. Material Science, Vol.18, June 1983, 1405.

113 Muller, W. and Gaube, E.
Kunststoffe, Vol.72, May 1982, 24.

114 Gebler, H.
Kunststoffe, Vol.73, 2, 1983, 9.

115 Reitemeyer, P.
Kunststoffe, Vol.71, 10, 1981, 665.

116 Cist, J.D. and Smith, J.G.
Plastics Engineering, Vol.34, No6, 1978, 41.

117 Schnur, G.
Kunststoffe, Vol.57, Oct. 1967.

118 Turner, A.
Fabrication of Thermoplastics.
Polymer - Applied Polymer Symposium, No17, 3
Wiley - Interscience, 1971.

119 Williams, J.G., Gray, A. and Hodgkinson, J.M.
Polymer Engineering and Science, Vol.21, Sept. 1981, 822-808.

120 Williams, J.G.
Plastics and Rubber Processing and Application, 1, 1981, 369-377.

121 Hodgkinson, J.M. and Williams, J.G.
Plastics and Rubber Processing and Application, Vol.3(1), 1983.

122 Marshall, G.P., Taylor, M.D. and Dickinson, A.J.
Proceeding of 5th International Conference, Plastic Pipes,
York University, Sept. 1982, Paper 7.

123 Gebler, H. and Racke, H.H.
Kunststoffe, Vol.72, Jan. 1982, 33.

124 Potente, H., Zeeuw, K. and Braches, E.
Schwessen and Schneiden, Vol.31, No5, May 1979, 192-195.

125 Reinke, M. and Potente, H.
ANTEC 1982, 59-61.

126 Young, R.J.
Introduction to Polymers, Chapman and Hall Ltd., London. 1981,
169, 278.

127 Gedde, U.W. and Jansson, J.F.
Polymer Testing, Vol.1. No4. 1980, 303.

128 Gedde, U.W., Terselius, B. and Jansson J.F.
Polymer Testing, Vol.2. No2. 1981, 85.

129 Gedde, U.W., Terselius, B. and Jansson J.F.
Polymer Testing, Vol.2. No3. 1981, 211.

130 Gedde, U.W., Terselius, B. and Jansson J.F.
Polymer Engineering and Science, Vol.22, No7. May 1982, 422.

131 Erikson, P. and Ifwarson, M.
Proceeding of 6th International Conference Plastic Pipes,
University of York, March 1985, Paper 40A and 40B.

132 Kirkland, F.J. (ed.)
Modern Practice of Liquid Chromatography, Wiley Interscience, 1971.

133 Loginov, V.S., Kashkovskaya, E.A. and Petrovskii, A.P.
Int. Polymer Science & Technology, Vol.6, No9, 1979, 729.

134 Loginov, V.S. and Kashkovskaya, E.A.
Int. Polymer Science & Technology, Vol.6, No.9, 1979, 183.

135 Schonefeld, C. and Wintergerst, S.
Kunststoffe, Vol.61, 1971, 33.

136 Mandelkern, L., Allou, A. G. and Gopalan, M.
J. Physical Chemistry, Vol.72, No1. Jan. 1968, 309.

137 Mandelkern, L., Price, J.M., Gopalan, N. and Faron, J.G.
J. Polymer Science, Polymer Physics, Ed.4, 1966, 385.

138 Hay, J.N.
British Polymer Jorunal, Vol.11, 1979, 137.

139 Still, R.H.
British Polymer Jorunal, Vol.11, 1979, 101.

140 Ghijsels, A., Waals, F.M. and Terselius, B.
Polymer Testing, Vol.1, 1980, 149.

141 Cooney, J.R.
J. Applied Polymer Science, Vol.8, 1964, 1889.

142 Andrews, E.H.
Fatigue in Polymers; Testing of Polymer, Vol. IV, W. Brownel ed.,
Interscience, N.Y. 1969, 237.

143 Plumbridge, W.T
J. Material Science, Vol.7, 1972, 939-962.

144 Hearle, J.W.S.
J. Material Science, Vol.2, 1967, 474-488.

145 Hertzberg, R.W. and Manson, J.A.
CRC Critical Review in Macromolecule Science, August 1973, 433.

146 Oberbach, K.
Kunststoffe, Vol.63, 1973, 35.

147 Kambor, R.P.
J. Polymer Science, Macromolecule Review, 7, 1, 1973, 1.

148 Andrews, E.H.
Fracture in Polymers, Oliver and Boyd, London 1968.

149 Schultz. J.M.
Treaties on Material Science and Technology, Part B, P599
Academic Press, N.Y. 1977.

150 Kausch, H.H.
Polymer/Properties and Application 2, Polymer Fracture.
Springer - Verlag, N.Y. 1978.

151 Hertzberg. R.W. and Manson, J.A.
Fatigue of Engineering Plastics, Academic Press. London 1980

152 Kinloch, J.A. and Young R.J.
Fracture Behaviour In Polymer. Applied Science Publishers Ltd,
Barking. 1983.

153 Ferry, J.D.
Viscoelastic Properties of Polymers, Wiely, N.Y. 1961.

154 Natov, M. and Glashkov, M.
Mekh. Polim. 6, 1009-1013.

155 Natov, M. and Glushkov, M.
Mekh. Polim. 7, 912-916.

156 Harris, J.S. and Ward, I.M.
J Material Science, 8, 1973, 165-1665.

157 Benham, P.P. and Hutchinson S.J.
Plast. Polym. 38, 1970, 259-264.

158 Ratner, S.B. and Korobov, V.I.
Mekh. Polim. 1 No3 1965, 93-100.

159 Mckenna, G.B. and Penn, R.W.
Polymer, Vol. 21,198, 213.

160 Zitvar, V.
J. Macromolecular Science; Physics B5 1971, 273-284.

161 Zilovar, V.
Plast. Polym. 39, 1971, 328-332.

162 Tauchert, T.R.
International J. Engineering and Science, 5, 1967, 353-365.

163 Crawford, R.J. and Benham, P.P.
J Material Science, 9, 1974, 18-28.

164 Sauer, J.A. and Richardson, G.C.
International J. Fracture, 16, 1980, 499.

165 Foden, E., Morrow, D.R. and Sauer, J.A.
J. Applied Polymer Science, 16, 1972, 519.

166 Crawford, R.J. and Benham, P.P
Polymer, 16, 1975, 908.

167 Andrews, E.H. and Walker, B.J.
Proceeding Royal Society, series A325, 1971, 57-97.

168 Rabinowitz, S., Krause, A.R. and Beardmore, P.
J Material Science, 8, 1973, 11-22.

169 Rabinowitz, S. and Beardmore, P.
J Material Science, 9, 1974, 81-99.

170 Feltner, C.E.
J. Applied Physics, 38, 1967, 3576-3584

171 Paris, P.C., Gomez, M.P. and Anderson, W.E.
Trends in Engineering, 13, 9, 1963.

172 Paris, P.C. and Erdogan, F.
J. Basic Engineering, 85, 1963, 528.

173 Hertzberg, R.W., Nordberg, H. and Manson, J.A.
J. Material Science, 5, 1970, 521.

174 Ramirez, A., Gaultier, P.M., Manson, J.A. and Hertzberg, R.W.
Proceeding International Conference on Fatigue Polymers, The Form Hotel, London. 1983.

175 Michel, A.C., Manson, J.A. and Hertzberg, R.W.
Proceeding 6th International Conference on Deformation, Yield and Fracture of Polymers, Churchill College, Cambridge, April 1985, Paper21.

176 Oberbach, K. and Heese, G.
Matericlprufung, Vol.14, 1972, 173.

177 Moore, D.R., Benham, P.p., Gotham, K.V., Hitch, M.J., and Littlewood, M.J.
Proceeding 4th International Conference Plastics Pipes, Brigthton, March 1979, Paper 27.

178 Van Crombrugge, R.
RILEM Symposium on Research and Reception Tests on Syntheic Materials for Construction, Final Report, Liege, 1974.

179 Kirstein, C.E.
Publication of the Institut fur Kunststoffprufung und Kunststoffbunder Universitat Stuttgart, 1972.

180 Feltner, C.E.
J. Applied Physics, 38 3576, 1967.

181 McEvily, A.J., Boettner, R.C. and Johnston, T.
Fatigue, An Interdisciplinary Approach, (Burke, J.J., Reed, N.L. and Weisgh, N. ed.), Syracuse University Press, Syracuse, N.Y. 1964.

182 Jacoby, G.H.
ASTM, STP 453, 1969, 147.

183 Zilvar, V., HarliccK, V. and Bouska, P.
Proceeding Conference Dimension, Strenghten, Calculations, Budapest, 11-471, 1974.

184 Laird, C. and Smith, C.G.
Phil. Mag., 7, 1962, 847.

185 Skibo, M.D., Hertzberg, R.W. and Manson, J.A.
J. Material Science, 11, 1976, 479.

186 Skibo, M.D., Hertzberg, R.W. and Manson, J.A.
J. Material Science, 12, 1977, 531.

187 Elinyck, J.P., Banwens, T.C. and Homes, G.
International J. Fracture Mechanics, 7, 1971, 277.

188 Mills, N.J. and Walker, N.
Polymer, 17, 1976, 335.

189 Williams, J.G.
J. Material Science, 12, 1977, 2525.

190 Mai, Y. and Williams, J.G.
J. Material Science, 14, 1973.

191 White, J.R. and Teh, J.W.
Polymer, Vol.20, 1979, 764.

192 De Charentenary, F.X., Laghouati, F. and Dewas, J.
Proceeding International Conference Deformation, Yield and Fracture of Polymer, Cambridge, 1979, Paper 6.

193 Bhatnagar, A. and Broutman, L.J.
Conference Proceeding for the SPE 43rd ANTEC Conference, Washington, D.C., 1985, 545-549.

194 Bauer, H.H., Christan, C.D. and O'Reilly, J.E. (ed.).
Instrumental Analysis, Allyn and Bacon, Inc., London, Chap.8. 201.

195 Menges, G.
DVS-Berichte, 62-65, E. Schmanchtenberg.

196 Menges, G.
AIF Reasearch Report, E. Schmachtenberg.

197 Gons, J.
Proceeding 4th International Conference Plastic Pipes, Brighton, March 1979, Paper 36.

198 Design Factors for Unreiforced Thermoplastics Products With Specific Reference to Pipes.
Plastics and Rubber Institute Design Booklet, 1976.

199 Hearn, E.J.
Mechanics of Materials, Pergamon Press, 1980, Chapters 9 and 10.

200 William, J.G.
Stress Analysis of Polymers (2nd Edition), Ellis Harwood, 1980.

201 Sternstein, S.S. and Ongehin, L.
American Chemical Society Polymer Preprints, Vol.10, 1969, 117.

202 Kubat, J., Rigdahl, M. and Seldon, R.
J. Polymer Science, Vol.20, 1976, 2799.

203 Bragaw. C.G.
Proceeding 4th International Conference Plastics Pipes, Brighton, March 1979, Paper 23.

204 Hannon, M.J.
J. Applied Polymer Science, Vol.18, 1974, 3761.

205 Folias, E.S.
International J. Fracture Mechanics, 3, 1967, 1-11.

206 Sanders, Jr., J.L.
ASME J. Applied Mechanics, 49, 1982, 103-107.

207 Sanders, Jr., J.L.
ASME J. Applied Mechanics, 50, 1983, 221.

208 Forman, R.G., Kickman, J.C. and Shivakumar, V.
Engineering Fracture Mechanics, Vol.21, No.3, 1985, 563-571.

209 Howard, J.
SPE ANTEC, 31, 1973, 408.

210 Scott. G. (ed.).
Developments in Polymer Stabilisation,
Applied Ssience Publishers Ltd., London. Part 2- Chap.5,
Part 3-Chap.4.